USE OF A VESSEL-MOUNTED ACOUSTIC DOPPLER CURRENT PROFILER TO STUDY CURRENTS AND ZOOPLANKTON BIOMASS DISTRIBUTION OVER THE VANCOUVER ISLAND CONTINENTAL MARGIN

By

Jesse Hoey

B.Sc. Physics, McGill University, 1992

A THESIS SUBMITTED IN PARTIAL FULFILLMENT OF

THE REQUIREMENTS FOR THE DEGREE OF

MASTER OF SCIENCE

in

THE FACULTY OF GRADUATE STUDIES

DEPARTMENT OF PHYSICS

We accept this thesis as conforming

to the required standard

THE UNIVERSITY OF BRITISH COLUMBIA

December, 1994

In presenting this thesis in partial fulfilment of the requirements for an advanced degree at the University of British Columbia, I agree that the Library shall make it freely available for reference and study. I further agree that permission for extensive copying of this thesis for scholarly purposes may be granted by the head of my department or by his or her representatives. It is understood that copying or publication of this thesis for financial gain shall not be allowed without my written permission.

Department of PHYSICS

The University of British Columbia
Vancouver, Canada

Date December 19th 1994

DE-6 (2/88)

Abstract

We examine currents and relative zooplankton scattering strengths measured with a vessel-mounted RD Instruments 150 kHz acoustic Doppler current profiler (ADCP) over the southwest Vancouver Island continental margin. Raw ADCP signal strengths are converted into relative zooplankton backscatter intensities using a method of residuals computed from average linear fits to depth profiles, which removes most system-dependent effects. An absolute calibration is not feasible without coincident net tows and a record of system characteristics. The problem of side-lobe contamination of near-bottom zooplankton backscatter estimates is given considerable attention and an objective method is developed to eliminate erroneous backscatter values. Ship-referenced water velocities are converted to absolute (earth-referenced) currents using bottom-tracking measurements of ship velocities. Methods of calculating absolute currents using ship velocities estimated from the change in (GPS) ship position are also examined. It is shown that the GPS positional errors of $\approx \pm 300$ m lead to velocity errors that are comparable to the currents. Only when bottom-tracking is available are absolute currents reliable.

The methods developed to process the data are applied to ADCP data collected in June 1993 over the southwest Vancouver Island continental margin. The currents and relative zooplankton scattering strengths are examined over a 20 hour period along a 14 km survey line which spans the shelf break. Zooplankton concentrations occupied the upper 50 m over the shelf and slope both day and night. Aggregations of scatterers were present over the shelf break at depths of 150–200 m during the day, and migrated to the surface waters at sunset. Mean upwards swimming speeds were 1–1.5 cm/s. Offshore flow and vertical shears of the order of $10^{-3}\,s^{-1}$ on the shelf were correlated with

horizontal movements of zooplankton, indicating that the distribution of zooplankton over the shelf and slope was influenced significantly by advection. A strong scattering layer with backscatter intensities 100 times higher than normal surface intensities was advected into the survey area over the shelf a few hours before sunrise on June 30^{th} 1993, and underwent downwards migration just prior to sunrise. Mean downwards swimming speeds were 3–4 cm/s. A southwestward flowing shelf-break current was observed in the upper 50 m with speeds of 15–20 cm/s. The contribution of tidal flows to the net current is determined and is found to be consistent with the predictions of Foreman's (1990) finite-element barotropic tidal model.

The ADCP data taken in June, 1993 are examined along eight 100 km long survey lines perpendicular to the coast of Vancouver Island. The eight survey lines span the region from the mouth of Juan de Fuca Strait to the mouth of Barkley Sound. Zooplankton concentrations occupied the upper 50 m over the shelf and slope both day and night. Aggregations of scatterers were present over the shelf break at depths of 150–200 m during the day. A southwestward flowing shelf-break current was observed in the upper 50 m with speeds of 15–20 cm/s. An estuarine type flow was observed at the mouth of Juan de Fuca Strait, with strong (>30 cm/s) outflow in the upper 80 m and weaker landward flow below 80 m. These currents are consistent with previous measurements in the region.

The ADCP data taken in June, 1993 are spatially averaged in order to characterize the summer mean zooplankton distribution and current pattern. Surface zooplankton concentrations were observed both day and night over the shelf and slope from Estevan Point to Juan de Fuca Canyon. High concentrations were found near the bottom along the shelf break from Estevan Point to Juan de Fuca Canyon. A southwestward flowing shelf break current with speeds of 15–20 cm/s was persistent along the shelf break from Estevan Point to Juan de Fuca Canyon. Surface outflow from Juan de Fuca Strait was

observed to persist up to about 50 km seaward over the shelf. A counterclockwise flowing eddy with a radius of about 30 km was observed over Juan de Fuca Canyon. Current speeds associated with the eddy were strongest near the surface and diminished gradually with depth.

Based on the limited data analyzed, it would appear that coastal ocean processes are too affected by high-frequency (tidal period) variability for ADCP surveys to provide synoptic views of the circulation and zooplankton biomass. However, this study demonstrates that the vessel-mounted ADCP is useful for observations of current velocity and zooplankton biomass distribution in confined spatial regions on diurnal time scales.

Table of Contents

List of Tables

List of Figures

Acknowledgements

I thank Dr. Rick Thomson for giving me the opportunity and the encouragement to study in oceanography and for devoting time and energy to this project. I also thank Dr. William Hsieh for supporting my studies in the U.B.C. Oceanography Department. I thank Luc Cuypers for his help with the maze of processing software and for help understanding ADCP data, Robin Brown for all his time spent in providing me with the data, and Steve Mihaly for being an indispensable liason at the Institute of Ocean Sciences. This research was supported by the National Sciences and Engineering Council of Canada. I am grateful for funds provided for me during my studies.

Brenda Burd, George Chase, Mike Foreman, Howard Freeland, and Rob Goldblatt were indispensable for their comments and contributions. I thank Susan Allen for support and encouragement and Denis Laplante for having all the answers.

I thank Tom Juhász, Bernard Minkley, Doug Yelland, Reg Bigham, Darren Tuele, Marie Robert, Rod Forbes, John Love and the officers and crew of the C.S.S. *J.P. Tully* for putting up with me for two weeks in a tin can. Special thanks go to Doug Boughton and the Capstan Bar for making me feel a little less sea-sick. I thank Judy Maxwell, Megan Hill, Carol Leven and Chris Mewis for help with forms, fax machines, administrative confusion, *etc.*....

I deeply thank my brother, Dylan, for his undying support in all this rain. I thank my parents for all their encouragement and guidance. Thanks go to Dave Timothy for raising hell and to Debby Ianson for calming conversations. I thank Greg Smith for his understanding of my decision to leave TRIUMF. Thanks to Scott Tinis, Roger Pieters, Mark Allen, Dave Jones and Jennifer Shore for helpful comments and for making the

annex an enjoyable place to work.

Lastly I would like to thank my motorcycle and a few stretches of the Great American Road for restoring my sanity.

Chapter 1

Introduction

The Vancouver Island continental margin encompasses a diversity of biological species whose distribution is closely coupled to the regional physical oceanography. The distribution of hake, herring, euphausiids and crab larvae are among the animals linked to the water property structure and circulation over the shelf. Since 1988, the Institute of Ocean Sciences, Sidney, B.C. has been collecting profile data using 150 kHz vessel-mounted acoustic Doppler current profiler units mounted on the hulls of the C.S.S. *Parizeau* (1988–1991) and the C.S.S. *J.P. Tully* (1992–). The ADCPs have collected one- to five-minute averaged current and backscatter profiles during twenty-seven cruises to the southwest coast of Vancouver Island, resulting in a data set consisting of over one hundred thousand profiles covering the shelf and slope out to distances of about 100 km from the coast. Such data can be used to study zooplankton distributions and current patterns from diurnal time scales to seasonal and interannual time scales.

Extensive research has been performed over the last ten years using ship-mounted acoustic Doppler current profilers to estimate ocean currents. One of the major focusses of the analysis has been to make accurate estimations of ship speed to obtain absolute water velocities. Joyce et al. (1982) used a 300 kHz profiler to measure currents in the western North Atlantic and found they could obtain accuracies of 5–10 cm/s in absolute currents using ship navigation from a LORAN-C receiver to calculate ship speed. Kosro (1985) and Trump (1986) outlined methods for calculating absolute currents using LORAN-C data, estimating that it is possible to obtain accuracies of less than 5 cm/s, providing one

is willing to sacrifice much of the spatial resolution of the Doppler data. Kosro's technique was used extensively in a large scale survey of the transition zone between coastal waters and the open ocean off northern California in winter and spring, 1987 (Kosro et al., 1991; Huyer et al., 1991; Ramp et al., 1991). Geyer and Signell (1990) used an ADCP to study tidal flows around a headland. Using bottom-tracking to estimate ship velocities, they obtained accuracies of 3–7 cm/s. Kaneko et al. (1990) used an ADCP on a towed fish to measure the currents in the upper 400 m of the Kuroshio and, using LORAN-C estimates of ship velocity, obtained accuracies of about 10 cm/s. Foreman and Walters (1990) describe two techniques for removing tidal currents from ADCP data.

Calibration of ship-mounted acoustic Doppler current profilers also has been the subject of study, with attention given to the misalignment angle of the transducer heads with respect to the ship and the scaling errors introduced by the instrument's conversion of Doppler shifts to water velocities. Pollard and Read (1989) outlined two calibration methods, one with bottom tracking and one without bottom-tracking, which enabled them to estimate the misalignment angle and the scaling factor to within 0.2° and 0.3%, respectively. They concluded that these errors limit the current accuracy to about 5 cm/s for a ship speed of 5 m/s. Kosro et al. (1991), using a 300 kHz transducer, reported a transducer misalignment angle of 1° and scaling errors of 0.3%. Ramp et al. (1991), using a 150 kHz ADCP, found a transducer misalignment angle of 1.4° and scaling errors of 1%. Bias induced in the velocity data by vertically migrating (swimming) zooplankton was studied by Wilson and Firing (1992). This work concluded that the fundamental assumption of acoustic Doppler current profiling - that horizontal swimming by the acoustic targets is incoherent - occasionally may be violated in strong sound scattering layers near topography.

Studies of the interaction of high frequency sound with zooplankters have been conducted by Pieper (1971), Greenlaw (1977), Holliday and Pieper (1980) and Richter (1984),

using a variety of sound sources and plankton distributions. Recently, interest in using the ADCP as a tool for measuring zooplankton abundances has grown. Flagg and Smith (1989) correlated the return signal strength from a 307 kHz ADCP to the abundance of zooplankton. They found that, with some modifications to the instrument and careful calibrations using net hauls, they could make estimates of biomass to within about $\pm 15\, mg/m^3$. Heywood et al. (1991) used a 150 kHz ADCP to measure the plankton distributions around the Indian Ocean island of Aldabra, also using separate net tows to obtain calibration constants. They were able to distinguish definite horizontal structures and vertical diel migrations. Both studies concluded that significant results were possible only after careful calibration of the transducers and processing electronics. Guerin-Ancey and David (1993) used a multifrequency sounder in concert with net tows and a fluid sphere scattering model to estimate the correlations between organism sizes and sound frequency.

Thomson et al. (1989a,1991) used a 150 kHz ADCP and a CTD-transmissometer mounted on a towed body to investigate the currents and biomass distribution near the hydrothermal plume emanating from vent sites on the Endeavour segment of Juan de Fuca Ridge in the northeast Pacific Ocean. They found a standard deviation of about $\pm$ 3 dB in echo amplitude and a standard error in current speed of about 1 cm/s. The ADCP profiles were used to estimate the biomass present in the water below 1800 m. Further work on the Endeavour Ridge hydrothermal plume by Thomson et al. (1992), Burd et al. (1992) and Burd and Thomson (1994) correlated the echo amplitude from an ADCP with net biomass samples using a set of five nets mounted on a towed body along with a 150 kHz ADCP and CTD-transmissometer package. Burd and Thomson (1993) used the orientation and velocity data from the ADCP on the same CTDT/ADCP net sampling package to estimate the total volume flow past the individual nets.

The performance of the ADCP in near-surface or near-bottom boundary layers was

studied by Appell et al. (1991). The nature of the data contamination near a boundary was determined and various methods of eliminating such contamination were suggested.

The purpose of this study is twofold. First, we wish to develop a consistent protocol for estimating zooplankton abundances and current flow from the raw ADCP data. We wish to show that this method is capable of removing most systematic or physical errors from the data, including contamination due to instrument noise, ship motion and sea floor variability. In doing so, we hope to determine the limitations of the instrument for such measurements and any modifications that could be applied to overcome them. Second, we wish to use the protocol to examine the spatial and temporal variability of zooplankton distributions off the southwest coast of Vancouver Island.

The thesis is organized as follows. Chapter 2 describes the study region in more detail, including the known physical and biological oceanography. The operation of the ADCP is discussed in chapter 3. Chapter 4 describes the processing techniques developed for the ADCP backscatter and current data, including the removal of bottom scattering effects, the calibration of the raw backscatter data, and the conversion from relative currents to absolute currents. The techniques presented are used in chapter 5 to examine the zooplankton distribution and its relationship in time and space to the local bathymetry and circulation. Two areas are studied separately. The first is a small area (14 km long by 1.5 km wide) located on the slope of a small canyon lying on the shelf break. The observations were taken during 19 consecutive hours. The second area encompasses most of the southwest coastal region off Vancouver Island out to a depth of about 2000 m. The measurements include 356 hours of data taken during a 21 day cruise in June of 1993, and are examined as a semi-synoptic survey of large spatial scales and of seasonal temporal scales.

Chapter 2

Region of Study

2.1 Bathymetry

The region under investigation stretches about 180 km along the west coast of Vancouver Island, from the mouth of Juan de Fuca Strait to Estevan Point, and extends out from the coast about 100 km to a depth of approximately 2000 m. The bathymetry is characterized by a narrow (35 km) continental shelf in the north and a wider (80 km) shelf in the south. The shelf is typically about 100–200 m deep, and is cut in the south by a series of deep (200–300 m depth) submarine canyons leading into Juan de Fuca Strait. The bottom shoals abruptly off the southeast corner of Barkley Sound forming a series of banks (70–100 m depth) and a network of semi-enclosed basins (150–200 m depth). The shelf break is located roughly along the 200 m isobath and the bottom falls of rapidly seaward of this line to a depth of 1000 m within 5–10 km. The shelf is cut by three shallow canyons (100–200 m depth) which penetrate about 10–20 km into the shelf at right angles to the mean shelf isobaths.

2.2 Physical Oceanography

2.2.1 Mean Currents

The region is typically divided into three major subregions, which will be discussed individually in terms of their water properties and current patterns: The shelf break and slope; the banks and basins of the inner shelf; and the southern shelf and submarine

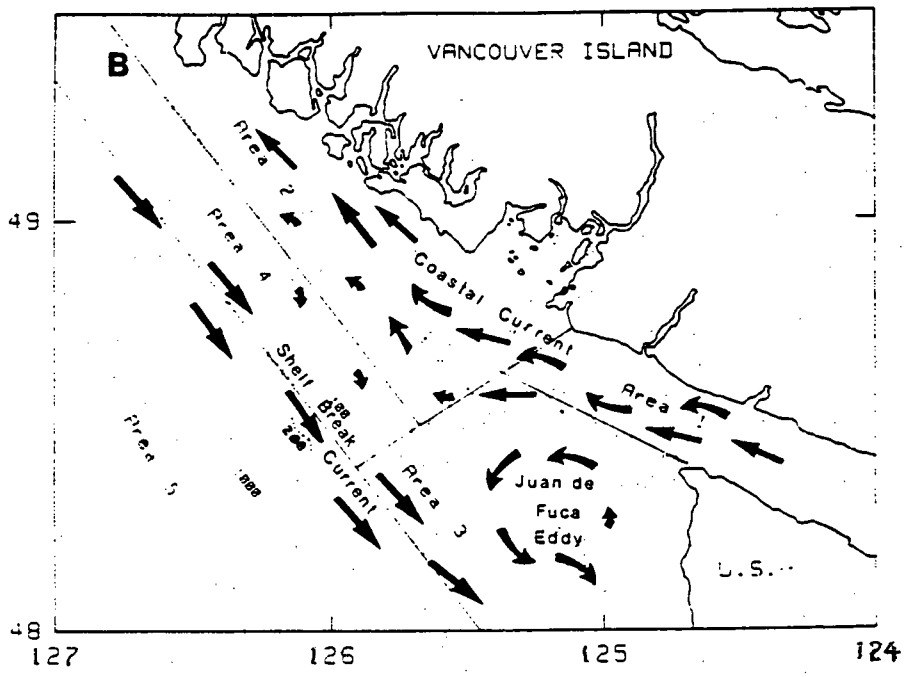

Figure 2.1: The west coast of Vancouver Island. The three subregions referred to in the text are shown as well as the local summer mean currents (Mackas, 1992).

canyon system west of the mouth of Juan de Fuca Strait (Figure 2.1).

The circulation over the shelf break in the upper 150 m is dominated by northwestward flows of order 30 cm/s in the winter and southeastward flows of the same magnitude in the summer (Freeland et al., 1984). The transition from winter to summer circulation occurs in February-April and coincides with the reversal from southeasterlies to northwesterlies in the prevailing winds (Ware and Thomson, 1988). Below 150 m there is a slower, quasi-permanent northwestward flow which is believed to be an extension of the California Undercurrent (Thomson et al., 1989b) Wind-driven upwelling in the summer transports the warm, dense, oxygen-depleted water of the undercurrent onto the shelf along the shelf break and into the submarine canyons to the south of Barkley Sound (Freeland and Denman, 1982). Such upwelling is thought to contribute significantly to the growth of phytoplankton on the shelf (Mackas, 1992), and is caused by the following series of events

(Freeland and Denman, 1982):

1. The prevailing coastal winds shift from southeasterly to northwesterly in February-April.

2. The northwesterly winds cause an upper-layer offshore transport, which is balanced by a return transport in the geostrophic interior.

3. The return flow is deflected upward over the continental slope which raises the deeper water to the surface over the outer shelf (upwelling). The cross-shelf sloping isopycnals generated by this process gives rise to the southeastward flowing summer shelf break current. It can be shown (Freeland et al., 1984; Thomson and Gower, 1985) that, assuming geostrophic flow, the along-shelf current is:

$$v \propto \frac{1}{H}\frac{dH}{dx} \tag{2.1}$$

   where H is the water depth. This simple model predicts an intensified flow just seaward of the shelf break, where $\left|\frac{dH}{dx}\right|$ is near maximum.

4. The southeastward flow pattern persists until the winds shift back to southeasterlies sometime in October-November.

5. Prevailing southeasterly winds cause onshore surface flow and downwelling at the shelf break, giving rise to prevailing northwestward flow in winter.

The inner shelf waters flow primarily to the northwest following the coastline, forming the Vancouver Island Coastal Current (VICC) which persists throughout the year. The primary forcing mechanisms for this current are considered to be coastal runoff from precipitation-fed streams on Vancouver Island and outflow of tidally mixed brackish water from the Juan de Fuca Strait (Freeland et al., 1984). The coastal runoff peaks

in fall and winter when the precipitation is a maximum, and acts as a line source of low density water along the coast. The Juan de Fuca Strait discharge peaks in summer due to snow melt in the mountains feeding the Fraser, Skagit and other rivers flowing into the Strait of Georgia-Puget Sound system, and acts as a point source feeding the VICC at the mouth of Juan de Fuca Strait. The outflow from Juan de Fuca Strait is deflected to the south by the La Pérouse Bank before turning north to form the VICC to the north of Barkley Sound. A transition zone of somewhat confused flow separates the shelf break current and the coastal current in the summer. This zone is wide (50 km) off Barkley Sound, and narrows progressively towards the north due to the narrowing of the continental shelf (Thomson et al., 1989b; Ware and Thomson, 1988). The VICC is a baroclinic current, roughly 15–25 km wide following the 50 m depth contour, with typical speeds in excess of 10 cm/s. The northwards pattern of this flow causes some downwelling along the small bottom slope near the 50 m isobath. In the summer months, the VICC opposes the prevailing northwesterly winds, and so the maximum speed of the current is typically found at depths of a few tens of metres. The shelf break upwelling, in concert with near shore downwelling, gives rise to a cross-shore structure in the subsurface water characterized by high salinity, low temperature, high density water lying roughly over the 100 m isobath, flanked by relatively low salinity, high temperature, low density water over the outer and inner portions of the shelf (Ware and Thomson, 1988).

The Juan de Fuca Eddy is located in the summer over the 200–500 m deep submarine canyons leading seaward from the mouth of Juan de Fuca Strait. It is a cyclonic (counter-clockwise) eddy with a radius of about 50 km and typical water speeds of 10–20 cm/s. The eddy sets up a pressure gradient towards its center, which is balanced in the surface waters by the outwards Coriolis force leading to a stable flow. However, within the various underlying canyons, due to topographic confinement, only the pressure gradient is felt, leading to upwelling at the eddy center of cold, dense California Undercurrent water. This

upwelled water is typically rich in nutrients, and this enhances phytoplankton growth and zooplankton aggregations within the eddy (Freeland and Denman, 1982; Simard and Mackas, 1989).

2.2.2 Tidal Currents

The tides on the west coast of Vancouver Island have been measured and modeled by Flather (1987,1988) and Foreman (1990). At the entrance to Juan de Fuca Strait, the tidal currents can be as large as 1 m/s. Their magnitude decreases northward along the shelf and westward towards the deep ocean.

The basic diurnal and semi-diurnal tidal currents in the area are modified by strong local effects due to the geography and all tidal constituents have significant baroclinic components. The semidiurnal tidal constituents (M_2, S_2, N_2 and K_2) predominantly consist of a barotropic Kelvin wave and internal tides, whereas the diurnal constituents (K_1, O_1, P_1 and Q_1) predominantly comprise a barotropic Kelvin wave and baroclinic shelf waves (Foreman and Walters, 1990; Foreman and Freeland, 1991). Due to the presence of these shelf waves, the diurnal period tidal currents will be stronger than that due to the astronomical tidal potential alone. The diurnal tides were first studied by Crawford and Thomson (1982, 1984), who found that the currents could be approximated by a free first-mode baroclinic shelf wave and a free barotropic Kelvin wave (Crawford and Thomson, 1982; Crawford and Thomson, 1984). The shelf wave originates near the entrance to Juan de Fuca Strait, and has a wavelength of about 200 km (Flather, 1987). It has a longer wavelength in the winter due to its interaction with the northwestward flowing mean currents. The shelf wave was found to dominate the tidal currents, whereas the Kelvin wave (wavelength of 13000 km) was found to dominate the amplitudes (Flather, 1987). The shelf wave only produced local amplitude variations.

2.3 Biological Oceanography

A large variety of marine life exists in the area under investigation, ranging from diverse and abundant phytoplankton to large vertebrate fishes. The primary interest of this study lies in the zooplankton community. Zooplankton are believed to be strongly linked to changes in the oceanic environment. They represent a dynamic element in the coastal ocean food chain, being influenced by the currents and having mobility to avoid predators and find food sources. The dominant zooplankton present off southern Vancouver Island are calanoid copepods and jellyfish over the inner shelf, calanoids and euphausiids over the southern shelf and submarine canyon system west of the mouth of Juan de Fuca Strait, and calanoids, euphausiids, chaetognaths, and salps along and seaward of the shelf break (Mackas, 1992). The primary scatterers of 150 kHz sound on the Vancouver Island continental margin are copepods and euphausiids. These two groups have different diurnal and seasonal cycles as well as vertical and horizontal spatial distributions. The distributions of zooplankton along the west coast of Vancouver Island were studied by Mackas et al. (1980) using an automated sampling system and by Simard and Mackas (1989) using high frequency acoustics and net tows. Mackas (1992) enumerated the major plankton communities in the region as well as their seasonal cycles from the results of a ten year study. Ware and Thomson (1988) and Thomson et al. (1992b) studied west coast fisheries and fishing vessel distributions and their relations to local oceanography. This section will first identify the various zooplankton species in each of the two major groups and give a brief description of their biological and acoustical properties, followed by a description of the spatial distributions of zooplankton in the region of study.

2.3.1 Zooplankton Species

Copepods form the most abundant zooplankton fauna off the southwest coast of Vancouver Island, accounting for over 50% of the total zooplankton biomass in spring and early summer. *Calanus marshallae*, *Pseudocalanus* spp. and *Metridia pacifica* account for 50–80% of the total copepod biomass over the shelf, and account for 20–40% over the shelf break and slope. Copepods endemic to the open subarctic Pacific (mostly *Neocalanus cristatus* and *Neocalanus plumchrus*) account for 20–70% of the total biomass in the spring and early summer over the shelf break and slope. The copepods found on the Vancouver Island continental margin typically weigh about 100 μg DW and have a mean length of 1–5 mm. Thus, at 150 kHz, they have an acoustic target strength of -100 dB to -120 dB (Figure 2.2) (Holliday and Pieper, 1980; Flagg and Smith, 1989; Mackas, 1992). *Calanus marshallae*, *Pseudocalanus* spp. and *Metridia pacifica* reside in the upper 100 m both day and night during the spring and summer. Only *Metridia pacifica* undergoes diel vertical migration, residing in the upper 50 m at night and descending below 100 m during the day (D.L. Mackas, *pers. comm.*). *Neocalanus* spp. reside in the surface layers both day and night in the early spring, and migrate to a depth of 200–400 m over the period from early July to December ('ontogenetic migration') (Parsons et al., 1984). Typical ontogenetic migration speeds are only about 10 m/day (D.L. Mackas, *pers. comm.*), and are therefore not important for the short term acoustic observations presented in this thesis. Significant changes in copepod biomass distribution due to ontogenetic migration occur over time scales of a few weeks, and will therefore contribute to vertical smoothing of long-term averages of acoustic backscatter data.

The euphausiids are comprised of two abundant species: *Euphausia pacifica* and *Thysanoessa spinifera* and one less abundant species; *Thysanoessa inspinata.* These species tend to concentrate close to the bottom at steep depth gradients such as at the

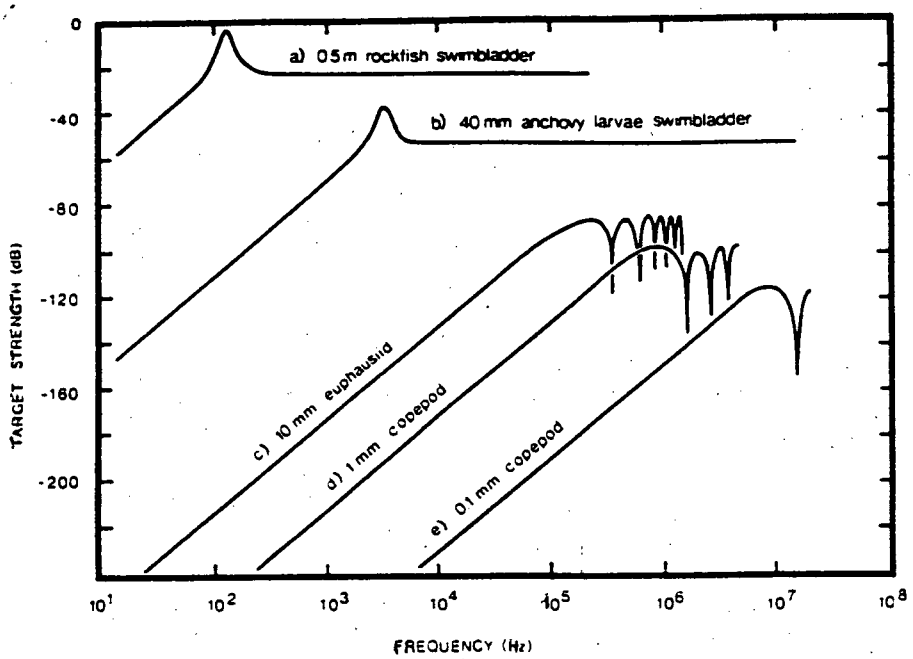

Figure 2.2: Theoretical acoustic signatures of several common types of marine organisms (Holliday and Pieper, 1980).

shelf break. They show strong diel migration, reaching the surface waters at dusk and descending to a daytime depth of about 100–200 m just before dawn (Simard and Mackas, 1989). Juvenile and adult euphausiids have a body weight of 1–10 mg DW, a length of 10–20 mm, and an acoustic target strength at 150 kHz of -80 dB to -100 dB (Pieper, 1971) (Figure 2.2). Therefore, juvenile and adult euphausiids have an acoustic target strength which is about two orders of magnitude larger than that of copepods (Flagg and Smith, 1989; Mackas, 1992).

2.3.2 Spatial Distributions

The biomass of the entire study area is primarily comprised of copepods in the upper layers (< 50 m) and euphausiids down deeper (100–200 m). It is thought that the net seasonal change in the copepod biomass is primarily due to two factors: (1) reproduction and food availability; and (2) horizontal and vertical advection by the currents (Mackas, 1992). Euphausiids have more mobility than copepods and spend more time in deep

water where the currents are slower, which causes them to be less susceptible to horizontal advection forces than the copepods. The horizontal distributions of the plankton depend on bathymetry and current structure and can be examined in three main sub-regions: The banks and basins of the inner shelf; the southern shelf and submarine canyon system west of the mouth of Juan de Fuca Strait; and the shelf break and slope (Figure 2.1).

The Inner shelf, comprised of the banks and basins shoreward of the 200 m depth contour, is populated primarily by the calanoid copepods. Euphausiids do not tend to inhabit this area because they cannot reach their typical daytime depths. This region has the lowest average biomass (annual average $3.2\,g/m^2$), the sharpest spring peak (up to about $8\,g/m^2$) and the lowest winter levels. The spring phytoplankton bloom in late March-early April leads to a rapid increase in zooplankton concentrations on the shelf. The initial nutrient supply is quickly exhausted, however, but is subsequently replenished by the onset of upwelling along the shelf break following the spring transition to northwesterly winds. Thus, the zooplankton biomass peaks in May-June following the phytoplankton blooms and then declines during the rest of the summer. This decline is due primarily to a decrease in the population of surface layer inhabitants (copepods), and is probably due to a high washout rate from upwelling and subsequent alongshore and seaward transport (Mackas, 1992).

The southern shelf and Juan de Fuca Eddy region is also dominated by copepods but has a higher average biomass (annual average $4.9\,g/m^2$) (Mackas, 1992). This region follows a similar cycle to that of the inner shelf, although the rate at which the biomass declines is lower in late summer. The eddy creates upwelling events which can cause spatially and temporally localized increases in zooplankton concentrations. Euphausiids also are more abundant here than on the inner shelf and are spread out in the deeper areas over most of this region (Simard and Mackas, 1989).

The outer shelf break and slope region has concentrations of copepods in the top 50 m

or so, while the deeper layers near the bottom contain large aggregations of euphausiids. The average biomass here is comparable to that in the southern shelf region ($4.6\,g/m^2$) (Mackas, 1992). This is the most stable planktonic structure on the coast, having an almost constant biomass throughout most of the summer and decreasing only slightly in the winter months (Oct-Feb) (Mackas, 1992). The plankton distributions are strongly affected by the shelf break current, especially in the summer months when a vertical shear is set up between the surface and the water at depth.

The summer euphausiid distributions in the area were studied by Simard and Mackas (1989). Horizontal distributions showed concentrations (1) at the shelf break and (2) in the ~150 m deep basins located between the La Pérouse Bank and Juan de Fuca Strait. The shelf break distributions showed high concentrations ($> 4.0\,g/m^2$) of biomass lying in a long narrow (2–3 km wide) filament, the center of which was always within about 5 km from the 200 m isobath. Upwelling along the shelf break contributes to the narrowness of the distribution by effectively 'cornering' the euphausiids between the upwelled water, the ocean bottom at the shelf break and the isolume barrier during the day (Simard et al., 1986; Simard and Mackas, 1989). At night the euphausiids move into the surface waters to feed. The basin aggregations were more spread out and less intense than at the shelf break. High concentrations were observed above Juan de Fuca Canyon, especially in the last week of August, when an upwelling event and a phytoplankton bloom were also noted in this area from salinity, density and chlorophyll profiles. Upwelling of the California Undercurrent waters in Juan de Fuca Canyon can account for the concentrations of plankton seen there, but it is not clear whether this population is resident or experiences large advective gains and losses (Simard and Mackas, 1989). It is also noted that the summer distribution of some of the major vertebrate fishes in the area such as pacific hake coincide almost exactly with the zooplankton distribution, giving an idea of the importance of the zooplankton to the higher trophic levels (Ware and Thomson, 1988).

Chapter 3

Instrument and Data

This chapter will describe in more detail how the ADCP measures currents, plankton abundances and ship speed from bottom-tracking, followed by a description of the internal data processing that occurs online and the shipboard data collection process.

3.1 Acoustic Doppler Current Profiling

3.1.1 Transducer Operation

The instrument used in this study is a narrow-band hull-mounted 153.6 kHz RDI acoustic Doppler current profiler (ADCP). It was mounted on the hull of the C.S.S. *J.P. Tully* from the fall of 1992 until the present. The vessel mounted ADCP configuration is shown in Figure 3.1. The ADCP has four transducer heads in a convex Janus configuration with each beam having a width of 4.0° at –3 dB and facing outwards at 30° from the vertical axis of the instrument. The instrument is oriented at 45° from the ship's bow-stern line, giving the four beams azimuthal angles of 45, 135, 225 and 315 degrees with respect to the ship's bow-stern line.

The ADCP takes an instantaneous water profile by emitting a pulse (*ping*) of sound from each of its four beams. Each pulse has a duration of about 3–6 milliseconds, or a length of about 4–8 m. The sound is scattered primarily off zooplankton in the water, and the return echo is range gated into bins of length 2^n (n=1,2,...) metres. A short delay between the pulse transmission and the beginning of processing allows the ringing

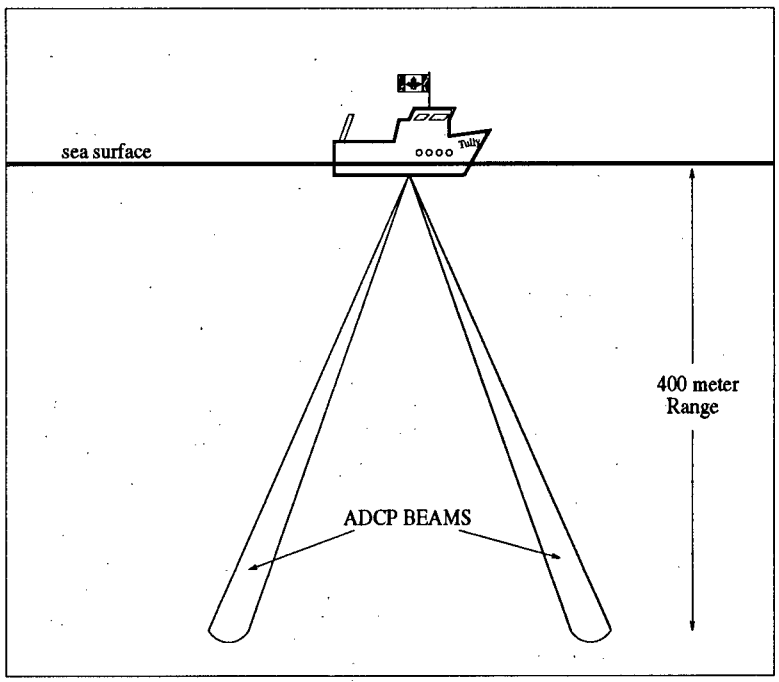

Figure 3.1: Side view of a typical VM ADCP. Two of the four beams are shown looking forward and aft, capable of measuring the along-ship currents and the plankton backscattering strength

in the transducer to die down, and defines a layer below the ship's hull (usually 1–4 m) in which no data is recorded, called the *blank-beyond-transmit.* The *blank-beyond-transmit* also ensures that the disturbances in the water caused by the ship's hull are not recorded. The ADCP records the frequency of the returning scattered sound for each bin, from which it determines a vertical profile of the water velocity relative to the ship. It also records the intensity of the return echo for each bin, which gives a vertical profile of the zooplankton acoustic scattering strength.

The ADCP has a nominal water profiling range of 400 metres. However, in rough seas, breaking waves generate bubbles which can be entrained under the ship's hull and inhibit the transmission of sound. Bubbles have been known to cause a reduction in profiling range of as much as 60% (RDI, 1989).

3.1.2 Relative Current Measurement

At 150 kHz, the primary sound scatterers in the ocean are zooplankton. The plankton have some mobility, but in general the motions of the animals tend to be uncorrelated. That is, they do not tend to school or swim in unison. Due to the large concentrations of plankton in the water, they appear as a group of scatterers passively advected by the local currents (Flagg and Smith, 1989). Thus, the return frequency in each beam will be Doppler shifted according to the motion of the water. The along-beam component of the water velocity, V, can be calculated using the Doppler shift relation:

$$V = \frac{1}{2} c \frac{F_d}{F_s} \tag{3.1}$$

where F_d is the Doppler shift, F_s is the output frequency, and c is the speed of sound in the water. The ADCP algorithm uses the along-beam velocities from each pair of horizontally opposed beams to calculate one horizontal water velocity component and the vertical water velocity component. This results in two horizontal velocity components in

the ship's reference frame, (u', v'), and two estimates of the vertical velocity component (w'). Finally, a rotation of the velocity reference frame from ship coordinates (along-ship, cross-ship, z) to earth-referenced coordinates (east, north, z) is made using the pitch, roll and heading angles of the ship determined from navigation devices, giving the velocities relative to the earth, (u, v, w).

Inherent in the ADCP algorithm to calculate (u', v', w') is the assumption that the water velocities are the same in each beam for a given bin depth. At a depth of 400 m, beam angles of 30° give rise to a maximum beam separation of 400 m, which sets the horizontal scale over which the assumption of uniformity must hold. Justification of this assumption is found in the *error velocity*, which is the difference between the two vertical velocity components. A large error velocity indicates that there are substantial differences in the velocities measured by each of the four ADCP beams, either due to transducer errors or because the actual currents are not horizontally homogeneous. The error velocity is a built-in means to estimate data quality (RDI, 1989).

3.1.3 Bottom-Tracking

Every second pulse the ADCP emits is designed exclusively to scatter off the bottom. This pulse is used to determine the local water depth and the speed of the ship over the bottom. It is referred to as a *bottom-tracking* ping and is implemented and processed separately from water profiling pings. It has a longer pulse length and is broken down into as many as 128 depth bins, each shorter than the transmit pulse. The ADCP searches through these depth cells to find the center of the strongest echo, which it chooses as the local water depth. It subsequently uses the measured Doppler shifts of the bottom echoes to estimate the ship's absolute (earth-referenced) velocity. The manufacturers claim that bottom-tracking pings are able to measure ship velocity with an accuracy of about 1 cm/s and bottom depth to within about 1 meter. The bottom tracking range is

roughly 50% greater than the water profiling range, or 600 m (RDI, 1989).

3.1.4 Absolute Current Measurement

As with the water velocity measurements, the estimates of the relative bottom velocity from the bottom-tracking pings are rotated to earth-referenced (east, north) coordinates and recorded for each profile. The absolute, earth-referenced, water velocities can then be computed for each depth bin by a simple subtraction of the bottom velocity from the relative water velocity.

If the bottom-tracking algorithm was unable to locate the bottom or was unable to make a reliable estimate of the relative bottom velocity, the ship's velocity must be estimated in some other way in order to compute absolute water velocities. This is typically done using navigational data from the ship's GPS or LORAN-C system.

In absence of any ship velocity estimates, only the vertical shears present in the water profiles can be examined. Most of the effects of the ship's motion can be removed by assuming a reference layer of 'no motion' within the profiling range, and subtracting the velocities measured in the layer of 'no motion' from the rest of the profiles. All velocities are then relative to the velocities in the layer of 'no motion', but will not include ship velocity effects. This method reveals horizontal shears on small spatial and temporal scales, while preserving the vertical structure in the water column.

3.1.5 Zooplankton Abundance Measurements

Typical input signal levels from scattered sound in the ocean vary by two or three orders of magnitude. This input signal must be amplified to a roughly constant level for the signal algorithms to accurately estimate the frequency. This amplification is accomplished by the *Automatic Gain Control* circuitry, which controls the gain with a voltage, V_g. The gain-control voltage, V_g, is converted to a logarithmic value and recorded as

a quantity called the AGC, which reflects the strength and thus the abundance of the sound scatterers. The AGC output is given by:

$$AGC = \gamma \log(\epsilon \frac{I_r}{I_a}) \tag{3.2}$$

where γ, ϵ are constants, I_r is the reflected intensity at the ADCP and I_a is some constant reference intensity. The backscatter intensity, S_v, in decibels is given by:

$$S_v = 10 \log(\frac{I_r}{I_i}) = 10 \log(\frac{\sigma_s}{4\pi}) \tag{3.3}$$

where I_r and I_i are the reflected and incident intensity measured at some reference distance from the scatterer, and σ_s is the total acoustic cross-section. In order to combine the two above equations, the implicit reference distance in (3.3) must be specified. The standard choice is a distance of 1 m, which is not feasible in the case of a ship-mounted ADCP. However, it can be set to the distance from the scatterer to the ADCP by adding the transmission loss of sound through the water due to attenuation and beam spreading. The result is:

$$S_v = k_c(AGC) + 20 \log R + 2\alpha R + A \tag{3.4}$$

where k_c and A are system-dependent constants, R is the ADCP-source distance in metres, and α is the coefficient of sound attenuation in the water in dB/m (Flagg and Smith, 1989). Equations (3.3) and (3.4) demonstrate that the AGC gives a measure of the backscatter strength which can subsequently be related to the acoustic cross-section and ultimately to the zooplankton biomass. This will be discussed in more detail in chapter 4.

3.1.6 Percent Good Estimate

The ADCP also makes an estimate of the signal-to-noise (S/N) ratio using a wide and a narrow band filter (Figure 3.2). If the energy passed by the narrow band filter is roughly

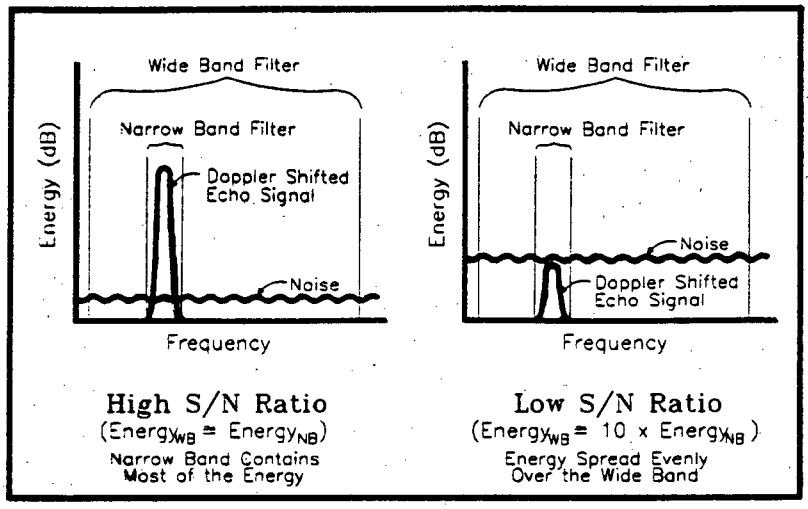

Figure 3.2: Filters used in estimating the percent good. Two extreme cases are shown for high and low S/N ratios (RDI, 1989).

equal to that passed by the wide band filter, then the signal must be many times greater than the noise, all its energy being passed by both filters. However, if the signal is small, the energy passed by the narrow filter will be much smaller than that passed by the wide one, since most of the total energy is noise. The S/N ratio is combined with the error velocity mentioned above to produce an estimate of the 'goodness' of the data. This estimate is called the *percent good* and is recorded for each depth bin. It provides a means of estimating the cut-off depth below which the acoustic data are too weak to yield acceptable results.

3.2 Internal Data Processing

Each ping emitted by the ADCP consists of four phases: overhead, transmit pulse, processing, and sleep (Figure 3.3). The overhead time is used to prepare for ping processing. The pulse is then transmitted, after which there is a short delay to allow for ringing to die down. The ADCP then begins to process the echo. After processing is complete the ADCP goes to sleep, unless it immediately starts another data collection cycle. Each

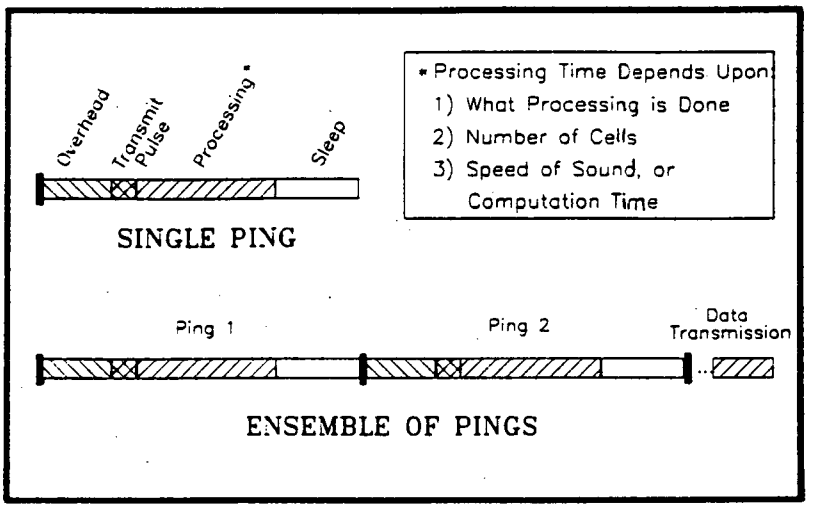

Figure 3.3: ADCP processing cycle (RDI, 1989).

ping takes about 1–2 seconds to transmit, receive and process, and the ADCP typically emits about 30 water profiling and 30 bottom-tracking pings in a two minute averaging interval. The bin-by-bin averages of the data are then transmitted to the data acquisition system (DAS) to be recorded on disk. The DAS produces records with the following three basic components:

Fixed Header This contains information pertinent to the entire *session.* A session is begun when the DAS is started and is ended when the data acquisition process is interrupted by a user. Typically a cruise will contain one or two sessions. The fixed header contains the ADCP setup, which includes such information as the length of each bin, the number of pings per averaging ensemble, the blank beyond transmit, the number of depth bins, the startup date and time, the cruise ID and various flags which show what parameters were recorded in the data itself.

Ensemble Header This contains information pertinent to each ensemble. It includes the recording date and time, the pitch, roll, heading, and temperature readings from ship navigation, the average bottom velocity from bottom-tracking pings,

the bottom depth, and the latitude and longitude from either GPS or LORAN navigation devices.

Ensemble Data This is the information that is transmitted to the DAS from the ADCP, including the full averaged velocity profile in ship-referenced coordinates, the averaged AGC profile and the percent good for each depth bin.

Chapter 4

Processing Techniques

This chapter will describe the basic processing techniques used to convert the raw AGC values into relative backscatter strengths and relative water velocities into absolute (earth-referenced) water velocities. The AGC conversions involve first removing all sections of the AGC profiles which include bottom scattering effects, then calibrating the raw AGC to obtain a clear picture of relative concentrations of zooplankton biomass. This chapter will open with a description of the data used in this study, including the various types of measurements made, the ADCP configuration, and the spatial and temporal coverage of the data. It will close with a description of the techniques used to average data temporally onto a regular grid and the algorithms used for the subsequent contouring.

4.1 Data Sets

The two different 150 kHz ADCPs used in this study were mounted on the hulls of two ships used extensively in the La Pérouse project. There were 24 cruises on the *C.S.S. Parizeau*: 9 in 1988, 6 in 1989, 4 in 1990 and 5 in 1991. There were 5 cruises on the *C.S.S. Tully* in 1993. These cruises typically lasted for 1–2 weeks during which the ship spatially covered 30–40% of the area delineated in Figure 4.1. The ship surveys involved primarily conductivity-temperature-depth (CTD) casts, hydro casts and plankton sampling along seven standard survey lines (Figure 4.1), as well as the deployment/recovery/servicing of current meters moored at selected positions. The CTD/Hydro data were initially edited

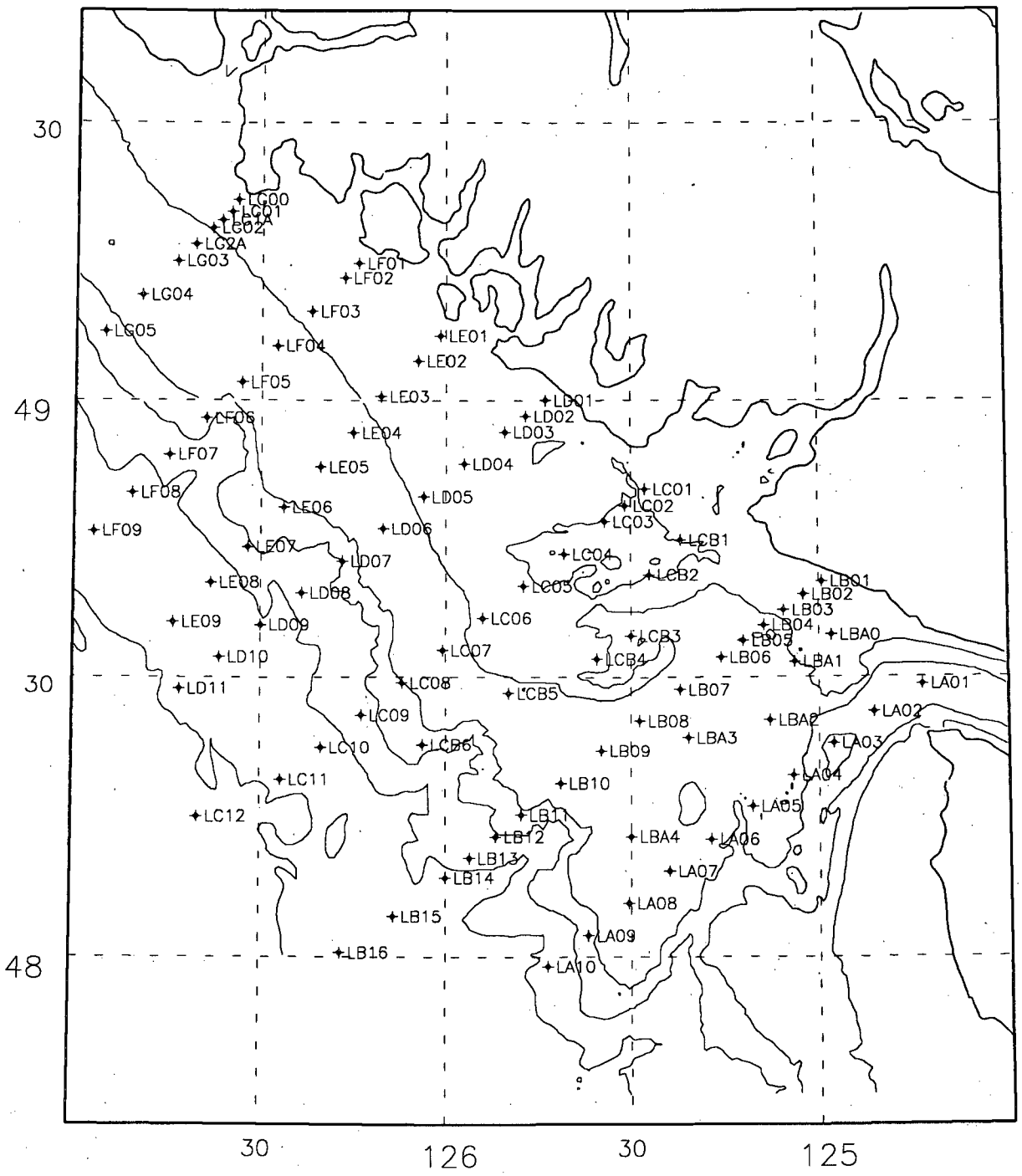

Figure 4.1: La Pérouse Bank CTD lines and profile stations.

Vessel	Sampling Interval (sec)	Number of depth bins	Bin Length (m)	Blank Beyond Transmit (m)	Mounting Depth (m)
Parizeau	300	49	8.0	1.0	5.0
Tully	120	128	4.0	4.0	4.0

Table 4.1: Typical ADCP set-up parameters

at the Institute of Ocean Sciences. The resulting archived products are described in (Ware and Thomson, 1992). The ADCP was typically set up with the characteristics given in Table 4.1 for each of the two vessels. Sampling was continuous throughout the cruises. The sampling intervals resulted in a spatial resolution at ship speeds of 10 knots of about 1500 m for the C.S.S. *Parizeau* and about 500 m for the C.S.S. *Tully*. A majority of the profiles were taken along the CTD lines, providing extensive spatial coverage in these areas. Other areas were only occasionally covered by the ship when in transit. Bottom-tracking was turned on for most cruises, giving accurate absolute velocities out to depths of about 450 m, or about 42 km offshore at Estevan Point to about 105 km offshore at the mouth of Juan de Fuca Strait. Most of the data have been edited and processed under contract to Hermes Computing Services (Luc Cuypers). Results include horizontal maps of absolute and relative currents, as well as vertical sections of contoured cross-shore and alongshore components of the water velocities. Contoured vertical sections of the backscatter intensity in decibels also were produced using a calibration technique similar to that described in Chapter 4.3.1. The data used in this study were pre-processed by Luc Cuypers to change the RDI format of the original data files into a more manageable format called *PHD300*. An extensive set of analysis programs developed by Luc Cuypers was modified for this study to implement the analysis techniques described in this chapter.

4.2 Bottom Effects

Due to the strength of the bottom echoes compared to that of zooplankton and other scatterers in the water column, sound scattering off the ocean floor is an important factor in both backscatter and velocity profiles when using an ADCP . This section discusses the various effects of the ocean floor on the acoustic echoes: First, the reliability of the ADCP bottom depth obtained from bottom-tracking pings; second, the effects of side-lobe scattering on the water profiles for a flat bottom; and third, the effects of the bathymetry for the cases of a constant-slope bottom and an irregular bathymetry.

4.2.1 ADCP Bottom Depth

The bottom depth is obtained from the ADCP bottom-tracking pings, which have a range roughly 50% more than the water profiling range , or about 600 m for a 150 kHz unit (RDI, 1989). The range is slightly smaller over the shelf break and slope since all four beams must be able to find the bottom. This correction is about 25 m for maximum slope angles of 4°, reducing the range to about 575 m. Beyond these depths, the bottom tracking velocity and the bottom depth are flagged and recorded as -19999.0 and -1, respectively. However, in cases where the bottom echo is weak or non-existent, the ADCP has a tendency to interpret any strong scattering layer in the upper 600m as a bottom echo and process the data accordingly, giving rise to a 'false bottom'. In other instances, the ADCP simply misjudges the bottom depth completely. Although the reasons are not yet fully understood, it is assumed that erroneous bottom depths occur because of excessive noise spikes in the bottom tracking data. Because of these problems, the ADCP's estimate of the bottom depth cannot be used in the following three cases:

1. The bottom is out of range and the bottom depth is flagged as incorrect;

2. a false bottom is found;

3. the ADCP 'misjudges' the bottom.

An external estimate of the local water depth is needed to check the reliability of the ADCP's estimate. These external bathymetry data were obtained from the Department of Energy, Mines and Resources and are contained in the 'Digital Terrain File', or DTF, which covers the west coast of Canada with a 1 km resolution grid (Luc Cuypers, *person. comm.*). An algorithm is used to find the closest DTF gridpoint to the profile's recorded position and the DTF depth is compared to the ADCP estimate. The ADCP estimate is taken as reliable if one of the following two conditions hold:

1. The ADCP depth is shallower than the bottom-tracking range of 580m *and* the DTF depth is below the same range following a correction, ΔD, for the grid resolution. The DTF grid resolution ($\pm 500m$) can give rise to maximum depth differences of

$$\Delta D = 500m \tan \phi \approx 35m$$

where $\phi \approx 4°$ is the maximum bottom slope. Thus, it is required that the ADCP depth is $< 580\,m$ *and* the DTF depth is $< 545\,m$.

2. The DTF and ADCP estimates of water depth are the same to within the resolution of the DTF grid of 35 m depth *and* the DTF depth is less than an upper limit for the ADCP range of 650 m corrected for the grid resolution, or $650\,m - \Delta D = 615\,m$.

Figure 4.2 presents a scatter plot of DTF depths versus ADCP estimates of depth for the June, 1993 cruise together with the limits applied to determine reliable bottom-tracking depths. Most bottom-tracking profiles agree well with the unflagged DTF estimates. A group of points at DTF depths of $\sim$ 750 m have consistently low ADCP estimates of depth, which can not be considered reliable. The October, 1993 cruise showed a similar

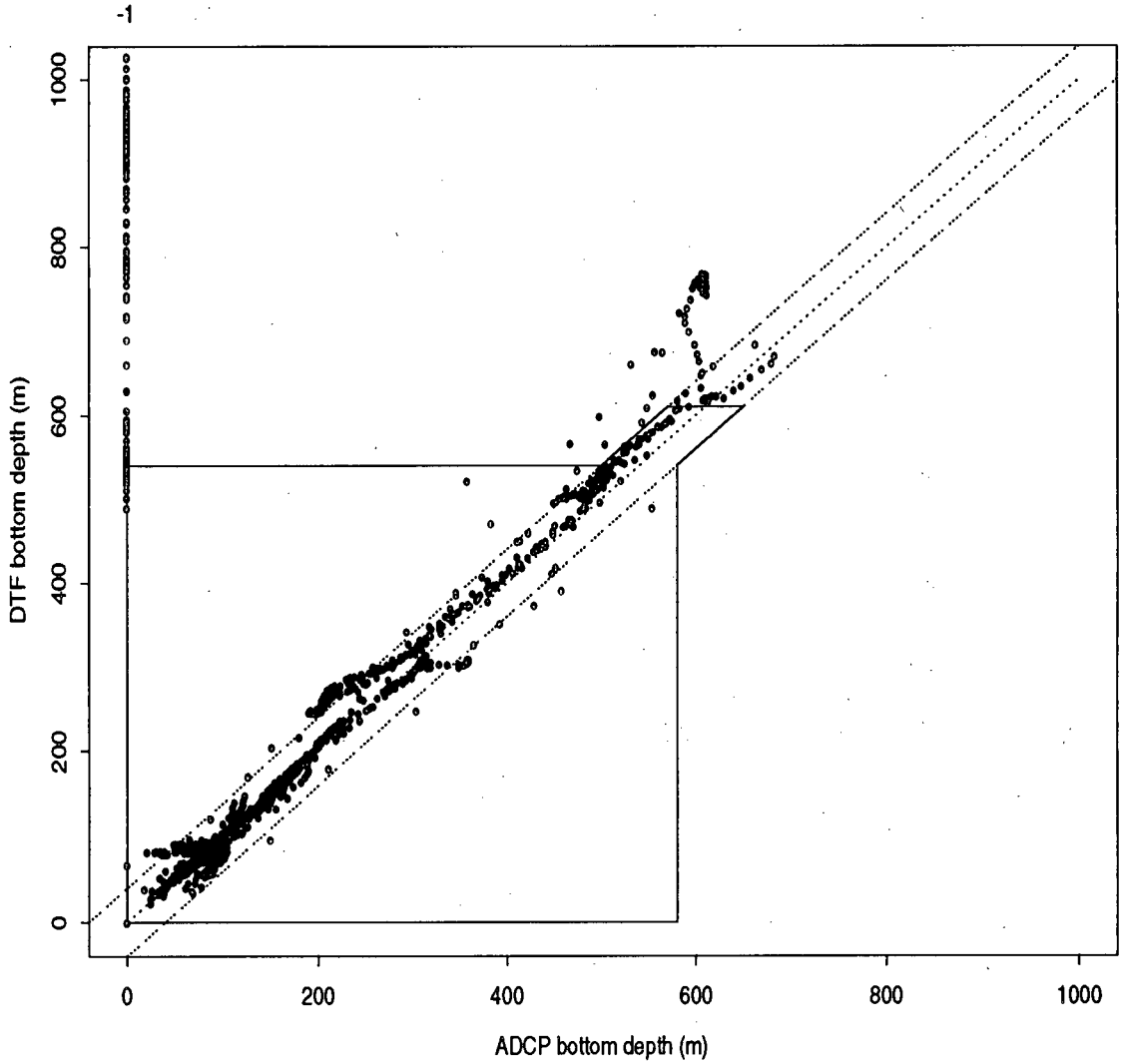

Figure 4.2: DTF vs. ADCP estimates of water depth for the June, 1993 cruise. The bottom-tracking depths are good inside the solid box. The profiles in which the bottom-tracking could not find a bottom have ADCP bottom depth = -1.

scatter plot (Figure 4.3). The aggregation of points just outside the box at ADCP depths of about 500–550 m are thought to differ slightly more from the DTF estimates due to decreased resolution of the DTF grid past the shelf break. This indicates that condition (2) can be increased to $\pm 60\,m$ without decreasing the reliability of our depth estimates. Henceforth, a profile's *water depth* will indicate either the ADCP bottom-tracking depth if criterion (1) or (2) was passed, or the DTF bottom depth otherwise.

4.2.2 Bottom Scattering: Side Lobes

The detected echo from the bottom is typically about 50 dB higher than the near-bottom water echoes. Due to side-lobe effects, the width of the bottom echo corresponds to about 40% of the water depth . The nature of these side-lobe effects are determined primarily by the ADCP transducer beam pattern (Figure 4.4). The centered main lobe has a beamwidth of 4.0° at the −3 dB level (RDI, 1989), and contains most of the beam power. The remaining power is contained in the sidelobes, which have strengths 30–40 dB below that of the main lobe. The ADCP transducers are sensitive to the two-way beam pattern because they both transmit and receive sound. Thus, the sidelobes are 60–80 dB below the main lobe — a factor of 100 million. Although this level may seem very small, sidelobe contributions become important when the ADCP is measuring signal strengths near the ocean floor. Rocky and sandy ocean floors reflect 100 kHz sound incident at an angle of 30° from normal at roughly the −25 dB level (Urick, 1983). This is 60 dB higher than typical zooplankton aggregation scattering strengths of −85 dB (RDI, 1990). Thus, sidelobe scattering off the bottom (≈ -85 to $-105\,dB$) is comparable to main lobe scattering off zooplankton ($\approx -85\,dB$), and can therefore contaminate the profile near the bottom. For a downward-looking ADCP with beams angled at 30° from the vertical, the echo from the side lobe facing the bottom will arrive at the transducer at the same time as that from the main lobe facing 30° from the vertical, so that the

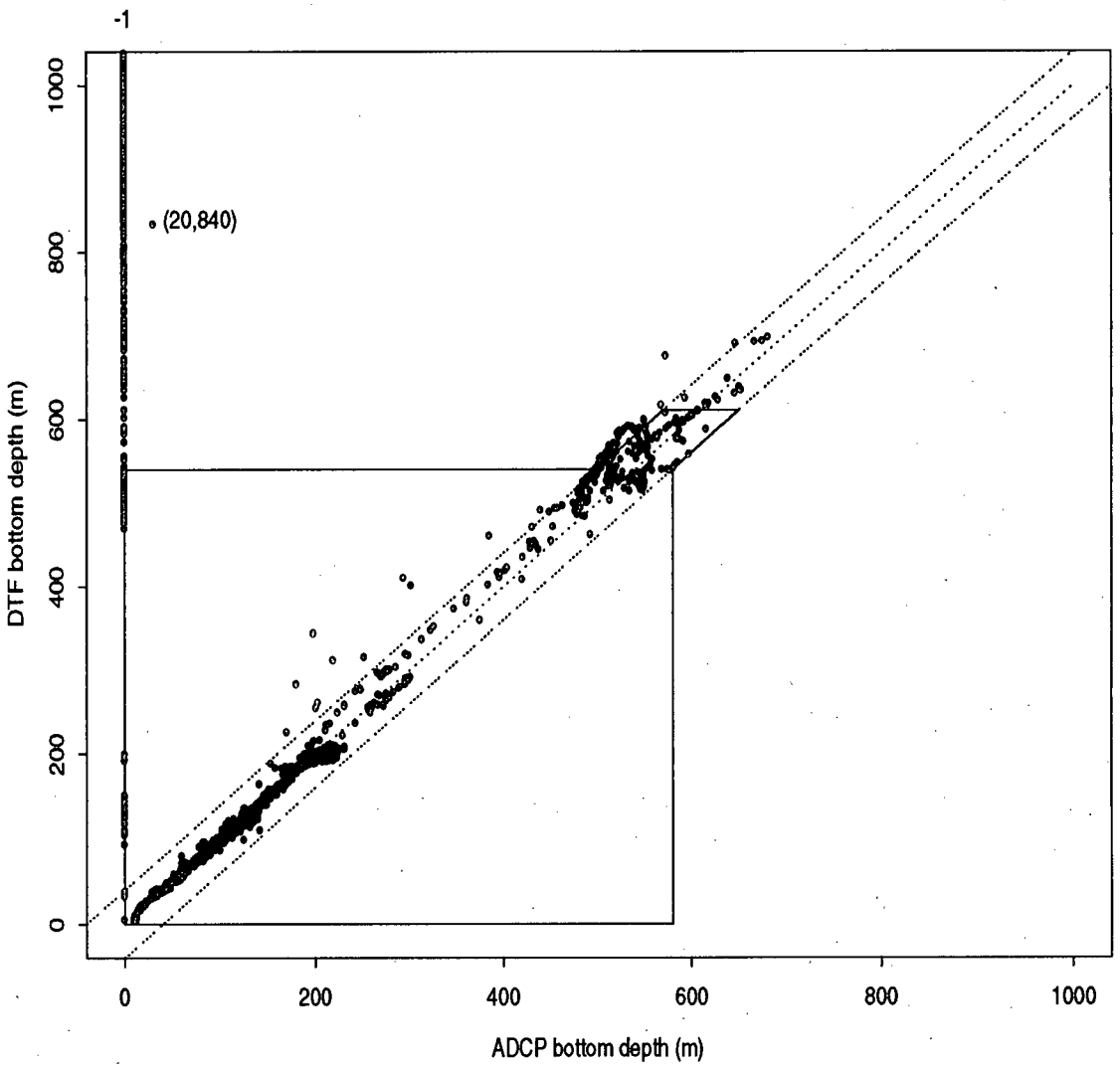

Figure 4.3: DTF vs. ADCP estimates of water depth for the October, 1993 cruise. The bottom-tracking depths are good inside the solid box. The profiles in which the bottom-tracking could not find a bottom have ADCP bottom depth = -1. A clear example of the ADCP finding a false bottom is located at about (20,820).

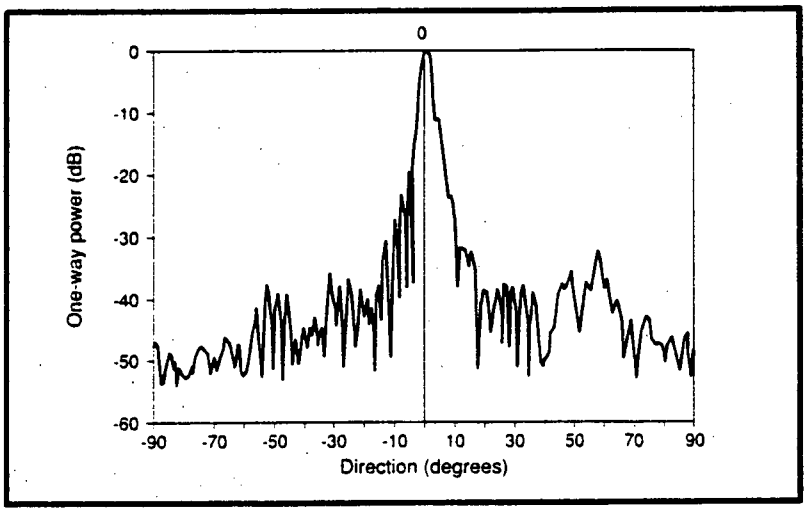

Figure 4.4: Typical ADCP transducer beam pattern. The beamwidth is defined at the –3 dB level. Side lobes are typically located at angles > 15° and are 30–40 dB below the main lobe level (RDI, 1989).

bottom 13% [= 1 − cos(30°)] will be contaminated by sidelobes (Figure 4.5). The pitch and roll of the ship also may contribute to the bottom contamination. Absolute values of ship pitch and roll angles taken from the ship's gyroscope are averaged throughout each ensemble interval and recorded for each profile. A 16 hour time series taken from 01:38 to 17:46 PDT on 29/06/93 of averaged absolute pitch and roll angles (Figure 4.6) reveals that roll angles were consistently higher than pitch angles. The maximum roll angles of about 2° will give rise to bottom contamination at the [1 − cos(30° + 2°)] = 15% level.

In practise, the width of the bottom echo is slightly larger than 15%. To demonstrate this, six consecutive vertical profiles of raw AGC taken from the June, 1993 cruise are examined (Figure 4.7). During the 12 minutes that these profiles were collected in, the ship was moving over a bottom of constant depth to within one bin length (4 m). The plots show a cut at 85% of the ADCP bottom depth and another at 80%. The 85% cut works well for about two thirds of the profiles, but includes a fraction of the bottom echo for the other third. This 'shoulder' could be a scattering layer sitting within 5 m of the bottom. However, since side-lobe bottom scattering and biological scatters leave

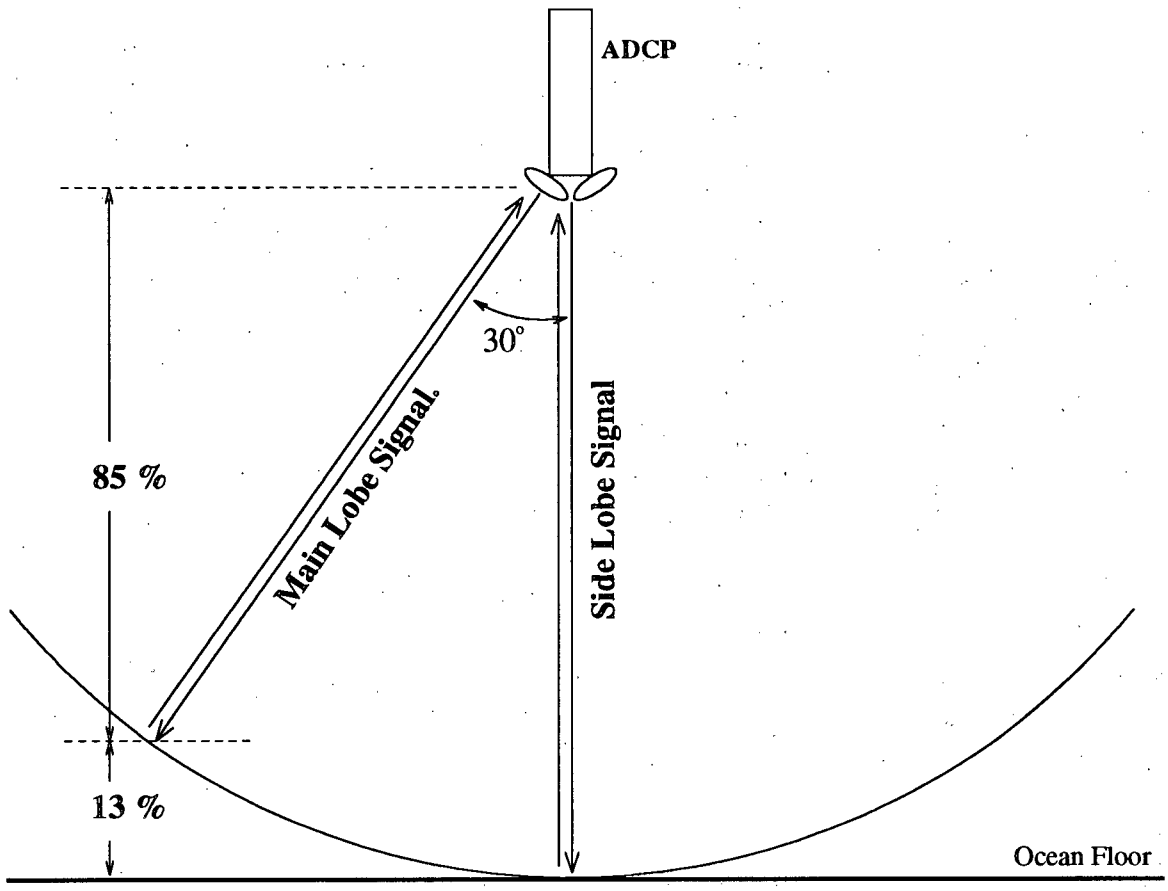

Figure 4.5: Backscattering from a downward-looking ADCP within range of the bottom. At this frequency and transducer orientation (30°), the bottom 13% of the profile is contaminated by sidelobe scattering from the bottom.

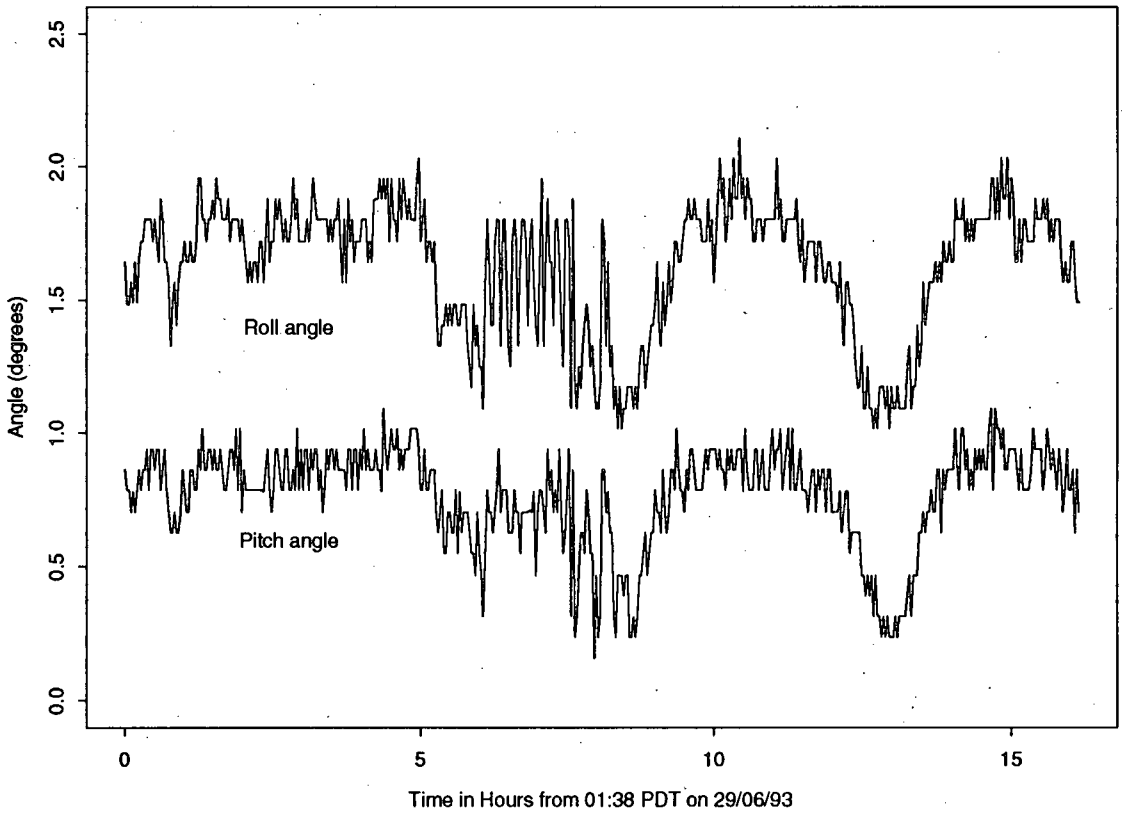

Figure 4.6: June 1993 time series of pitch and roll angles taken every 2 minutes. Data was recorded from 01:38 to 17:46 PDT on 29/06/93.

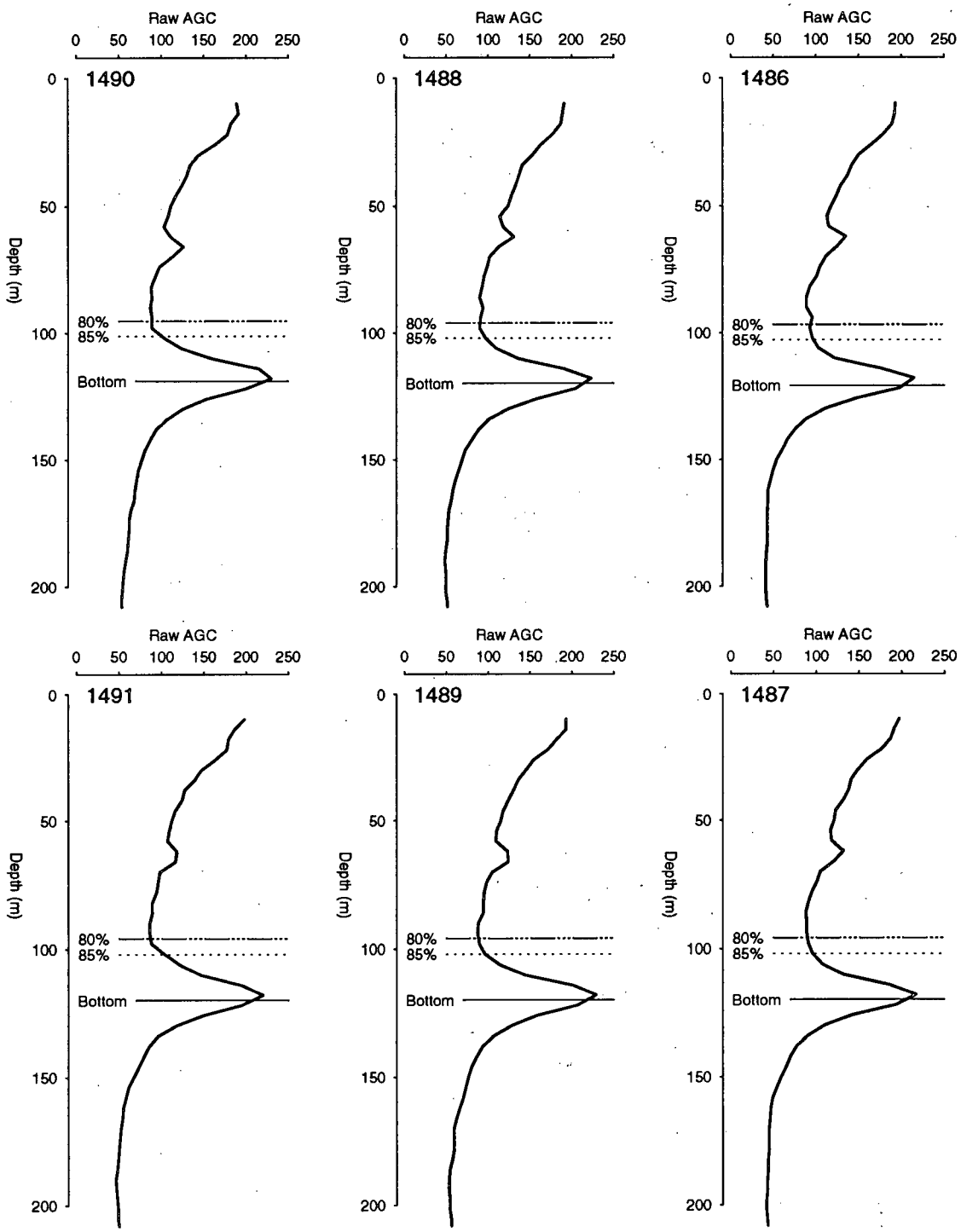

Figure 4.7: Six consecutive profiles of raw AGC vs. depth taken on 26/06/93 at 09:46 – 09:58 PDT. ADCP estimates of depth from bottom-tracking are shown with a solid line, whereas the 85% cut and 80% cuts are shown with dotted and dashed lines, respectively.

virtually identical signatures, it is not feasible to try and make the distinction on such a small vertical scale. Thus, the bottom 20% of each water profile is removed in order to get rid of all bottom scattering effects for a flat bottom.

4.2.3 Removing Bottom Scattering Effects for a Constant-Slope Bottom

A two-minute averaged profile during which the ship is moving over a flat bottom will be contaminated by bottom scattering at 20% of the minimum depth encountered during the averaging interval. The depth recorded by the ADCP is an average and represents the bottom depth somewhere near the middle of the averaging period. Thus, a bottom sloped at θ degrees from the horizontal will result in bottom scattering contamination at a percentage of the ADCP bottom depth, D, of:

$$\left[1 - \frac{(D - \frac{1}{2}|V_s| I \tan\theta) \times 0.8}{D}\right] \times 100\% \tag{4.1}$$

where V_s is the mean ship speed in m/s, and I is the ensemble averaging interval in seconds. At a ship speed of 10 knots, the maximum Vancouver Island shelf slope angle of 4° causes a change in bottom depth of about 40 m in a 2 minute averaging period. For a minimum shelf depth of 200 m, (4.1) allows contamination at the 28% level, which represents a maximal percentage for the study region. For $V_s = 0$, (4.1) reduces to the 20% contamination value discussed in the previous subsection.

An implementation of the above formula for computing the effects of a sloped bottom involves making a best estimate of the bottom slope and hence the minimum depth encountered using the bathymetric information available, which consists of the following six bottom depths:

1. Present profile's water depth

2. Next profile's water depth

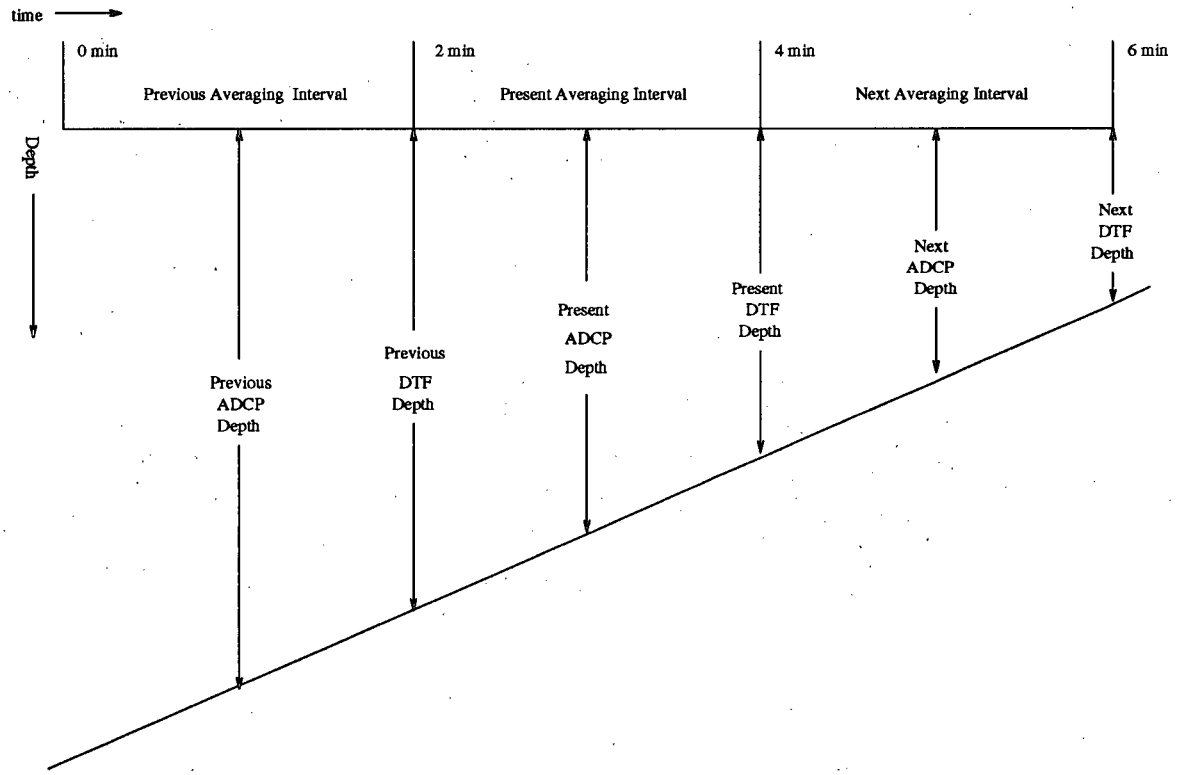

Figure 4.8: Schematic of three averaging intervals for a ship moving over a constant slope bottom. The various estimates of depth are shown in their respective positions in time and space.

3. Previous profile's water depth

4. Present profile's independent (DTF) water depth estimate

5. Next profile's independent (DTF) water depth estimate

6. Previous profile's independent (DTF) water depth estimate

Figure 4.8 is a schematic of these six depths showing what depth they represent for a ship moving at a constant rate over a bottom with a uniform slope. The DTF depths represent the bottom depth somewhere near the end of the averaging interval as that is when the ADCP queries the ship navigation devices for positional information.

Therefore, assuming the bottom has a uniform slope, the profile can be cut at 20% of the minimum of the two endpoints in the averaging interval. These endpoints can be found either by averaging water depths, or simply by looking at the DTF depths. Therefore, for a uniform slope bottom, the minimum depth is taken to be the minimum of the following four depths:

1. Average of the present water depth and the next profile's water depth.
2. Average of the present water depth and the previous profile's water depth.
3. The DTF depth for the present profile.
4. The DTF depth for the previous profile.

The effect of this depth selection process can be seen by examining a series of 12 consecutive profiles recorded on June 26^{th}, 1993 from 10:48–11:08 PDT, with the ship moving at about 10 knots over a spur canyon to the north and west of the Juan de Fuca canyon at latitude 48.26° N, longitude 125.2° W (Figure 4.9). The cuts at 80% of the ADCP water depth and at 80% of the minimum of the four depths given above are shown as solid and dotted lines, respectively.

Over the 20 minute period covered by the data segment the bottom depth increased from about 120 m to about 220 m and then decreased to 100 m. The largest jumps, ΔH, in bottom depth were between profiles 1324–1325 of $\Delta H = 44\,m$ and between profiles 1329–1330 of $\Delta H = -43\,m$. Although the average bottom depth for profile 1325 was close to 180 m, the depth was clearly shallower than this at the beginning of the averaging interval, resulting in the apparent 'scattering layer' situated at a depth of about 120 m. Further evidence that the 120 m scattering layer in profile 1325 was not biological is found in the next three profiles (1326–1328), where this layer was no longer visible. Profile 1329 also shows a similar amount of bottom backscatter influence which occurred when the

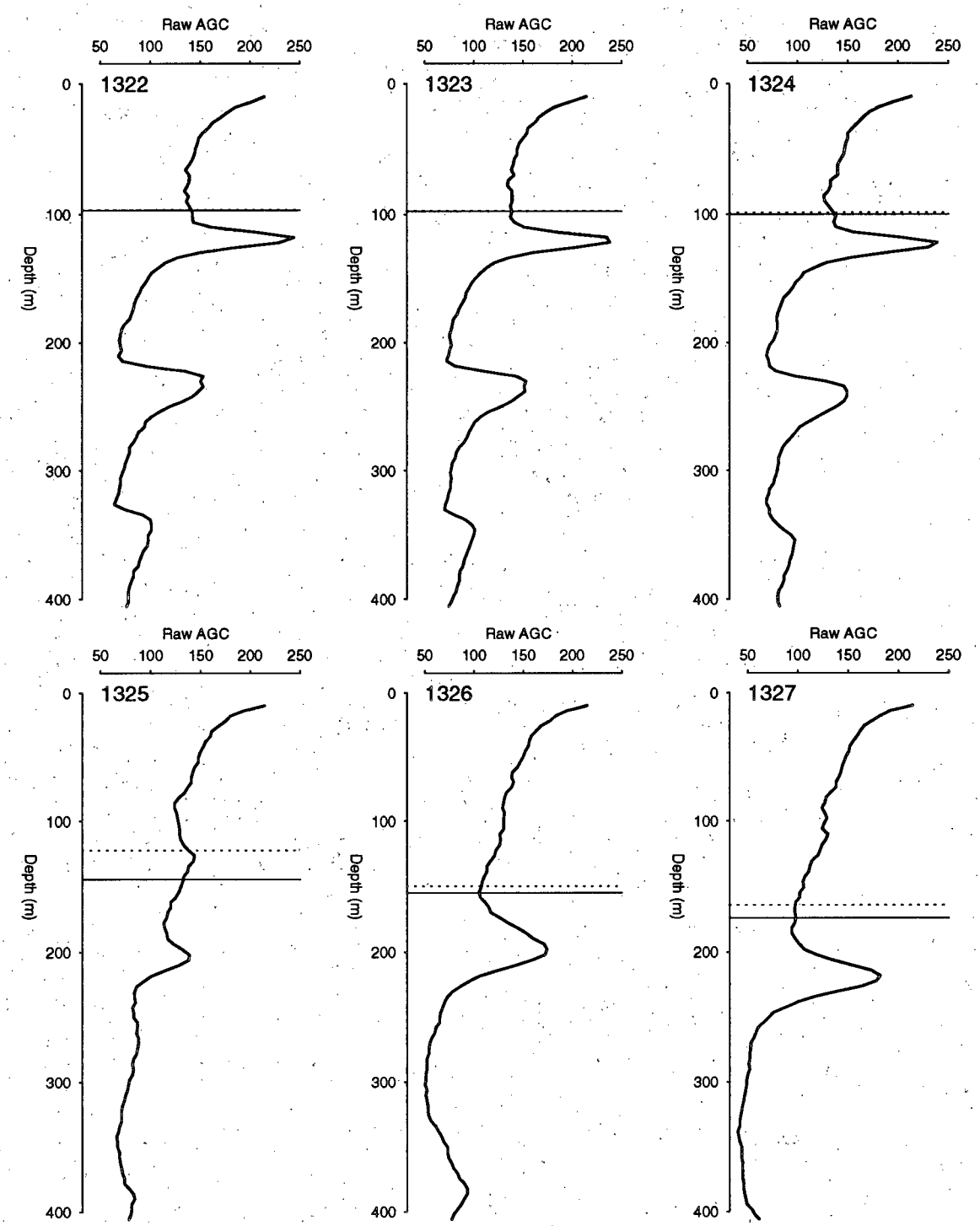

Figure 4.9: Twelve consecutive profiles of raw AGC vs. depth taken on 26/06/93 at 10:48–11:08 PDT Ship speed was about 10 knots. The solid lines show the cut at 80% of the ADCP water depth, the dotted lines show 80% of the minimum of four depths as explained in the text.

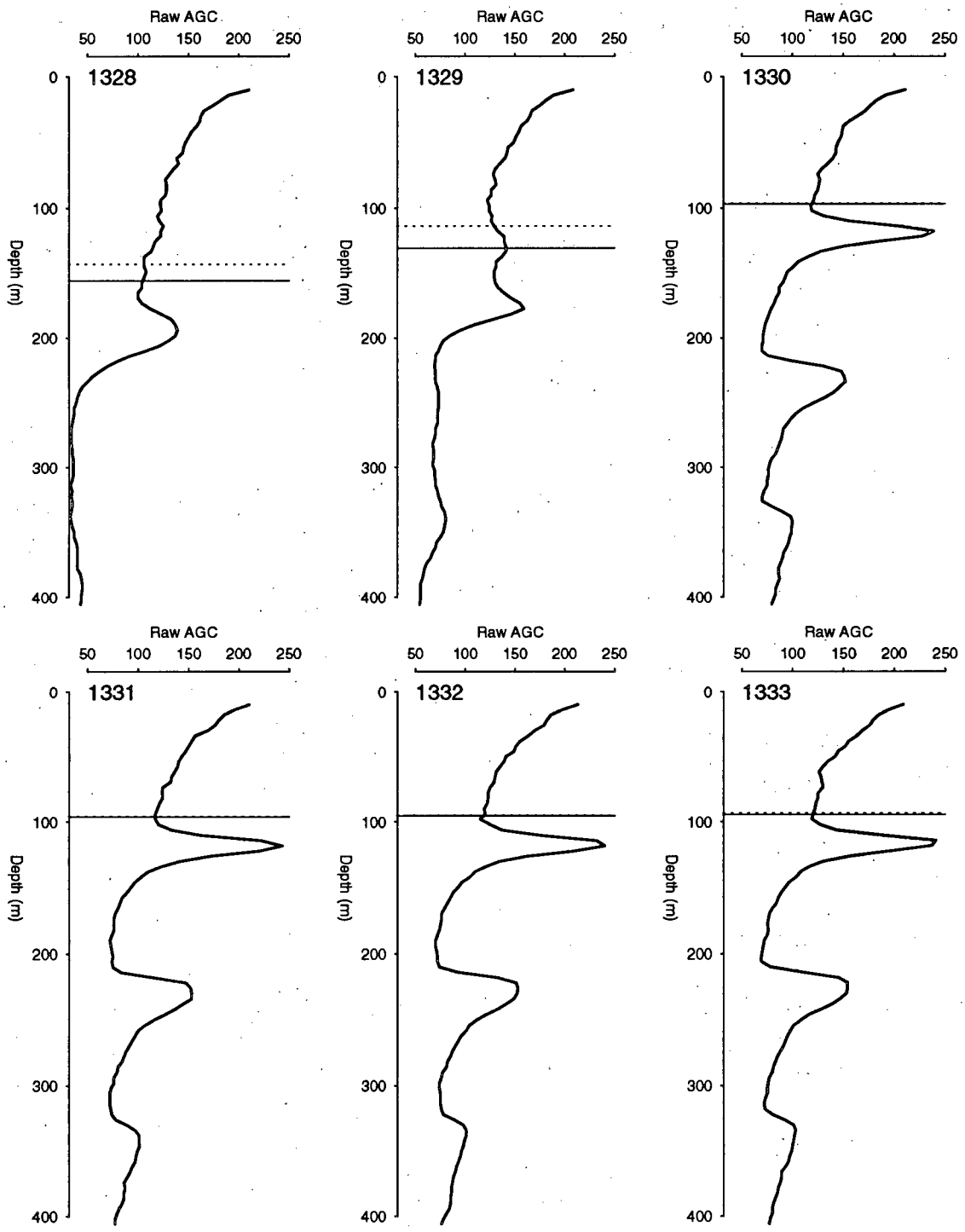

Figure 4.9: *(continued)*

ship was moving from a depth of 164 m to 121 m. Both of these suspect profiles admit the possibility of bottom scattering accounting for the extra scattering layer observed, and must be cut so as to remove the contaminated bins. Figure 4.9 shows that the assumption of a uniform slope bottom is not validated, as the cut developed above does not remove all the bottom scattering effects from profile 1325, leaving a substantial shoulder which is not apparent in the profiles that followed. However, the cut removes nearly all of the shoulder in profile 1329, which can be attributed to the bottom slope being more uniform over the averaging interval of profile 1329 than over the averaging interval of profile 1325.

Irregularities in the bottom slope can lead to bottom scattering effects which are not accounted for by a uniform slope model, and so a stricter cut must be devised.

4.2.4 Removing Bottom Scattering Effects for an Irregular Bottom

The analysis of the profile data indicates that the only reliable way to remove all bottom scattering effects from ADCP data is to cut on 80% of the minimum of the following five depth estimates:

1. Present profile's water depth
2. Next profile's water depth
3. Previous profile's water depth
4. Present profile's independent (DTF) water depth estimate
5. Next profile's independent (DTF) water depth estimate

This cut will successfully account for most irregular bottom topography occurring on length scales of about 500 m. It will not account for 'bumps' in the ocean floor which have horizontal length scales smaller than about 500 m and vertical scales greater than

4 m. The effects of this cut are examined on the same twelve consecutive profiles as in Figure 4.9 (Figure 4.10). The dotted lines now represent the above objective cut using the minimum of the five possible depths. The bottom scattering effects in profiles 1325 and 1329 are fully removed by this cut.

The five-depth cut overestimates the amount of bottom scattering present in the data, which can become a problem when trying to observe near-bottom biological scatterers. However, as pointed out previously, the acoustic signatures of such scatterers and side-lobe bottom scattering are too similar to be distinguished regardless of the processing approach. Thus, if there is a possibility of bottom scattering effects in the dynamic transducer/ocean-floor configuration, then elimination of these effects must take precedence over the possibility of biological scatterers to avoid any ambiguities in the final results. For example, consider six consecutive profiles taken on June 29^{th}, 1993 from 13:50–14:00 PDT at latitude 48.05° N, longitude 125.6° W on the shelf break near the southern entrance to the Juan de Fuca Canyon (Figure 4.11). The bottom increases from a depth of about 140 m at profile 1414 to a depth of about 280 m at profile 1417, with the biggest jump ($\Delta H = 52\,m$) between profiles 1414–1415. The effect of this 52 m change in bottom depth is manifested in profile 1415 as an apparent 'scattering layer' similar to what was seen in the profiles of Figure 4.9. However, in this case, the successive profiles also show a similar structure lying about 100 m above the bottom. This would seem to indicate that the 'scattering layer' in profile 1415 is due, at least in part, to biological scattering. It still must be removed because it is possibly due in part to bottom scattering of acoustic side-lobes from the shallower depths recorded near the beginning of the averaging interval. The corresponding scattering layers in profiles 1416–1420 are not removed by the cut, and so the presence of this biological feature is not altogether lost.

The most efficient method for removing all bottom scattering effects would be to record the minimum depth encountered in each averaging interval.

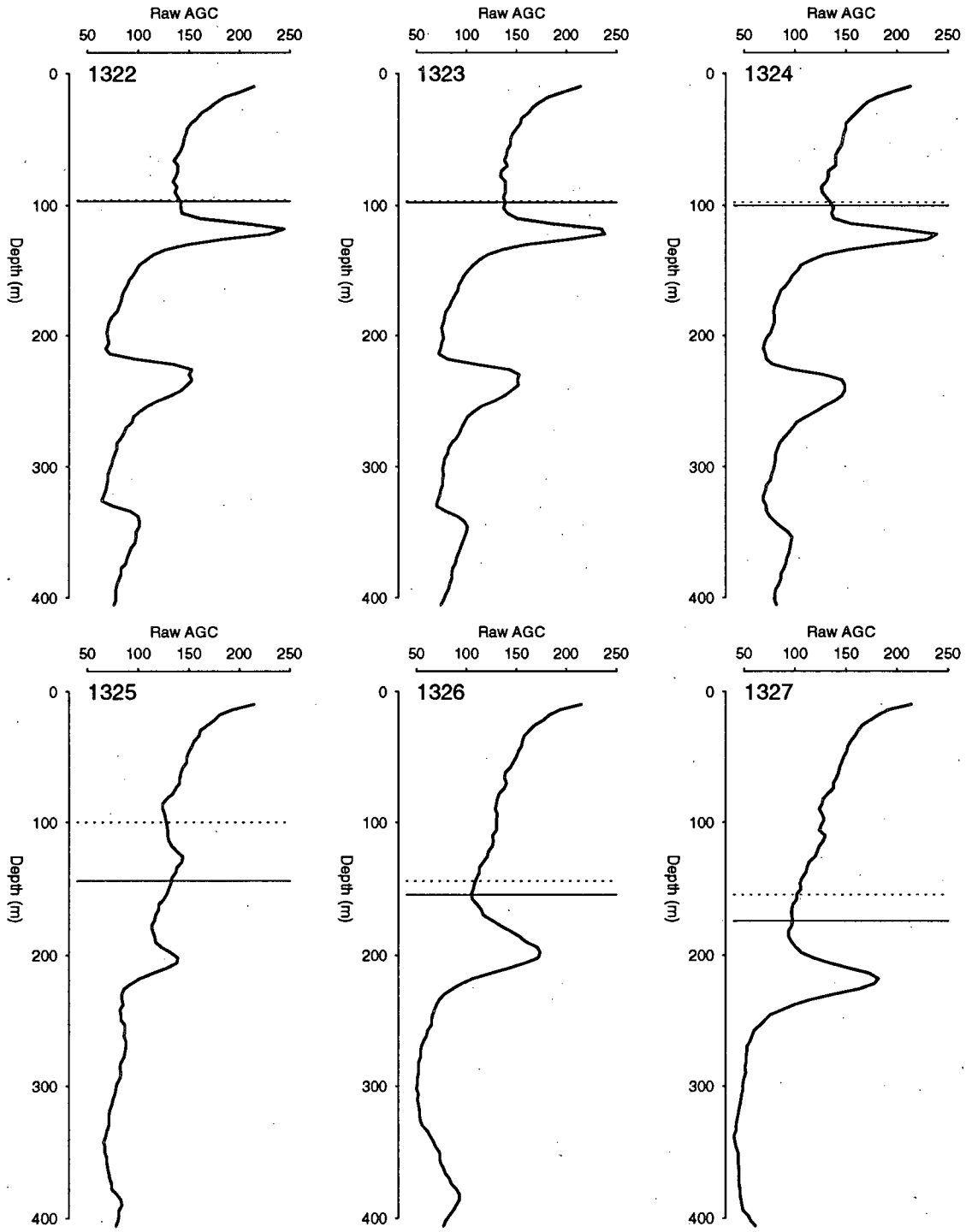

Figure 4.10: Twelve consecutive profiles of raw AGC vs. depth taken on 26/06/93 at 10:48–11:08 PDT. Ship speed was about 10 knots. The solid lines show the cut at 80% of the ADCP water depth, the dotted lines show 80% of the minimum of five depths as explained in the text.

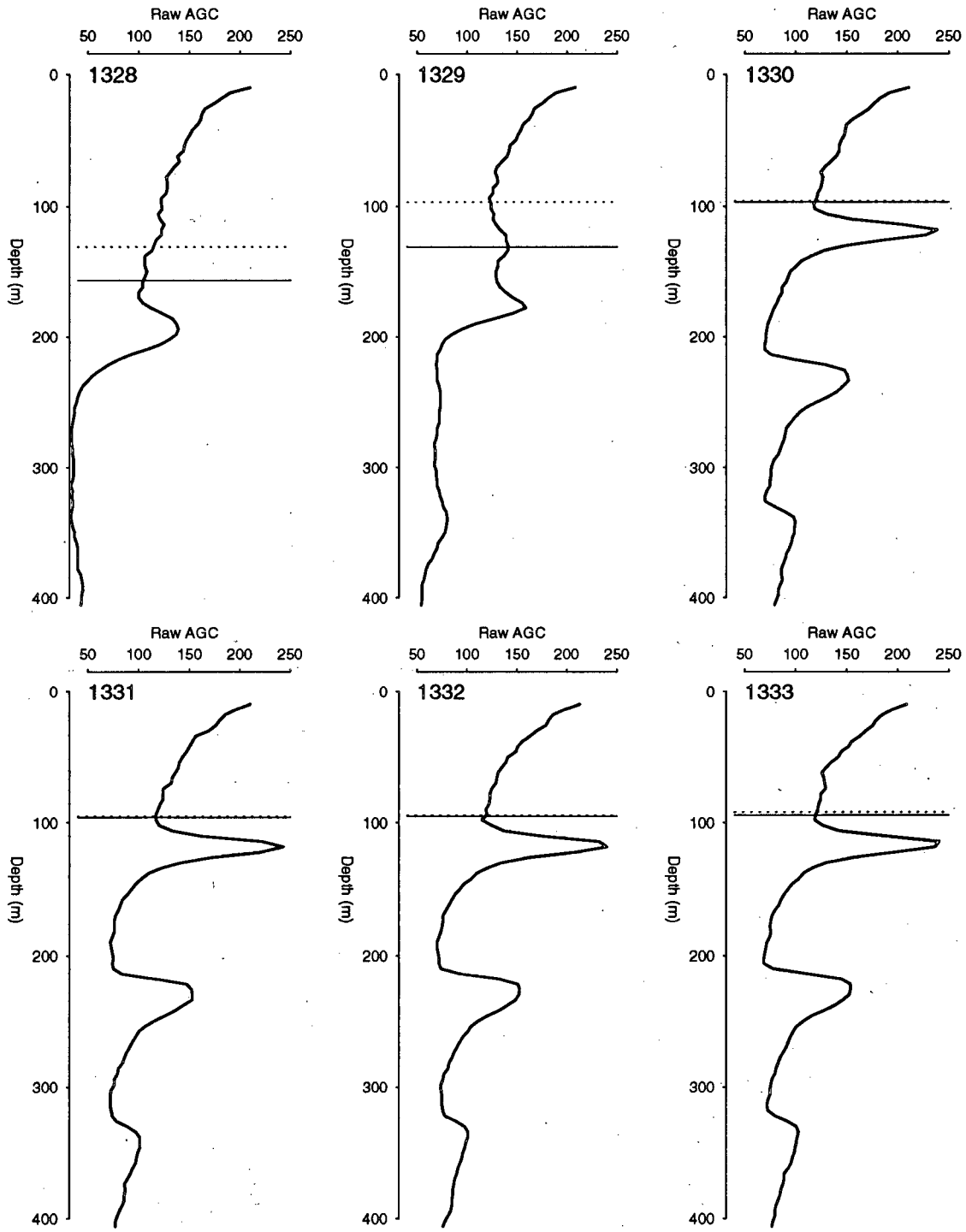

Figure 4.10: *(continued)*

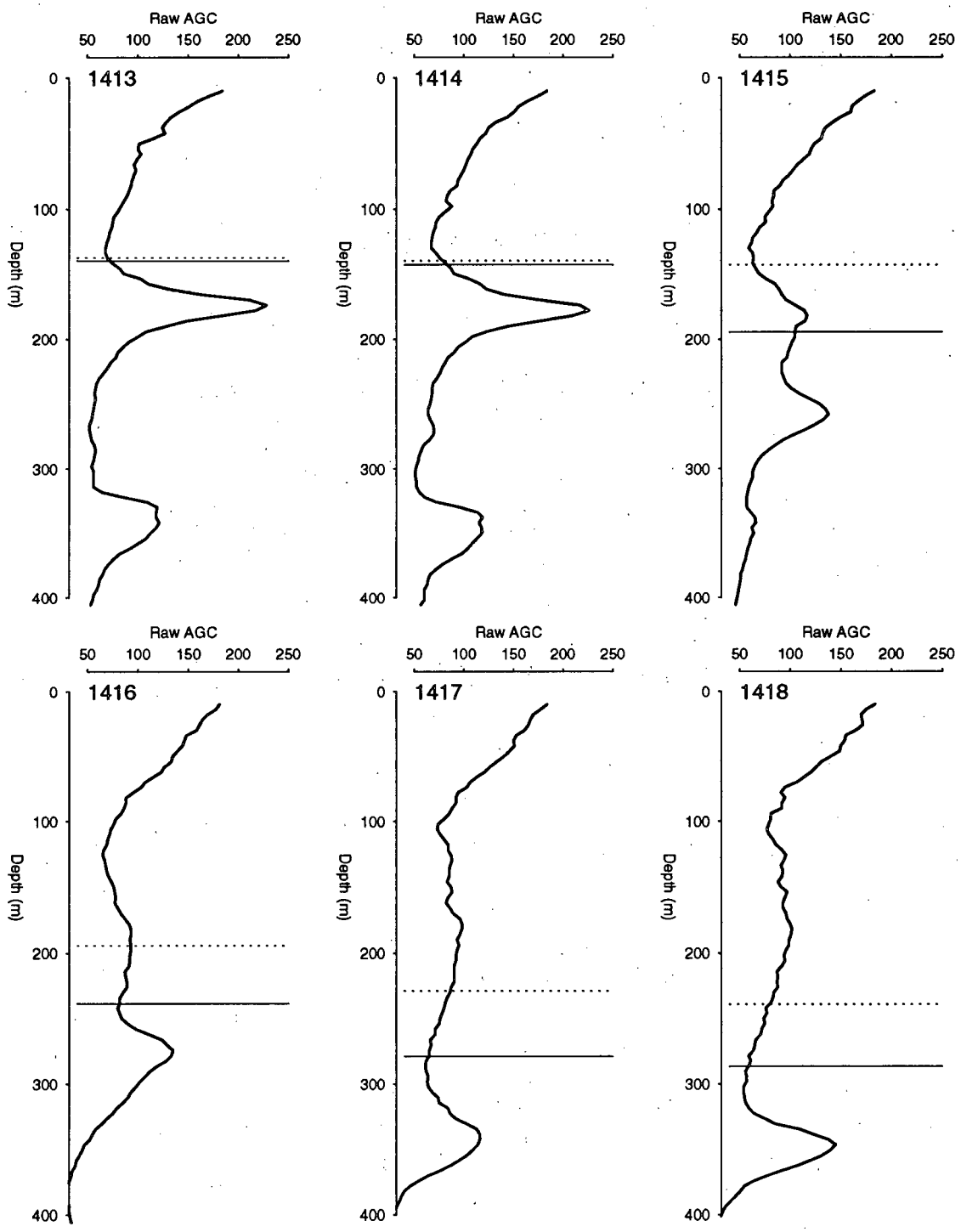

Figure 4.11: Six consecutive profiles of raw AGC vs. depth taken on 29/06/93 at 13:50–14:00 PDT. Ship speed was about 10 knots. The solid lines show the cut at 80% of the ADCP water depth, the dotted lines show 80% of the minimum of five depths as explained in the text.

4.3 AGC Calibration

The relation between the raw AGC and the backscatter strength, S_v, was given by (3.4):

$$S_v = k_c(AGC) + 20\log R + 2\alpha R + A \tag{4.2}$$

The AGC can be calibrated to give absolute backscatter strength and thus the acoustic cross-section by estimating the constants k_c and A. In absence of such an estimate, residuals can be calculated from fits of the vertical profiles of AGC vs. $20\log R + 2\alpha R$, yielding relative acoustic backscatter only. These two methods are discussed in the following sections.

4.3.1 Absolute Calibration

The unknown constants k_c and A in (4.2) are functions of system dependent parameters, a breakdown of which is obtained by expanding the sonar equation using the system characteristics (RDI, 1990; Urick, 1983):

$$\begin{aligned} S_v \;=\; & 10\log(4.47\times 10^{-20} k_2 k_s (T_x + 273)) \\ & + 10\log(10^{k_c(E-E_r)/10} - 1) \\ & + 20\log R + 2\alpha R \\ & - 10\log(cP) - 10\log K_1 \end{aligned} \tag{4.3}$$

where $k_2 = 4.3$,

$k_s = 4.17 \times 10^5$,

$T_x =$ temperature of transducer head ($^\circ C$),

$k_c = 127.3/(T_e + 273)$,

$T_e =$ temperature of electronics ($^\circ C$),

$E =$ AGC in counts,

Parameter	Depends on	Range	ΔS_v	Value
T_x	water $T°$	$[5,15]°C$	0.15dB	10°
k_c	electronics $T°$	$[5,20]°C$	3dB	18°
E_r	noise	[25,35]dB	4dB	30dB
α	depth	$[0,400]m$	1dB	0.044
α	water $T°$	$[5,15]°C$	0.5dB	0.044
c	sound speed	$[1460,1530]m/s$	0.2dB	1475.1 m/s
V_s	Voltage	[219,221] V	3dB	220 V

Table 4.2: Parameters from (4.3) and their effect on S_v. Values given in the last column are those used in this study.

E_r = Reference level of echo intensity (electronics noise) in counts,

R = Along-beam distance from transducer to depth bin (m),

α = attenuation coefficient (dB/m),

c = speed of sound in water (m/s),

P = Pulse length (m) (typically P = bin length),

K_1= Power into the water = $\left[\frac{(V_s \times a)-b}{n}\right]^2 \times K_{1c}$ (W),

V_s = VAC input,

a = 1.397,

b = 4.27,

n = 37.14,

K_{1c} = 3.3 (W).

The values of k_2, k_s, a, b, n, and K_{1c} in (4.3) are nominal values given in (RDI, 1990), and contribute errors of less than $\pm 2dB$ to the estimation of S_v (RDI, 1990). The remaining six parameters: T_x, k_c, E_r, α, c and V_s must be measured independently for each instrument. Table 4.2 shows these six parameters, what they depend upon, how strongly typical variations in the dependencies will affect an estimate of S_v using constant parameters, and a best estimate of the values.

The temperature of the transducer head, T_x, can be taken as the temperature of the water under the ship's hull. Due to its small effect on S_v, T_x can be set to a constant value of $10°C$, a characteristic temperature for the outer coast near 5 m depth. The temperature of the electronics, T_e, on the other hand, can have a substantial effect on S_v. A small change in T_e, δT_e, causes a change in S_v, δS_v, of:

$$\delta S_v = E\,\delta k_c = E\left|\frac{dk_c}{dT_e}\right|\delta T_e = E\,\frac{127.3}{(T_e+273)^2}\,\delta T_e \tag{4.4}$$

For characteristic values of $E = 200$ counts and $T_e = 18°$, (4.4) gives $\delta S_v = 0.3\,\delta T_e$. Thus, to reduce δS_v below 2 dB, the temperature of the electronics unit must be kept at constant temperature to within about $\pm 3°C$. The unit which houses the ADCP electronics was located in the lower laboratory on the *C.S.S. Tully*, which is generally heated to a uniform temperature. A $\delta T_e < 6°C$ is assumed for the data used in this study. Only a consistent record of the temperature near the electronics unit could reduce the error in S_v induced by δT_e further.

Changes in the speed of sound affect the estimation of S_v very minimally, and can be ignored. The ADCP uses a value of 1475.1 m/s for depth cell size calculations, and this value is adopted for the calculations in this analysis.

The attenuation coefficient, α, changes with the temperature of the water, and so will be variable above the thermocline and roughly constant below it, where the water temperature is more homogeneous. A variation of $\pm 2°C$ in the deep water causes a change in α of less than 0.001 dB/m. Thus, a specified nominal value of α for seawater at $4°C$ and 35ppt of 0.044 dB/m (Urick, 1983; RDI, 1990) is good to within about 2% (0.001 dB/m) in the deep, isothermal water. The nominal value will be about 0.008 dB/m low in the shallow water. However, at these depths it has little effect on S_v, since the $2\alpha R$ term increases linearly with depth. Use of the deep-water value of α will therefore induce an error in S_v of less than 0.1 dB at 50 m, increasing to about 0.8 dB at 400 m.

The AC power to the transducer head most probably underwent a smaller range of variability than the one given in Table 4.2. Consequently, the error in S_v due to variations in K_1 could probably be reduced to below 1 dB with a single measurement of V_s. To reduce this error further would involve monitoring the transducer power for a longer period of time to detect any changes and to correct for them.

There are two methods to estimate the background noise in the ADCP electronics, E_r (RDI, 1990): (1) The approximation method, in which the value of E_{rc} given by RDI is adjusted for real-time electronics and transducer temperatures, giving E_r; (2) The *in-situ* method, in which the value of E_r is obtained from the data set by examining echo intensity values taken from depth bins from which no anomalous echo is present. Since E_r is a measure of the thermal noise of the ADCP electronics, care must be taken to insure that there are no other interfering noise sources contributing to the returning echoes. Thus, these measurements should be taken while the ship is motionless on a calm sea with engines off. The range of the profile and the bottom depth must be large enough so that propagation losses reduce the signal-to-noise ratio well below unity. At this point, the recorded value of the AGC is the noise level, E_r. Heywood et al. (1991) chose to estimate E_r when the *percent good* parameter had fallen to zero. A similar analysis was used for the October, 1993 cruise. The result was a noise level of $30\,dB \pm 5\,dB$. A specific calibration run would be necessary to obtain this value to any degree of accuracy.

RDI recommends a separate calibration of E_{rc} before each experiment and suggest the *in situ* method because the ADCP is measuring the reference value in real-time (RDI, 1990).

The summed errors on all the parameter estimates will result in a total systematic error on S_v of about 5 dB. This yields a systematic error on the scattering cross-sections calculated from S_v of roughly the same magnitude as the cross-sections. Therefore, more precise calibration of S_v is needed to make this approach useful.

4.3.2 Residuals

The computation of residuals presented in this section offers an alternative to the absolute calibration method described in this previous section. Although it makes no claim at being able to determine absolute zooplankton scattering strengths, it gives a good estimate of the relative structure. The proposed residual method makes the assumption that the backscatter strength, S_v, consists of a constant background level, S_v^*, plus a small depth-dependent perturbation or residual, $S_v'(R)$:

$$S_v(R) = S_v^* + S_v'(R). \tag{4.5}$$

Equation (4.2) then becomes:

$$E = -\frac{1}{k_c}(20\log R + 2\alpha R) + \frac{1}{k_c}(S_v^* - A) + \frac{1}{k_c}S_v'. \tag{4.6}$$

k_c and A are constant (in R) since they depend only on characteristics of the transducer and the electronics. Thus, a linear fit of E vs. the transmission losses, $(20\log R + 2\alpha R)$, will result in a slope and intercept of:

$$slope = \frac{\partial E}{\partial(20\log R + 2\alpha R)} = -\frac{1}{k_c} + \frac{1}{k_c}\frac{R}{(20 + 2\alpha R)}\frac{\partial S_v'}{\partial R}, \tag{4.7}$$

$$intercept = E|_{(20\log R + 2\alpha R = 0)} = \frac{1}{k_c}(S_v^* - A) + \frac{1}{k_c}(S_v')|_{(20\log R + 2\alpha R = 0)}. \tag{4.8}$$

Since $(20\log R + 2\alpha R) = 0$ at $R \approx 0.99$, which is less than the *blank-beyond-transmit*, the value of $(S_v')|_{(20\log R + 2\alpha R = 0)}$ is arbitrary and is chosen to be $(S_v')|_{(20\log R + 2\alpha R = 0)} \equiv 0$, leaving the intercept $= -\frac{1}{k_c}(S_v^* - A)$. If the backscatter residuals are uniform, such that:

$$\frac{\partial S_v'}{\partial R} \ll \frac{(20 + 2\alpha R)}{R}, \tag{4.9}$$

then the slope $\approx -\frac{1}{k_c}$ which, together with the intercept $(= -\frac{1}{k_c}(S_v^* - A))$, yields values of k_c and $(S_v^* - A)$, enabling calculation of the residuals using (4.6):

$$S_v' = k_c E + 20\log R + 2\alpha R - (S_v^* - A) \tag{4.10}$$

The residuals calculated in (4.10) give the vertical structure of zooplankton scattering strengths for each profile separately. In order to examine horizontal structures or to compare two profiles, the residuals must be computed from the same fit parameters, which are chosen as the mean fit parameters for the entire data set in question. Such an averaging procedure relies on the assumption that S_v^*, A, and k_c remain constant throughout the study period. If this assumption holds, the fitting procedure will effectively remove all the system-dependent components from the backscatter profiles, leaving a cruise-independent set of backscatter strength estimates.

There were two assumptions made in the preceding development which are now discussed. To verify the first assumption (4.9) , the average fit parameters ($\overline{k_c}$ and $\overline{S_v^* - A}$) are calculated using all the profiles taken on the Vancouver Island continental margin during two 1993 cruises (Table 4.3). The profiles are broken down into five groups depending on their bottom depths. All profiles are included in the first group (*bottom depth*> 0 m), and only those taken over bottom depths >320 m are included in the last group (*bottom depth*> 320 m). The mean fit parameters ($\overline{k_c}$ and $\overline{S_v^* - A}$) for profiles taken over the slope only (*bottom depth*>240 m) have standard deviations of about 10% (Table 4.3). If the profiles taken over the shelf (*bottom depth*<240 m) are included in the averages in Table 4.3, the standard deviations increase to 30–50%. This increase indicates that the scattering distributions over the slope are more uniform (more in accordance with (4.9)) than over the shelf. The fits to profiles taken over the slope are therefore more representative of the transmission losses. Fitted values of $\overline{k_c}$ and $\overline{S_v^* - A}$ for profiles taken over the slope only are assumed to approximate the actual values more reliably than the fitted values for all profiles together. Physical oceanographic processes over the shelf and shelf break appear to be responsible for more localized high concentrations of scatterers in the shelf and shelf-break waters which lead to the higher variances in the fitted parameters observed. The standard deviations in Table 4.3 indicate that the best estimates of $\overline{k_c}$

		k_c		$S_v^* - A$	
cruise	*bottom depth >*	*mean*	*std.dev.*	*mean*	*std.dev.*
	0	0.45	0.19	103.0	26.0
9317	80	0.47	0.20	104.4	27.4
June	160	0.53	0.07	109.3	5.73
1993	240	0.54	0.06	110.3	4.62
	320	0.54	0.06	110.1	4.32
	0	0.41	0.14	92.7	20.2
9335	80	0.45	0.15	98.9	20.4
October	160	0.58	0.12	115.6	13.2
1993	240	0.57	0.08	114.1	6.9
	320	0.56	0.06	113.2	4.0

Table 4.3: Fitted parameters for the June and October, 1993 cruises in the study area. Profiles with bottom depths greater than the value in the first column (*bottom depth >*) are included in the averages. A value of *bottom depth* >0 indicates that all profiles were used in the average.

and $\overline{S_v^* - A}$ were obtained from fits to profiles with bottom depths >320 m, and hence averages of only fit parameters from fits to profiles taken over the slope are used in the residual calculations.

The second assumption was that S_v^*, A, and k_c were constant throughout the study period. Following the analysis of Chapter 4.2.1, the only parameter which could seriously weaken this assumption is the electronics noise, E_r. All others are stable enough to not affect S_v by more than about 2 dB. The electronics noise undergoes changes primarily due to the temperature of the electronics. The effect of temperature on E_r is roughly given by (RDI, 1990):

$$E_r = constant - 0.9T_e - 0.1T_x \tag{4.11}$$

Thus, the changes in T_e and T_x described above will result in a change in E_r of about 1 dB. The ranges of the dependencies in Table 4.2 can be used to calculate the variability in k_c and A which are expected during either cruise:

$$\sigma_{k_c} = 0.005\, dB/m \tag{4.12}$$

$$\sigma_A = 2\,dB. \tag{4.13}$$

Thus, the assumption that S_v^*, A, and k_c are constant holds to within about 2%.

The variances in Table 4.3 are due to a combination of the effects of (4.9) being violated too strongly and of changing system characteristics (as in Table 4.2). Increased violation of (4.9) only yields greater variances in the fit parameters. However, this type of error can be reduced by including many samples in the averaged fits. For the 10000–sample average used to obtain the fit parameters for the June, 1993 cruise in Table 4.3, the error in $\overline{k_c}$ and $\overline{S_v^* - A}$ due to violation of (4.9) is reduced to under 0.1%. The bias errors in k_c and A due to changing system characteristics, on the other hand, cannot be reduced with increased sampling, are given by (4.12) and (4.13). Using (4.10) and a representative value of E=200 counts, the errors in S_v due to σ_{k_c} and σ_A are found to be roughly 2 dB. Therefore, the values of the average fit parameters are accurate enough to remove all system-dependent effects from the backscatter residuals to within about 2 dB.

4.3.3 Biomass

Zooplankton biomass can be calculated by first making estimates of the relative abundances of the various species of zooplankton in the water, and then specifying a scattering model for each species. A simple calculation starting from (3.3) gives the total biomass per unit volume, W (see appendix A):

$$W = 4\pi 10^{\frac{S_v}{10}} \left(\frac{\sum_i \xi_i w_i}{\sum_i \xi_i \sigma_i} \right) \tag{4.14}$$

where W = Biomass per unit volume (g/m^3),

S_v = Acoustic backscatter per unit volume (dB),

ξ_i = relative number abundance of species i,

$= \frac{n_i}{\sum_i n_i}$ where n_i is the number of plankton of species i,

w_i = average weight of individual member of species i (g),

σ_i = scattering cross section of individual member of species i, model estimate.

The relative abundances of plankton, ξ_i, can be obtained from net tows done coincidentally with the ADCP profiles. Scattering models typically model the plankton as a fluid sphere. This results in an equation of the form $\sigma \propto r^n$, where σ is the acoustical backscattering cross-section, r is the equivalent spherical radius of the zooplankter, and n is some power. For example, Flagg and Smith (1989) use an empirical model determined from net tows taken in conjunction with a moored upward looking ADCP:

$$\sigma(mm^2) = 1.209(0.130 + 0.019r^3)^{2/3} \tag{4.15}$$

where r is the mean length for all crustaceans in millimetres. Guerin-Ancey and David (1993) use a theoretical model which takes into account density differences. Greenlaw (1977) gives a good review of fluid sphere scattering models and their limitations.

An error of 5 dB in S_v would induce a factor of 2 or 3 error in the biomass estimate, even before the accuracy of the scattering model and the estimate of relative zooplankton abundances were taken into account. Thus, only an estimate of S_v to within about $\pm\frac{1}{2}dB$. and coincident calibration net tows would give a reasonable estimate of the biomass.

4.4 Absolute Currents

The vessel mounted ADCP is used to measure currents relative to the ship. These relative currents are only useful for looking at vertical shears in the water column. Any horizontal structure will be completely 'overwhelmed' by ship motion, since ship velocities (~300 cm/s) are typically an order of magnitude greater than earth-referenced (absolute) water velocities (~20 cm/s). Since the area of study contains substantial horizontal water velocity gradients associated with the prevailing flow regimes and intense tidal currents,

and these are important to the study of the zooplankton distributions, a conversion from relative currents to absolute currents is necessary. This requires an estimate of the earth-referenced ship velocity, which can be obtained by one of two methods: Acoustic bottom-tracking measurements, or change in ship position as a function of time. In both cases, the relative water velocities and ship velocities are always converted to the earth's coordinate system (east,north,z) first and then subtracted to obtain absolute water velocities. The ADCP bottom-tracking estimate is used whenever the ADCP estimate of bottom depth was deemed reliable, as per the method described in Chapter 4.2.1. This removes all profiles for which the ADCP located a 'false bottom', which would cause strong systematic errors in the estimates of ship speed from bottom-tracking. The ADCP automatically corrects for ship pitch and roll in calculating the velocities. The final step in processing the absolute current data is to remove the segments of the profiles which contain effects due to side-lobe scattering off the bottom.

The remainder of this section comprises: First, the bottom-scattering contamination removal protocol; second, a brief analysis of the errors involved in estimating the absolute water velocity; third, the bottom-tracking estimates of ship velocity and associated errors; fourth, the GPS change-in-position estimates of ship velocity and associated errors; and finally, a description of the barotropic tidal model used to estimate the tidal currents.

4.4.1 Removal of Side-Lobe Scattering Effects

Side-lobe scattering from the bottom has serious effects on the water velocities, causing errors of 4 cm/s to 10 cm/s in the bottom 15% of the water column when the bottom is in range of the ADCP (Appell et al., 1991). Such errors are typically 50–100% of the water velocities. The signal-to-noise ratio will reflect this corruption from bottom scattering. Typically, the *percent good* parameter falls from 90–100% when no bottom scattering effects are present to 0% when side-lobe scattering from the bottom comes

into range (85% of depth). Thus, in order to remove the side-lobe scattering effects, the currents in depth bins for which the *percent good* has fallen below 50% are removed from each profile.

4.4.2 Velocity Errors

Estimates of the absolute water velocity in the earth's coordinate system (east, north) involve two kinds of errors. The first arises from the random error and bias in the measurement of horizontal water and bottom velocity components, and the second arises from errors in the compass headings used to convert from ship coordinates to earth coordinates. Random error in the horizontal water velocities for an ADCP using 30° transducers is (RDI, 1989):

$$\sigma_w = \frac{1.6 \times 10^4}{\sqrt{f^2 D^2 N}} \tag{4.16}$$

where σ_w = standard deviation in water velocity (cm/s),

f = frequency (kHz) = 153.6 kHz,

D = depth cell size (m) = 4 or 8 m (in present configurations),

N = number of pings averaged together in a velocity estimate.

The number of pings averaged in a two-minute ensemble is typically about 30–35. Equation (4.16) thus gives a random error of $\sigma_w \approx 5\,cm/s$ for 4 m bins. This is reduced when averaging many profiles onto a grid. For typical ship speeds of 5 knots and intergridpoint spacing of 5 km, about 10–15 two-minute ensembles will be averaged together onto a single grid point, reducing the random error in the average velocities for each grid point to $\sigma_w \approx 1.5\,cm/s$.

Velocity data are recorded in (east, north) earth coordinates and thus require a ship heading obtained from the ship's compass. This ship heading will have some random error, σ_θ, associated with it. Pollard and Read (1989) reported short period errors of up

to 2° in heading persisting for up to 10–15 minutes after a sharp turn. Fortunately, these ship heading errors are present in both bottom-tracking ship velocity estimates and in relative velocities, so that when the two are subtracted, the errors exactly cancel, leaving much smaller errors in the absolute water velocities derived from bottom-tracking (RDI, 1989; also see appendix B).

Bias usually falls into two categories: (1) Scaling bias which is the systematic error in the conversion of Doppler shifts to relative water velocities; and (2) misalignment angle which is the angle between the ship's bow-stern line and the transducer's principal axis. Scaling bias affects the value of each velocity component and depends on various parameters such as temperature and signal-to-noise ratio. The misalignment angle introduces a systematic bias in velocity directions.

Estimates of bias are difficult and usually involve separate calibration runs with specific ship speeds and directions. Using a 150 kHz vessel-mounted ADCP, Pollard and Read (1989) found the scaling bias for the water velocities to be about 1.5% of ship speed and the misalignment angle to be $\phi \approx 4°$, causing systematic errors in water velocities of 8 cm/s due to scaling bias and 36 cm/s due to misalignment angle (for a 10 knot ship speed). Scaling bias for the bottom velocity was found to be about 0.3% of ship speed which resulted in a systematic error in water velocities of 1.5 cm/s. Ramp et al. (1991), also using a 150 kHz vessel-mounted ADCP, found a scaling bias of 0.3% and a misalignment angle of only 1°, leading to errors of about 10 cm/s in water velocities. The misalignment angle for the ADCP being used in this study has never been measured with any precision. Ship pitch and roll typically introduces errors of $\sim$1 cm/s in the horizontal currents (Kosro, 1985; RDI, 1989).

4.4.3 Bottom-Tracking

A bottom-tracking ping is emitted for each water profiling ping, and the resulting bottom velocities are converted to earth-referenced coordinates (east, north), which can then be subtracted from the relative water velocities to obtain the absolute water velocities. Random error in the bottom-tracking velocity is quoted by RDI as being $\sigma_b \approx 1\,cm/s$ (RDI, 1989).

The earth-referenced absolute velocities, $(u,\ v)$, are found from the ship-referenced velocities using a rotation matrix:

$$\begin{pmatrix} u \\ v \end{pmatrix} = \begin{pmatrix} \sin\theta & -\cos\theta \\ \cos\theta & \sin\theta \end{pmatrix} \begin{pmatrix} (V_w)_{\|} - V_b \\ (V_w)_{\perp} \end{pmatrix} \tag{4.17}$$

where (Figure 4.12) $(V_w)_{\|}$= along-ship component of relative water velocity (cm/s) (positive to left of direction of ship motion),

$(V_w)_{\perp}$= cross-ship component of relative water velocity (cm/s) (positive in direction of ship motion),

θ = ship heading from compass (degrees clockwise from north) ,

V_b = bottom speed (cm/s).

The errors on the earth-referenced absolute velocities, $(\sigma_u,\ \sigma_v)$, can be shown to be (see appendix B):

$$\begin{aligned} \sigma_u^2 &= \left[((V_w)_{\|} - V_b)^2 + (V_w)_{\perp}^2 \tan^2\theta + 2\tan\theta((V_w)_{\|} - V_b)(V_w)_{\perp}\right]\cos^2\theta\,\sigma_\theta^2 \\ &\quad + \sigma_w^2 + \sin^2\theta\,\sigma_b^2 \end{aligned} \tag{4.18}$$

$$\begin{aligned} \sigma_v^2 &= \left[(V_w)_{\perp}^2 + ((V_w)_{\|} - V_b)^2\tan^2\theta + 2\tan\theta((V_w)_{\|} - V_b)(V_w)_{\perp}\right]\cos^2\theta\,\sigma_\theta^2 \\ &\quad + \sigma_w^2 + \cos^2\theta\,\sigma_b^2 \end{aligned} \tag{4.19}$$

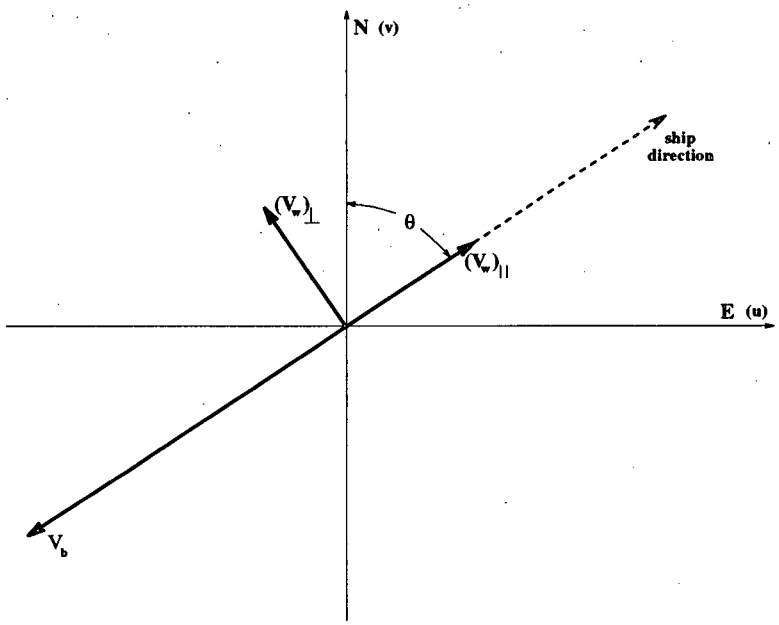

Figure 4.12: Geometric relationships between the ship-referenced water velocity coordinate system $[(V_w)_{\|}, (V_w)_{\perp}]$ and the earth-referenced coordinate system [east, north] as described in (4.17). The ship direction of motion is shown with a dashed arrow. θ is the ship heading measured clockwise from north, and V_b is the bottom velocity relative to the ship.

where σ_θ = heading error (random error + heading bias) (degrees),

σ_w = water velocity random error (cm/s),

σ_b = bottom velocity error (cm/s).

For water speeds less than $30\,cm/s$ and heading errors less than 4°, (4.18) and (4.19) can be approximated (to within about $0.4\,cm/s$) as (see appendix B):

$$\sigma_u = \sqrt{\sigma_w^2 + \sin^2\theta\,\sigma_b^2}, \tag{4.20}$$

$$\sigma_v = \sqrt{\sigma_w^2 + \cos^2\theta\,\sigma_b^2}, \tag{4.21}$$

showing that the heading errors in the relative water velocity and the ship velocity estimates have cancelled, resulting in smaller errors.

For $\sigma_w \approx 5\,cm/s$ before averaging and $\sigma_b \approx 1cm/s$, (4.20) and (4.21) give $\sigma_u = \sigma_v \approx 5\,cm/s$ for any heading angle, θ. It may be possible to reduce this to about 1–2 cm/s using 10–15 profile spatial averages (using a spatial grid).

4.4.4 Change in Position

The ADCP interrogates the ship's navigation system for positioning at the end of each averaging period and records the coincident latitude (ϕ) and longitude (λ). The vector-average ship velocity for each profile can be calculated using the previous (ϕ_1, λ_1) and the present (ϕ_2, λ_2) positions and the β-plane approximation:

$$\Delta x = R\cos\phi_2 \sin(\lambda_2 - \lambda_1) \tag{4.22}$$

$$\Delta y = R\sin(\phi_2 - \phi_1) \tag{4.23}$$

$$V_s = \frac{1}{\Delta t}\sqrt{\delta x^2 + \delta y^2} \tag{4.24}$$

$$\theta_n = \pi - \arctan(\frac{\Delta x}{\Delta y}) - \frac{\pi}{2} \times sign(\Delta x) \tag{4.25}$$

where Δx is the distance covered by the ship in the east direction (m),

Δy is the distance covered by the ship in the north direction (m),

V_s is the ship speed from GPS change in position (m/s),

θ_n is the ship heading from GPS change in position,

R is the radius of the earth (m),

Δt is the ensemble averaging period (usually 120 seconds).

The components of ship speed in earth-referenced coordinates (east, north) are $(\frac{\Delta x}{\Delta t}, \frac{\Delta y}{\Delta t})$. To estimate how precise such estimates are, they are compared to the bottom-tracking velocities in areas where the bottom is within range of the ADCP. Figure 4.13 (a) and (b) show the east and north ship speed estimates, respectively, from bottom-tracking and from GPS change in position estimates for a 6.5 hour period during the June 1993 cruise from 21:29 PDT on 18/06/93 to 04:07 PDT on 19/06/93.

The two estimates corresponded well on time scales greater than about 30 min, but short period (< 10 min) variations of the order of 20–50 cm/s were present in the GPS estimates of ship velocity which were not present in the estimates from bottom-tracking. Furthermore, when the ship underwent any large rapid changes in direction (while turning), the GPS estimates of ship velocity sometimes differed from the bottom-tracking estimates by over 100 cm/s (such at T=5.2 hours in Figure 4.13). The differences between GPS and bottom-tracking ship velocity estimates are plotted for the first 130 hours of the June 1993 cruise from 21:29 PDT on 18/06/93 to 08:14 PDT on 24/06/93 (Figure 4.14). Typical short period variations in GPS estimates of ship velocity lead to differences between the two estimates of ship velocity of 20–50 cm/s throughout the cruise. Differences of 100–300 cm/s were also apparent throughout the cruise, due primarily to errors in the GPS estimates of ship velocity while the ship was turning. The

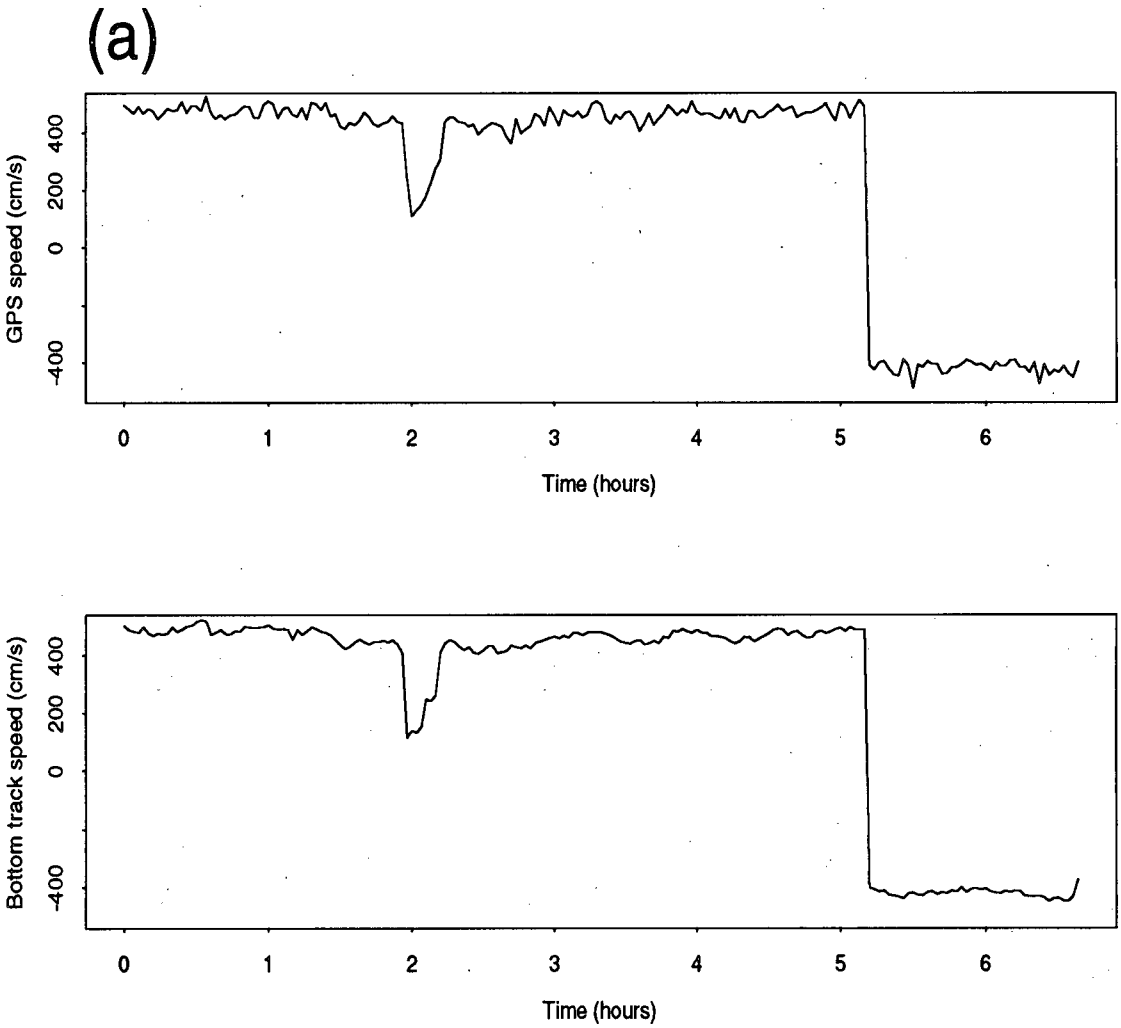

Figure 4.13: Comparison of GPS (top) and bottom-tracking (bottom) estimates of ship velocity for a 6.5 hour period during the June, 1993 cruise from 21:29 PDT on 18/06/93 to 04:07 PDT on 19/06/93. (a) East component.

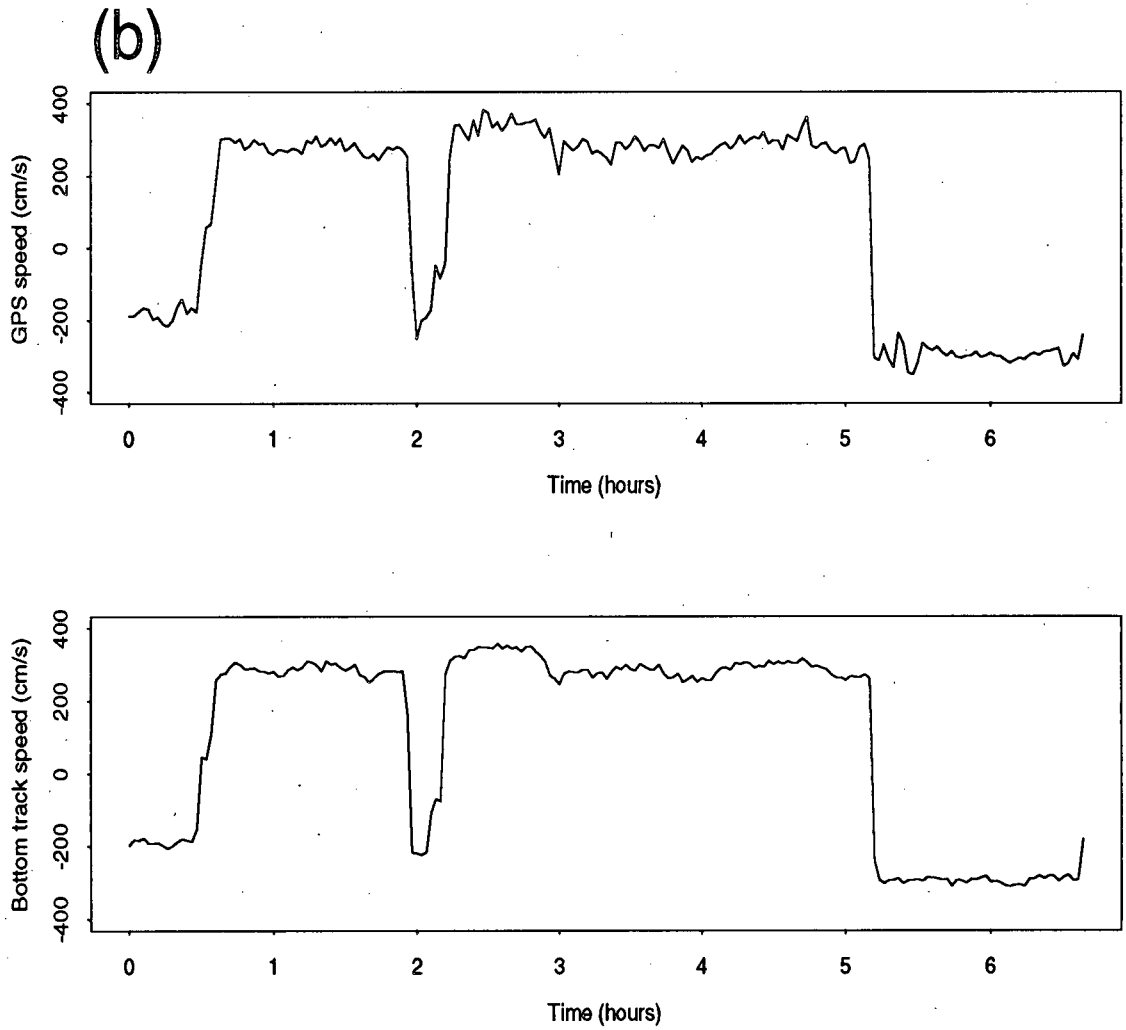

Figure 4.13: (b) North component

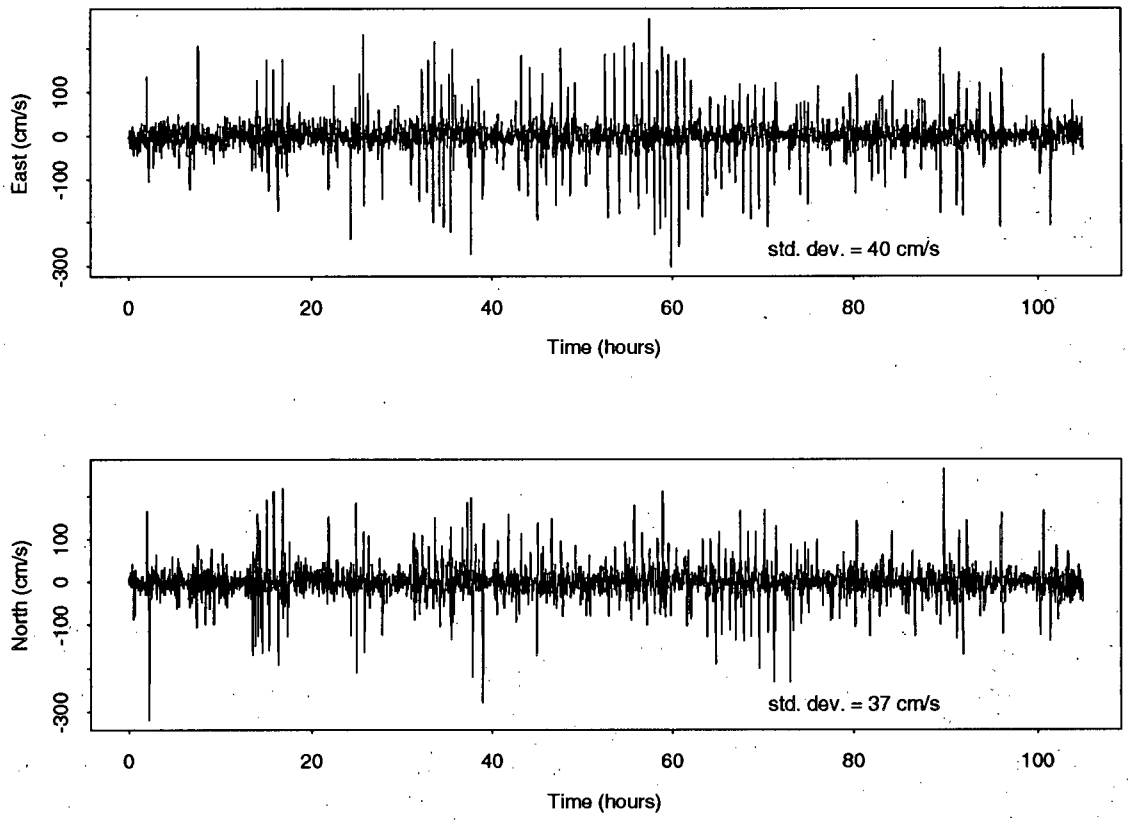

Figure 4.14: Differences between GPS and bottom-tracking estimates of ship velocity (top) east and (bottom) north components for the June 1993 cruise. The standard deviations are shown.

standard deviations in the mean ship speed differences shown in Figure 4.14 include errors from both bottom-tracking and GPS estimates of ship velocity. However, the errors in the bottom-tracking estimates were of order 1 cm/s, and so the errors in the GPS estimates of ship velocity alone, $(\sigma_u)_{GPS}, (\sigma_v)_{GPS}$, were roughly:

$$(\sigma_u)_{GPS} = 40\,cm/s \tag{4.26}$$

$$(\sigma_v)_{GPS} = 37\,cm/s \tag{4.27}$$

The errors in absolute water velocities will be higher than those in (4.26) and (4.27), due primarily to the differences between the heading estimates from the relative water velocities, θ, and from the GPS-derived ship velocities, θ_n. In any case, the resulting absolute water velocity errors will greatly exceed the typical currents of 10–20 cm/s. As a consequence, individual GPS estimates provide unacceptable surrogates of bottom-tracking velocity.

The spatial averaging onto a grid substantially reduces the variability in the GPS velocities. Since at least 10–15 water profiles are averaged onto each initialized grid point, the standard deviations should be reduced by a factor of 3–4. The differences in GPS and bottom-tracking estimates of spatially averaged ship speeds are presented in histogram form in Figure 4.15. Again, the standard deviations in Figure 4.15 include errors from both bottom-tracking and GPS estimates of ship velocity. However, the errors in the spatially averaged bottom tracking estimates are also a factor of 3 to 4 smaller (<0.5 cm/s), and so the errors in the spatially averaged GPS estimates of ship velocity are roughly 10–12 cm/s. Such errors represent a minimum value obtainable on the spatially averaged absolute water velocities, due to heading differences as described above. The minimum errors in spatially averaged water velocities are still of the same magnitude as the typical flows to be measured, indicating that only very strong ($\gg 10\,cm/s$), large-scale water flow patterns will be resolved when using spatially averaged GPS estimates of

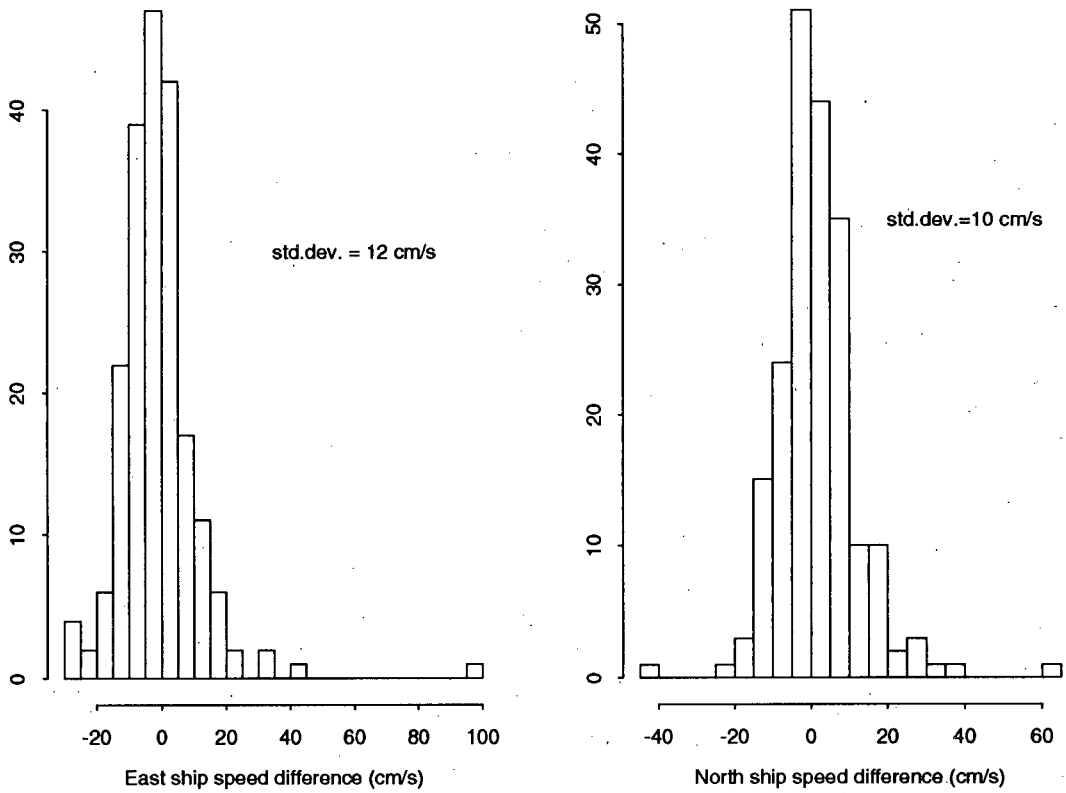

Figure 4.15: Histograms of differences between spatially averaged ship speed estimates in east and north components for the June, 1993 cruise. The standard deviations are shown.

ship velocity. Furthermore, very strong outlying errors ($> 50cm/s$) occur (Figure 4.15) and will dominate the water velocities. These outliers typically are the result of only one or two profiles being averaged onto a grid point and could be eliminated by requiring a certain number of profiles for each included grid point.

4.4.5 Barotropic Tidal Model

A finite-element, barotropic tidal model developed by Foreman and Walters (1990) is used to give a rough estimate of the magnitude of the tidal currents in the study area. The model uses a triangular grid with 2050 nodes and 3597 elements covering most of the area of interest to this study, extending from Juan de Fuca Strait to the southern tip of Estevan Point and from the coast to a distance of about 150 km offshore. Since the baroclinic tidal effects have small sea surface manifestations, such a barotropic model can reproduce the surface elevations accurately. However, the model cannot account for the baroclinic tidal currents in the region.

The tides predicted by the model were compared with extensive tide-gauge and current meter observations, and expected accuracies in the amplitudes were obtained (Foreman and Walters, 1990). The tidal currents did not compare as favorably as the tidal elevations, although the differences in the current ellipse parameters between the model and the observations were only around 1–2 cm/s (major and minor semi-axes) and $5°-15°$ (phase lag). Significant differences with depth were also observed in the M_2 component, and are due primarily to the combined effects of a barotropic Kelvin wave and an internal tide. The predicted tides were also compared with Flather's finite-difference model (Foreman and Walters, 1990; Flather, 1987), and both predicted high tidal currents (10–20 cm/s) close to the mouth of the Juan de Fuca Strait, decreasing north and west to about 2–5 cm/s along the shelf break.

The barotropic model will only be used in this thesis as a qualitative measure of the

large scale tidal effects. The circulation patterns discussed in chapter 5 will be comprised of both mean and tidal currents, and the model will be used to isolate any major tidal effects which dominate the local mean currents.

4.5 Averaging Grids

4.5.1 Interpolation Methods

In order to facilitate contouring of vertical sections and horizontal maps of both currents and backscatter intensity, the data are smoothed (spatially averaged) on a regular grid. This is done simply by locating the nearest grid point to each profile's position and assigning to that grid point the absolute currents and raw AGC. The AGC data are separated into night and day profiles, using code written by Luc Cuypers, adapted from code provided by Chris Aikman of the Dominion Astrophysical Observatory. The sunrise and sunset are both 'upper limb' values, meaning a 0° angle between the top of the sun's disc and the horizon. A record is kept during the averaging process of the number of samples added to each grid point, which is used after all profiles have been processed to average them on each grid point.

The data in Table 4.4 are recorded for each grid point. The number of cruises is always 1, unless averaging multiple cruises together. Grid points or depth bins with no data are flagged with -0.1E+05.

4.5.2 Grids

Two grids are used in this study. The first is a large grid which covers the entire area of interest to this study with a resolution of 3.5 km in the cross-shore direction and 8.0 km in the alongshore direction (Figure 4.16). The grid rows are at angles of 39° to the west-east direction, so as to roughly follow the general trend of the CTD survey lines,

1. Depth (m)		
2. Total residual backscatter intensity (dB)		3. Total time in (2) (min.) 4. Number of samples in (2) 5. Number of cruises in (2)
6. Night residual backscatter intensity (dB)		7. Total time in (6) (min.) 8. Number of samples in (6) 9. Number of cruises in (6)
10. Day residual backscatter intensity (dB)		11. Total time in (10) (min.) 12. Number of samples in (10) 13. Number of cruises in (10)
14. $\vec{u}$ absolute (cm/s)	15. $\vec{v}$ absolute (cm/s)	16. Total time in (14),(15) (min.) 17. Number of samples in (14),(15) 18. Number of cruises in (14),(15) 19. Percent good for (14),(15)
20. $\vec{u}$ relative (cm/s)	21. $\vec{v}$ relative (cm/s)	22. Total time in (20),(21) (min.) 23. Number of samples in (20),(21) 24. Number of cruises in (20),(21) 25. Percent good for (20),(21)

Table 4.4: Data recorded for each grid point.

which lie in a cross-shore direction. The second grid is a smaller one used for the June 1993 ADCP line data, and is comprised of 2 columns and 64 rows, with a gridpoint spacing of about 1.8 km by 0.5 km. Most of the data is centered along a line which runs close (within about 0.3 km) to one of the grid columns.

4.5.3 Contouring Algorithms

Two interpolation algorithms are used in the analysis. Both define a regular grid onto which the data is interpolated. The gridded data is then contoured. The first is an inverse distance method, in which the data is weighted according to the inverse of the square of the distance between data point and grid point. The region of influence of grid points is two grid units, meaning that a data point value influences grid points two grid units away from it (Cuypers, 1993). The second is a linear method, where the surface is approximated by triangular patches joining groups of three data points, and linear interpolation is used within the triangle. (Stat. Sci., 1991; Becker et al., 1988).

Most of the data used in this study was averaged onto a regular grid prior to the use of interpolation and contouring algorithms, so that the interpolation grid size used was that of the original grid. In the cases where the data was not gridded prior to interpolation, an interpolation grid size was chosen which reflected the distribution of the data. For this type of previously un-gridded plot, the raw data was examined to ensure that the grid size was appropriate, and that the contours did not cause any spurious elements to appear in the surface.

The inverse distance method is used for all plots done with the *Oceanplot*[1] software package. This package produces contours which are rounded using two arcs per straight line segment, resulting in few sharp edges in the contours. The linear method is used for

[1] *Oceanplot Version 1.01*, ©1993 Hermes Computing Services

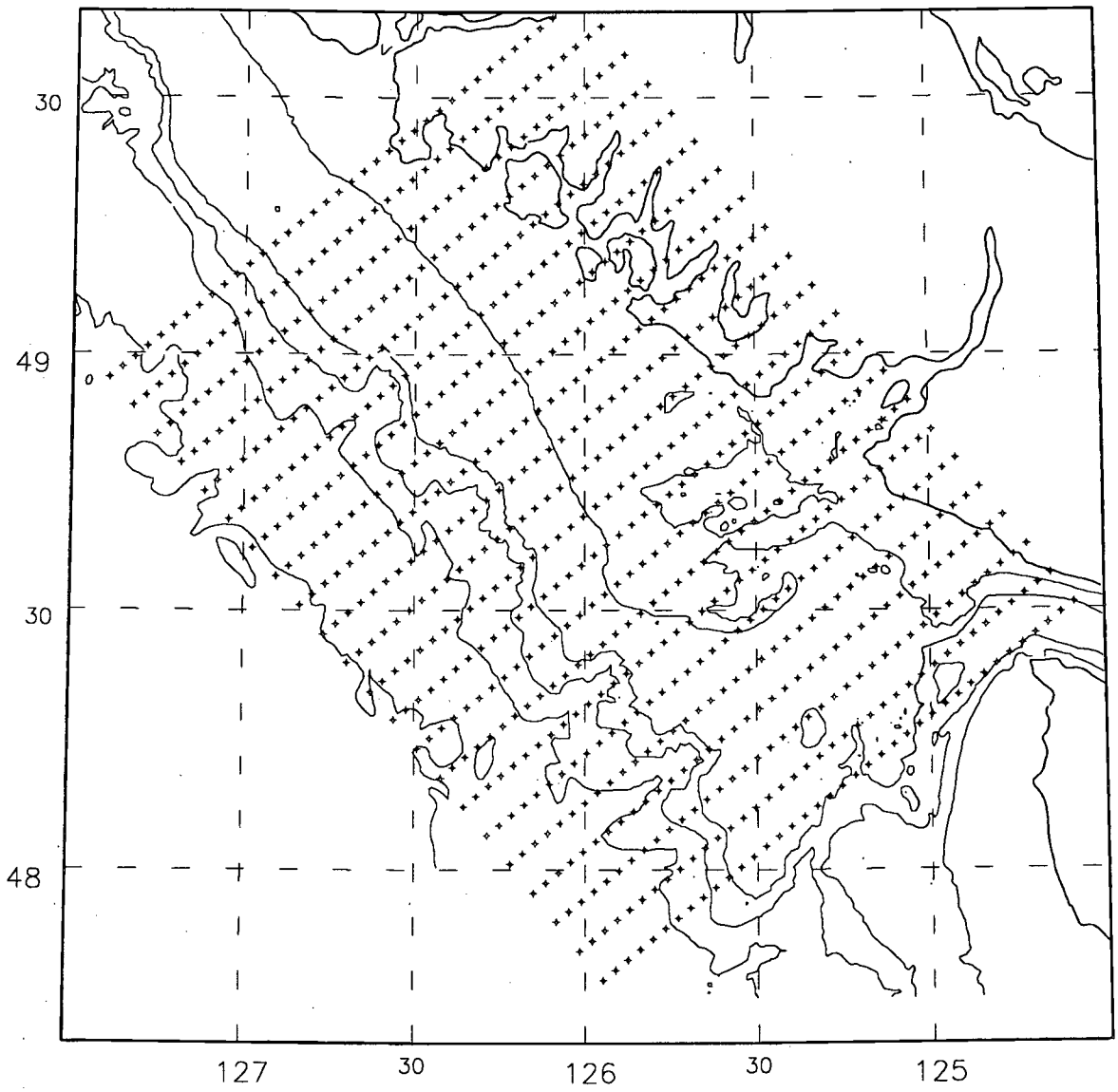

Figure 4.16: ADCP seasonal averaging grid. The grid spacing is $3.5 \times 8.0km$ and the grid rows are angled at 39° counterclockwise to the eastward direction.

all plots done with the *S-Plus* [2] plotting software. This package produces straight-line contours with no smoothing, usually resulting in sharp edges at each grid point.

4.6 Summary of Procedures

Figure 4.17 shows the data processing procedure, starting with the raw data files (ping-data.***) produced by the ADCP data acquisition system. *Phd300* and *gridadcp* are Microsoft *QuickBasic* and *FORTRAN* programs, respectively, written by Luc Cuypers and modified by the author to implement the processing techniques described earlier in this chapter. *Newbinrs* and *newavgrs* are also Microsoft *FORTRAN* programs, written by the author, which fit the raw AGC profiles to determine the average fit parameters, compute the residuals using these average fits, and change the vertical structure from 4 m to 8 m bins. *Velout* is also a Microsoft *FORTRAN*, which is used to produce ASCII listings of the fitted data files for use with the *S-Plus* [3] plotting software. *Oceanplot* [4] is a software package used to produce vertical sections and horizontal maps.

[2] *S-Plus version 3.0*, © 1991, Statistical Sciences, Inc.
[3] *S-Plus version 3.0*, © 1991, Statistical Sciences, Inc.
[4] *Oceanplot Version 1.01*, ©1993 Hermes Computing Services

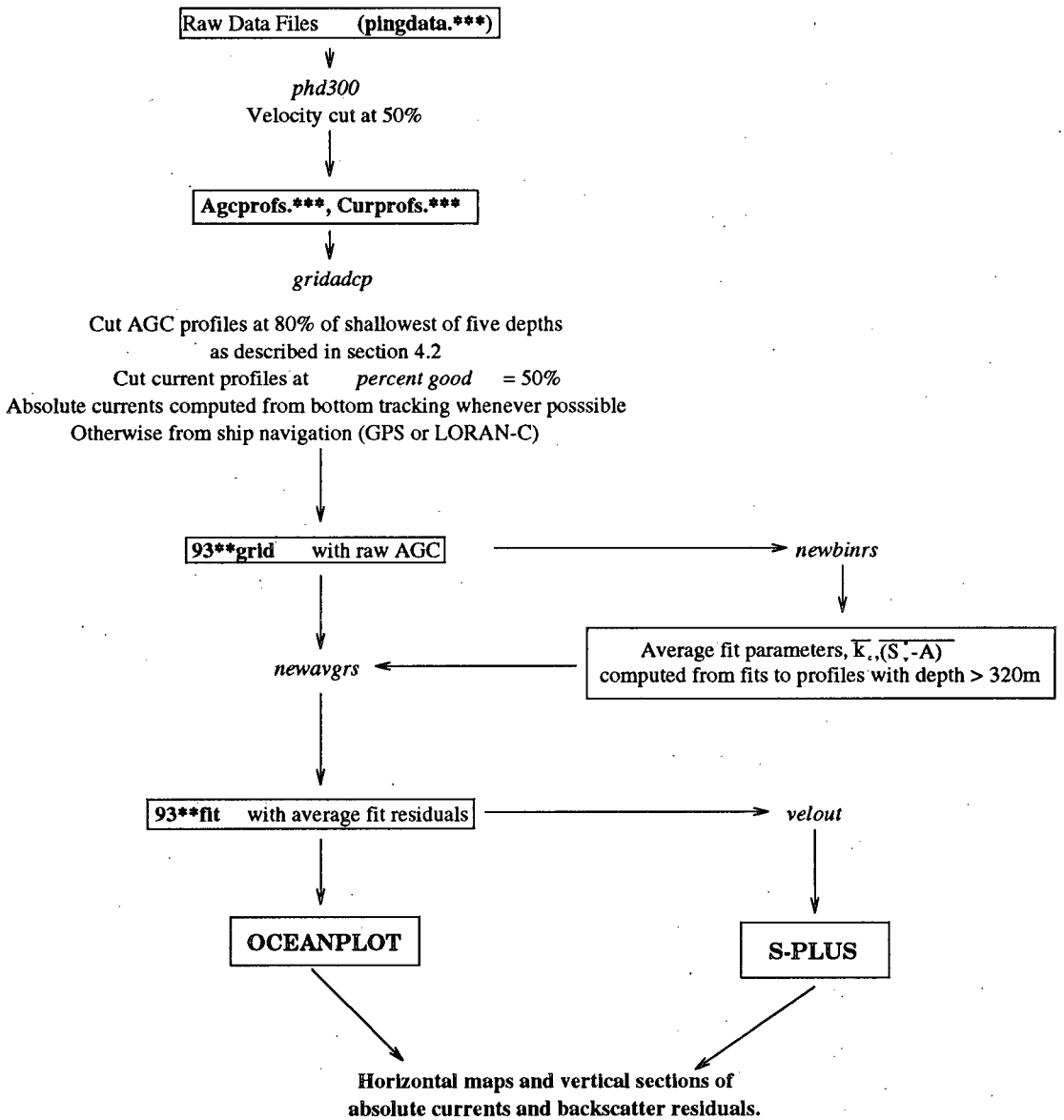

Figure 4.17: Flow chart for processing ADCP data. *Italicized* names are Fortran or QuickBasic programs, **boldface** names are data files.

Chapter 5

Results

This chapter describes results obtained from ADCP data collected during the June, 1993 La Pérouse cruise from 19/06/93 to 07/07/93, using the processing techniques developed in the last chapter. Chapter 5.1 examines a subset of the data which covers a small spatial area (14 km by 1.5 km) and has a short (19 h) duration. The basic zooplankton distributions as well as the current patterns are described. Correlations between the zooplankton distributions and the current patterns are determined. Chapter 5.2 describes all the data taken during the June, 1993 cruise over the southwest Vancouver Island continental margin. The data are first examined *in-situ* on temporal scales of about 10 hours and spatial scales of 100 km cross-shore and 20 km alongshore. Then, the data are examined as an average over the entire cruise period and over spatial scales of 100 km cross-shore and 200 km alongshore. All times referred to in this chapter are in PDT.

5.1 Mesoscale Cross-Shelf Survey

5.1.1 The Survey Line

During the June, 1993, La Pérouse cruise, a 19-hour period was devoted exclusively to steaming back and forth over a survey line to gather a time series for a small area over the Vancouver Island shelf break and slope. Figure 5.1 is a map of the ship's track during this period. The ship started at the southwest corner (48.22° N, 125.80° W), on June 26, 1993 at 10:10, and proceeded to steam the survey line ten times. Onshore steaming

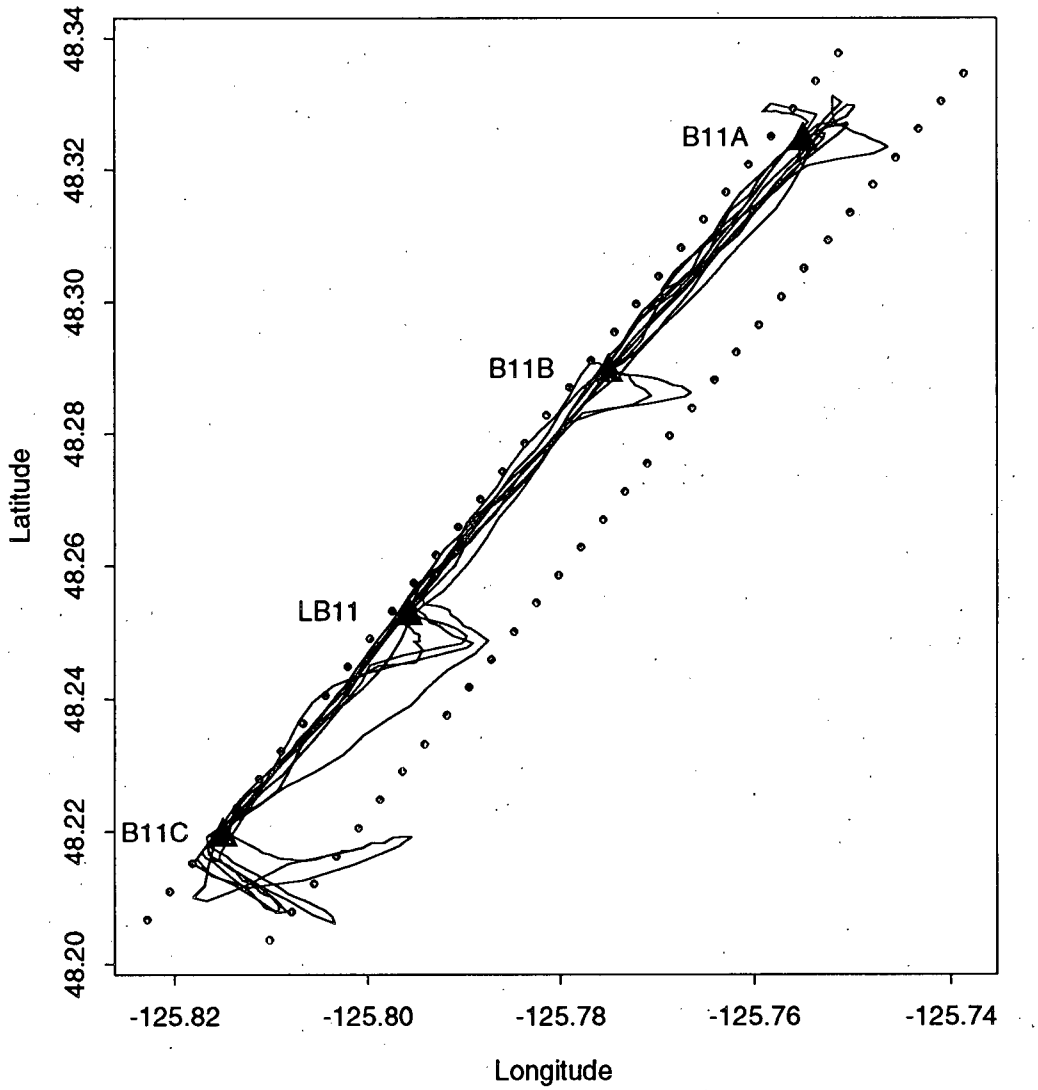

Figure 5.1: The ADCP line ship track for June, 1993. The ship started at the southwest corner at 10:10 on 29/06/93, and left from the northeast corner at 5:54 on 30/06/93. The dots denote averaging grid centers. The four CTD stations B11C, LB11, B11B and B11A are shown as solid triangles.

was at a constant ship speed of around 5 knots, and required about 1.0–1.5 hours for each leg. Offshore steaming included 10–20 minute stops for CTD casts at four standard CTD stations labeled B11C, LB11, B11B, and B11A (Figure 5.1). Steaming between CTD stations was at ship speeds of about 5 knots. Each offshore leg of the ADCP line took about 2.0–2.5 hours. Upper limb sunset occurred at 21:28 on 29/06/93 , during the 6^{th} leg of the ADCP line. The program continued throughout the night with four more passes over the line. Upper limb sunrise occurred at 05:24 on 30/06/93, just before the ship left the area from the northeast corner (48.33° N, 125.75° W) at 05:54 PDT. The first 9 legs covered about the same 14 km, of the shelf-slope region, whereas the 10^{th} leg only covered the northeasternmost 3 km of the line. A total of 591 vertical profiles of currents and AGC were recorded at 2 minute intervals.

The local bathymetry determined from DTF depths is shown in Figure 5.2. The survey line was located along the northwest side of a small canyon which penetrates about 10 km into the shelf in a northeastward direction. The survey line was roughly perpendicular to the local isobaths, although with an angle of 70° from the east, it was somewhat askew to the general direction of the shelf isobaths, which run perpendicular to about 40° from the east. The deepest water encountered was just over 600 m at the southwest corner of the survey line, the shallowest about 180 m at the northeast corner. Most ADCP bottom depths from bottom-tracking were reliable, with only about 5% of the depths rejected by the criteria presented in Chapter 4.2.4. Rejected depths were always in the far southwest corner of the line, and primarily during the last 4 legs of the survey session. Since the ship was usually turning when sampling over the deepest water, the areas where the GPS estimates of ship velocity were used in place of the bottom-tracking velocities have unreliable absolute water velocities, and hence are not included in the current analysis.

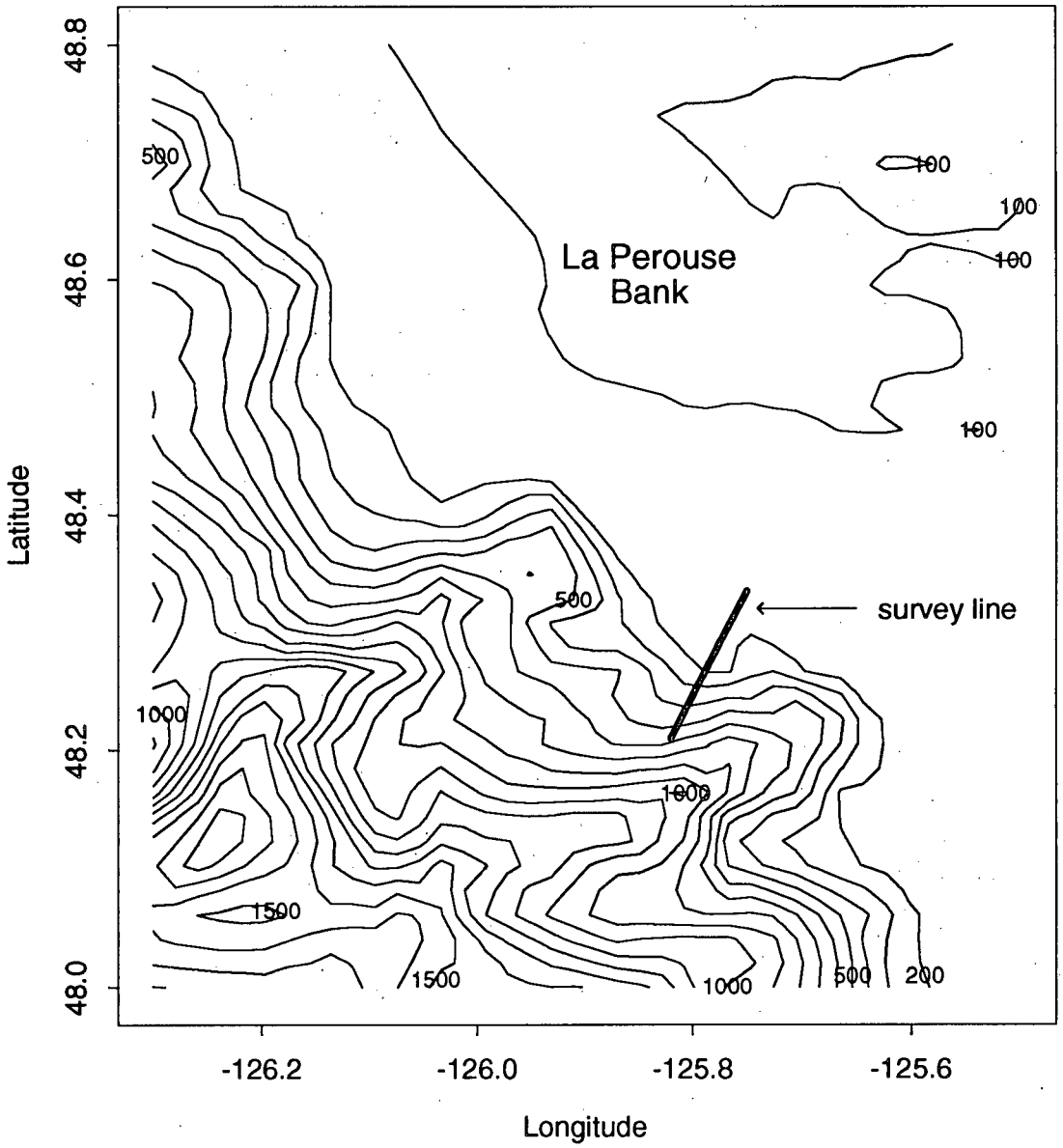

Figure 5.2: Survey line and local bathymetry for the June, 1993, ADCP survey (Depths in metres).

5.1.2 Survey Data

The ADCP data collection during the survey period provided a time series of vertical sections along the survey line. The current and backscatter data are functions of the form: $\vec{V}(d,t,z_k)$ and $S'_v(d,t,z_k)$, where d is the distance from the southwest corner of the survey line, t is the time, and z_k is the depth of bin k. $\vec{V}$ and S'_v are defined at a series of irregular (in d and t) and regular (in z) points in the three dimensional space (d,t,z). The times, t, for each of the 591 profiles in the survey are plotted in Figure 5.3, as a function of the distance, d. The cruise legs are labeled 1 through 10, each of which is nearly an instantaneous picture of $\vec{V}$ and S'_v over the vertical section d *versus* z_k for $t \approx$ constant (to within 1–2 hours). There are two other types of sections that can be generated to visualize the four-dimensional nature of this time series. The first are plots of $\vec{V}$ and S'_v as functions of z_k and t only [$\vec{V}(z_k,t)$ and $S'_v(z_k,t)$ for fixed d], which reveal the time evolution of the vertical structure for each point along the survey line. The second are plots of $\vec{V}$ and S'_v as functions of d and t only, [$\vec{V}(d,t)$ and $S'_v(d,t)$ for fixed z_k], which reveal the time evolution of the horizontal structure for each depth.

The grid in Figure 5.1 was used for the plots of (d, z_k) and (z_k, t) to average the data as described in Chapter 4.5. The northernmost grid row is used for most data points; the southern grid row is used only for short periods when the ship drifted off the main survey line. Only the northernmost grid row is used in the following analysis. The averaging process results in current and backscatter values defined at regular points in all three dimensions, or functions of the form $\vec{V}(d_i,t_j,z_k)$ and $S'_v(d_i,t_j,z_k)$, where d_i is the distance from the SW corner to grid-point i, (i =1 to 32), z_k is the depth of bin k, and $t_j = t(d_i,j)$ is an array containing a set of 32 PDT times for each of the ten legs of the survey line. Each $t(d_i,j)$ is calculated as the mean of the recording times of all profiles averaged onto grid-point d_i during cruise leg j. Throughout this analysis, the

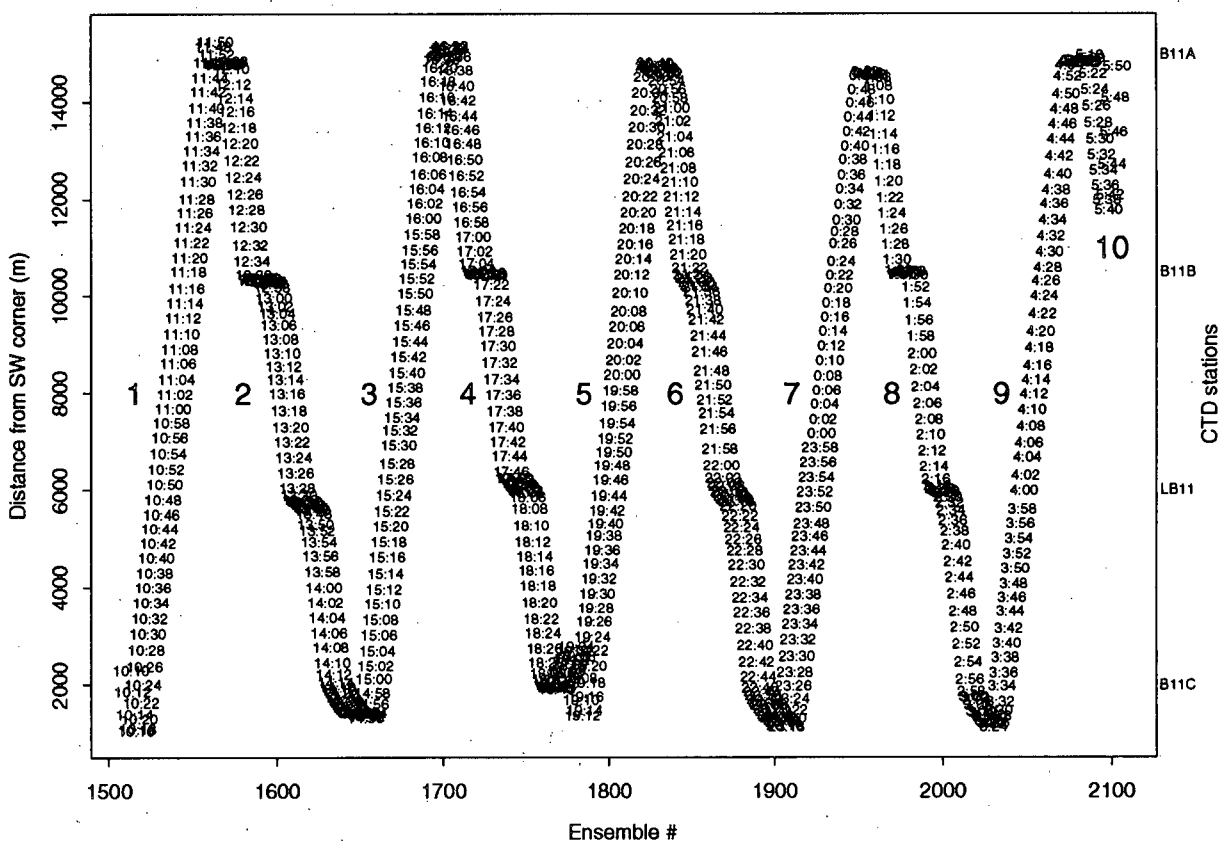

Figure 5.3: ADCP survey line profile recording times and distances for the June, 1993 survey. CTD stations and the leg numbers (1-10) are displayed. Times are PDT.

times, t, will usually be given in hours from the beginning of the survey period (10:10 on 29/06/93).

The first 9 legs each typically covered about 90% of the northern grid row, leaving out the top and bottom two grid-points. Each grid-point usually contains an average of 1–3 profiles, with those near the CTD stations and the end-points (grid-points 8, 22, 44 and 58) containing more than 5 profiles. Raw backscatter data is converted to residuals using average fit parameters determined from fits to all profiles in the June, 1993, cruise with bottom depths greater than 320 m. Profiles have been cut at 80% of the minimum of 5 recorded depths as described in Chapter 4.2.4. Absolute currents are determined from bottom-tracking velocities only. Profiles with erroneous ship velocity estimates are flagged, then discarded. Bottom-tracking gave erroneous estimates of ship velocity at the southeastern corner of the survey line (grid-points 3, 5, 6 and 8) for 31 of 591 profiles, with 2 during the 2^{nd} leg, 8 during the 6^{th} leg and 21 during the 8^{th} and 9^{th} legs.

The following sub-sections describe the backscatter and current data observed during the survey period. Chapter 5.1.3 examines the backscatter residuals in plots of all combinations of the three variables (d, t, z). It closes with an examination of the last hour of the survey period. Chapter 5.1.4 examines the current data as vertical sections in (d, z) to outline the vertical shears, and as horizontal time series in (d, t) to outline the temporal variations. It also discusses the tidal currents predicted and observed during the survey period. Chapter 5.1.5 summarizes the plankton and current structures and their correlations.

5.1.3 Backscatter Residuals

Quasi-instantaneous vertical sections

Figures 5.4a-j are contoured vertical sections in (d_i, z_k)-space of the backscatter residuals averaged onto the grid. These sections are not exactly instantaneous, as each spans a time between 1 and 3 hours (except the 10^{th} leg, which only spans 30 minutes). The bathymetry is determined from the DTF only, and so is only a rough approximation to the actual bottom. The 4^{th} leg and the 6^{th} leg have data missing at $d \sim 5km$, when the ship was closer to the southernmost grid row. These data were not included to ensure little along-shelf variability in backscatter in the vertical sections.

The structure during the first 9 hours (Figures 5.4a-d; legs 1–4) remained approximately the same. High plankton concentrations were observed near the ocean surface in a layer 20–30 m thick over the continental slope (southwest sector) and 70–100 m thick over the shelf (northeast sector). A 'depletion layer' filled the area below the surface scattering layer, with scattering levels 15–20 dB lower than at the surface. The extent (in depth) of this depletion layer in the southwest over the slope was from 50 to 100 m. In the center of the line over the shelf break, the depletion layer extended from the surface to 150 m. In the northeast sector of the line over the shelf, the depletion layer extended from 50 m to the bottom. This depletion layer was found throughout the coastwide survey discussed in Chapter 5.2. The deep water seaward of the shelf break contained the highest concentrations of scatterers, reaching levels 10–15 dB higher than at the surface. These deep water scatterers were concentrated primarily at a depth of about 200 m, 4–5 km seaward of the shelf break, in slope water 500–700 m deep.

During the first two legs, the near-surface scattering layer in the northeast sector occupied the upper 80 m and extended 4–5 km along the survey line. It moved seaward during the first four legs, covering the surface waters out to the shelf break by about

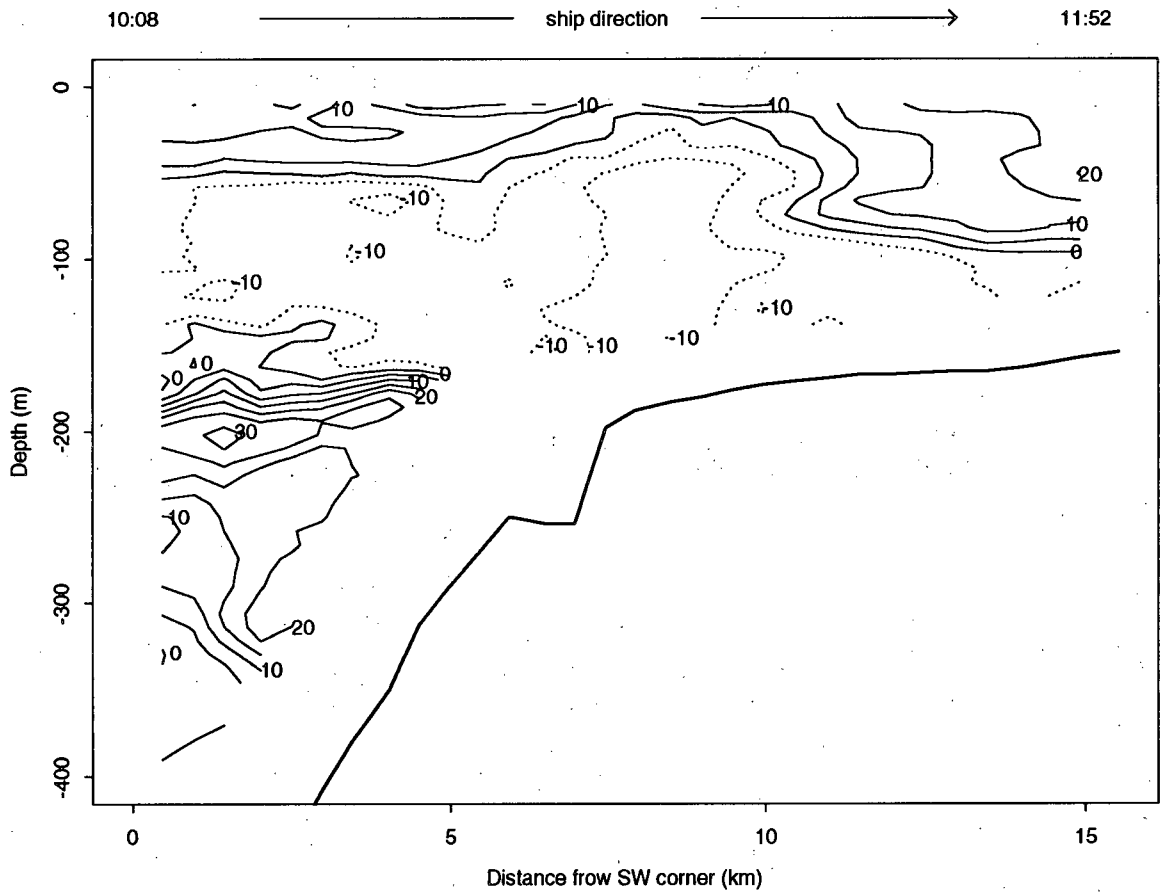

Figure 5.4: Backscatter residuals (dB) for the June, 1993 ADCP line. (a) Leg 1. Collection times are from 10:08 - 11:52 PDT on 29/06/93 with the ship steaming onshore.

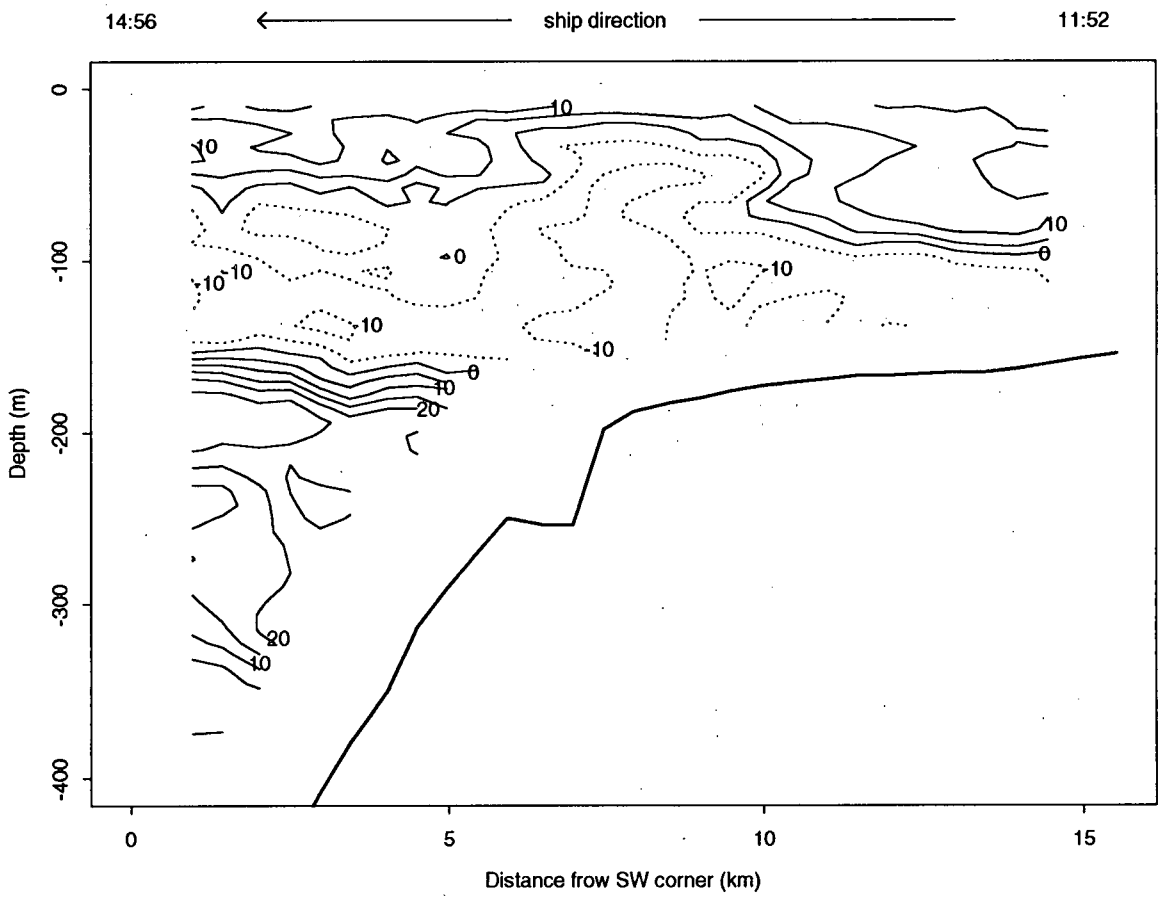

Figure 5.4: (b) Leg 2. Collection times are from 11:52 - 14:56 PDT on 29/06/93 with the ship steaming offshore.

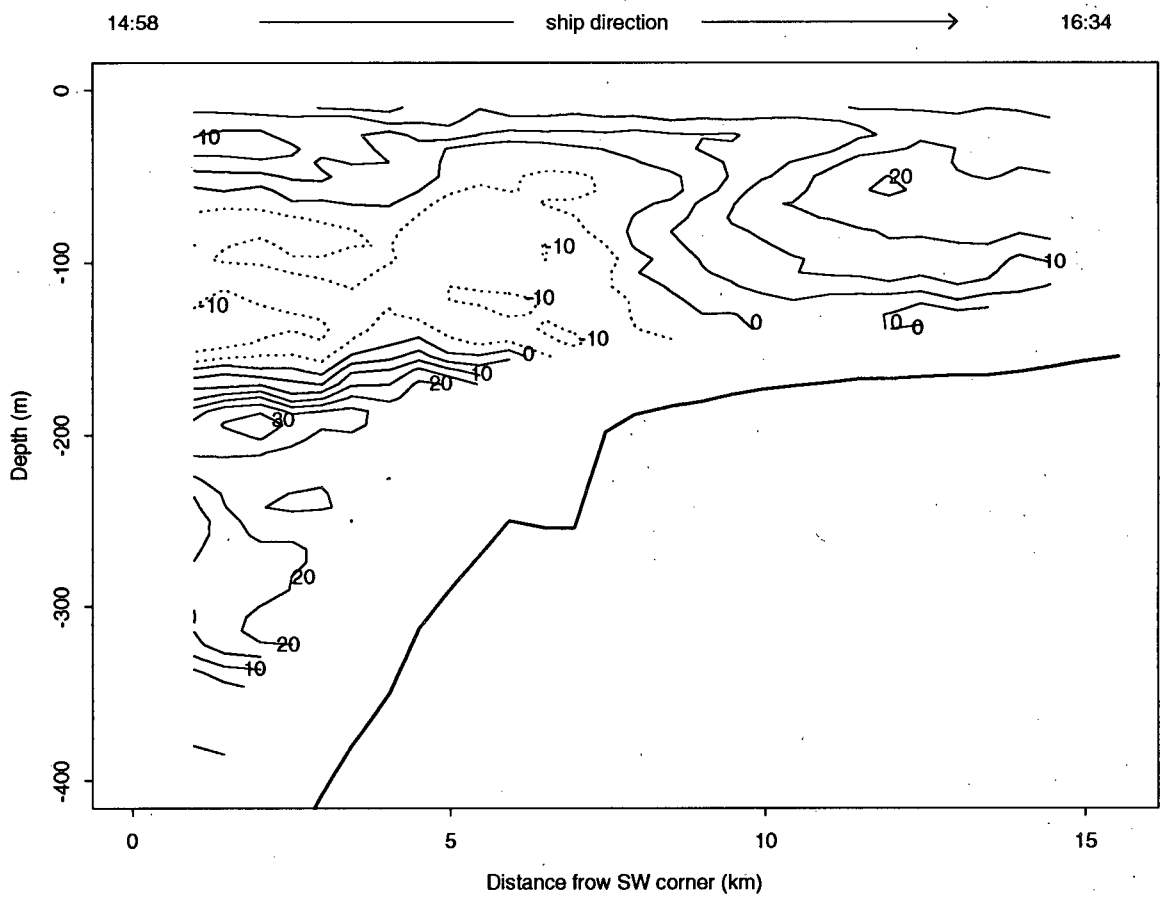

Figure 5.4: (c) Leg 3. Collection times are from 14:58 - 16:34 PDT on 29/06/93 with the ship steaming onshore.

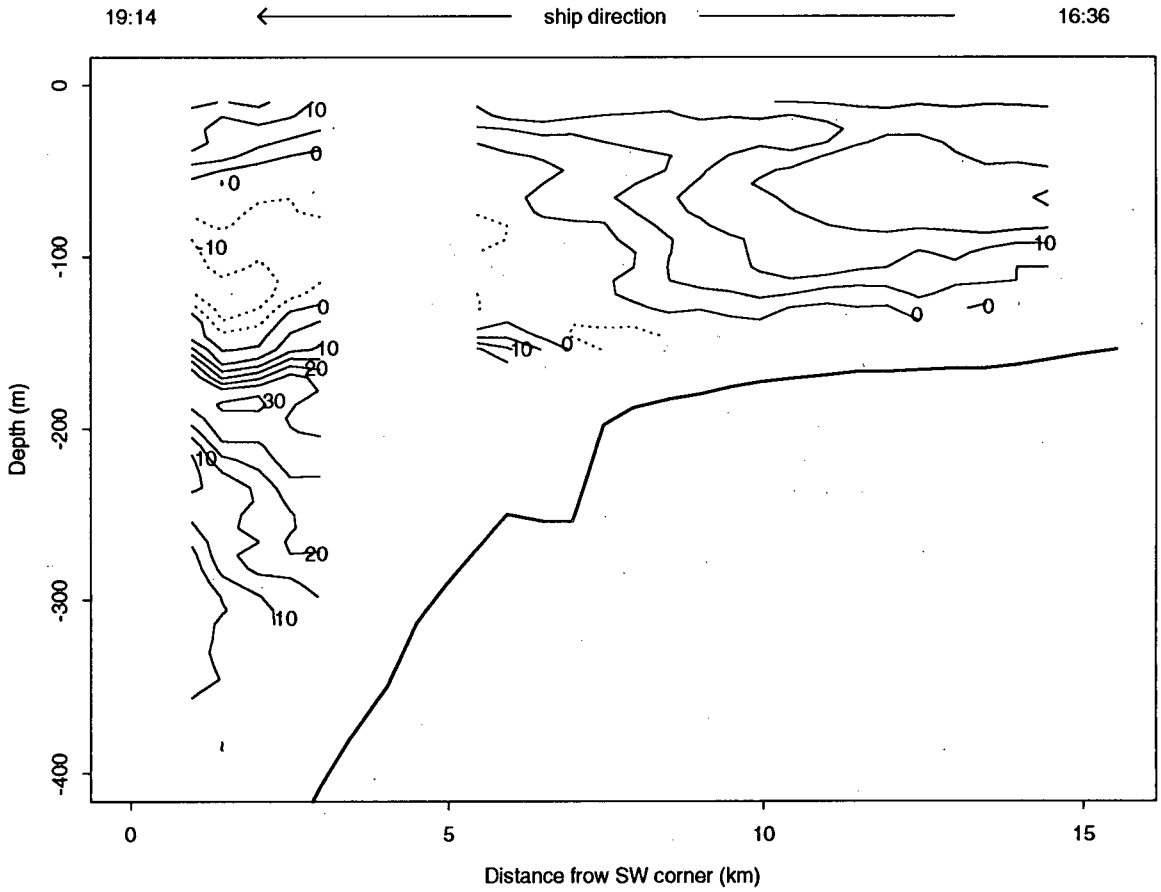

Figure 5.4: (d) Leg 4. Collection times are from 16:36 - 19:14 PDT on 29/06/93 with the ship steaming offshore.

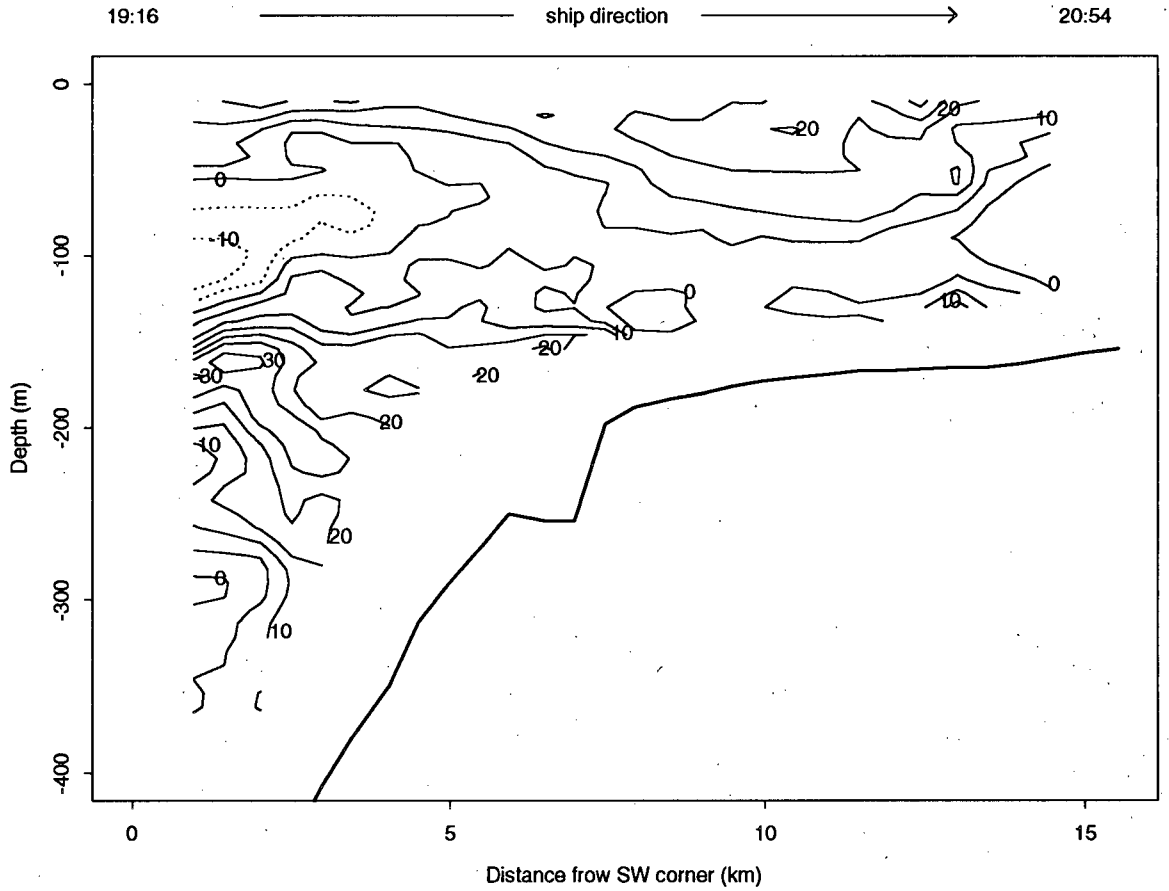

Figure 5.4: (e) Leg 5. Collection times are from 19:16 - 20:54 PDT on 29/06/93 with the ship steaming onshore.

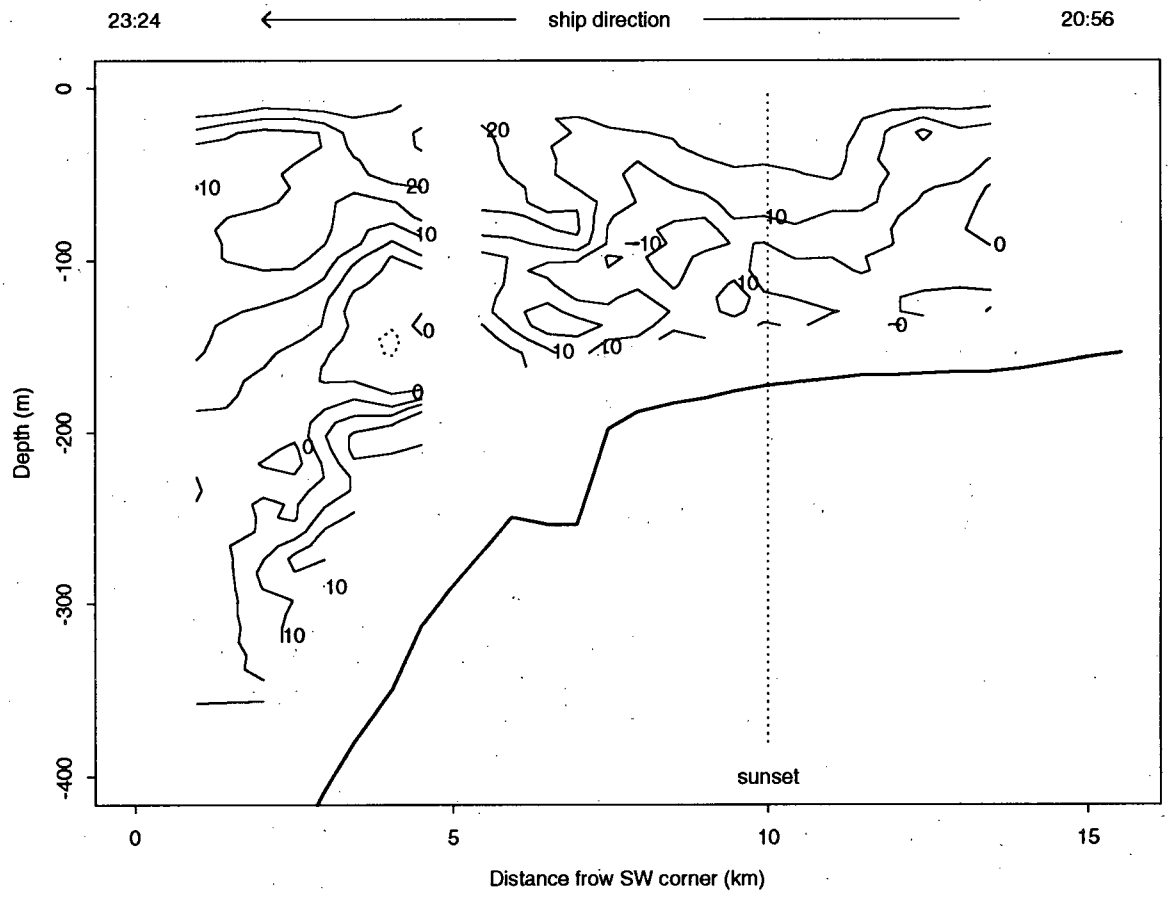

Figure 5.4: (f) Leg 6. Collection times are from 20:56 - 23:24 PDT on 29/06/93 with the ship steaming offshore. Sunset occurred at 21:28 PDT, as shown by the dotted line.

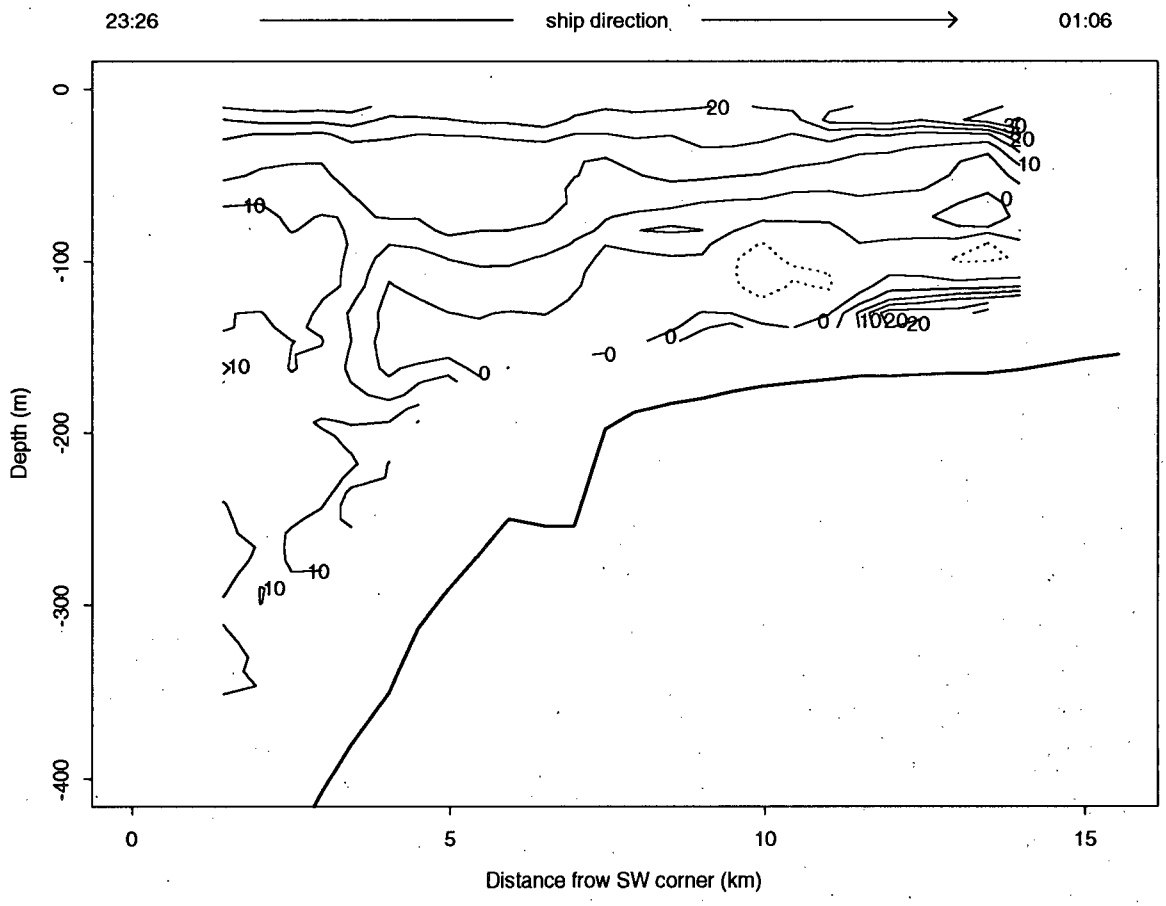

Figure 5.4: (g) Leg 7. Collection times are from 23:26 PDT on 29/06/93 to 01:06 PDT on 30/06/93 with the ship steaming onshore.

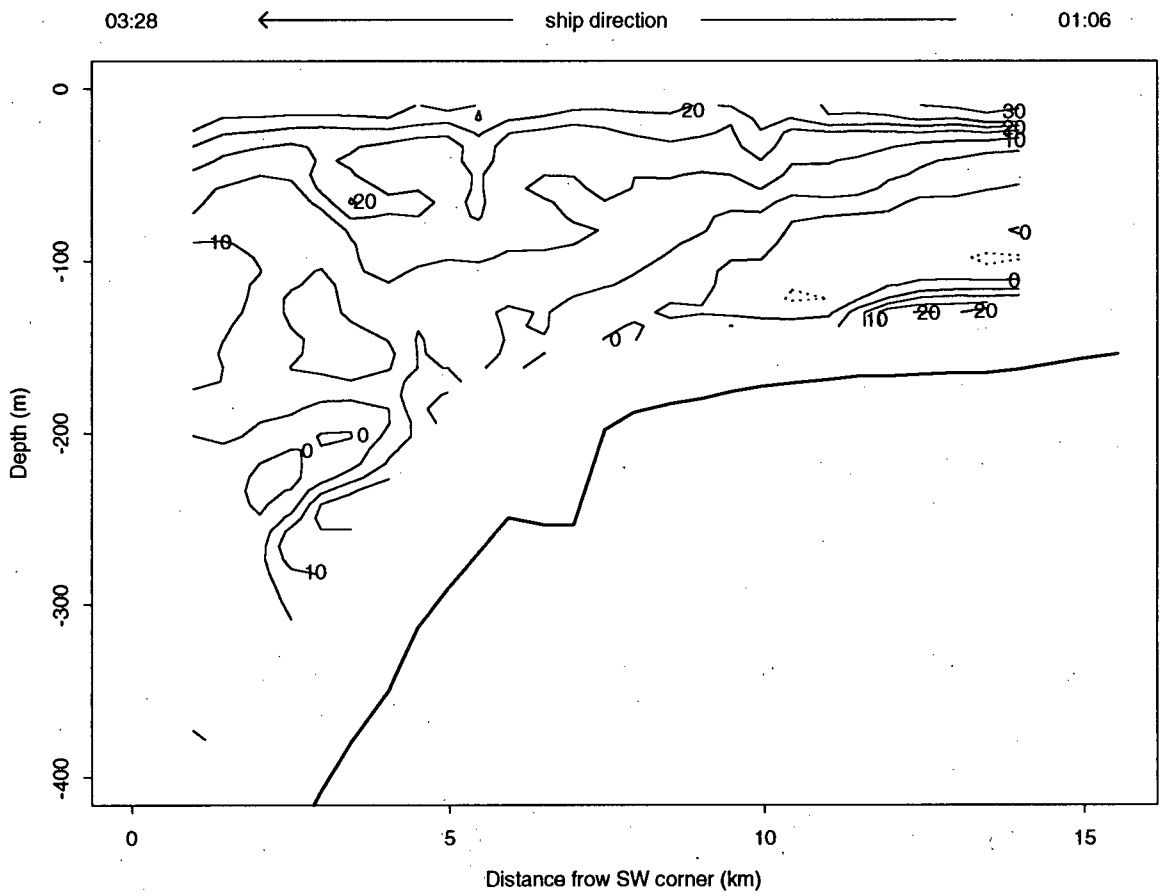

Figure 5.4: (h) Leg 8. Collection times are from 01:06 - 03:28 PDT on 30/06/93 with the ship steaming offshore.

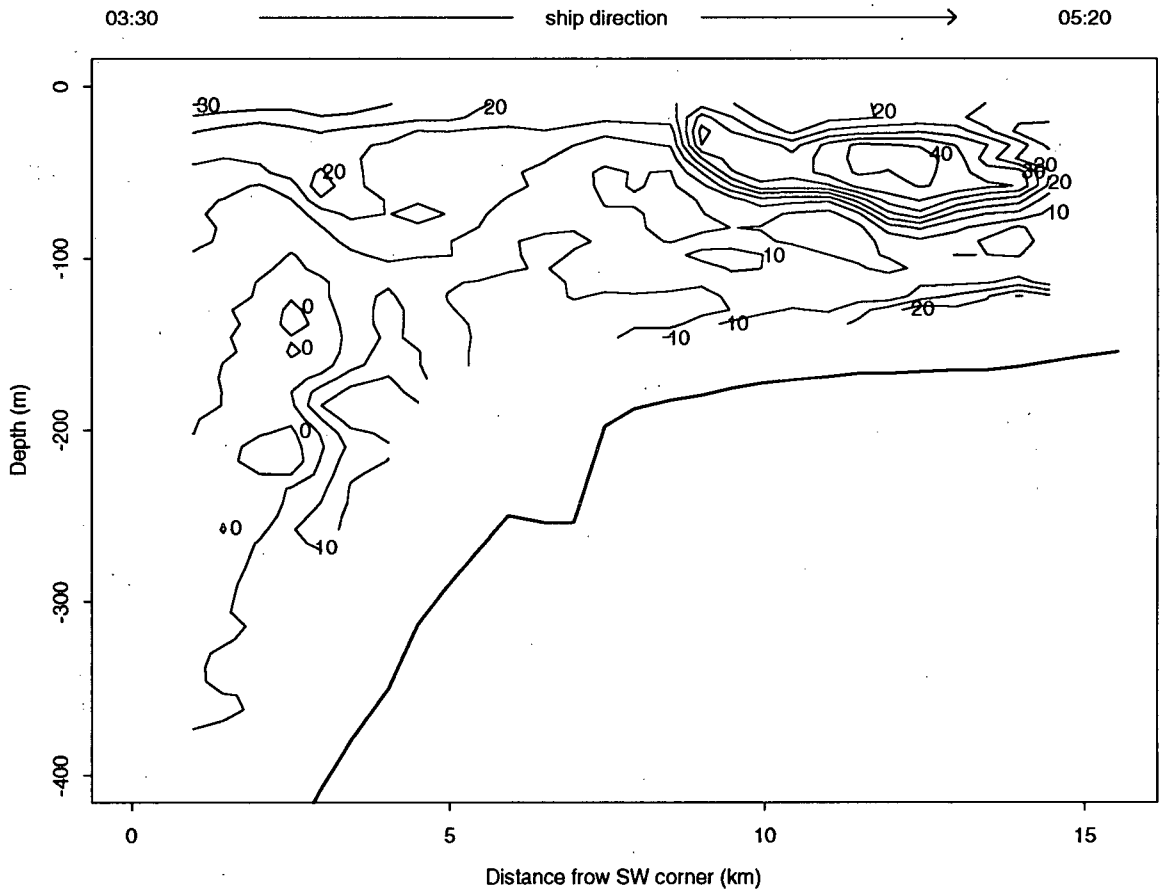

Figure 5.4: (i) Leg 9. Collection times are from 03:28 - 05:20 PDT on 30/06/93 with the ship steaming onshore. Sunrise occurred at 5:24 PDT, just after the ship reached the end of the section

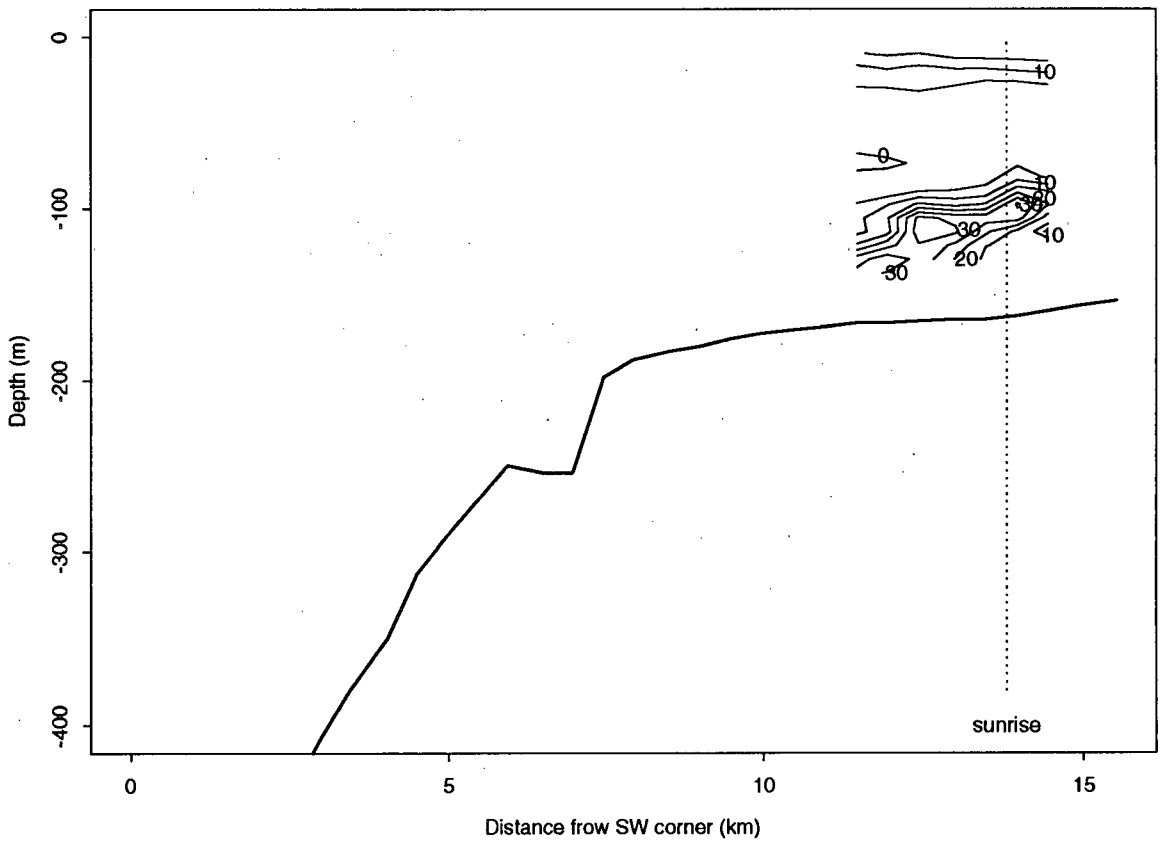

Figure 5.4: (j) Leg 10. Collection times are from 05:20 - 05:50 PDT on 30/06/93. Sunrise occurred at 5:24 PDT, as shown by the dotted line.

17:30 during the 4^{th} leg. This surface scattering layer expanded between 12:00 on the second leg and about 16:00 on the third leg to fill the entire water column to a depth of 130 m and over a distance of 6 km. The cross-shelf movement of the shelf scattering layer was related to strong cross-shelf currents, as will be shown in Chapter 5.1.5. The scattering layer over the slope moved up slightly during the fourth leg, from a depth of 200 m to a depth of about 180 m.

The backscatter structure during the 5^{th} leg was somewhat similar to that observed during the first four legs. The slight vertical rise in the deep water scatterers during the 4^{th} leg continued during the 5^{th} leg, lifting the centre of the scattering layer to about 165 m depth. A depletion of the shelf water scatterers occurred in the bottom 40 m at a distance of $d \approx 10\,km$, and in the bottom 100 m further to the northeast (at a distance d=13–14 km).

Sunset occurred during the sixth leg of the cruise (Figure 5.4f) and the planktonic structure changed drastically. The upper 50 m contained higher backscatter levels, with the largest concentration above the 250 m isobath at $d \approx 4\,km$. The intensity of the scattering layer over the slope was reduced by 10–15 dB, and had moved to lie within about 2–3 km of the shelf break. The mid-depth depletion layer observed during the first 5 legs was nearly gone, with only a small area centered at about 150 m depth, at $d \approx 3\,km$.

The structure remained approximately the same for the next 6 hours (legs 7-9; Figures 5.4g-i). High concentrations filled the upper 50 m across the entire survey line. The deep water scatterers remained at a constant level and stationary near the bottom as in the 6^{th} leg. The only major difference was a depletion layer which formed between the sixth and seventh legs of the cruise, extending over 100–150 m depth in the shallow water from the northeast corner out to 2 km beyond the shelf break. This depletion layer was reduced during the 8^{th} leg and had disappeared by the time the ship returned over the

shelf during the 9^{th} leg.

A strong scattering layer appeared at a depth of about 30 m over the shelf near the northeast corner of the survey line during the ninth leg. This aggregation was only about 2–3 km wide and had backscatter levels about 20 dB higher than typical shallow water levels, which corresponds to a 100-fold increase in acoustic cross-section. It was not present at 01:00–02:00 during the 8^{th} leg and had disappeared by 05:30 when the ship returned on the 10^{th} leg. The 10^{th} leg revealed, instead, a strong scattering layer just above the bottom at a depth of about 110 m. These bottom scatterers in the northeast corner of the survey line over the shelf appeared first during the 7^{th} leg, with backscatter levels of about + 10 dB, remained at this level during the 8^{th} and 9^{th} legs, intensifying to about + 25 dB in the early morning hours between the 9^{th} and the 10^{th} legs.

The strong scattering layer which appeared in the surface waters during the ninth leg is thought to be a patch of euphausiids which was advected into the survey area between 02:00 and 04:30, and which subsequently descended to the deep waters near the bottom just prior to sunrise (05:30). In Chapters 5.1.4 and 5.1.5, it is shown that the appearance of the patch was correlated with a reversal of the local water flow from southeastward to northwestward. The composition of the patch will be discussed further in Chapter 5.1.5.

Vertical time series

To get a better idea of the major changes occurring in the survey region near sunset, the data were plotted as time series for each grid point, or $S'_v(z_k, t_j)$ for fixed d_i. Figures 5.5a-e are contoured time series for each of five grid-points 8, 10, 14, 24, and 48, which are located at survey line distances of d=1, 1.5, 2.5, 7.5, and 19.5 km, and over water depths of 600, 500, 400, 250, and 170 m, respectively. Sunset occurred at t=11.3 hours. Sunrise occurred at t=19.3 hours, which is only relevant for grid-point 48, since data were only taken in the early morning at the northeastern corner of the survey line (grid-points

48–64).

Grid-points 8, 10 and 14 over the continental slope revealed nearly identical variability with depth and time. A strong deep scattering layer was present near depths of 200 m from t=0 to t=7 hours, with residuals of 20–30 dB. The upper layers (0–50 m) during this period had scattering levels of about 10 dB, whereas the mid-depths (50–150 m) had levels about 20 dB lower, or about -10 dB. The structure underwent a major change after about 18:00 (t=8 hours). The deep water (>150 m) scattering levels were reduced by about 20 dB, whereas the surface waters underwent a 10–15 dB increase and the mid-depth waters underwent a 20–25 dB increase.

The change in structure at $t = 8$ hours in the time series for Grid-points 8, 10 and 14 is attributed to an upwards migration of zooplankton. The possibility of horizontal advection of zooplankton into the depths between 50 and 150 m can be ruled out. The deep scattering layer, which extended over about 50 m prior to 18:00, rose to occupy the upper 100 m by sunset (t=11.3 hours). This sets the mean vertical swimming speeds at 1–1.5 cm/s. Vertical migrations on these speed and distance scales are common for euphausiids. Hardy and Bainbridge (1954) measured the average swimming speed of a euphausiid at 2.5 cm/s. Pieper (1971) observed euphausiids in Saanich Inlet, British Columbia migrating upwards at sunset with mean speeds of about 2 cm/s. Maximum swimming speeds for euphausiids have been measured by Kampa (1975) at 5–6.5 cm/s. Simard and Mackas (1989) observed *Euphausia pacifica* on the Vancouver Island continental margin occupying daytime depths of 100–150 m (on the shelf) and 150–200 m (at the shelf break), and rising to occupy the surface waters at dusk. Bollens et al. (1992) observed *Euphausia pacifica* in Puget Sound occupying 50–125 m during the day and the upper 25 m at night. Genin et al. (1988) observed *Euphausia pacifica* in the Southern California Bight residing below 200 m during the day and rising to the upper 50 m at night.

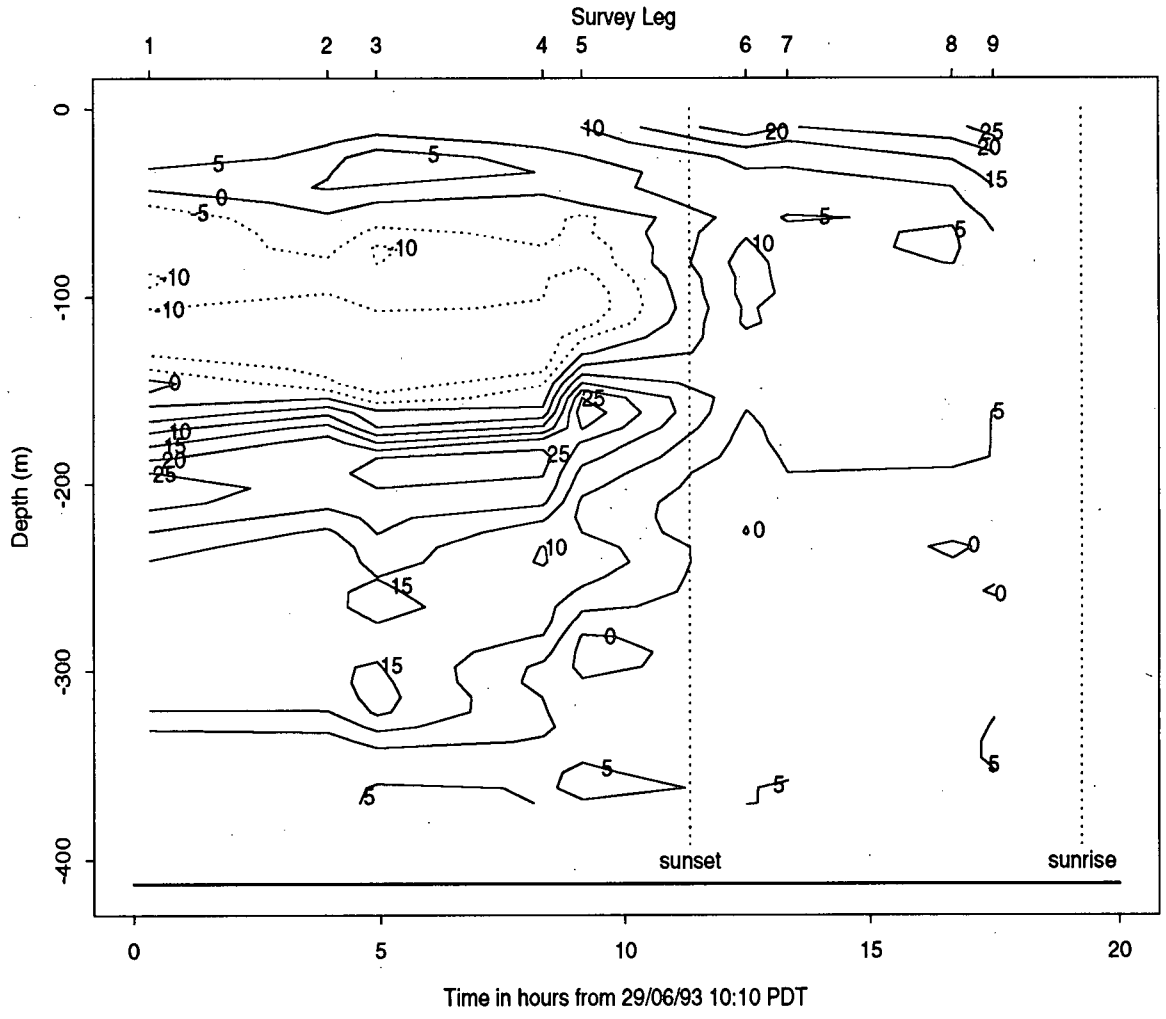

Figure 5.5: (a) Time series of backscatter residuals $S'_v(z_k, d_i)$(dB) at grid-point–8. The water depth is shown with a solid horizontal line at depth = 413 m.

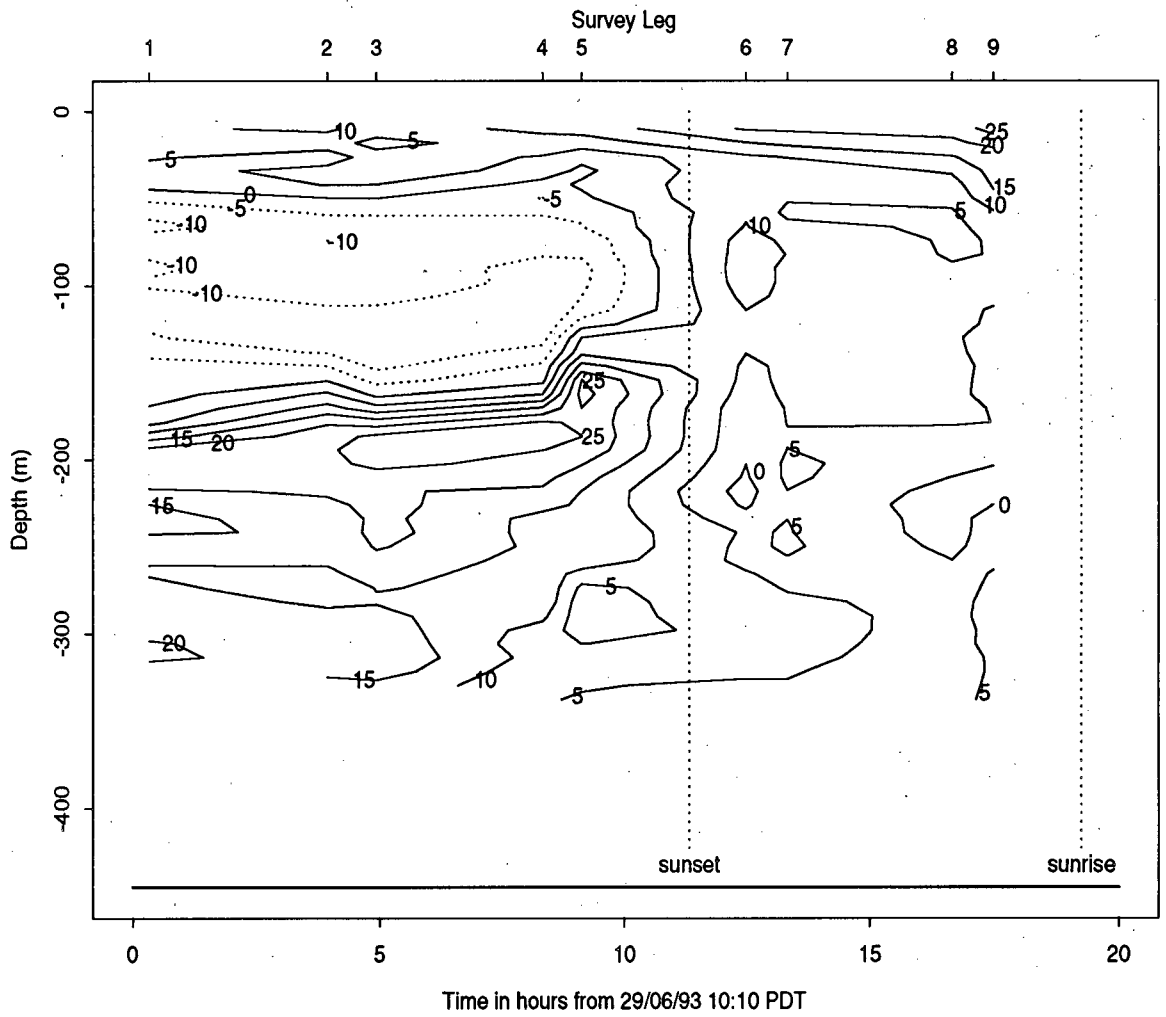

Figure 5.5: (b) Same as Figure 5.5a but at grid-point–10, water depth = 445 m.

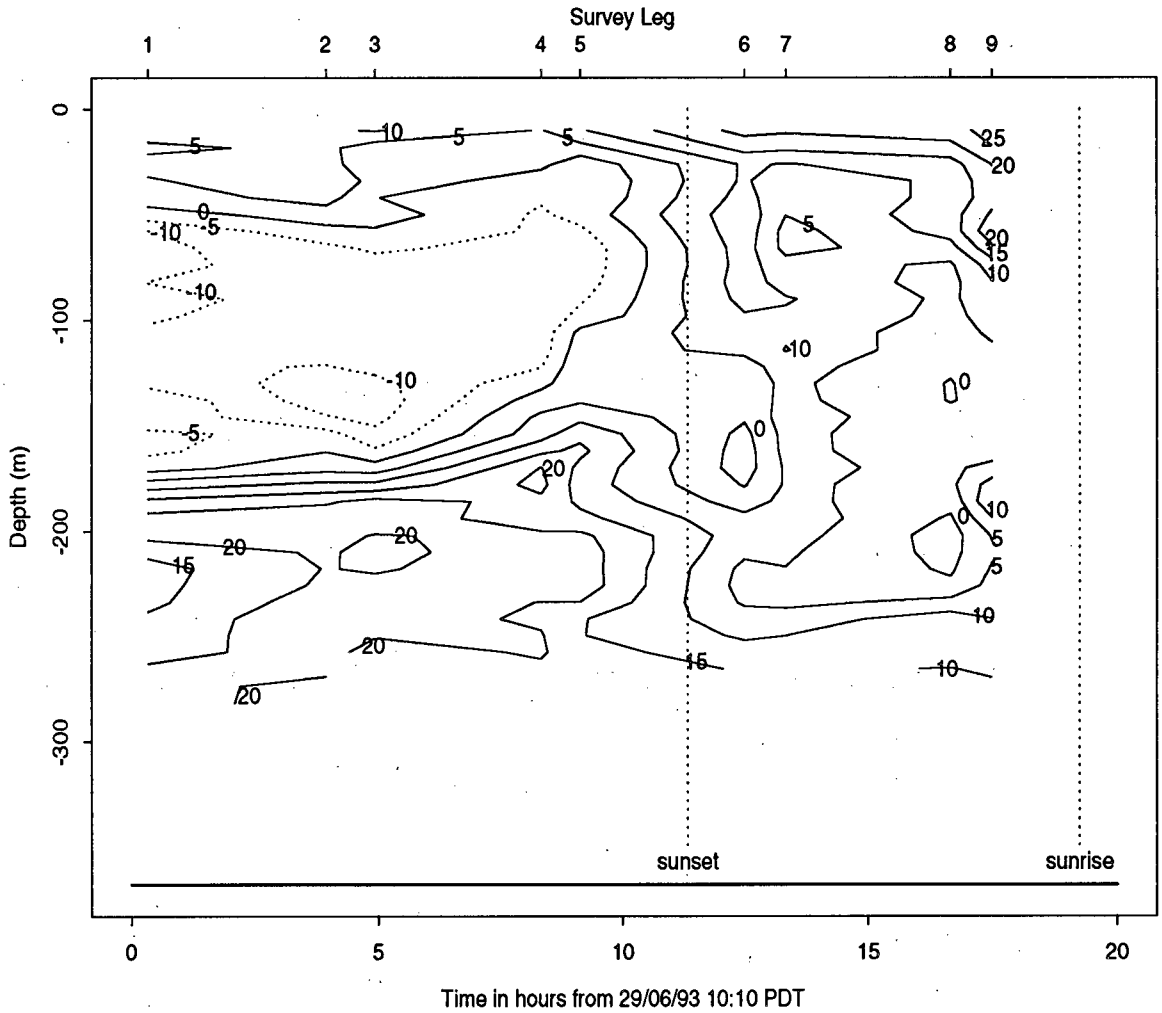

Figure 5.5: (c) Same as Figure 5.5a but at grid-point–14, water depth = 367 m.

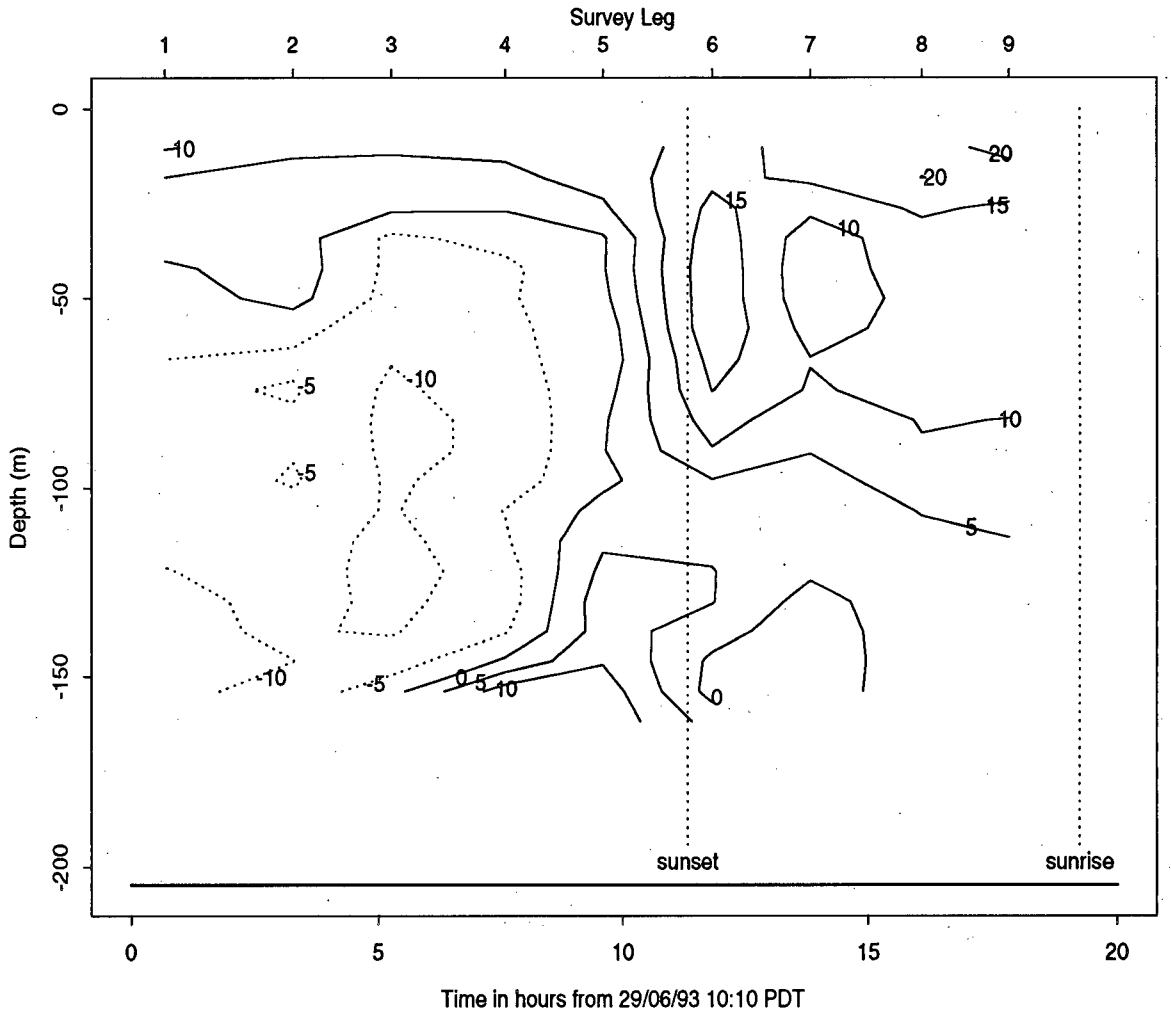

Figure 5.5: (d) Same as Figure 5.5a but at grid-point–24, water depth = 205 m.

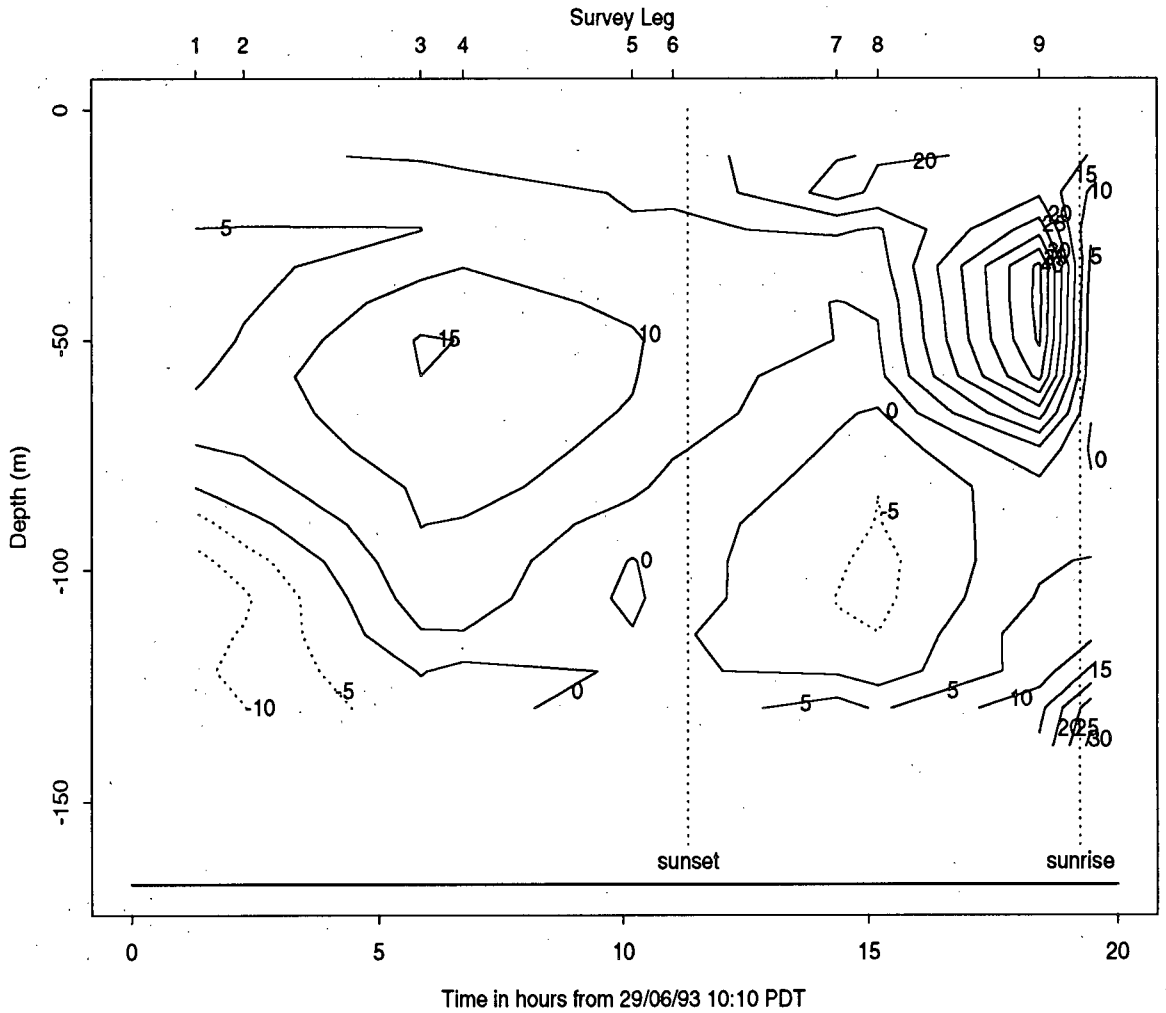

Figure 5.5: (e) Same as Figure 5.5a but at grid-point–48, water depth = 168 m.

The vertical migration at sunset is apparent in the time series for grid-point–24 as well (Figure 5.5d). The top of the deep scattering layer is visible for a few hours prior to sunset at about 150 m. This scattering layer is no longer apparent after t=11 hours. The surface water concentrations of scatterers increased by 10–15 dB about an hour prior to sunset, and remained at this higher level for the remainder of the time series. This nighttime shallow water scattering layer extended from the surface down to about 100 m depth.

Grid-point–48, over the shelf, had a different scattering layer variability than the profiles over the slope. During the first 5 hours (survey legs 1–3), the concentrations at depths of 80–100 m increased by about 15 dB, as observed in Figure 5.4b and Figure 5.4d, while the scattering levels in the shallower waters remained constant. A slight vertical migration of the deep water scatterers started at about t=7 hours, simultaneously with an increase in surface water scattering levels of about 10 dB. The most remarkable feature of this time series is the strong scattering layer which appeared abruptly at t=16 hours (01:00 on 30/06/93). This feature also appears in Figure 5.4i. It is visible as well in similar time series for grid-points 50, 52, 54 and 56. As discussed above, this patch is thought to have been advected into the survey area and then to have descended into the near-bottom waters just prior to sunrise. This downward migration is visible in Figure 5.5e, with a strong scattering layer (25 dB) appearing at t=19.5 hours in the water below 130 m.

Last hour time series

In order to see more clearly what happened during the last hour of the survey period, the profiles taken from 04:36 to 05:50 in the morning of the 30^{th} of June, 1993 are examined more closely. Figure 5.6 is a map of the ship track during this 74 minute period, with the recording times for each profile, and the approximate length scales important for the

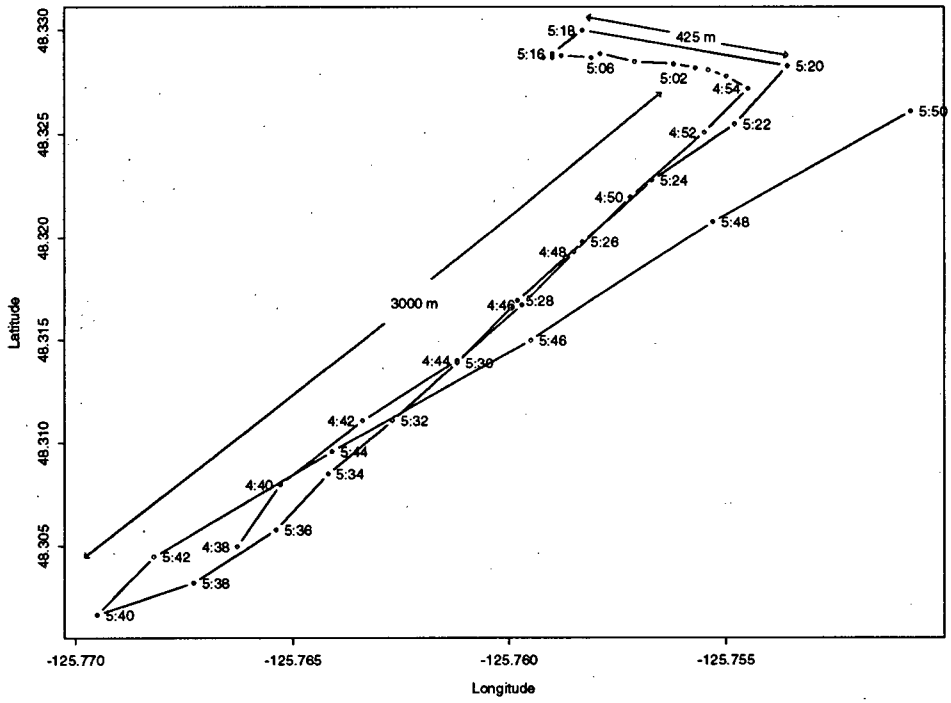

Figure 5.6: Ship track for the last 74 minutes of the survey period. PDT times are given as well as approximate length scales.

analysis. The ship traveled up an 'L' shaped path from 04:36–05:16, then back down the same path from 05:18–05:40, and returned up nearly the same way from 05:40–05:50. The ship moved over a distance of about 3 km during the first 14 minutes, and again over the last 30 minutes. However, from 04:54–05:20, the ship was stationary to within 500 m. At any given time, horizontal homogeneity is assumed for the region covered by the ship. This assumption allows the backscatter residual profiles to be contoured as a time series (Figure 5.7). The strong scattering layer was located in the upper 70 m during the first 20 minutes of this time series (see also Figures 5.4i and 5.5e). Following twilight start at 04:45, this layer underwent a slight decrease in scattering level (5–10 dB), as well as a slight increase in depth (10–20 m). Just after 05:00, about 20 minutes prior to

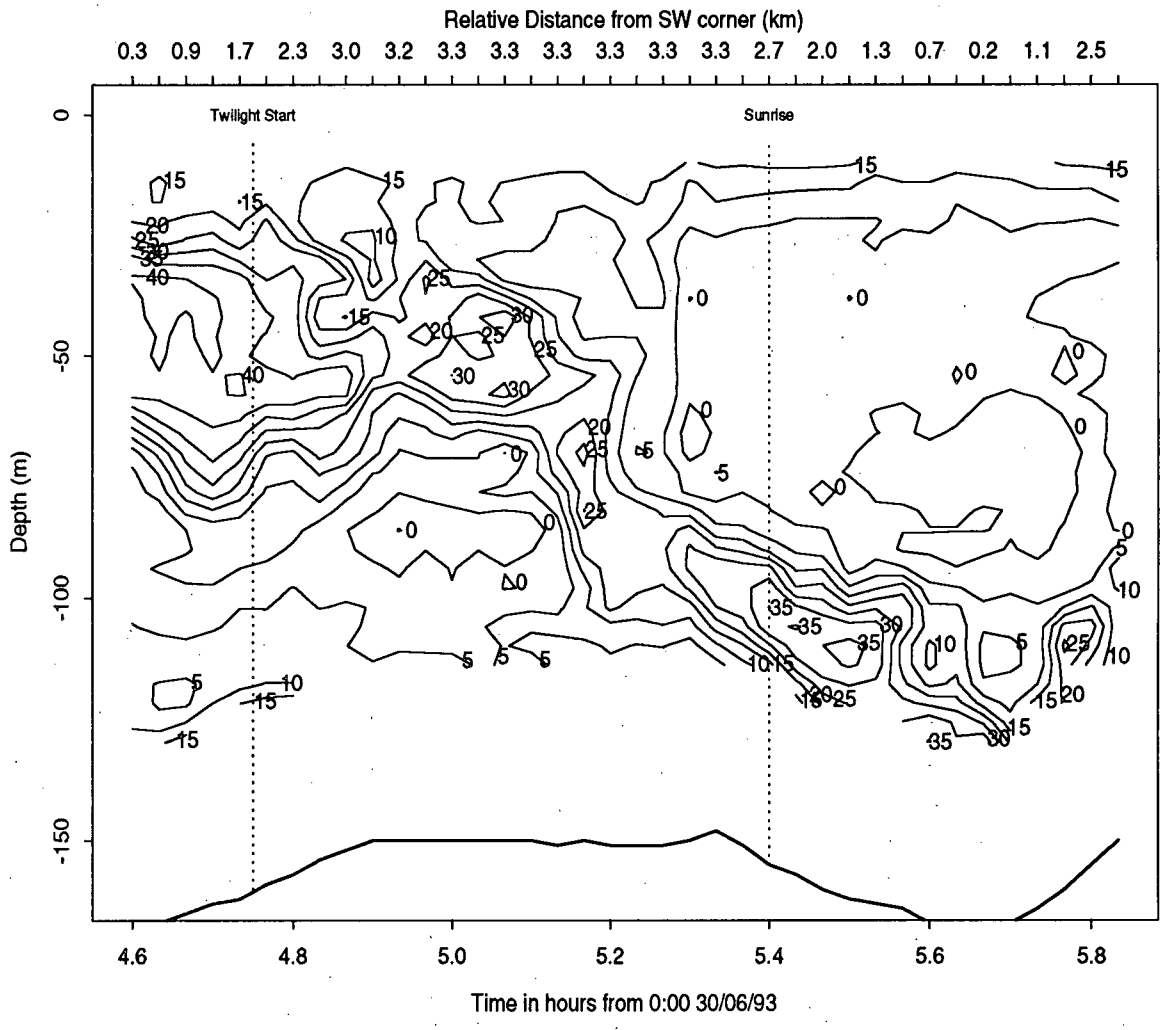

Figure 5.7: Time series of backscatter residuals (dB) for profiles taken from 4:36 to 5:50 on 30/06/93. Civil twilight start and upper limb sunrise are shown as dotted lines at 4:45 and 5:24, respectively.

sunrise, the scattering layer underwent an abrupt descent, reaching a depth of 100–120 m at about 05:30, or about 10 minutes after sunrise. It remained at this depth near the bottom from 05:30 to the end of the time series at 05:50. The time and length scales of this descent gives mean swimming speeds of 3–4 cm/s. These rates are a factor of two higher than the rates observed for the scattering layer migrating upwards at sunset, and are consistent with Pieper (1971), who observed downwards migratory speeds at sunrise of about 3 cm/s. The major temporal changes in the overall zooplankton structure dominated any spatial variations during this time series, justifying the assumption of horizontal homogeneity.

Horizontal time series

The final method of observing the various advective and migrational motions of the zooplankton aggregations is to look at horizontal time series, or contour plots of $S'_v(d,t)$ for constant z_k. Figures 5.8a-i are such horizontal time series, in 24 m depth bins from 6 m to 224 m.

The shallow water (6–80 m) scattering levels (Figures 5.8a-c) increased over the south-west half of the survey line (d=2–11 km) by about 10 dB from t=7 to t=12 hours (17:00–22:00). This increase is due to the upwards migration of zooplankton at sunset. The scattering levels over the shelf (from d=11 to d=14 km) remained roughly constant over this time period, but underwent a 5–10 dB increase from t=11 to t=15 hours. A strong scattering layer (also see Figures 5.4i and 5.5e) appeared at d=10–12 km and t=18 hours in the two shallowest bins (6–56 m), disappearing during the 10^{th} leg at t=19 hours.

The scattering levels at mid-depths (80–128 m) (Figures 5.8d-e) increased by 10–15 dB just prior to sunset over the slope (d=2–10 km), and between t=3 and t=5 hours (13:00–15:00) over the shelf (d=10–12 km). The increase over the shelf corresponds to

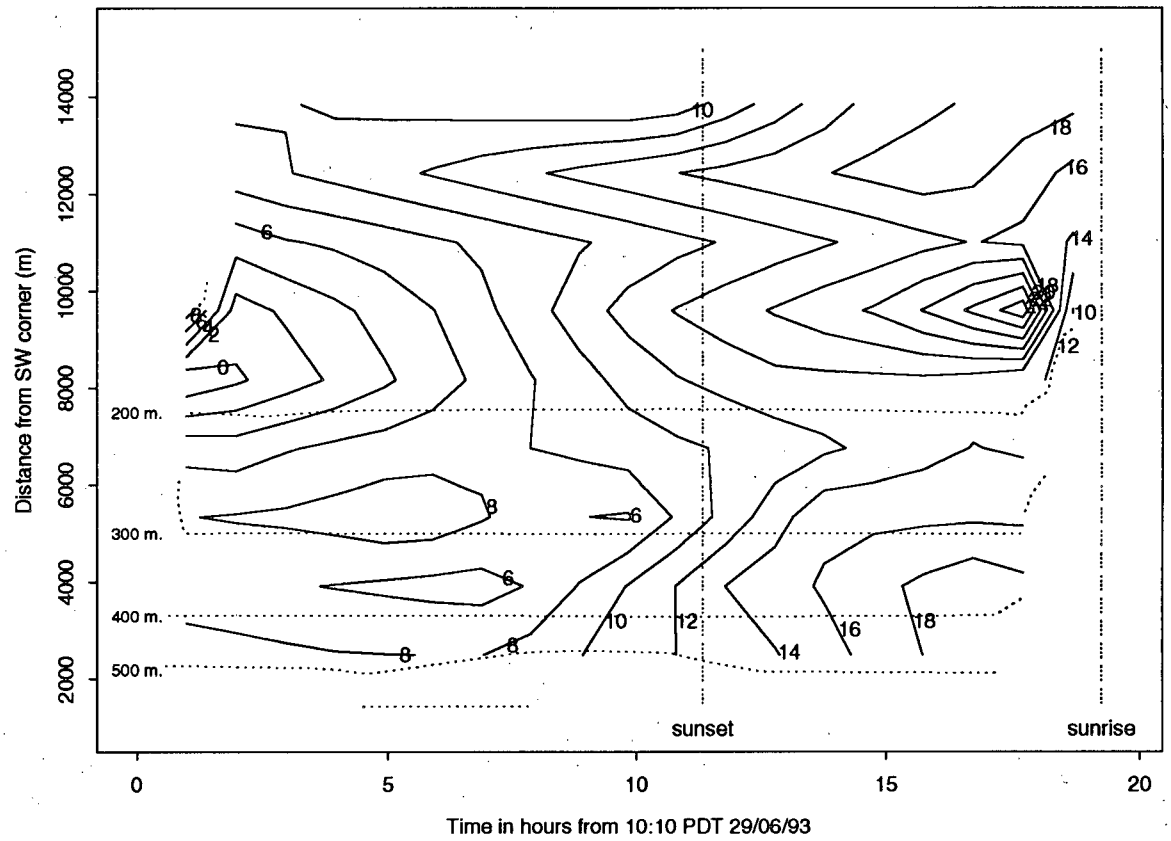

Figure 5.8: Survey line horizontal time series of backscatter residuals (dB). Bottom contours are shown as horizontal dotted lines at depths of 200, 300, 400 and 500 m. Sunrise and sunset are indicated by dashed-dotted lines at 11.33 hours and 19.25 hours, respectively. (a) Averaged over the acoustic depth range [6:32] m.

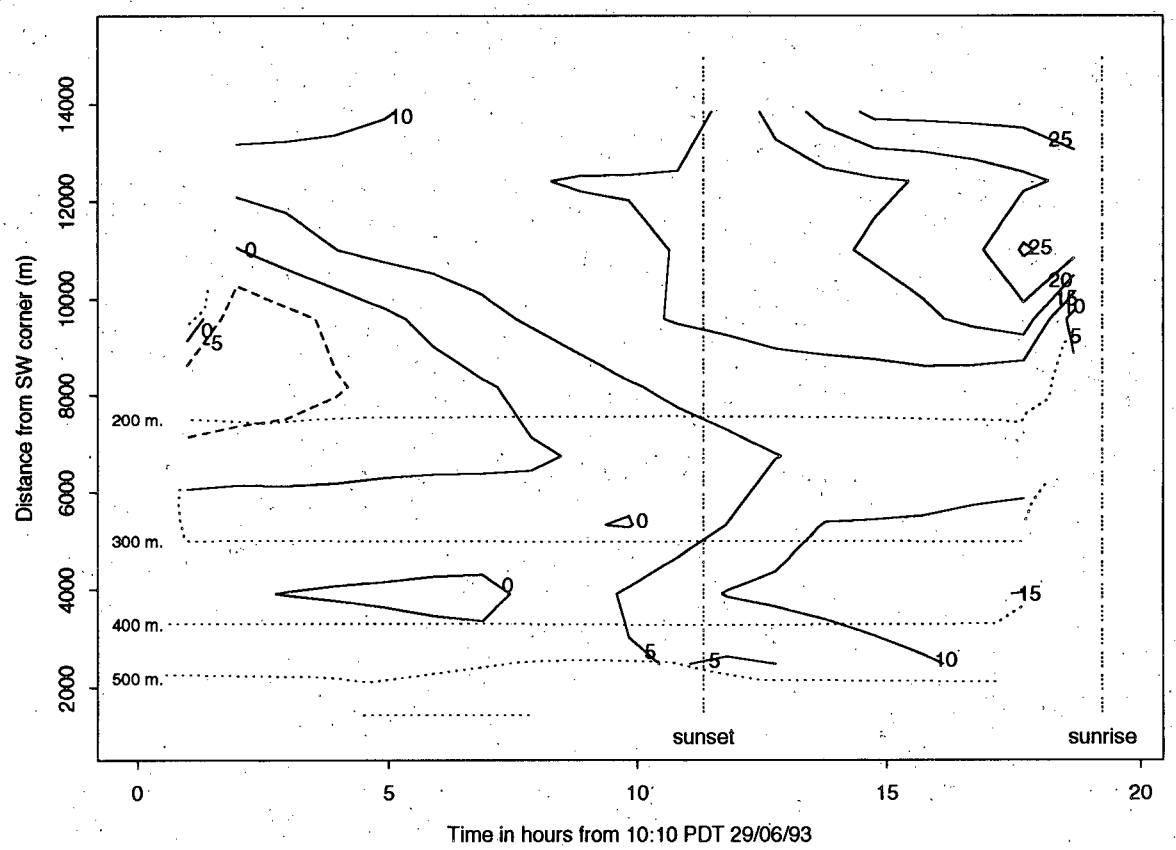

Figure 5.8: (b) Averaged over the acoustic depth range [32:56] m.

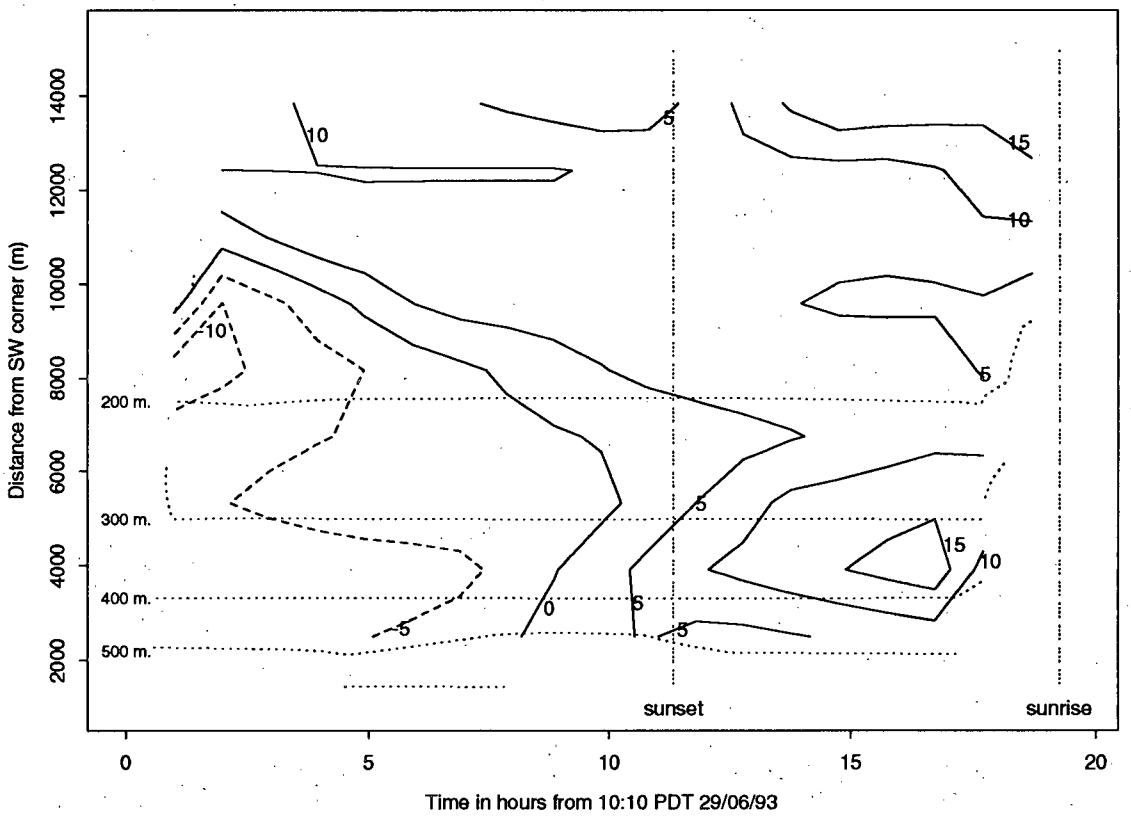

Figure 5.8: (c) Averaged over the acoustic depth range [56:80] m.

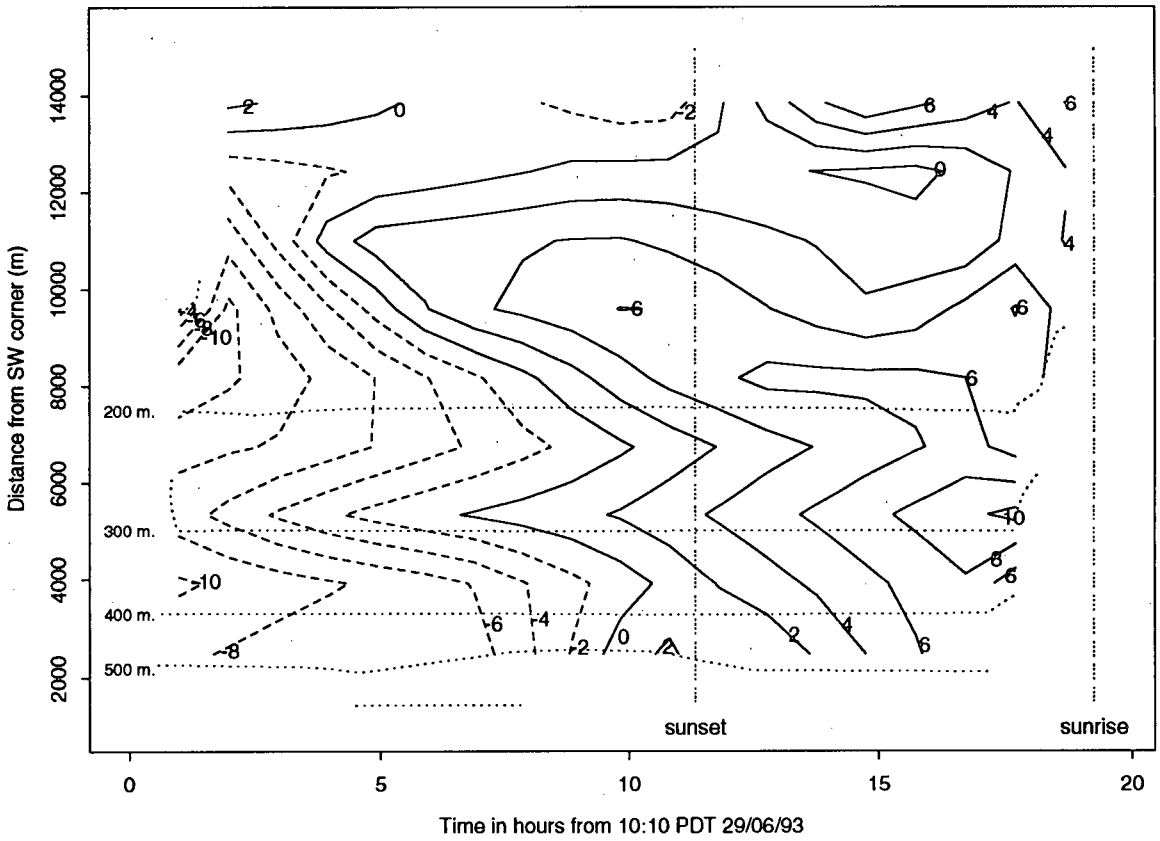

Figure 5.8: (d) Averaged over the acoustic depth range [80:104] m.

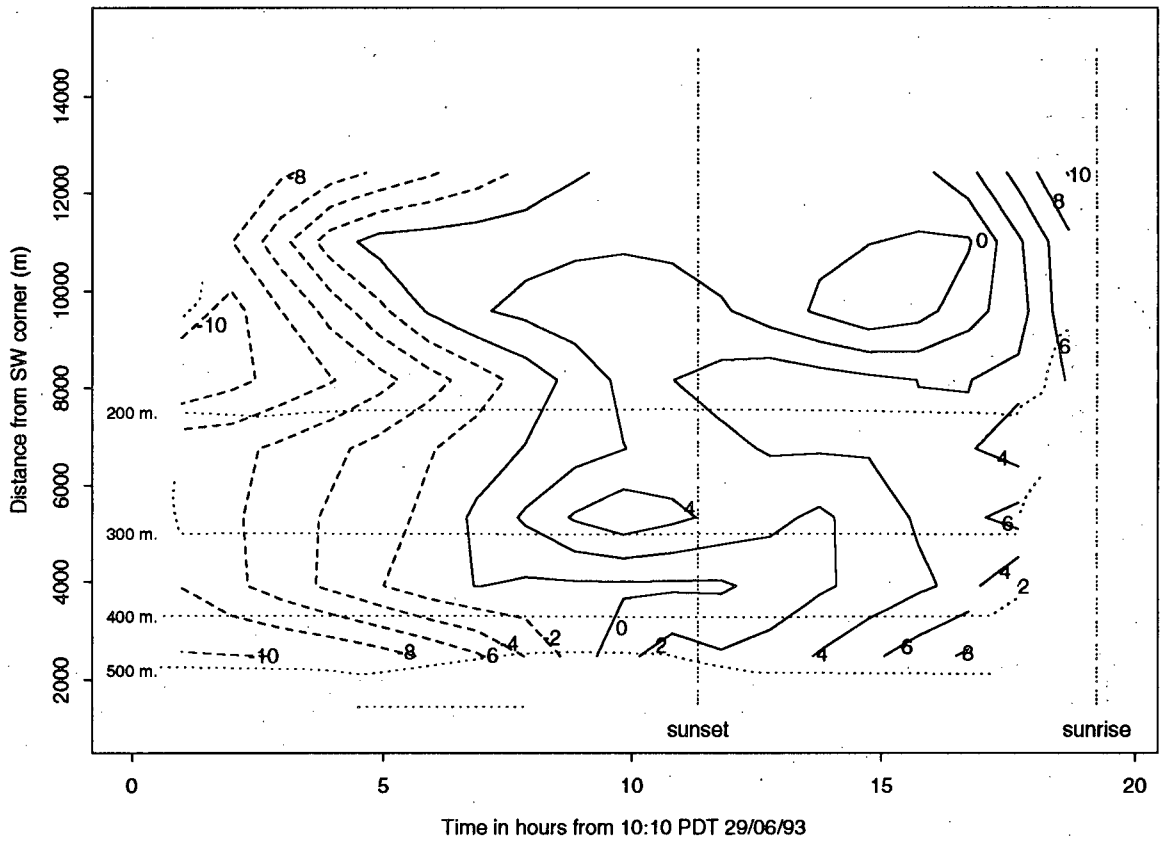

Figure 5.8: (e) Averaged over the acoustic depth range [104:128] m.

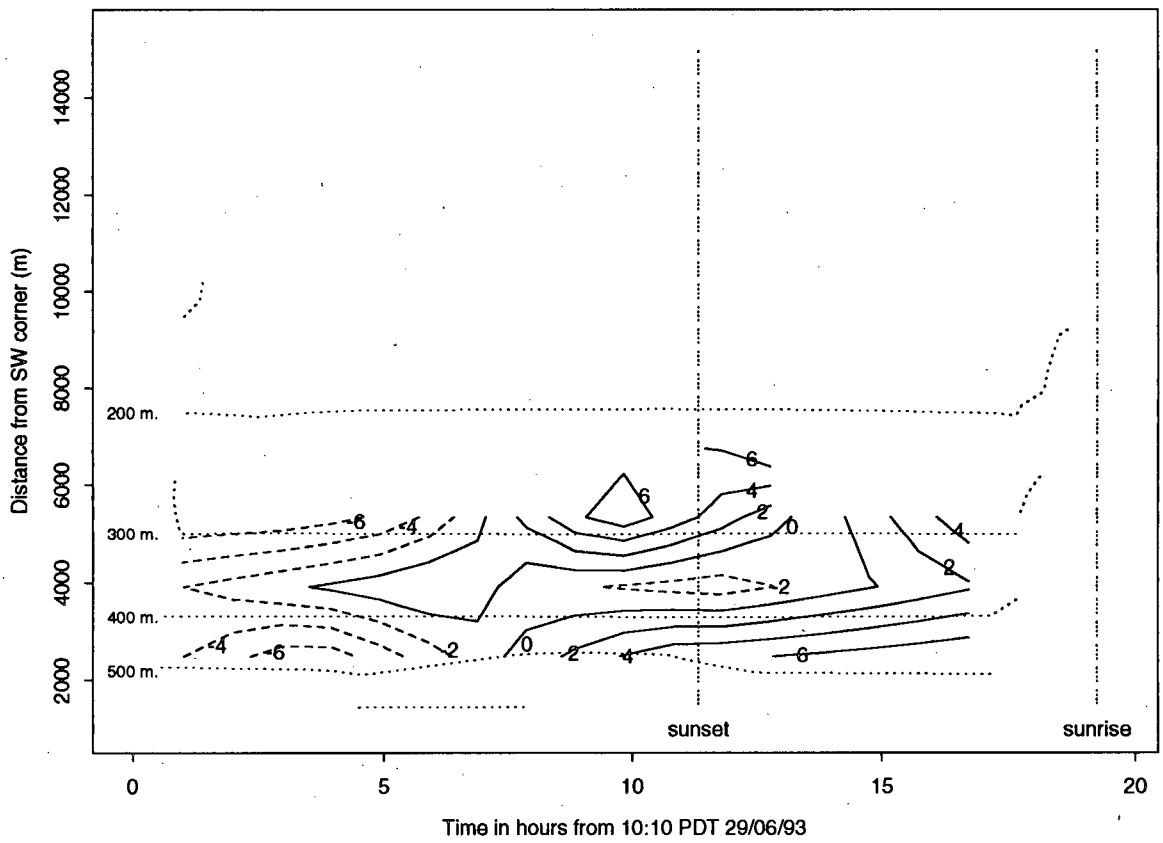

Figure 5.8: (f) Averaged over the acoustic depth range [128:152] m.

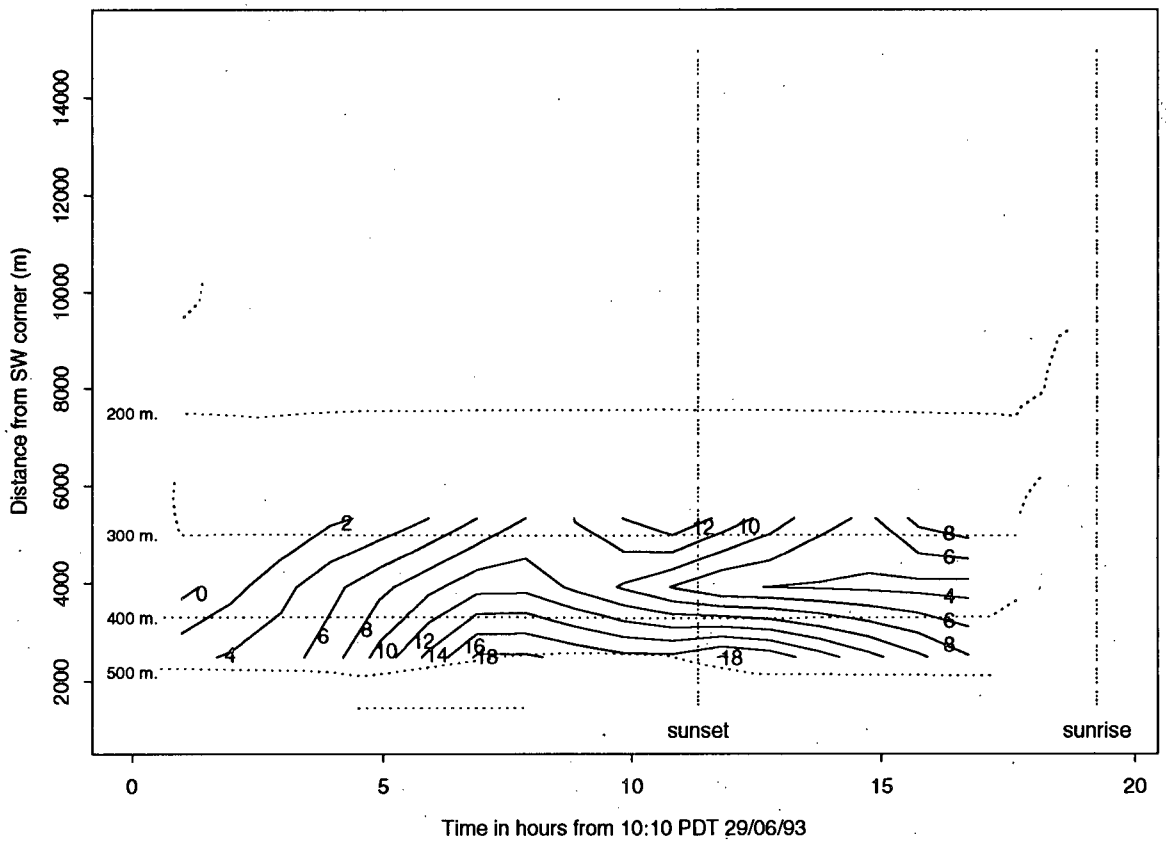

Figure 5.8: (g) Averaged over the acoustic depth range [152:176] m.

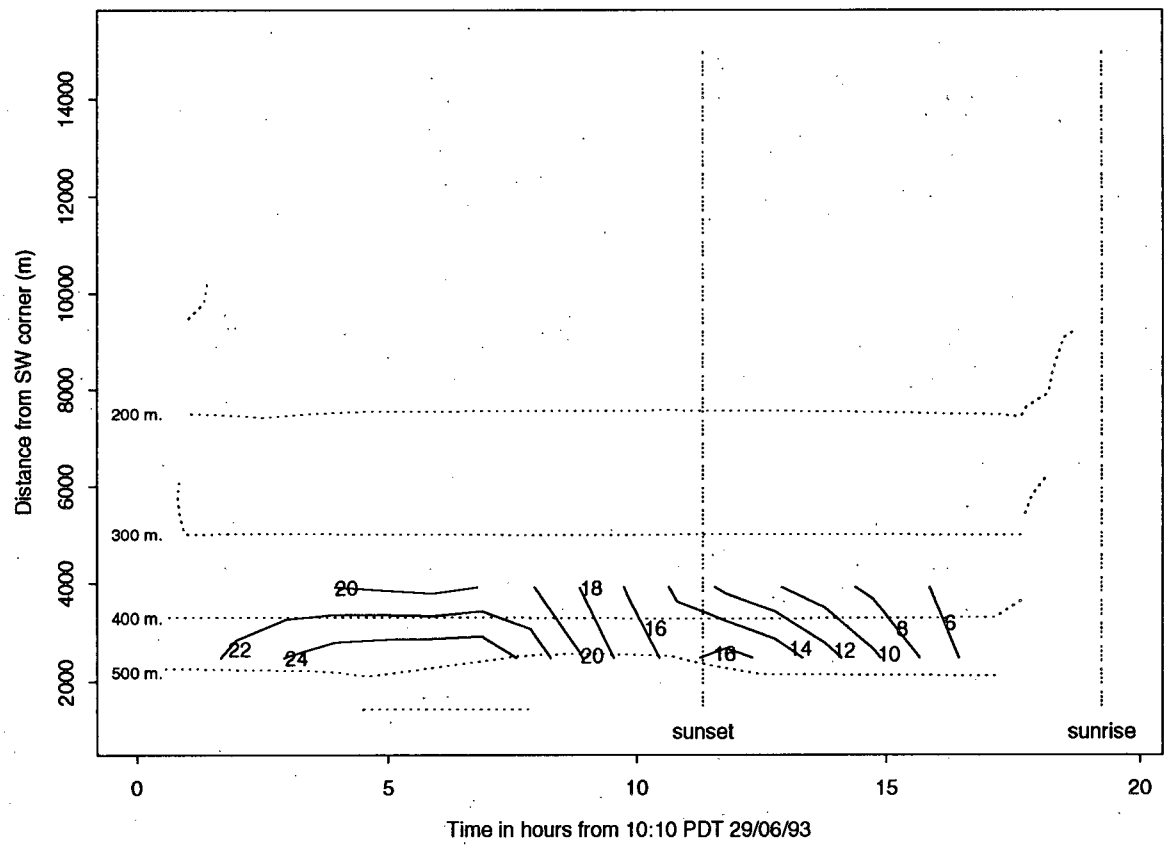

Figure 5.8: (h) Averaged over the acoustic depth range [176:200] m.

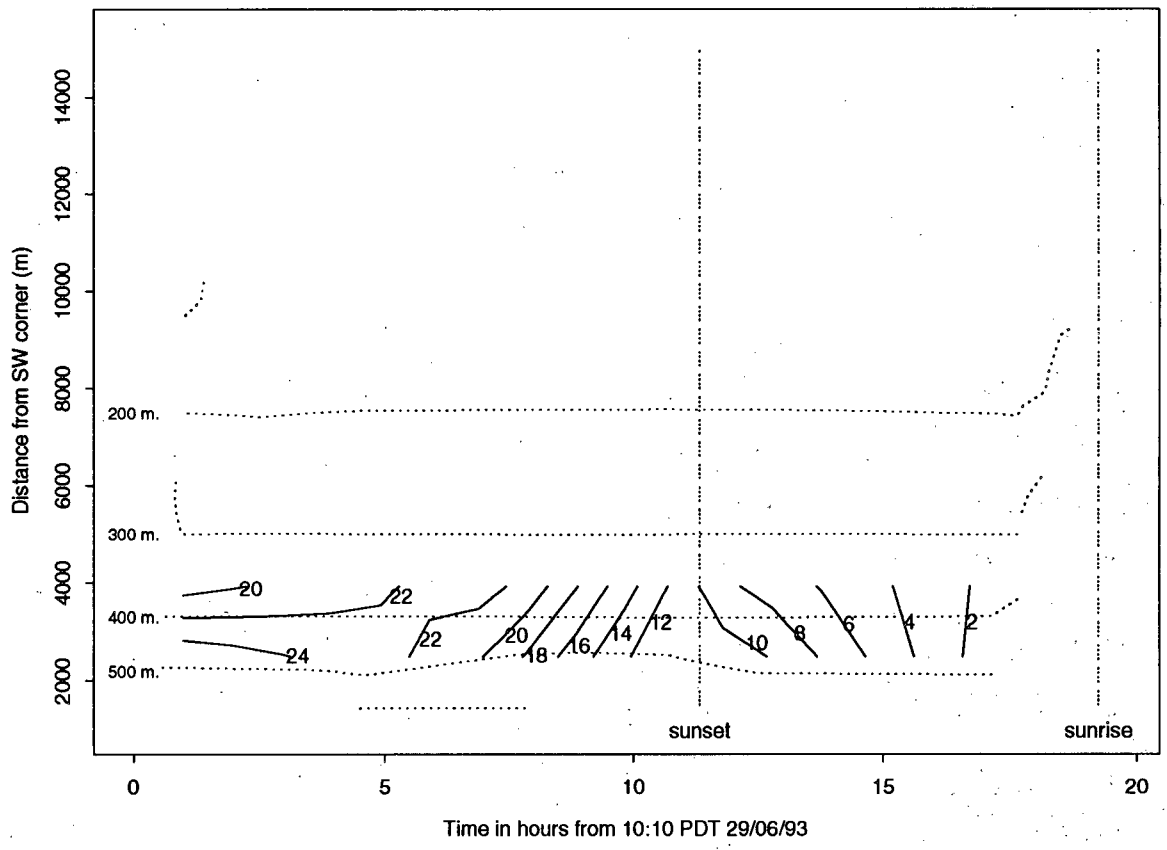

Figure 5.8: (i) Averaged over the acoustic depth range [200:224] m.

the increase observed in Figures 5.4b–c, and Figure 5.5e. The depletion layer seen over the shelf at depths of 100–150 m in Figures 5.4g and 5.4h is also visible in Figures 5.8d and 5.8e between t=14 and t=15 hours.

The deep water (128–176 m) scattering levels (Figures 5.8f-g) over the slope increased by about 10 dB from t=7 to t=12 hours, followed by a slight decrease ($\approx 5\,dB$) from t=12 to t=16 hours, corresponding to the vertical migration of the zooplankton past these depths on their way up to the shallower water. The scattering levels in the deepest bins (176–224 m) (Figures 5.8h-i) decreased from t=7 to t=12 hours by about 10 dB, corresponding once again to the upwards migration of zooplankton out of these depths.

Summary of Scattering Layer Distributions

Four major changes in zooplankton structure were observed during the survey period. Two of these relate to vertical migration of zooplankton upwards at sunset and downwards at sunrise. The other two are probably due to advection by the currents.

1. An upwards vertical migration of deep water (150–200 m) scatterers to the surface layers at sunset, from 17:00-22:00 on 29/06/93, with estimated swimming speeds of 1–2 cm/s. Some of the deep water scatterers also appeared to remain at their daytime depths, only moving in closer to the shelf break.

2. A quick downwards vertical migration of the scatterers in the surface waters over the shelf from the surface waters (30–50 m) to the near bottom waters (100–120 m) just before sunrise on 30/06/93, with swimming speeds about twice those observed during the upwards migration at sunset, or 3–4 cm/s.

3. An increase in scattering levels over the shelf at depths of 80–130 m between t=3 and t=5 hours. This does not appear to be vertical migration of plankton

downwards, because the concentrations in the upper layers (10–80 m) maintain a constant scattering level, and so is probably due to horizontal advection into the near-bottom water. Analysis of the currents measured by the ADCP confirm this; see Chapter 5.1.5.

4. An abrupt increase in scattering levels over the shelf break in the upper 50 m during the 9^{th} leg of the survey. This group of scatterers had a very strong acoustic signature, with 100 times the scattering cross-section of neighboring surface aggregations. The surface waters are usually populated primarily with copepods. Typical surface-water concentrations of copepods on the Vancouver Island continental margin range from $1 - 30\,\ell^{-1}$ (Mackas et al., 1980;Mackas, 1992; R. Goldblatt, *pers. comm.*). Thus, if the patch were also composed of copepods, it would contain concentrations of about $10^2 - 10^3\,\ell^{-1}$, which are unlikely. However, if it were composed of euphausiids, which have acoustic target strengths $10^3 - 10^4$ times larger than that of medium sized copepods (Holliday and Pieper, 1980), the concentrations would be about $10^{-2} - 10^{-1}\,\ell^{-1}$. Typical euphausiid concentrations reported by (Simard and Mackas, 1989) are $10^2 - 10^3$ per $100\,m^3$, or $10^{-3} - 10^{-2}\,\ell^{-1}$. Other studies along the Pacific coast of North America report concentrations of *Euphausia pacifica* ranging from $10^{-3} - 10^{-1}\,\ell^{-1}$ (Genin et al., 1988; Bollens et al., 1992). Concentrations of euphausiids about 10 times higher than normal are more probable than concentrations of copepods 100 times higher than normal (R. Goldblatt, *pers. comm.*). Furthermore, the patch migrated downwards very quickly (3–4 cm/s) just prior to sunrise, remaining spatially localized during the migration. The swimming speeds, the spatial 'grouping', and the high scattering levels of the patch lend credibility to the claim that it is composed of euphausiids with concentrations about 10 times higher than normal shelf concentrations. The advection of the patch into the survey

area will be discussed in conjunction with the local currents in the next sections.

5.1.4 Currents

The total currents in the survey area are the sum of a mean, southeastward flow and tidal flows dominated by the diurnal and semidiurnal constituents. To begin this section, the simulated tidal flows will be examined using the barotropic model discussed in Chapter 4.4.5. The data will then be examined in a similar fashion and the correlation with the predicted tidal flows will be discussed. This will be followed by observations of the vertical shears present in this time series, and their effect on the observed zooplankton distributions.

Tidal Currents

Figure 5.9 shows tidal currents derived from the barotropic current model for each of the locations and times when ADCP profiles were recorded. The stick plot along the bottom of this figure shows the same currents plotted as a time series independent of location. All angles are true in both plots.

Diurnal (predominantly K_1) and semi-diurnal (predominantly M_2) tidal constituents are evident in this time series. The M_2 component is manifested as a clockwise rotation of the current vectors through 360° after about 11 hours, or through 590° after 19.5 hours. The diurnal component adds constructively to the semi-diurnal current at the beginning and at the end of the survey period, giving rise to tidal currents of about 5–10 cm/s. In the middle of the survey period (t=5 to 15 hours), the interference is destructive, resulting in small tidal currents ($< 5cm/s$).

Southeastward flowing tidal currents add to the mean, southeastward currents during the first two legs of the survey period, while northwestward tidal currents subtract from

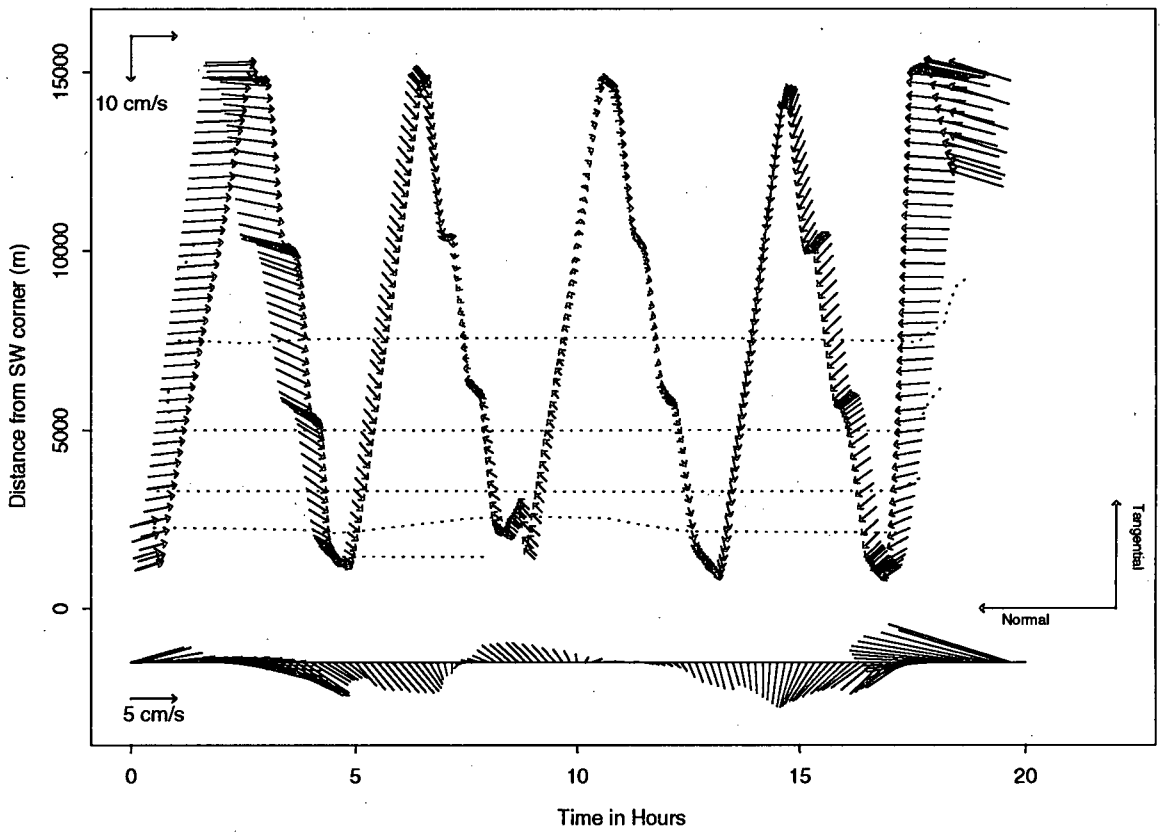

Figure 5.9: Time series of the barotropic model estimates of tidal currents. The vectors are plotted in the reference frame of the survey line (normal and tangential to the survey line). The stick plot along the bottom of this figure shows the same currents plotted as a time series independent of location. All angles are true. Bottom contours are dotted lines at 200, 300, 400 and 500 m.

the mean flow during the last two legs. The contribution from the tidal currents to the overall flow during the period from t=5 to t=15 hours was small.

Horizontal time series

Figures 5.10a-e show the current vectors for each recorded profile as a function of distance along the survey line and time from the beginning of the survey period in five 24 m bins. The coordinate system for the current vectors (tangential to the survey line, normal to the survey line) is coincident with the axes of the plot (d,-t), and is shown in the lower right corner of each time series. The vector length scales for both components are in the upper left corner. These length scales are square, so the angles are true. Note that these vector scales are different from those in Figure 5.9.

A southeastward flow dominated for the first 15 hours of the time series for all depths (legs 1-7), with speeds of 10-25 cm/s. The only exception to this was a rotation to northeastward flowing water in the northeast corner of the 1^{st} and 2^{nd} legs at depths of [80:128] metres. This represents a vertical shear in the currents tangential to the survey line of about 20 cm/s, and will be examined more closely later in this section and in Chapter 5.1.5.

At the end of the 8^{th} leg and the beginning of the 9^{th} leg, (in the SW corner) the flow turned more towards the southwest in the water at mid depth (56–128 m). The currents in shallow (6–32 m) and deep water (152–224 m) at the end of the 8^{th} leg and the deep water (152–224 m) at the beginning of the 9^{th} leg remained strong to the southeast. The shallow water (6–80 m) at the beginning of the 9^{th} leg had weak and confused flows of less than 5 cm/s. In the upper layers (6–80 m) at the end of the 9^{th} leg and during the entire 10^{th} leg, the flows were still weak throughout the water column, but reflected an overall northwestward flow. The deeper water (104–128 m) flows at the end of the 9^{th} leg and during the entire 10^{th} leg were predominantly to the southwest, indicating a vertical

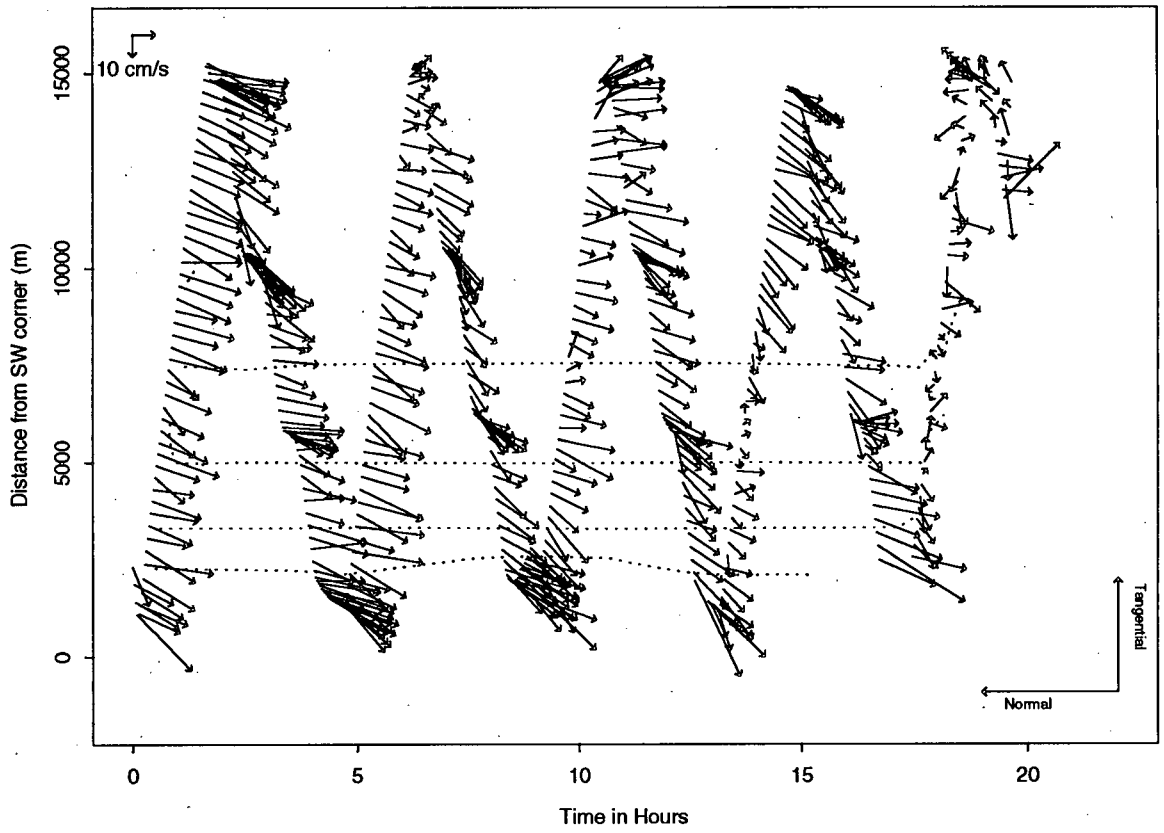

Figure 5.10: (a) Survey line horizontal time series of current vectors over depths [6,32] m. The coordinate system for the current vectors (normal to the survey line, tangential to the survey line) is in the lower right hand corner. All angles are true. Bottom contours are shown as dotted lines at 200, 300, 400 and 500 m.

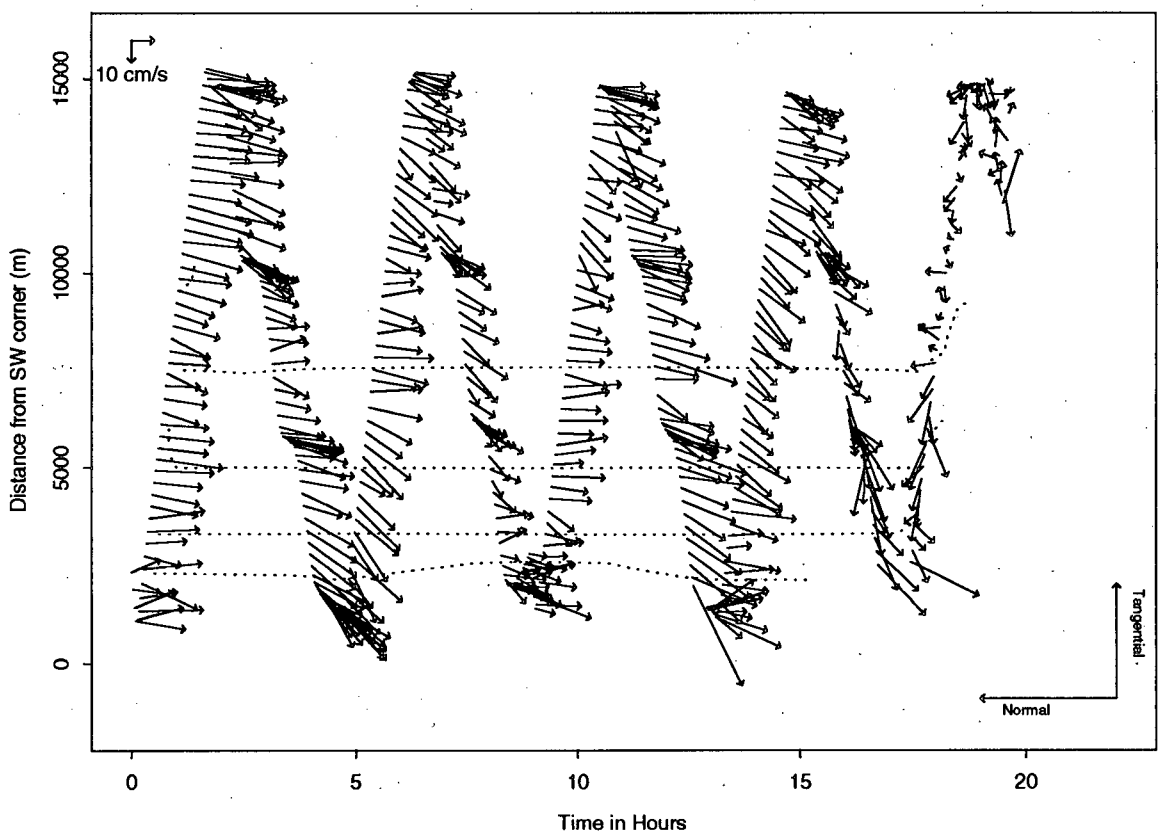

Figure 5.10: (b) Same as (a) but for depth range [56:80] m.

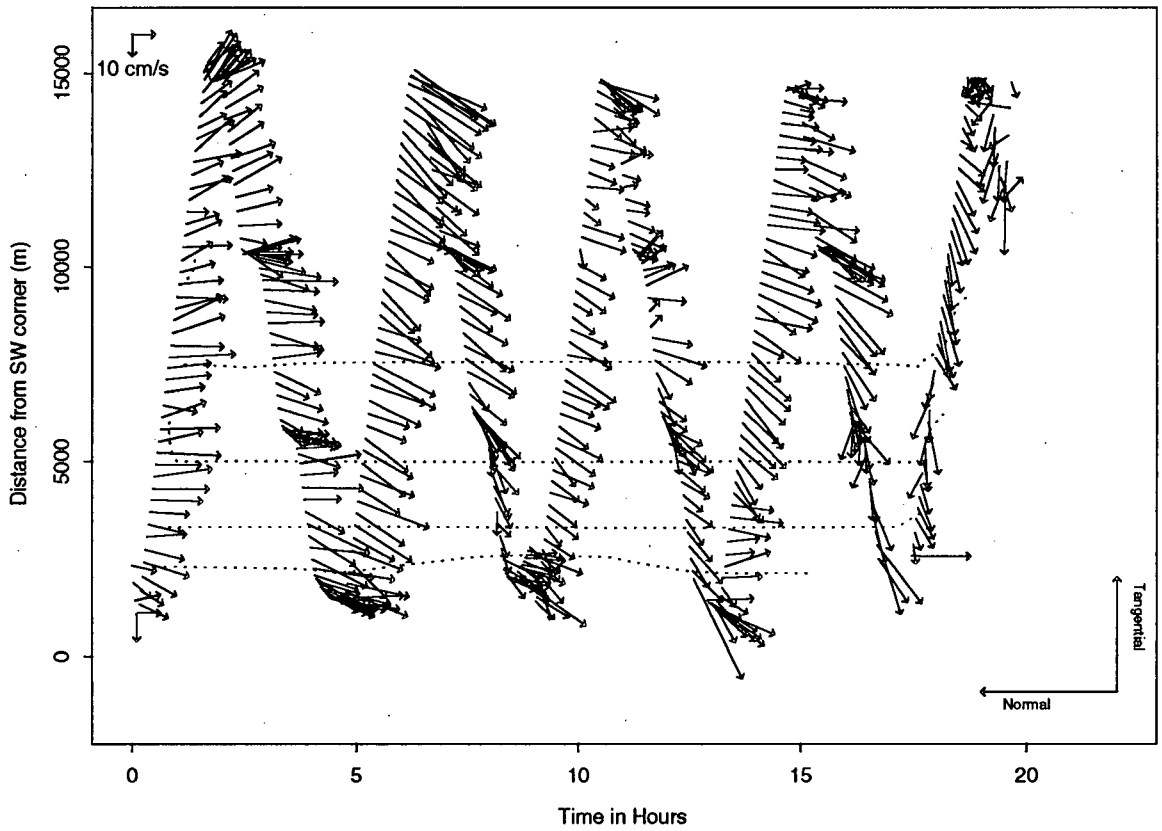

Figure 5.10: (c) Same as (a) but for depth range [104:128] m.

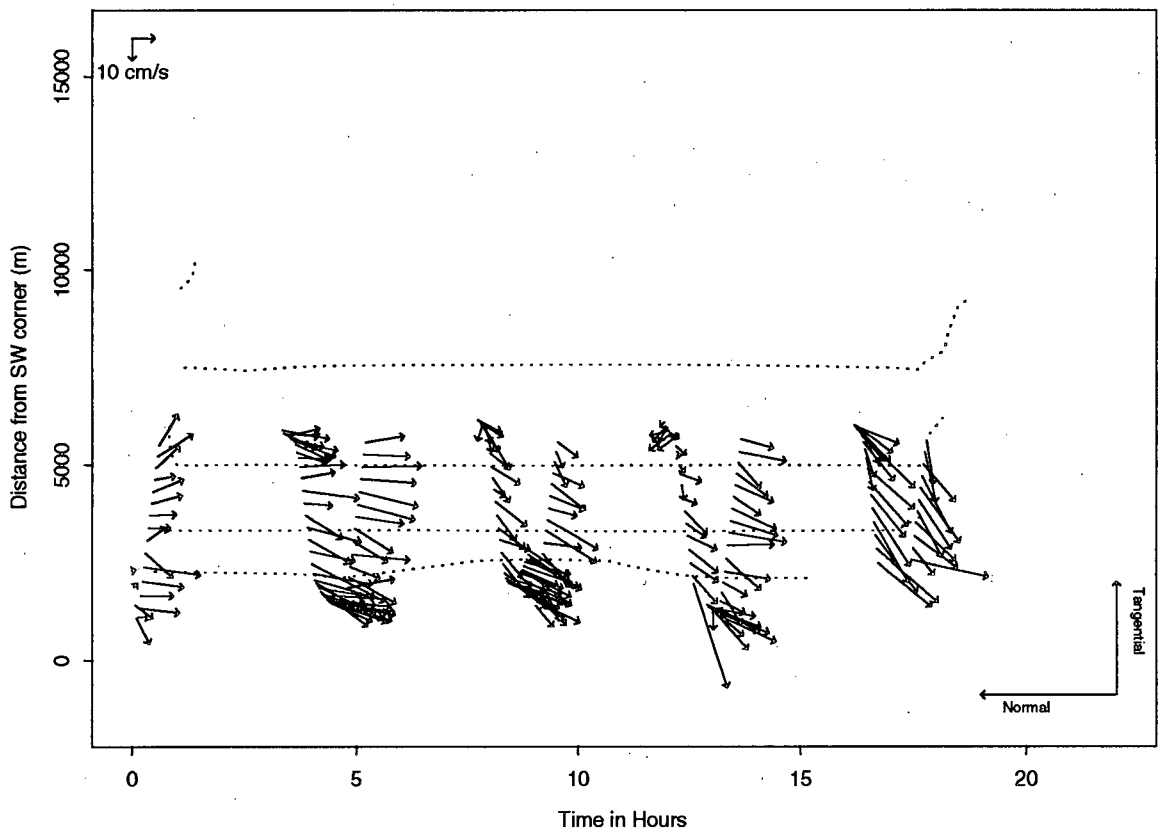

Figure 5.10: (d) Same as (a) but for depth range [152:176] m.

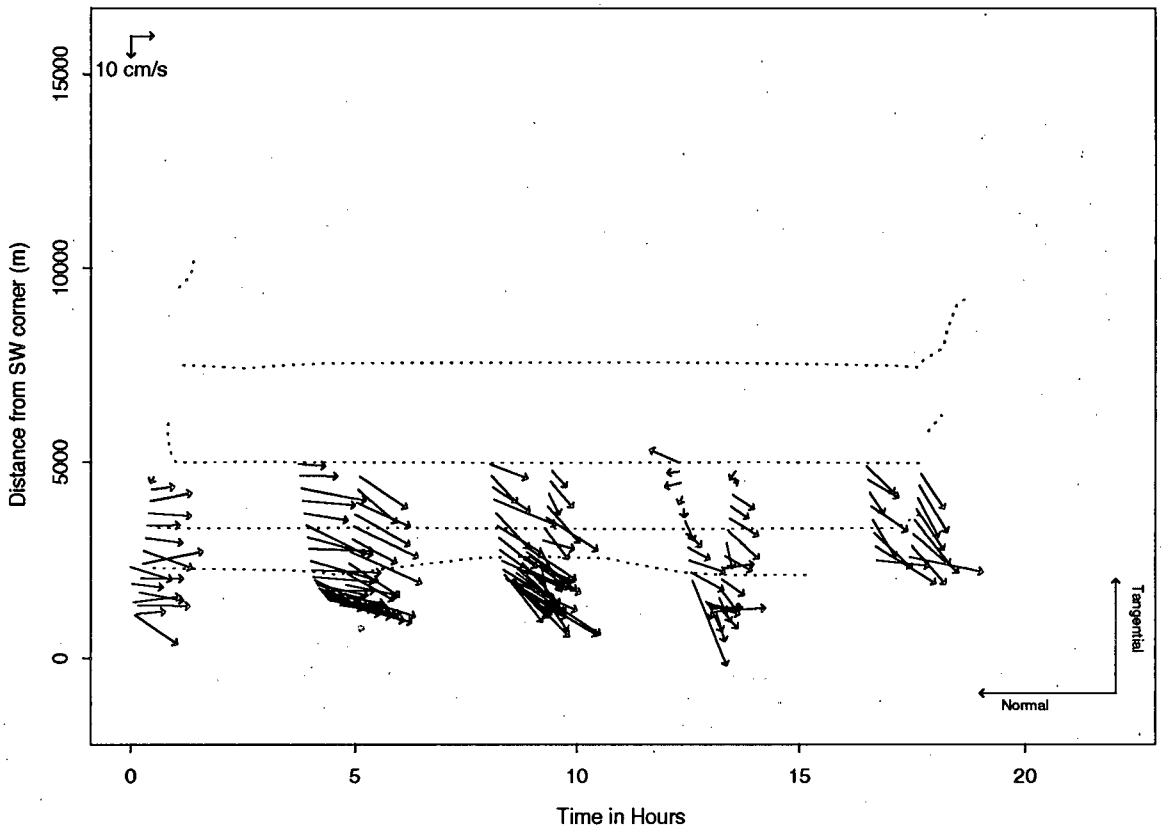

Figure 5.10: (e) Same as (a) but for depth range [200:224] m.

shear of about 10–15 cm/s over 100 m at the very end of the time series.

Quasi-Instantaneous Vertical Sections

Vertical sections of the absolute water velocities, $\vec{V}(d_i, z_k)$ for $t \approx$ constant, computed only when bottom tracking was available, are presented in Figures 5.11a - j. Each figure has two contour plots, corresponding to components of velocity normal to and tangential to the survey line. Positive normal components point 'into' the page, in a northwestward direction. Positive tangential components point to the right, in a northeastward direction.

The tangential currents were predominantly in the offshore direction (southwestward flow), with typical speeds of 10–20 cm/s. Currents were in the onshore direction below 90 m depth during the 1^{st} and 2^{nd} legs over the shelf and the shelf break. This onshore flow extended beyond the shelf break during the first leg, but was confined to the shelf during the second leg, and was replaced by offshore flowing water during the 3^{rd}, 4^{th} and 5^{th} legs. During the 6^{th} and 7^{th} legs, onshore flows were again found close to the bottom over the shelf and shelf break. The strong vertical shear in the tangential component over the shelf and slope in legs 1 and 2 and then again in legs 6 and 7 suggest 12 hourly baroclinic tidal motions. The 7^{th} leg revealed almost no cross-shelf flow in the water above 30 m depth over the southwestern half of the survey line. Small ($< 2\,km$ wide) patches of weak onshore flow ($< 5\,cm/s$) at the surface were also observed during the ninth leg. Stronger onshore flow (5–10 cm/s) was then observed during the 10^{th} leg in the surface waters (30–50 m) over a distance of 4–5 km. The deeper waters (50–180 m) during this last leg were once again dominated by offshore flows with speeds of 10–15 cm/s.

The normal currents were predominantly to the southeast for the first 8 legs of the survey, with typical speeds of 15–25 cm/s. Northwestward flows were observed during the 1^{st} and 6^{th} legs close to the bottom over the shelf break, at depths of 180–300 m. The vertical shear in the normal component over the shelf and slope during leg 1 and then again

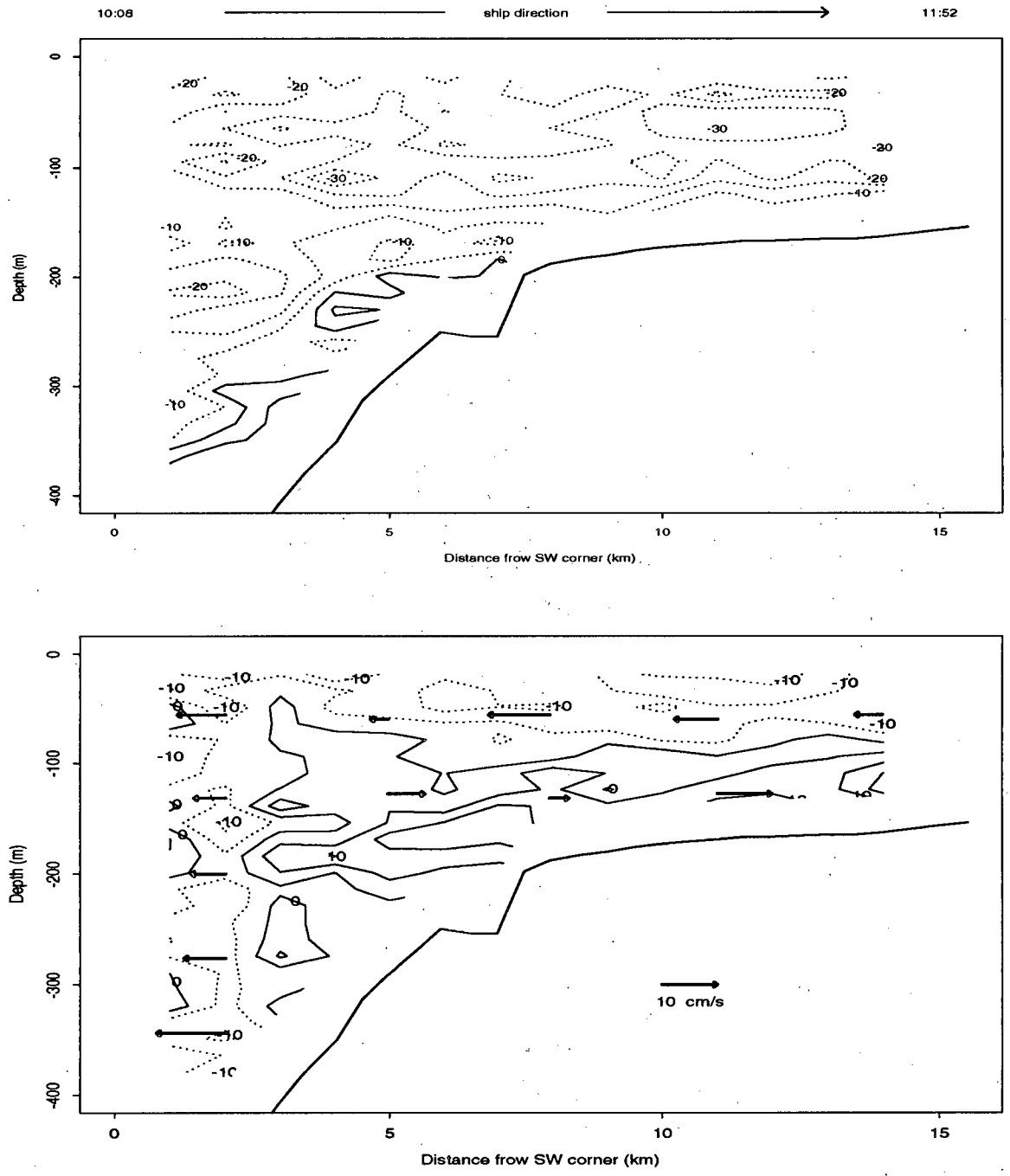

Figure 5.11: Absolute water velocities (cm/s) normal (top) and tangential (bottom) to the survey line for the June 1993 ADCP line, computed from bottom-tracking only. Negative values are contoured with dotted lines, positive values with solid lines. Positive normal components point 'into' the page, in a northwestward direction. Positive tangential components point to the right, in a northeastward direction. Vectors are also shown for some tangential values. (a) Leg 1. Collection times are from 10:08 - 11:52 on 29/06/93 with the ship steaming onshore.

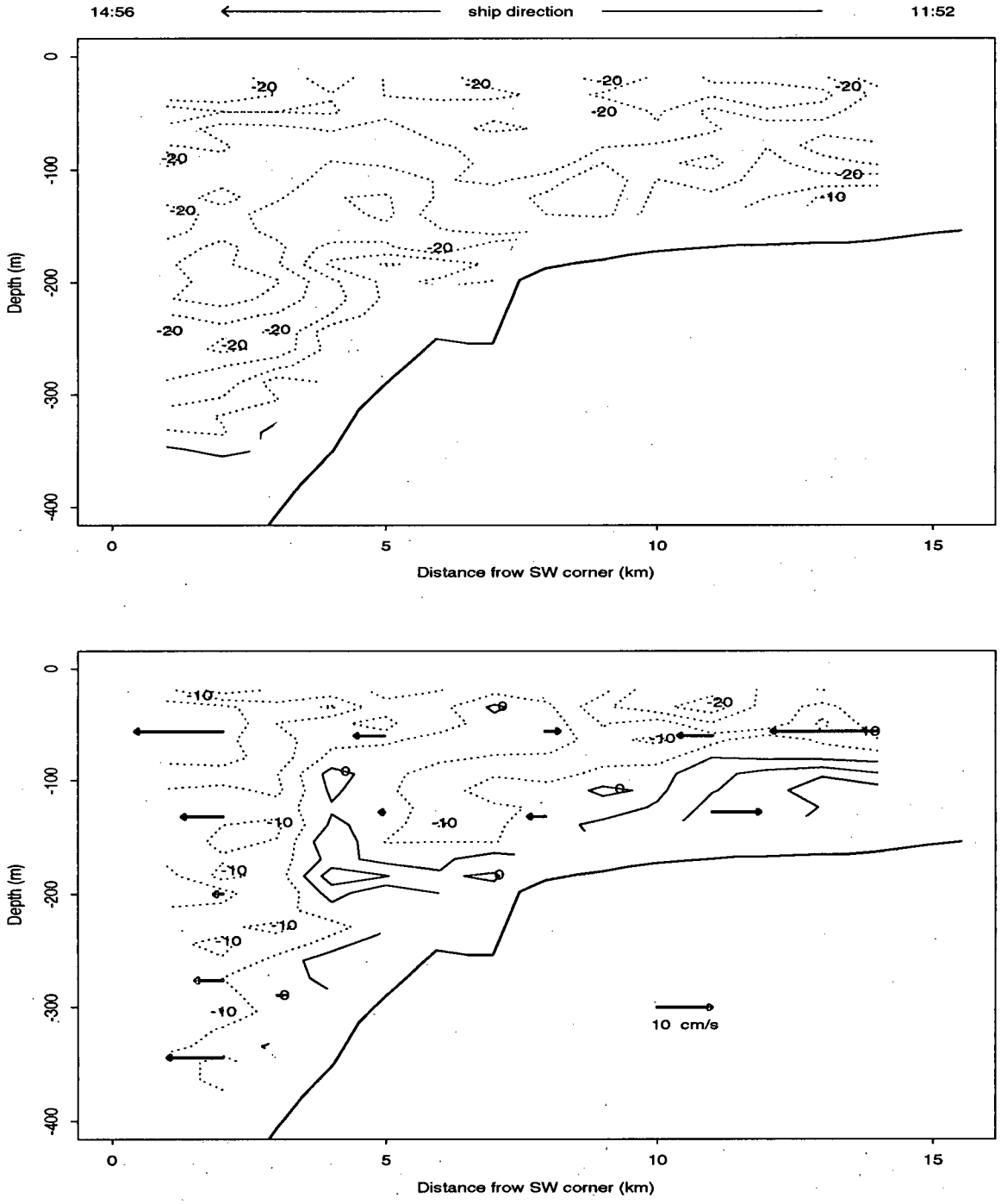

Figure 5.11: (b) Leg 2. Collection times are from 11:52 - 14:56 on 29/06/93 with the ship steaming offshore.

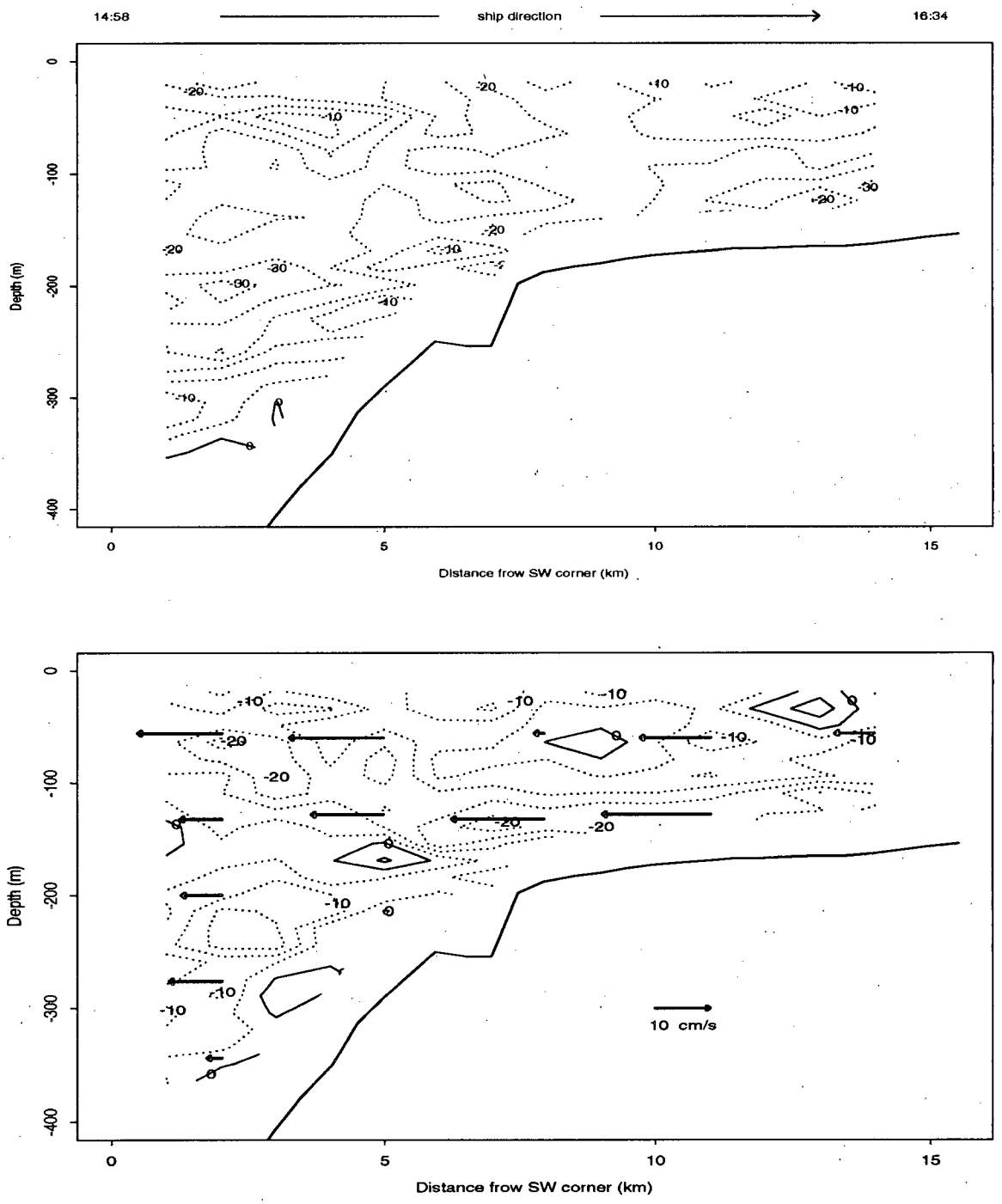

Figure 5.11: (c) Leg 3. Collection times are from 14:58 - 16:34 on 29/06/93 with the ship steaming onshore.

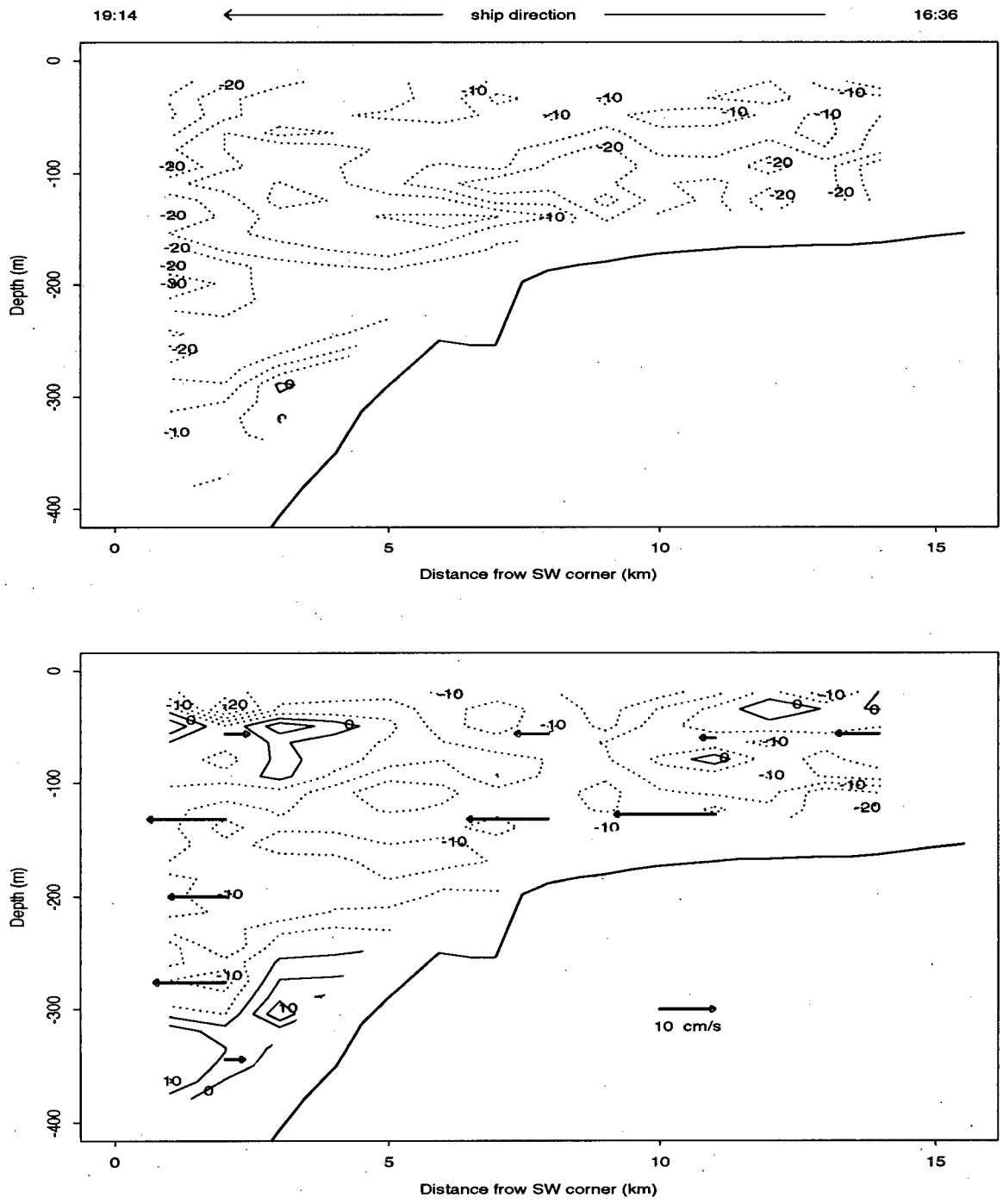

Figure 5.11: (d) Leg 4. Collection times are from 16:36 - 19:14 on 29/06/93 with the ship steaming offshore.

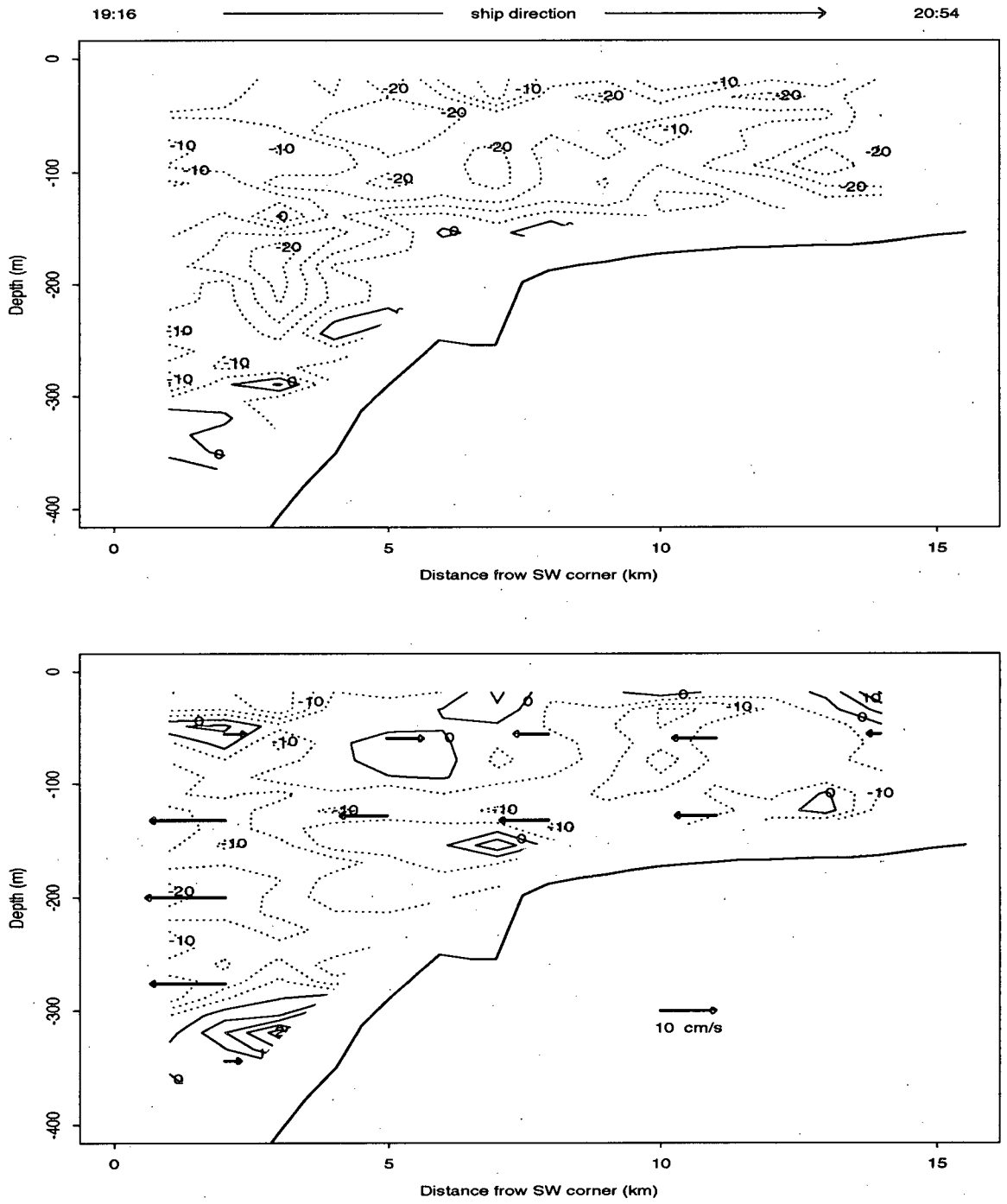

Figure 5.11: (e) Leg 5. Collection times are from 19:16 - 20:54 on 29/06/93 with the ship steaming onshore.

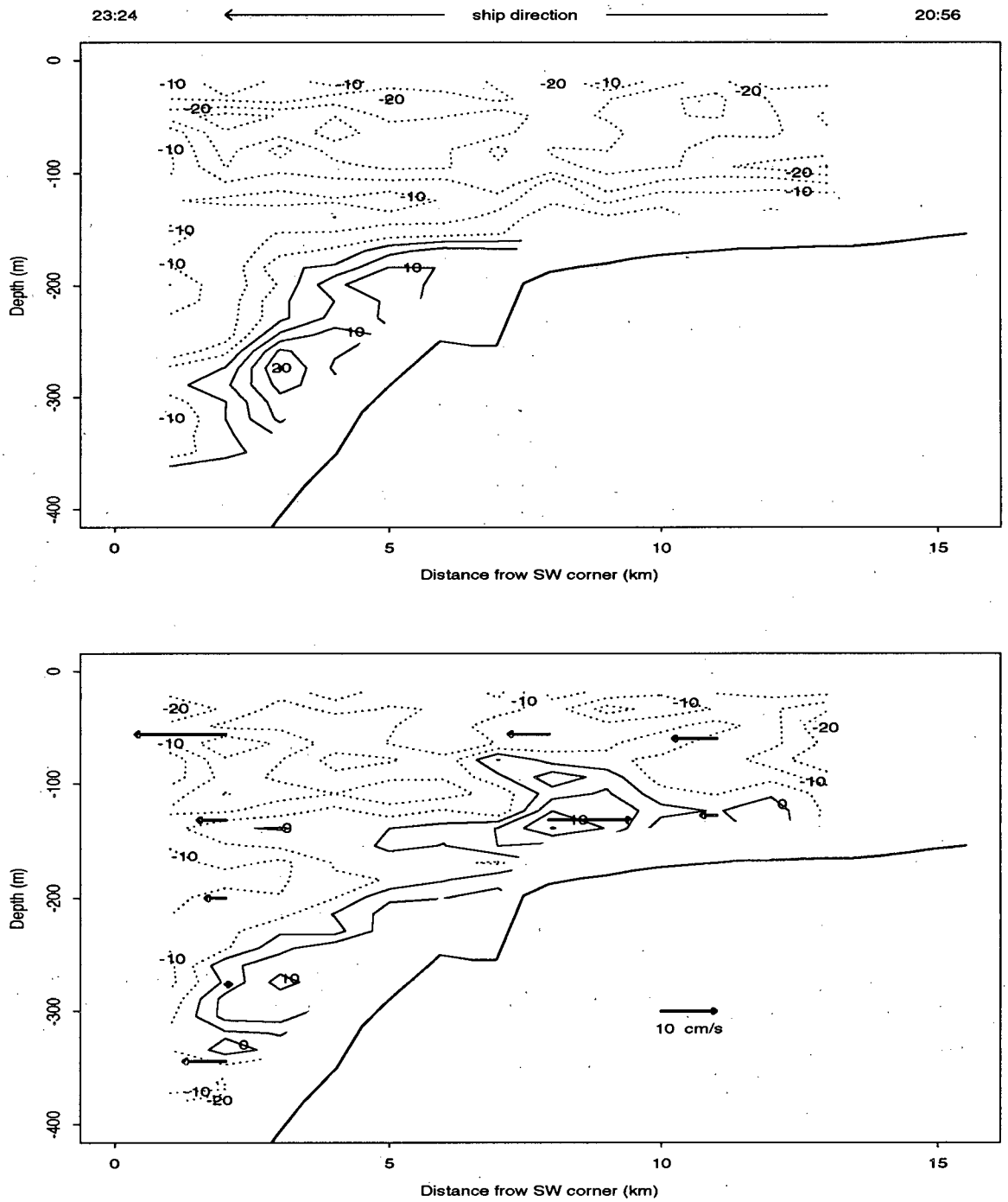

Figure 5.11: (f) Leg 6. Collection times are from 20:56 - 23:24 on 29/06/93 with the ship steaming offshore.

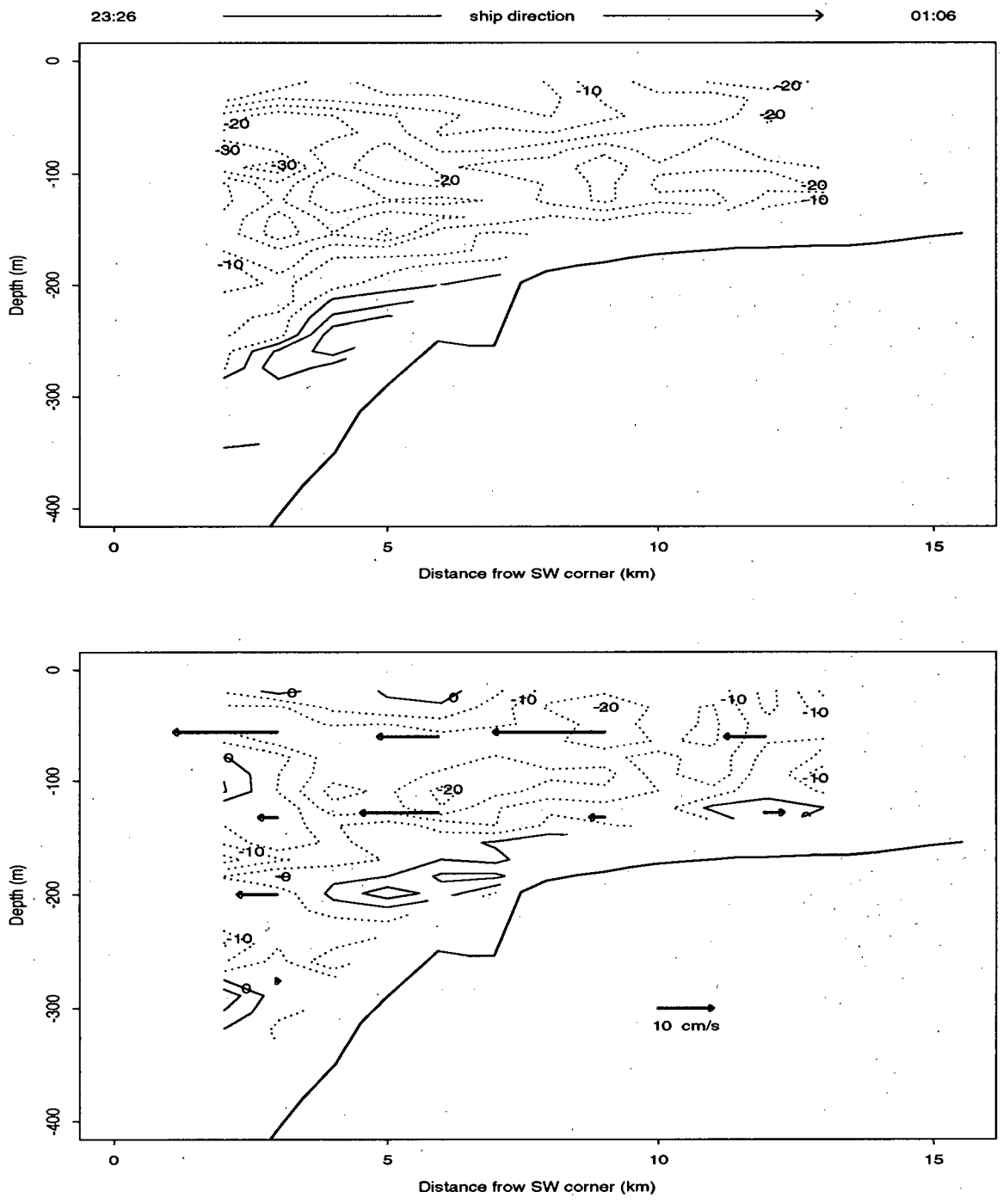

Figure 5.11: (g) Leg 7. Collection times are from 23:26 on 29/06/93 to 01:06 on 30/06/93 with the ship steaming onshore.

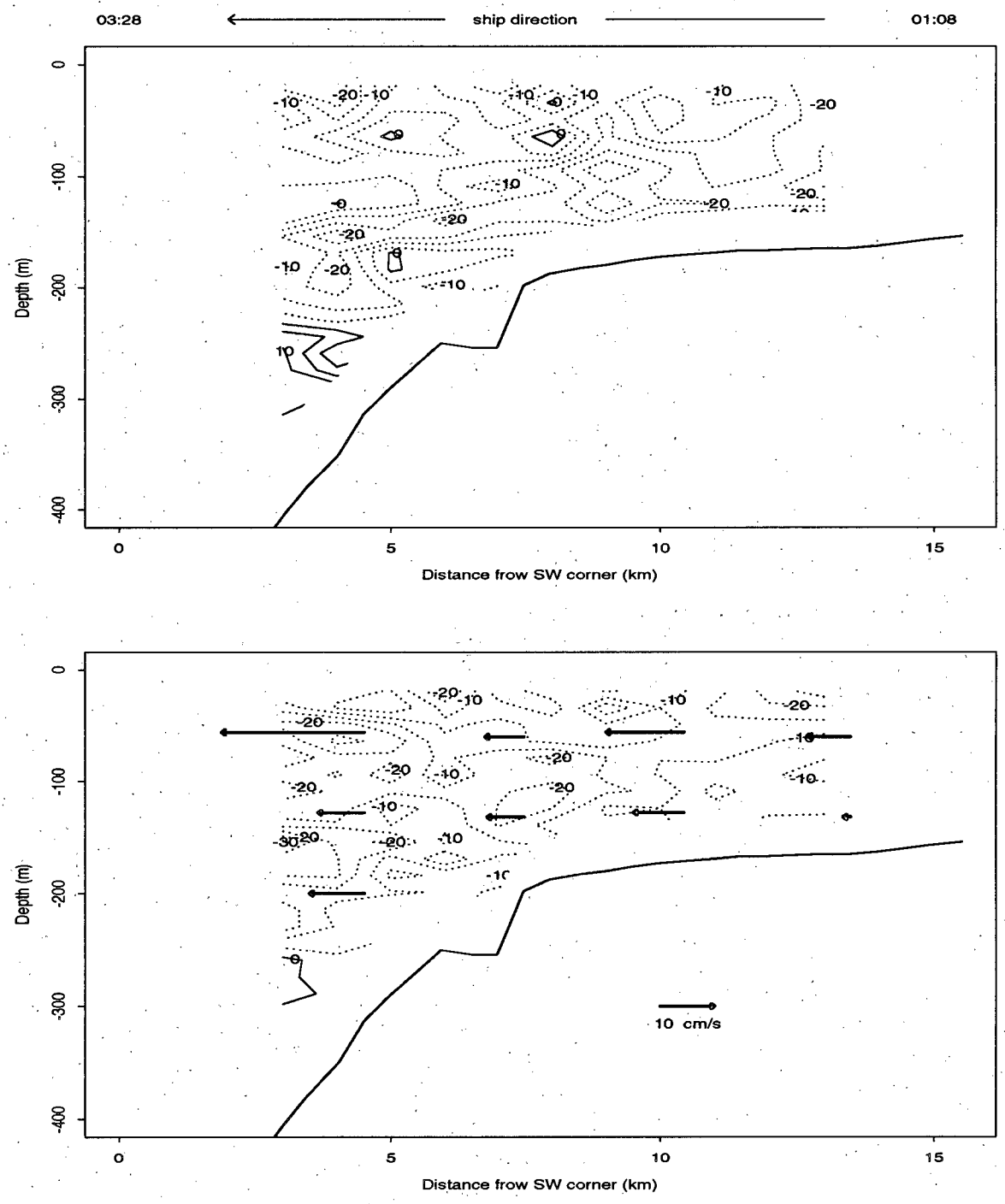

Figure 5.11: (h) Leg 8. Collection times are from 01:06 - 03:28 on 30/06/93 with the ship steaming offshore.

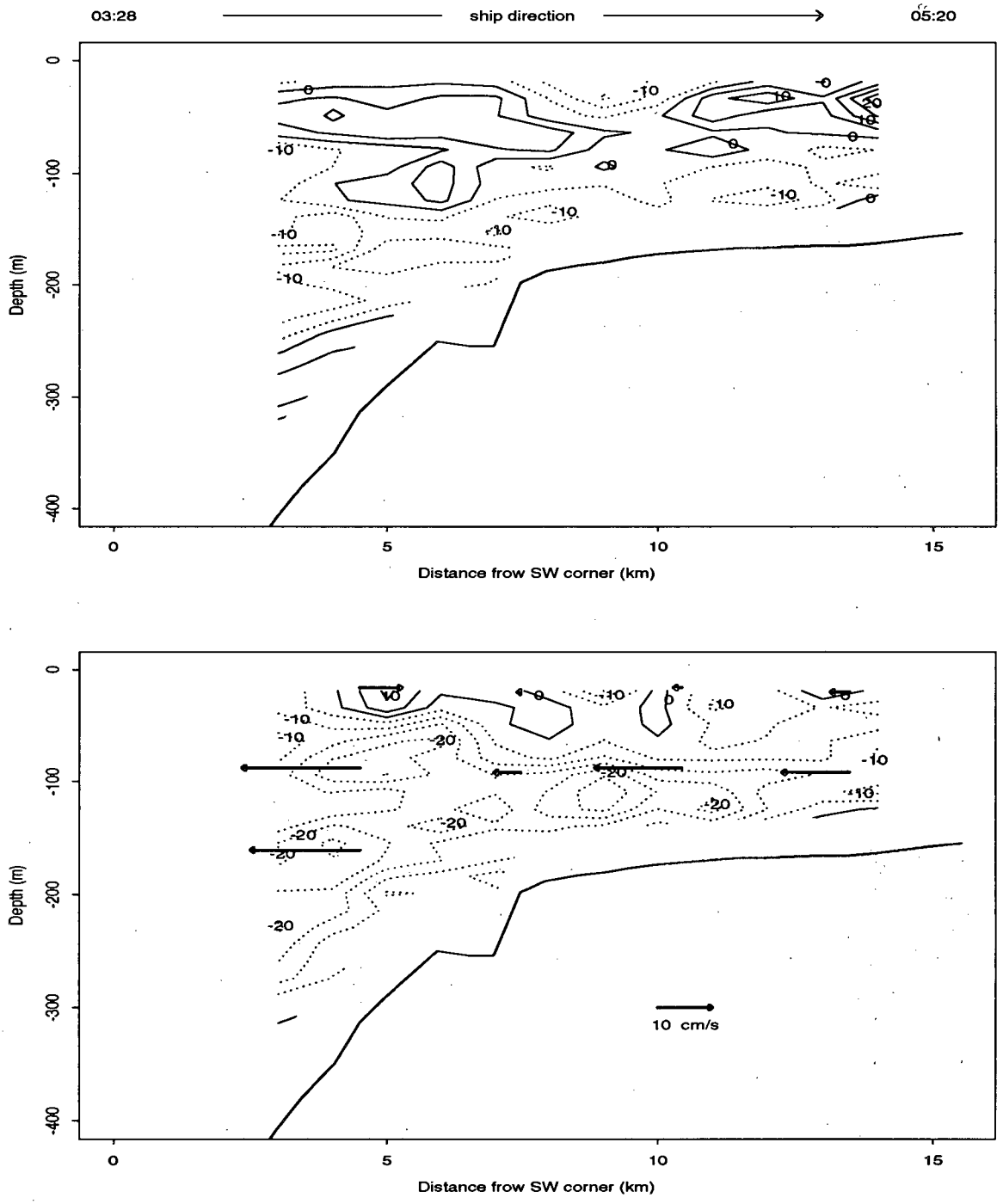

Figure 5.11: (i) Leg 9. Collection times are from 03:28 - 05:20 on 30/06/93 with the ship steaming onshore.

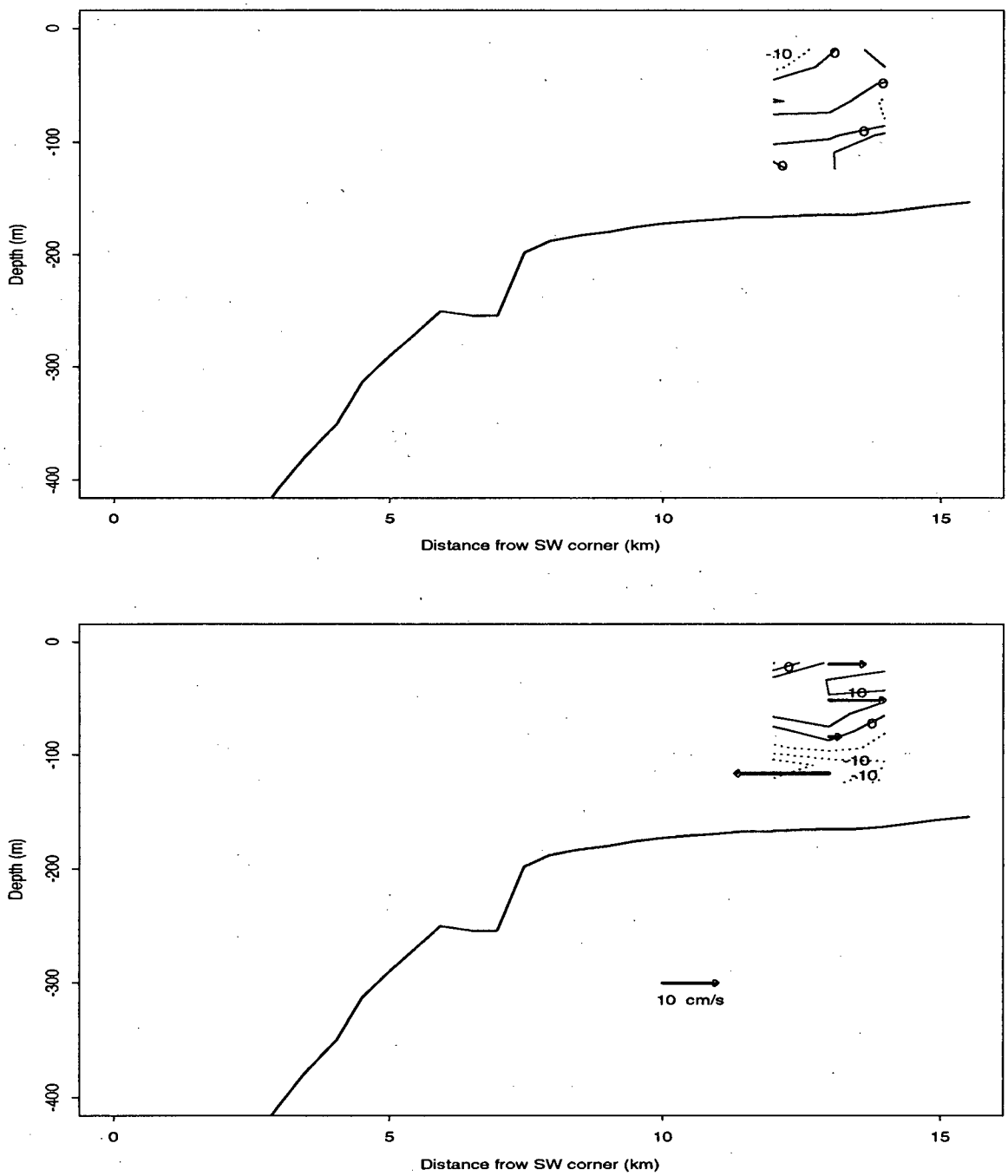

Figure 5.11: (j) Leg 10. Collection times are from 05:20 - 05:50 on 30/06/93.

during leg 6 also suggest semidiurnal baroclinic tidal motions as were observed in the tangential component. The ninth leg revealed baroclinic shear in the normal component, with weak southeastward flows ($\approx$ 5–10 cm/s) below 100 m, and weak northwestward flows ($\approx$ 0–5 cm/s) in the surface waters (30–100 m). The 10^{th} leg currents were weak and to the northwest throughout the water column, with small patches of water flowing weakly in the opposite direction.

Summary of Currents

The overall current pattern was a strong ($\approx 20\,cm/s$) southeastward flow throughout the water column during the first 16 hours (legs 1-8). The speeds during the next three hours (legs 9–10) in the shallow waters (0–80 m) over the shelf and shelf break were reversed to weak northwestward flows. The deep water (> 80 m depth) during legs 9–10 still revealed southeastward flows. Vertical shears in tangential component were observed at the northeast corner of the survey line over the shelf during the 1^{st} and 2^{nd} legs, and again in the same area during the 6^{th} and 7^{th} legs. Vertical shears in the normal component were observed over the shelf break and slope during the 1^{st} leg and again during the 6^{th} leg.

The reversal in flow from southeastward to northwestward agrees with the predictions of the barotropic tidal model (Chapter 5.1.4). However, strong vertical shears over the shelf and shelf break suggest that the tidal motions have strong 1^{st} and 2^{nd} mode baroclinic components.

The current vectors taken in the same area at the same time in Figures 5.10a-e exhibit variability of about $\pm 5\,cm/s$ in speed and $\pm 20°$ in direction. These fluctuations were most probably due to the combined effects of random errors in the water and bottom velocity estimates. In Chapter 4.4.3, a rough prediction of these errors yielded $\sigma_u = \sigma_v = 5\,cm/s$. The errors can be calculated from the data taken during the survey line by assuming

horizontal homogeneity in the current components over the length scales covered by the ship between profiles (about 500 m). If this assumption holds, then the mean difference in absolute water velocity components between neighboring profiles ($\langle \Delta u \rangle$ and $\langle \Delta v \rangle$ over the ADCP sampling interval, Δt) should be zero:

$$\langle \Delta u \rangle = \langle u(t) - u(t - \Delta t) \rangle = 0, \tag{5.1}$$

$$\langle \Delta v \rangle = \langle v(t) - v(t - \Delta t) \rangle = 0. \tag{5.2}$$

Therefore, the variances in $\langle \Delta u \rangle$ and $\langle \Delta v \rangle$ give estimates of σ_u and σ_v:

$$\sigma_{\langle \Delta u \rangle} = \sqrt{2\sigma_u^2} \tag{5.3}$$

$$\sigma_{\langle \Delta v \rangle} = \sqrt{2\sigma_v^2}, \tag{5.4}$$

The currents in the area usually have maximum horizontal shear just over the shelf break, where the ADCP survey was taken. Freeland et al. (1984) fitted data taken over the shelf break off Estevan Point to a model of the alongshore current (see discussion in Chapter 2.2), which yields an estimate of horizontal shears:

$$\frac{dv}{dx} = \frac{u f}{\beta \sin\theta} \left(\frac{1}{H} \frac{dH}{dx} \right)^2 = \frac{\beta \sin\theta}{u f} v^2 \tag{5.5}$$

where u is the onshore flow component, and θ is the angle between the latitude lines and the coastline. Using the same values as in (Freeland et al., 1984) of $u = 0.026\, cm/s$, $v = 20\, cm/s$ at the shelf break, and $\theta = 45°$, (5.5) yields:

$$\frac{dv}{dx} = 1.5 \times 10^{-5}\, (cm/s)/cm, \tag{5.6}$$

which represents a change in the alongshore flow of about 1 cm/s over the length scale of 500 m typically covered by the ship during a two minute averaging period. The result (5.6) verifies that the assumption of horizontal homogeneity holds for the ADCP sampling rate to within 1 cm/s.

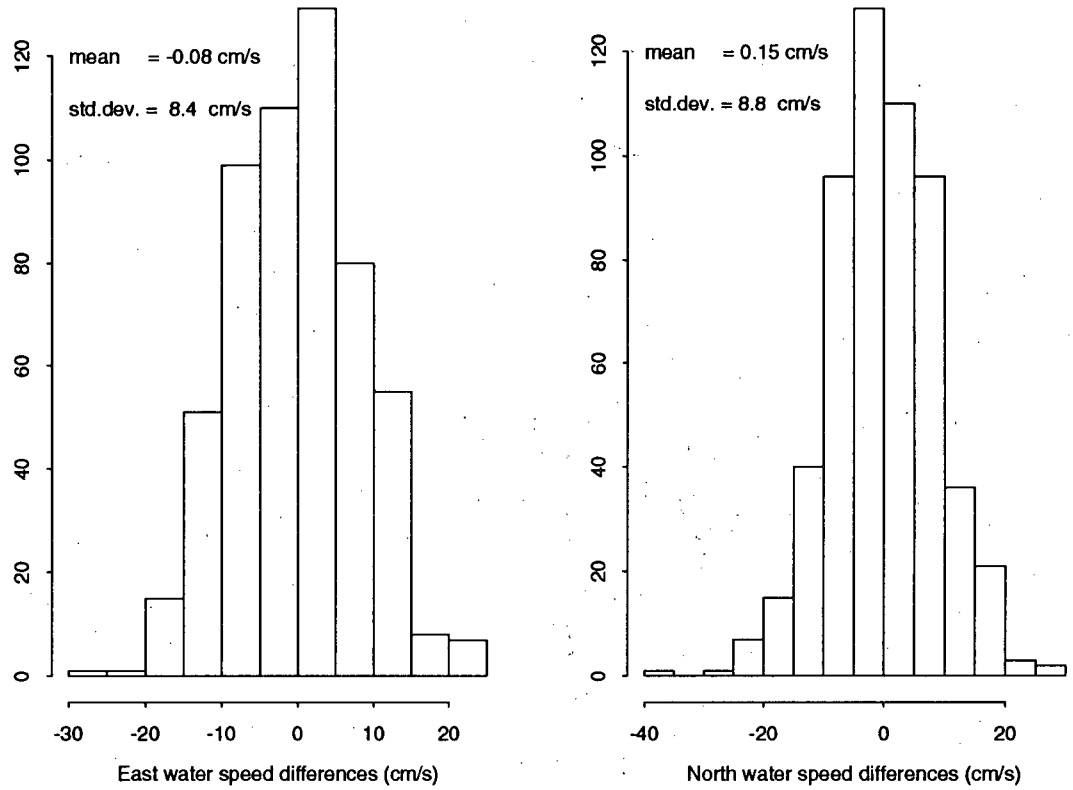

Figure 5.12: Histograms of the differences in the current components East, $\langle \Delta u \rangle$, and North, $\langle \Delta v \rangle$, between neighboring profiles at 86 m depth for the survey line. Means and standard deviations are shown.

Histograms of the differences, ($\langle \Delta u \rangle$ and $\langle \Delta v \rangle$), in the current components between all neighboring profiles taken during the survey line are shown in Figure 5.12 for the 4 m depth bin centered at a depth of 86 m. Figure 5.12 shows that $\sigma_{\langle \Delta u \rangle} = 8.4\, cm/s$ and $\sigma_{\langle \Delta v \rangle} = 8.8\, cm/s$. Therefore, using (5.3) and (5.4), the random errors in the absolute water velocity components at 86 m are found to be:

$$\sigma_u = \frac{1}{\sqrt{2}} \sigma_{\langle \Delta u \rangle} = 5.9\, cm/s \tag{5.7}$$

$$\sigma_v = \frac{1}{\sqrt{2}} \sigma_{\langle \Delta v \rangle} = 6.2\, cm/s \tag{5.8}$$

All other depth bins exhibit approximately the same variability, with σ_u and σ_v varying between 5.5 cm/s and 7.5 cm/s, with no apparent overall change in variability with depth. These measurements agree with the predictions in Chapter 4.4.3, indicating that the estimates of $\sigma_w = 5\,cm/s$ and $\sigma_b = 1\,cm/s$ are roughly correct.

5.1.5 Zooplankton-Current Correlations

Of the four major changes in zooplankton structure discussed in Chapter 5.1.3, two could be accounted for by vertical migration of zooplankton at sunset and sunrise. The other two could only be accounted for by advection by the local currents. The current patterns in Chapter 5.1.4 were used as evidence of such advection. A closer examination of the current patterns and zooplankton distributions revealed that there are three major areas where advection of zooplankton was evident:

1. During the first 9 hours of the ADCP line time series, a large aggregation of scatterers was advected into the survey area over the shelf in the northeast sector (Figures 5.4a-d). This layer had a definite, vertical 'edge' in the shallow water (0–80 m), which moved from a distance d=12 km during the first leg to a distance d=7.5 km during the fourth leg. The layer traveled 2–3 km in about 6 hours, for a mean advection speed of about 10 cm/s. The coincident tangential water speeds were also about 10 cm/s (Figures 5.11a-e), and thus the appearance of the patch over the shelf can be accounted for by southeastward advection. The water over the shelf between depths of 80 m and the bottom contained very low scattering levels during the first two legs (Figures 5.4a-b), which were replaced by higher levels during the 3^{rd} and 4^{th} legs (Figures 5.4c-d). The depletion in the deep water ($> 80\,m$) for the first 2 legs was correlated with onshore flowing water below 80 m

depth. The subsequent reversal to offshore flow sometime after 13:00 or 14:00 enabled advection of the deep water ($> 80\,m$) scatterers into the survey area along with the surface water ($< 80\,m$) scatterers.

2. During the 6^{th} leg of the survey, a northwestward current developed just over the shelf-slope at about 100 m from the bottom (Figure 5.11f). It extended from d=2–5 km and from a depth of 180 m to 300 m. At the same time and location, an aggregation of zooplankton was observed with the same spatial structure in z and d as the water velocities (Figure 5.4f). This aggregation was originally thought to be a remnant of the deep scattering layer which has already begun its upwards migration. However, the possibility also exists of horizontal advection by localized currents. The near-bottom plankton aggregation remained in its initial position for the remainder of the survey period, whereas the modified current pattern was much weaker in the seventh leg, and completely gone by the eighth leg. Whether the zooplankton were advected in from the south or whether they remained at depth after sunset, they stayed near the bottom just past the shelf break throughout the night, regardless of the current variations.

3. During the 9^{th} leg of the survey, a strong scattering layer appeared in the area, as discussed above (Figure 5.4i). This layer was not present at about 2:00 in the morning during the eighth leg, and migrated quickly downwards to the bottom layers just before sunrise, where it was found during the tenth leg. Therefore, this scattering layer must have been advected into the survey area between 2:00 and 4:00 on the morning of 30/06/93. If it was present at 2:00 just outside the range of the grid-points, it would have been advected by approximately 1 km in the two following hours before the ship returned, giving an estimate for the advection speed of about 10 cm/s. This is roughly corroborated by the current data, which

shows speeds normal to the section of about 5–10 cm/s throughout the ninth leg (Figure 5.11i). A better visualization of the correlation between the appearance of this aggregation of scatterers and the current structure is obtained by plotting the normal currents as a function of time for grid-point–48 (Figure 5.13), and comparing this to Figure 5.5e. The change in normal currents in the depth range 30–80 m from southwestward to northeastward flows is clearly seen at $t \approx 17$ hours, and is correlated with an almost identical structure in the zooplankton concentrations in Figure 5.5e. The advection of this high concentration seems certain, leaving only the question of its origin. Advection from the south-east seems to indicate an origin over the small canyon located a few kilometres to the south of the survey line (see Figure 5.2).

5.2 Semi-Synoptic Continental Margin Survey

This section examines the currents and zooplankton distributions observed during the June, 1993 cruise within the area defined by the grid in Figure 4.16. The spatial and temporal scales are larger here than for the ADCP survey line described in the last section, and the coverage of data for each location is more sparse. After a brief description of the June 1993 cruise, the data are examined as cross-shelf *in-situ* vertical sections about 100 km long at various times in June, 1993. The persistent features in these vertical sections are discussed. Then, the data are horizontally averaged to produce maps of the entire southwest Vancouver Island continental margin. Such average distributions must be approached with caution, as high temporal variabilities on diurnal time scales in backscatter residuals due to advection and migration and in water velocities due to tidal flows were observed during the ADCP survey line (Chapter 5.1). A single cruise, which

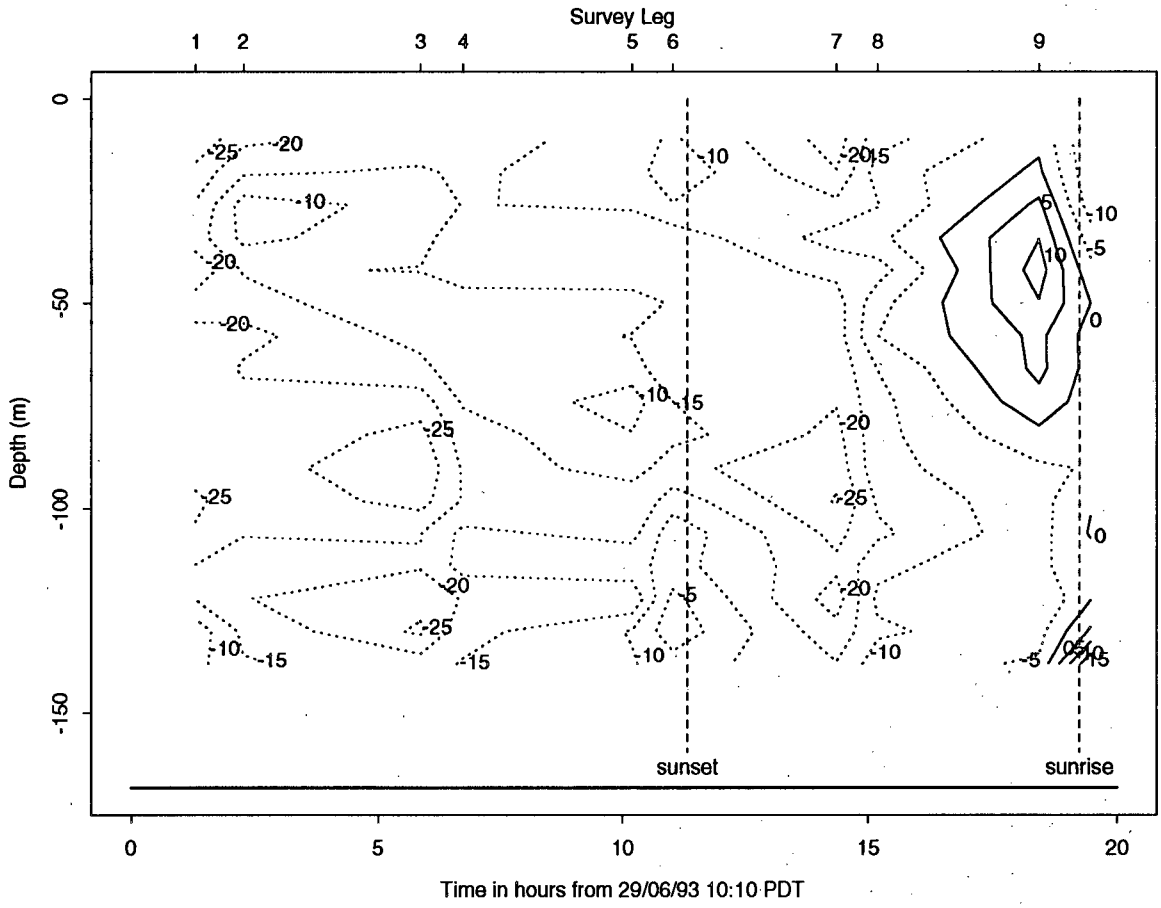

Figure 5.13: Grid-point 48 time series of normal currents $v(z_k, t_j)$ (cm/s). Negative values are contoured with dotted lines, positive values with solid lines. Positive normal components point 'into' the page, in a northwestward direction. Positive tangential components point to the right, in a northeastward direction.

typically results in 2–3 sampling periods [1] averaged onto each grid-point, will not contain enough sampling periods to yield accurate seasonal mean values. Thus, the averages can only be used to represent the persistent features found in the *in-situ* vertical sections over larger horizontal spatial scales.

5.2.1 June, 1993 Cruise and Data

During the June, 1993 La Pérouse cruise, the C.S.S.*J.P.Tully* spent 356 hours in the area defined by the grid in Figure 4.16, recording a total of 10680 ADCP profiles. Figure 5.14 shows the ship's tracks within the area defined by the grid in Figure 4.16. Each of eight survey lines perpendicular to the coast are numbered (1–8) in Figure 5.14, and will be discussed later in this section. During the cruise, the ship was collecting water property data and servicing moorings along the west coast from Juan de Fuca Strait to Brooks Peninsula. It entered the area from the mouth of Juan de Fuca Strait at 01:19 on 19/06/93, and proceeded up the coast over the deeper waters, steaming back and forth in lines parallel to the grid rows, covering the first 6-20 columns of the grid on each pass. It left the area from the northwest corner $(49°N, 125.0°W)$ at 03:28 on 22/06/93, proceeding north to Brooks Peninsula. It returned to the northwest corner of the area at 02:14 on 26/06/93 and proceeded to Barkley Sound $(48.7°N, 125.0°W)$, where it arrived at about 10:00 on 27/06/93. It subsequently steamed along nearly three complete grid rows, before arriving at the ADCP survey line (described in Chapter 5.1) at 10:10 on 29/06/93. Following the survey, it proceeded to the Barkley Sound area again, arriving at 12:00 on 30/06/93. It left at 21:30 on the same day and steamed along one complete grid row on its way to Endeavour Ridge, $(46.0°N, 130.0°W)$, leaving the area at 23:00 on 30/06/93. It returned to the area at 18:00 on 08/07/93 over the slope near the southwest

[1] A 'sampling period' denotes a period of time during which all ADCP profiles were sequential and averaged onto the same grid point

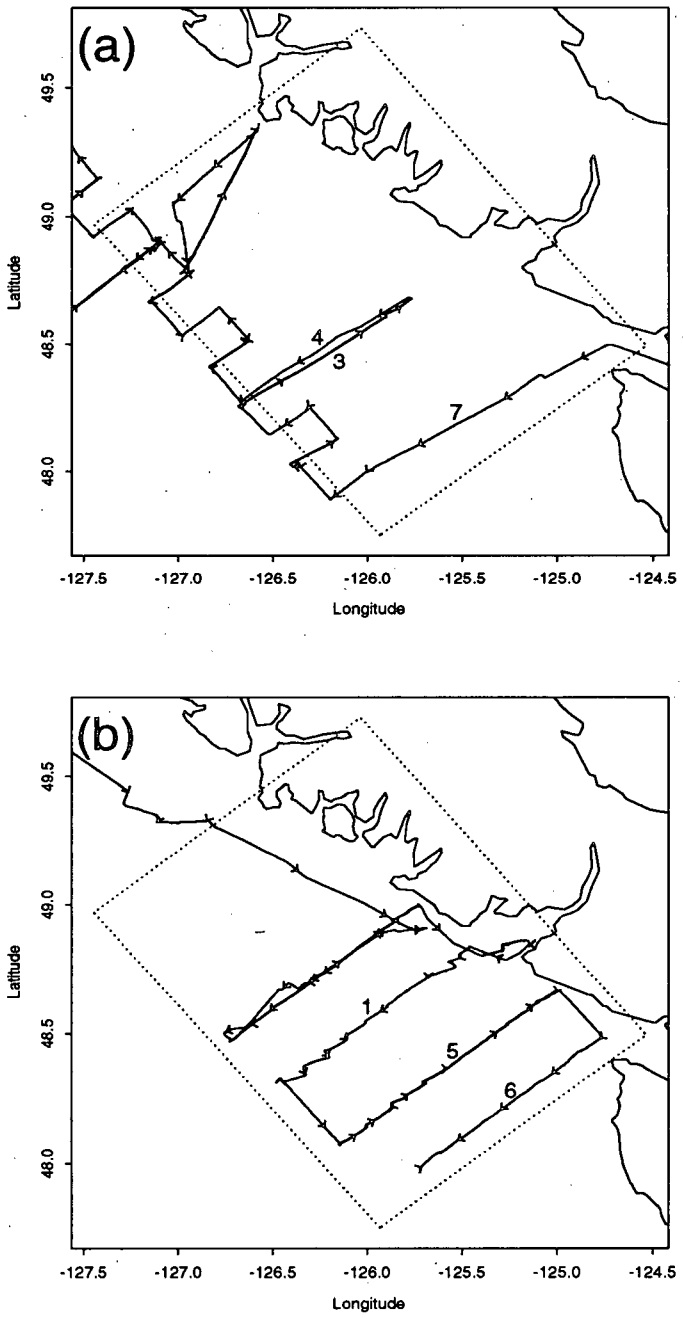

Figure 5.14: June 1993 ship tracks within the area of interest. Eight survey lines are numbered (1–8) (see Table 5.1). Arrow heads are spaced at 2 hour intervals along the ship tracks. The area covered by the grid is delineated by a dotted line. (a) From 01:19 on 19/06/93 to 03:30 on 22/06/93, (b) from 02:00 on 26/06/93 to 10:00 on 29/06/93.

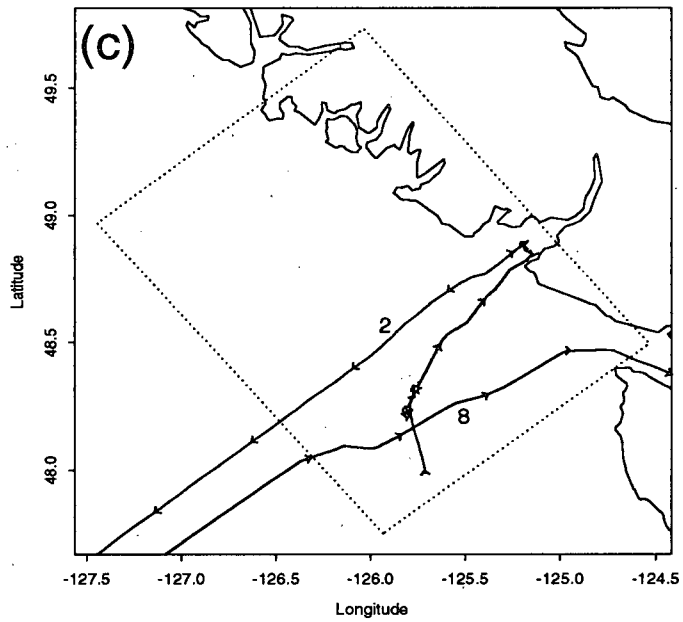

Figure 5.14: (c) From 10:00 on 29/06/93 to 23:00 on 30/06/93 and from 18:00 on 08/07/93 to 01:00 on 08/07/93.

Section Number	Start-End Grid Column	Grid Row(s)	Start-End Date;Time (PDT)	Δt (hours)	Day or Night
1	2-34	10	27/06;11:44 - 28/06;03:44	12	Both
2	5-34	9	30/06;17:44 - 30/06;22:44	5	Both
3	1-21	10-11	19/06;22:28 - 20/06;05:28	7	Night
4	1-21	10-11	20/06;05:28 - 20/06;11:28	6	Day
5	2-34	6	28/06;07:44 - 28/06;22:44	15	Day
6	8-33	2	29/06;00:44 - 29/06;08:44	8	Both
7	4-36	3-4	19/06;00:27 - 19/06;10:28	11	Both
8	1-35	1-6	07/07;17:58 - 07/07;23:58	7	Both

Table 5.1: Eight June vertical sections taken along grid rows and their time and length scales. The ship tracks for these sections are shown in Figure 5.14.

corner of the grid, and went directly to the mouth of Juan de Fuca Strait, leaving the area from the south east corner at 01:00 on the same day.

The data set described above includes eight vertical sections (numbered 1–8 in Figure 5.14) taken as the ship steamed onshore or offshore. During each one of these sections, the ship usually stayed within about 4 km of a grid row, and covered most of the length of the grid, or about 100 km, in 5 to 15 hours. Table 5.1 presents the temporal and spatial coverage of these eight sections, as well as their alongshore locations in terms of grid rows, and whether the data was taken at night or during the day. Sections 1 through 4 were taken perpendicular to the coast off the mouth of Barkley Sound. They covered most of the grid length, out to a distance of 100 km from the coast, but only covered about three grid rows, or about 20 km in an alongshore direction. Sections 5-8 covered a larger area towards the south of the grid, spanning the grid length (100 km) and about six grid rows or 50 km in an alongshore direction.

The ADCP was set to record 120-second averages of profiles, using a 4 m bin length, a 4 m *blank beyond-transmit*, and a total of 128 depth bins. Ship speeds during the cruise varied from about 0 knots during water property measurements to about 15 knots as the ship steamed from Barkley Sound to Endeavour Ridge. The spatial coverage of the

profiles therefore had a resolution of about 0–1 km, with an average of about 500 m at normal cruising speeds (10 knots).

5.2.2 *In-Situ* Scattering Layer Distributions

Figures 5.15–5.18 are contoured vertical sections of backscatter residuals for sections 1–4, respectively. The horizontal axes at the bottom give the relative distance in kilometres measured from the most westward point in the section. The axes at the top give the consecutive numbers of the grid-points, which are numbered from south to north, west to east. The tick marks on the right axes show the location of 8 m bins. The bathymetry is estimated from Digital Terrain File (DTF) depths only, and so is only an approximation of the true bottom depths.

All four sections had a similar structure, with the highest scattering levels occurring in the upper 50 m over the entire section length, reaching +25 dB at night and about +15 dB during the day. A depletion region occupied the mid-depths (50–150 m) over the slope, with residual levels of -5 dB to -10 dB. The scattering levels in deep water (150–400 m) were higher than in the mid-depths, usually reaching 5–8 dB.

ADCP measurements taken over the shelf break at mid-depth range of 50–150 m along cross-sections 1, 2 and 3 (measured at night) revealed scattering levels comparable to the levels in the surface waters, leading to near-uniform scattering levels throughout the water column over the shelf break. Cross-section 4 (measured during the day), however, revealed depleted scattering levels during the day of -5 dB to -3 dB in the mid-depth range (50–150 m) over the shelf break and a strong scattering layer in the deeper water (150–200 m) over the shelf break. This strong shelf-break bottom scattering layer was probably euphausiids at their daytime depth. Such a scattering layer was not observed in the sections where the ship steamed over the shelf break at night (sections 1 and 3 - Figures 5.15 and 5.17), when the euphausiids had presumably risen to the

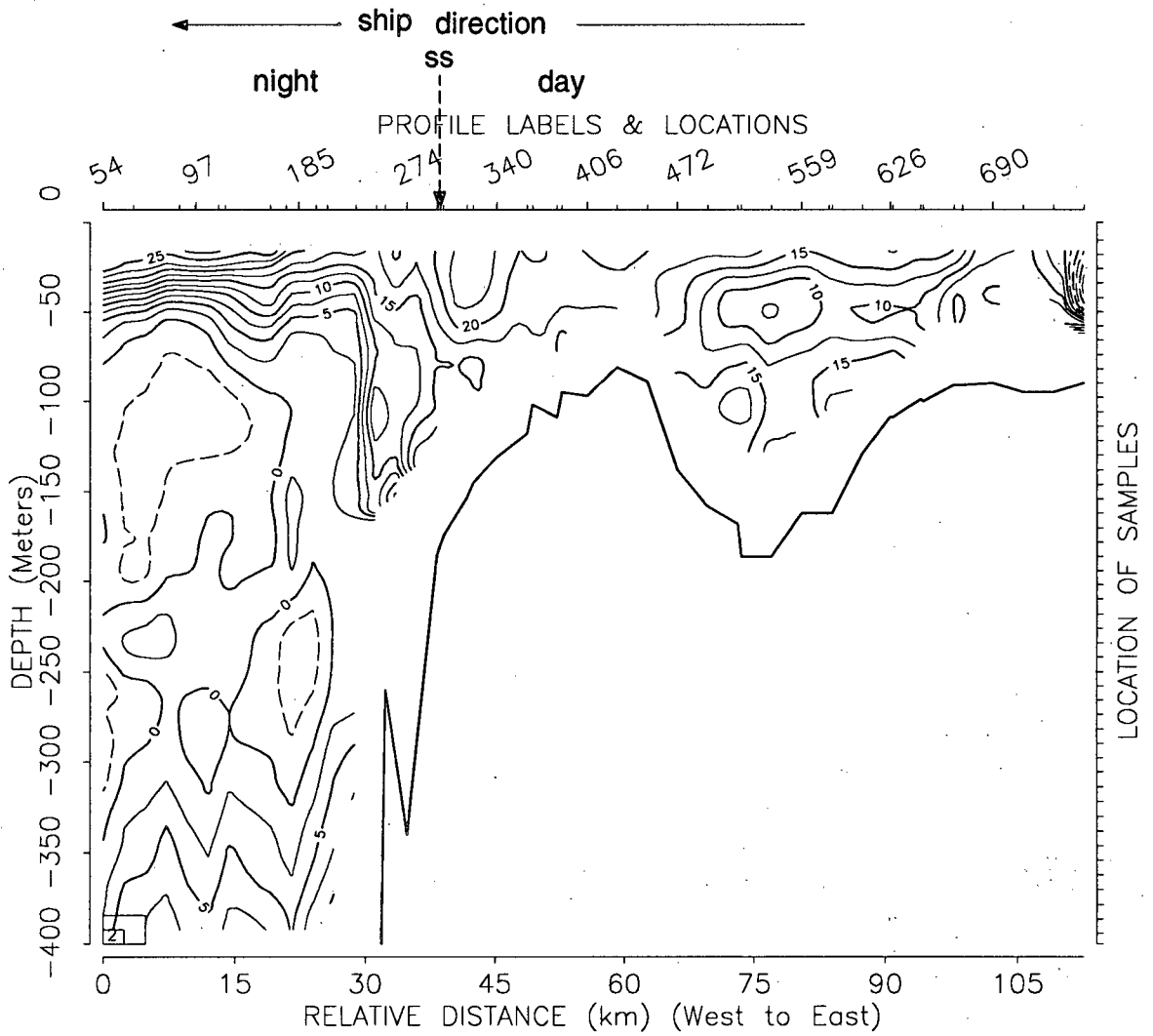

Figure 5.15: Contoured backscatter residuals (dB) for section 1. Data was collected from 11:44 PDT on 27/06/93 to 03:44 PDT on 28/06/93, with the ship steaming offshore. Sunset occurred at 21:30 PDT on 27/06/93, when the ship was over the shelf break, at a relative distance of $\approx 40km$, as indicated by the dashed arrow.

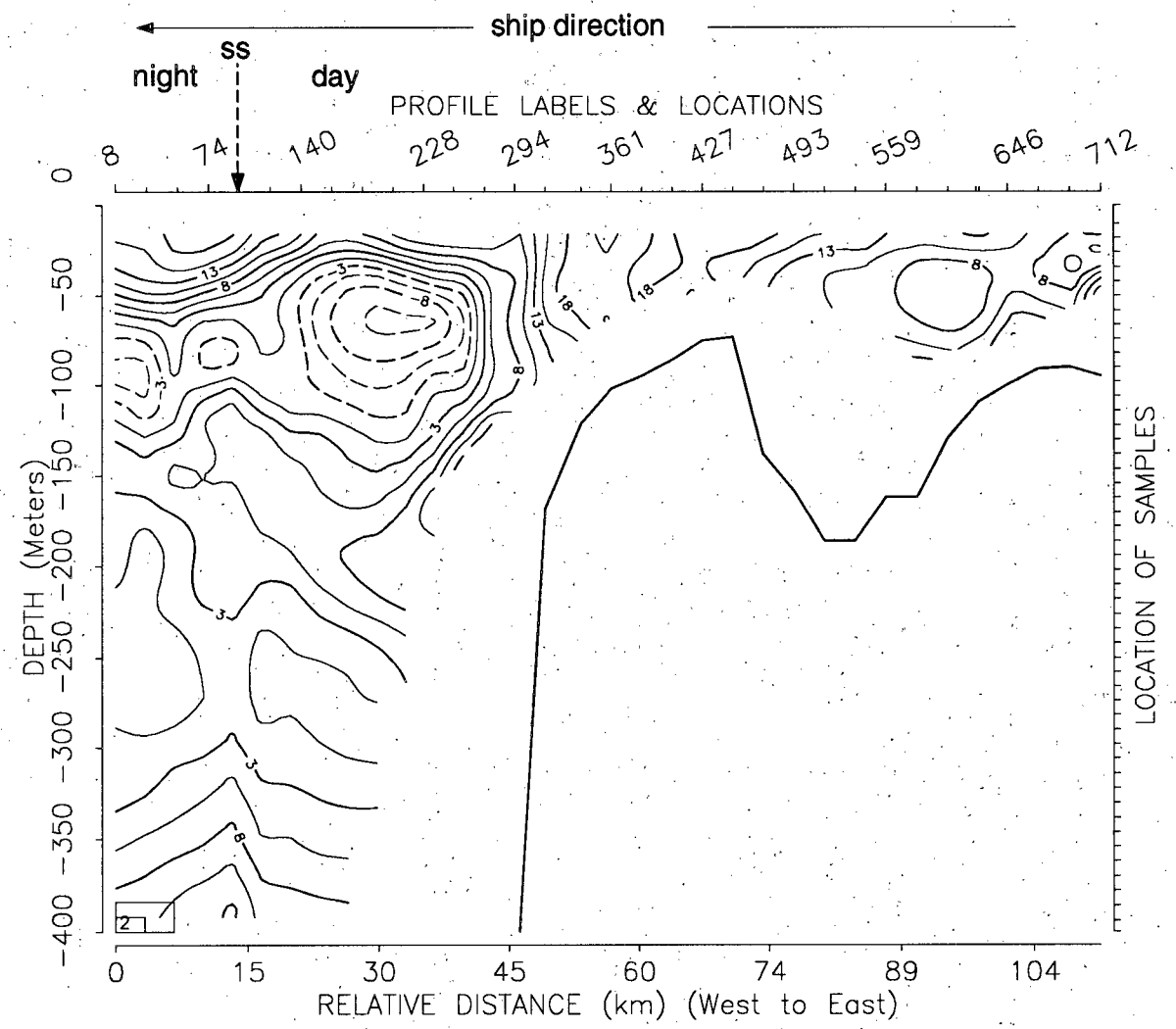

Figure 5.16: Contoured backscatter residuals (dB) for section 2. Data was collected from 17:44 to 22:44 PDT on 30/06/93, with the ship steaming offshore. Sunset occurred at 21:30 PDT, when the ship was over the deep water, at a relative distance of $\approx 15km$, as indicated by the dashed arrow.

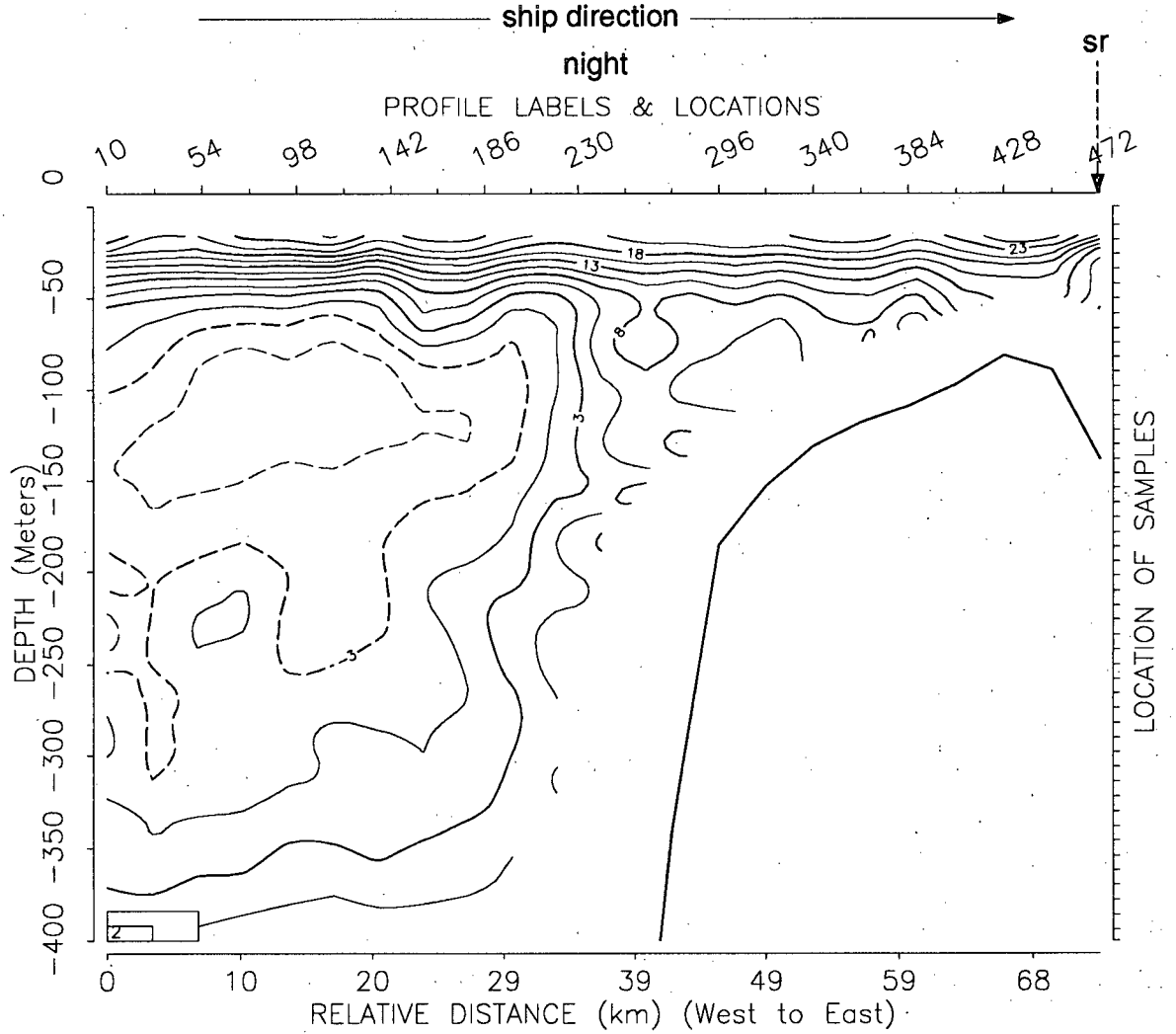

Figure 5.17: Contoured backscatter residuals (dB) for section 3. Data was collected from 22:28 PDT on 19/06/93 to 05:28 PDT on 20/06/93, with the ship steaming onshore. Sunrise occurred at 05:24 PDT on 20/06/93, just as the ship reached the end of the section, as indicated by the dashed arrow.

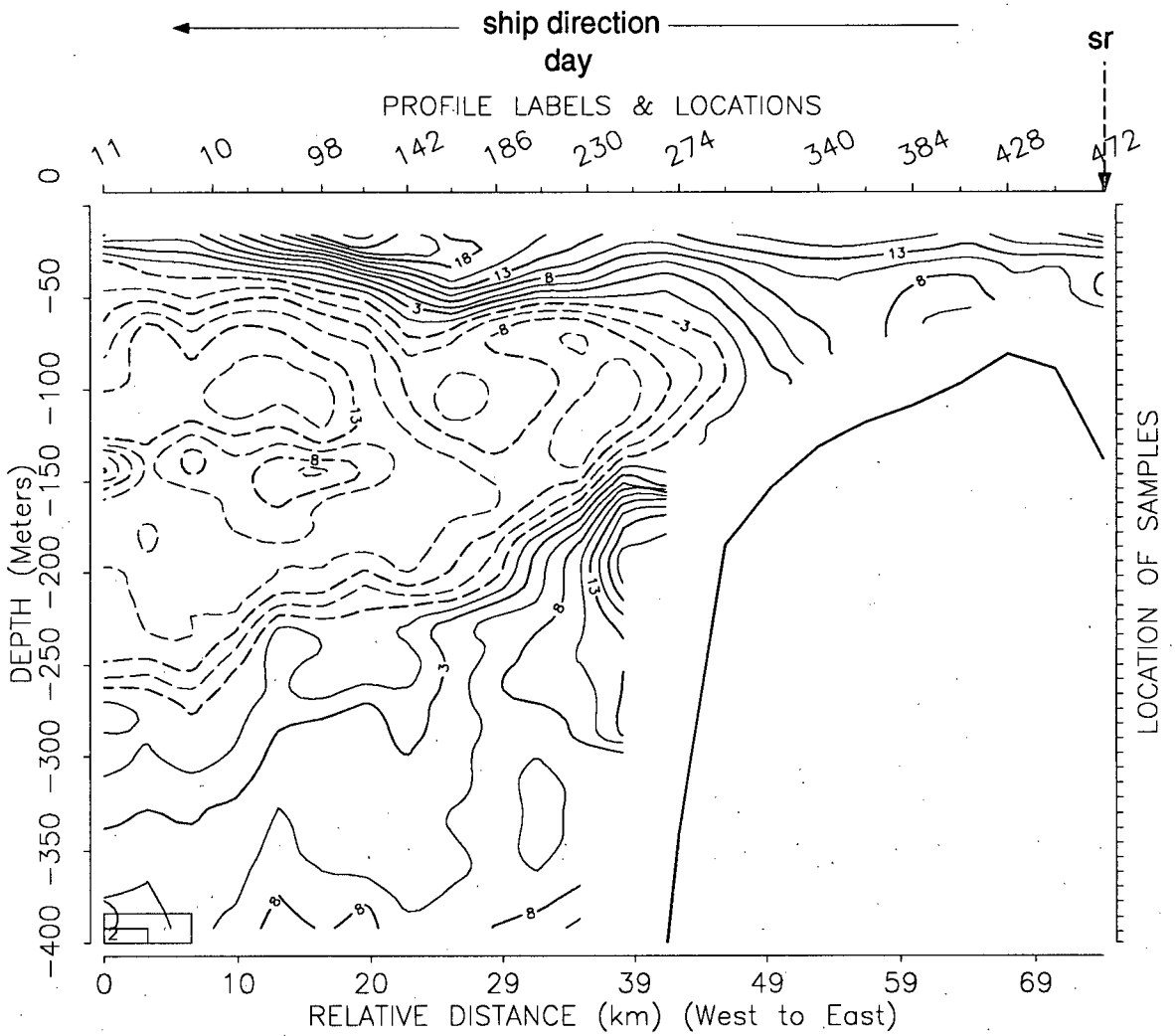

Figure 5.18: Contoured backscatter residuals (dB) for section 4. Data was collected from 05:28 to 11:28 PDT on 20/06/93, with the ship steaming offshore. Sunrise occurred at 05:24 PDT on 20/06/93, just before the ship started the section, as indicated by the dashed arrow.

surface. A shelf-break bottom scattering layer was not observed in cross-section 2 either (Figure 5.16), even though the ship steamed over the shelf break during the day. However, the ship was moving at about 20 knots along section 2, and so it steamed over the shelf-break about an hour prior to sunset. The euphausiids over the shelf-break had probably started their upwards migration, accounting for the lack of a shelf-break bottom scattering layer at this time. The water over the shelf in sections 1 and 2 had a uniform structure, with scattering levels for the entire water column ranging between 8 and 15 dB. A slight depletion region (levels 3–5 dB lower than in the surrounding water) was observed in both sections over the 100 m deep basin at relative distances of 70 to 90 km.

Figures 5.19–5.22 are contoured vertical sections of backscatter residuals for sections 5–8, respectively. The parts of these sections over the shelf break and slope were taken during daylight, and had a similar structure as in section 4 (see Figure 5.18). Aggregations of scatterers were found at the surface and at depths of 150–250 m near the shelf-break. A depletion layer occupied the depths from 50–150 m over the shelf-break and slope, and extended a few kilometres onto the shelf. The resulting definite separation between the shallow-water and the deep-water scattering layers was most likely due to euphausiids at their daytime depths over the shelf break, as observed in section 4. The structure over the shelf in sections 5–8 was again uniform, as in sections 1 and 2 (Figures 5.15 and 5.16). The only high ($> 15dB$) scattering layer was in section 5 close to the bottom over a shallow basin in the shelf, at relative distances of 70–90 km.

5.2.3 *In-Situ* Current Patterns

The errors in the absolute water velocities due to inaccuracies in ship velocity estimates can be calculated in a manner similar to that in Chapter 5.1.4. The currents are assumed uniform (to within 1 cm/s) over the length scales covered by the ship in an averaging period, so the differences in current components between neighboring profiles give variances

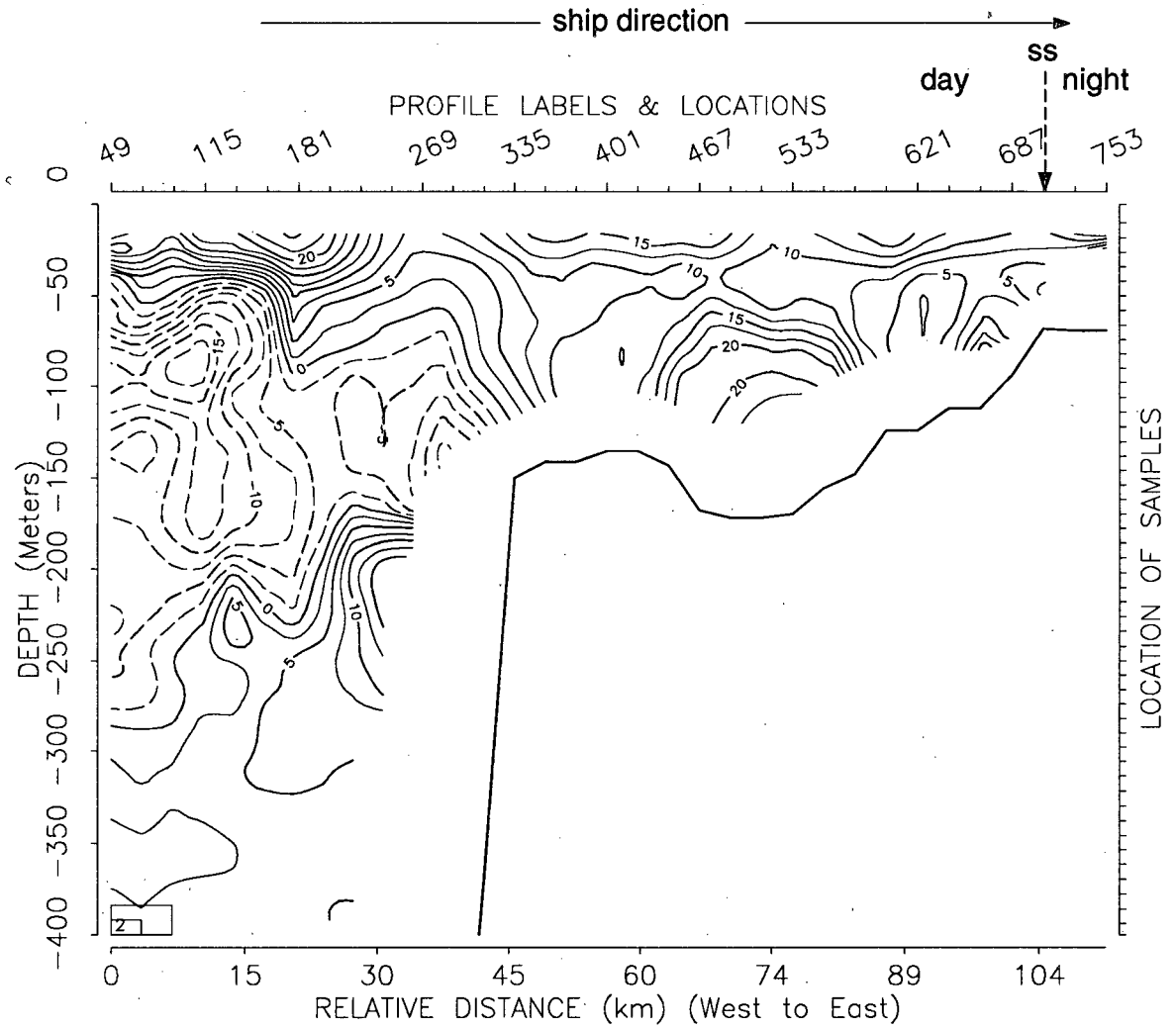

Figure 5.19: Contoured backscatter residuals (dB) for section 5. Data was collected from 07:44 to 22:44 PDT on 28/06/93, with the ship steaming onshore. Sunset occurred at 21:30 PDT on 28/06/93 when the ship was over the shelf at a relative distance of ≈ 105 km, as indicated by the dashed arrow.

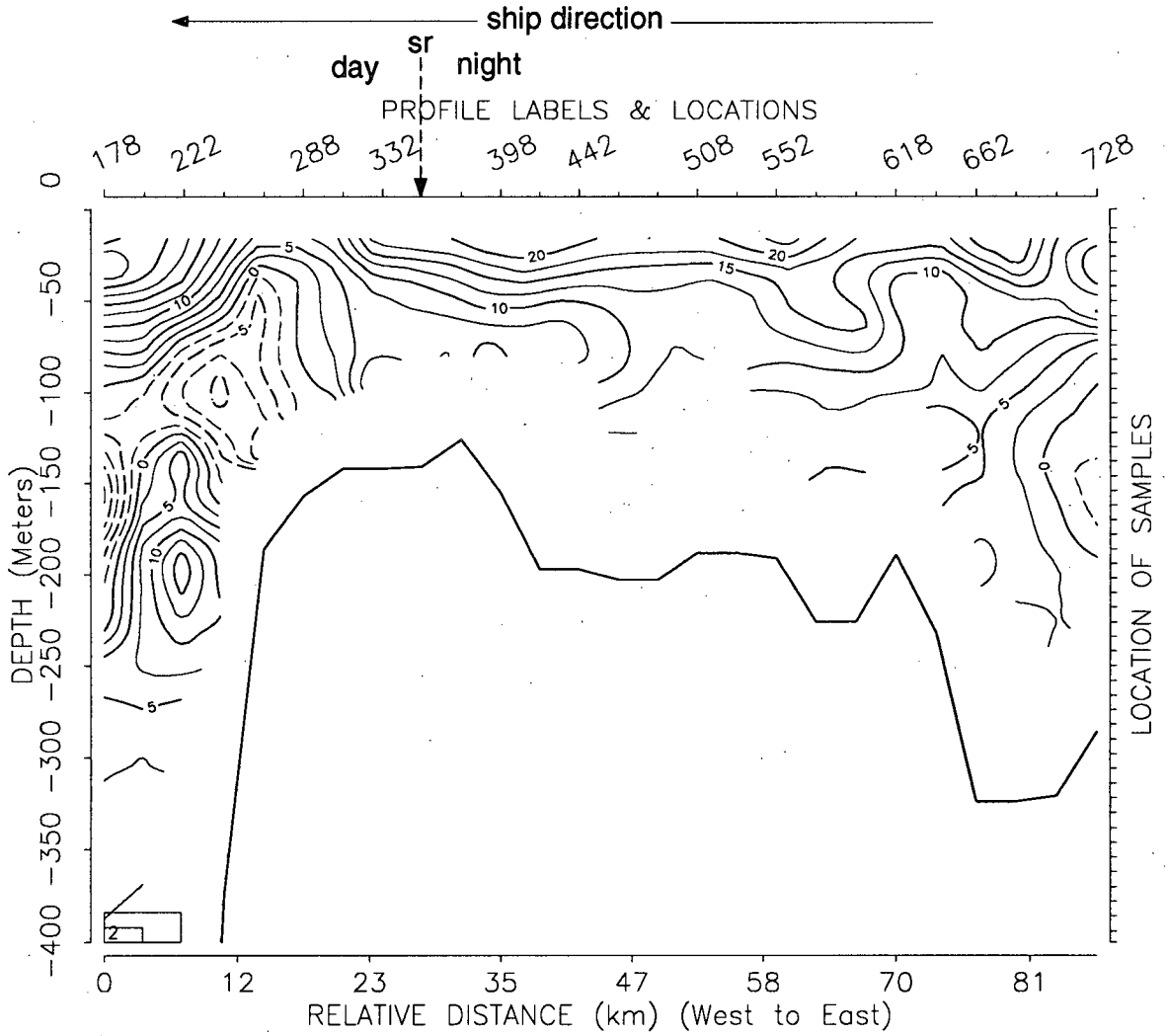

Figure 5.20: Contoured backscatter residuals (dB) for section 6. Data was collected from 00:44 to 08:44 PDT on 29/06/93, with the ship steaming offshore. Sunrise occurred at 05:30 PDT when the ship was over the shelf at a relative distance of $\approx 25km$, as indicated by the dashed arrow.

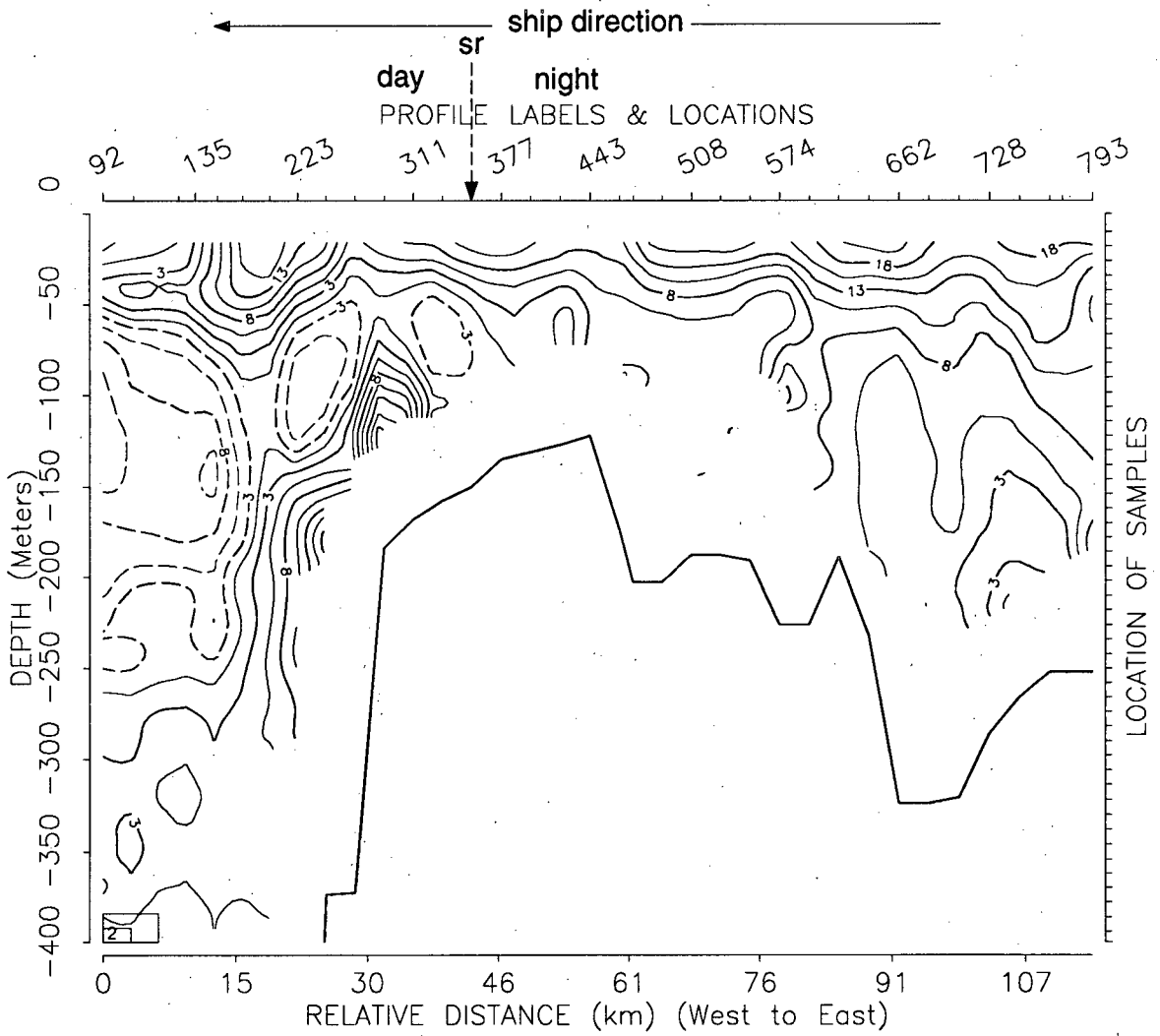

Figure 5.21: Contoured backscatter residuals (dB) for section 7. Data was collected from 00:27 to 10:28 PDT on 19/06/93, with the ship steaming offshore. Sunrise occurred at 05:30 PDT when the ship was over the shelf at a relative distance of $\approx 40km$, as indicated by the dashed arrow.

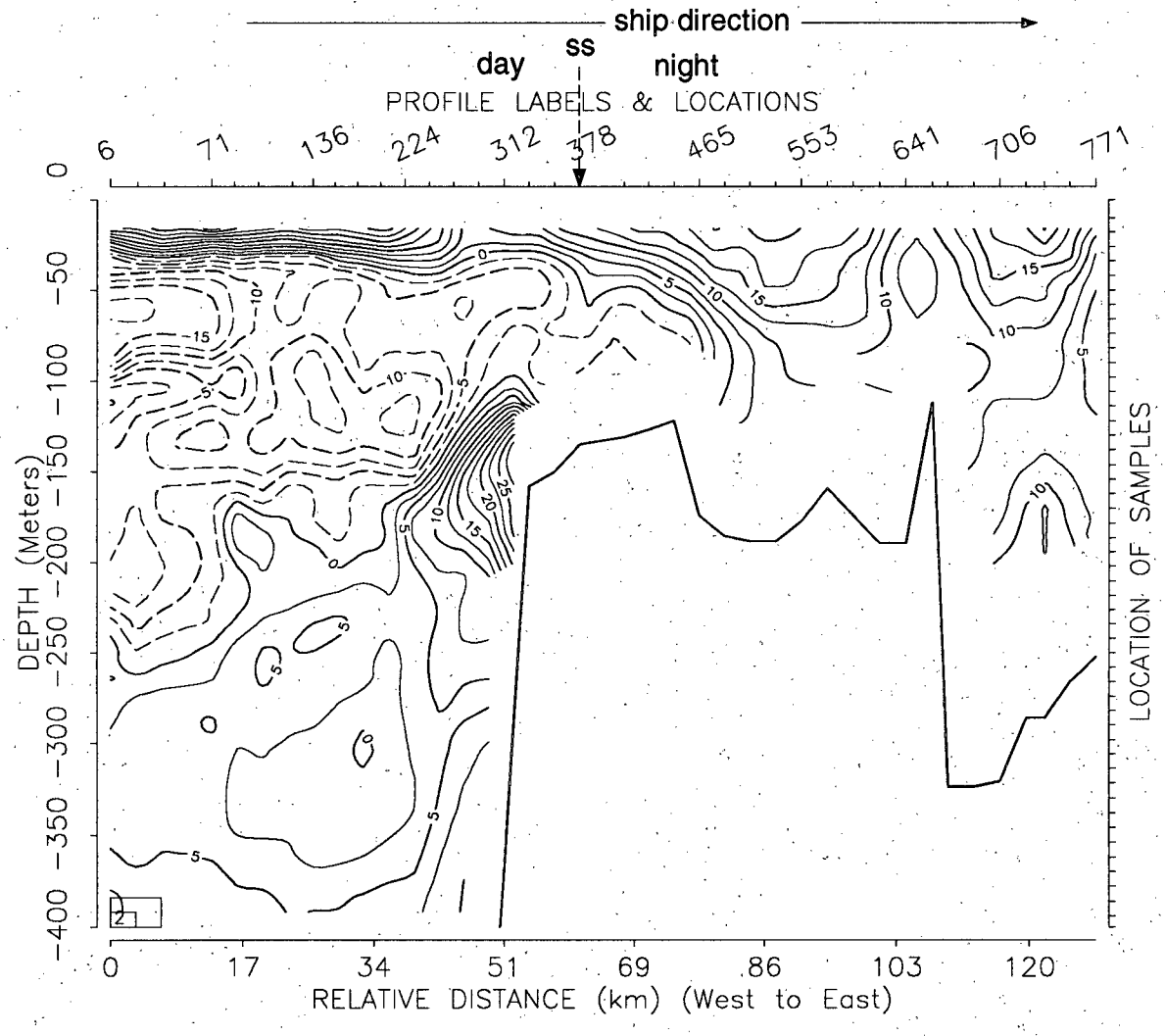

Figure 5.22: Contoured backscatter residuals (dB) for section 8. Data was collected from 17:58 to 23:58 PDT on 07/07/93, with the ship steaming onshore. Sunset occurred at 21:30 PDT on 07/07/93, when the ship was over the shelf, at a relative distance of $\approx 60km$, as indicated by the dashed arrow.

Absolute currents from:	σ_u (cm/s)	σ_v (cm/s)
bottom-tracking	8	7
GPS change in position	31	32

Table 5.2: Standard deviations on differences in neighboring profile currents at 10 m.

in the current components. Table 5.2 gives standard deviations (σ_u,σ_v) on the differences in the current components (u,v) calculated from 2576 profiles taken from 27/06/93 at 07:46 to 02/07/93 at 19:32, for profiles which used bottom-tracking and GPS change in position separately. The standard deviations of 7–8 cm/s in the currents obtained from bottom-tracking are only slightly (1–2 cm/s) higher than those calculated from the ADCP survey line (Chapter 5.1.4). The currents estimated from GPS change in position are a factor of four higher, or 31–32 cm/s. This is lower than the estimate of 40 cm/s made in Chapter 4.4.4 by comparing the GPS absolute currents with the bottom-tracking absolute currents. However, the estimate of about 30 cm/s is probably more accurate as it does not involve errors in bottom-tracking estimates. The mean number of profiles averaged onto a grid point is about 10, and so the spatial averaging will reduce the standard deviations on the absolute velocities calculated from GPS estimates of ship velocity to:

$$\sigma_u \approx \sigma_v \approx \frac{32}{\sqrt{10}} = 10\ cm/s. \tag{5.9}$$

Absolute currents over the slope calculated from GPS estimates of ship velocity showed large changes ($\pm 30\ cm/s$) in the horizontal direction over distances of about 10 km. It was concluded that the GPS estimates of ship velocity were not reliable enough to yield accurate results. The remainder of this chapter will only look at absolute currents from bottom-tracking estimates of ship velocity.

The current structure was examined for the eight vertical sections in Table 5.1. Figures 5.23 - 5.30 are contoured vertical sections of the absolute water speeds normal and

tangential to the section planes. Normal currents are positive to the northwest, tangential currents are positive to the northeast.

The persistent features in sections 1–4 (Figures 5.23 – 5.26) were: (1) A southeastward flowing shelf break current (20–25 cm/s) in the upper 150 m over the shelf break; (2) a northwestward flow (10–15 cm/s) in the water over the shelf.

All four sections (1–4) showed negative (southeastward) normal components of about 20–25 cm/s and negative (southwestward) tangential currents of about 20 cm/s in the upper 150 m over the shelf break and slope. The 4^{th} vertical section over the shelf had positive normal flow in upper 50 m and negative normal flow below 50 m, with a shear of about 20 cm/s over 100 m. Vertical shears of equivalent magnitudes were also observed in sections 1 and 2 over the shelf break. Sections 1 and 2 (Figures 5.23 and 5.24) show positive tangential ($\approx 15\,cm/s$) currents and normal currents of -5 to 10 cm/s over the shallow basin in the shelf at relative distances of 45–65 km.

The persistent features in sections 5–8 (Figures 5.27–5.30) were: (1) a west-northwestward flow (20–70 cm/s) in the upper 50–100 m at the northeastern corner of the sections (near the mouth of Juan de Fuca Strait at relative distances of 55–90 km - see Figure 5.14), probably due to outflow from Juan de Fuca Strait; (2) a south-southeastward flow (20–60 cm/s) in the upper 50–100 m over the shelf, just seaward of the northwestward flow in (1) and probably due to the Juan de Fuca Eddy; and (3) southward and eastward flows (15–20 cm/s) over the shelf break, due to the shelf break current.

Sections 6 and 7 both revealed vertical shears in the normal components over Juan de Fuca Canyon at relative distances of 65–75 km of about 35 cm/s over 100 m, with normal flows reversing from southeastwards in the upper 50 m to northwestward in the deeper water. The tangential components over Juan de Fuca Canyon in the northeastern corner of sections 6 and 7 revealed shears of about 70–80 cm/s over 200 m, with tangential flows reversing from southwestward in the upper 50 m to northeastward in the deeper water.

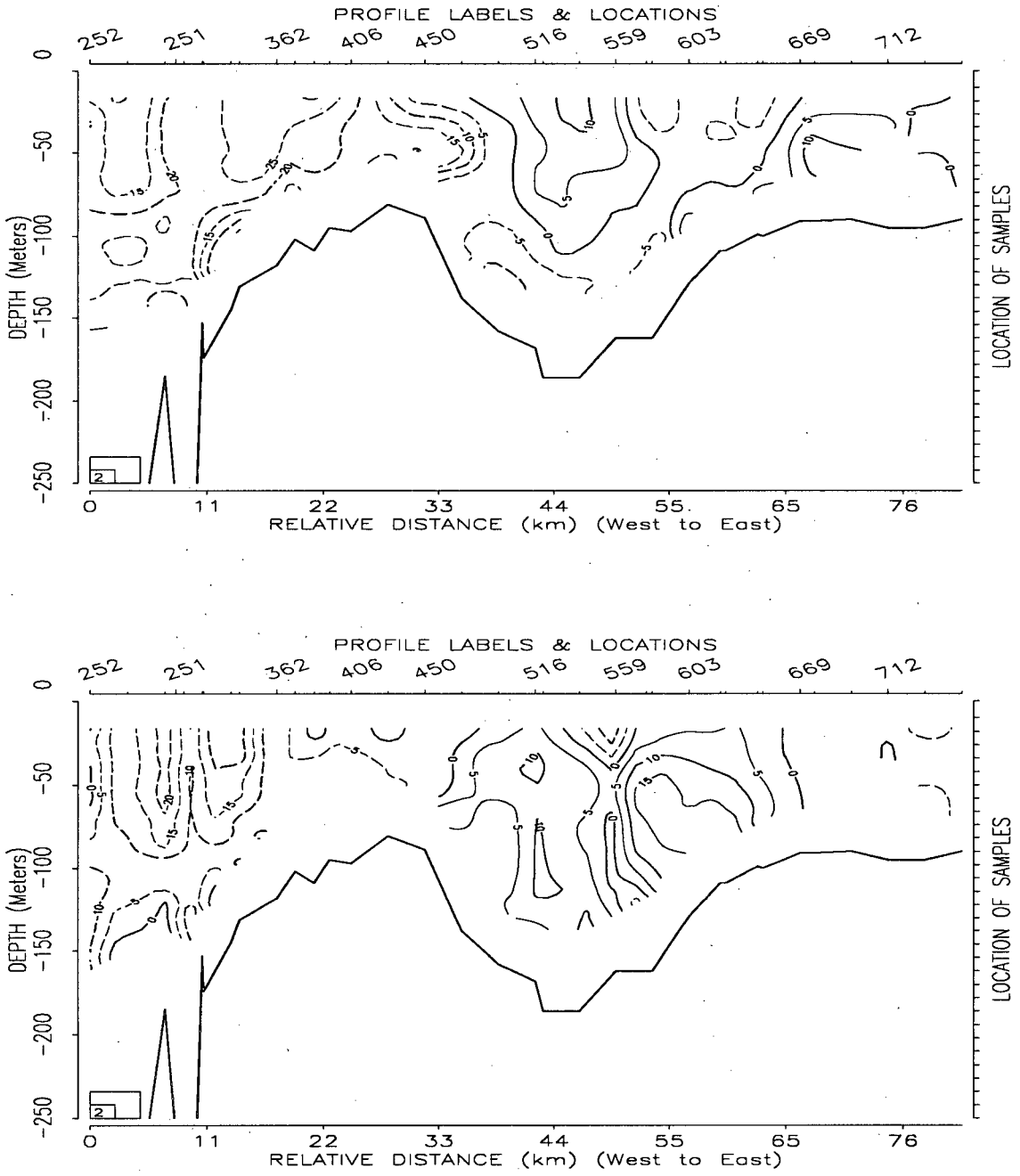

Figure 5.23: Contoured normal (top) and tangential (bottom) currents (cm/s) for section 1. Normal currents are positive to the northwest, tangential currents are positive to the northeast. Data was collected from 11:44 PDT on 27/06/93 to 03:44 PDT on 28/06/93, with the ship steaming offshore.

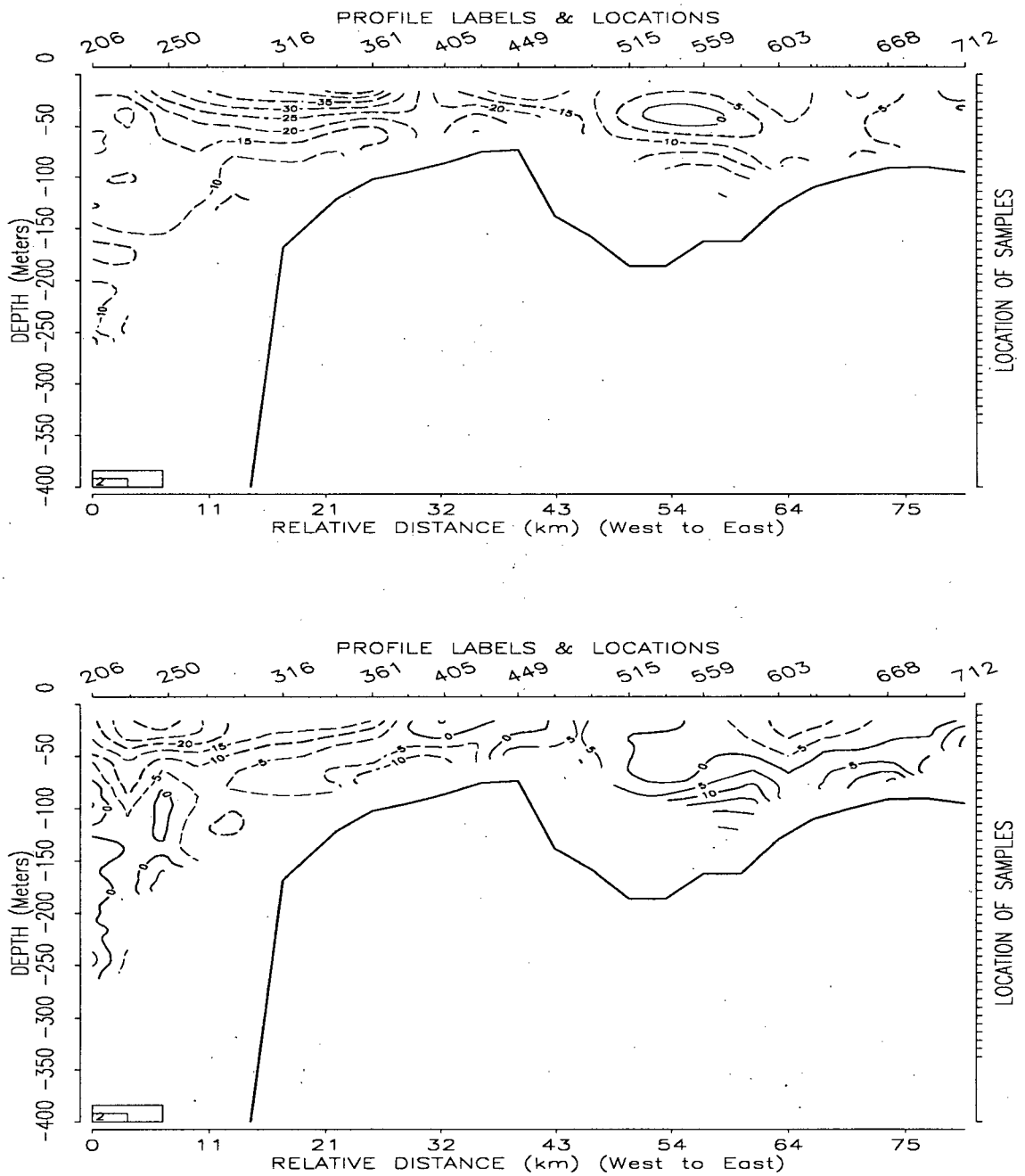

Figure 5.24: Contoured normal (top) and tangential (bottom) currents (cm/s) for section 2. Normal currents are positive to the northwest, tangential currents are positive to the northeast. Data was collected from 17:44 to 22:44 PDT on 30/06/93, with the ship steaming offshore.

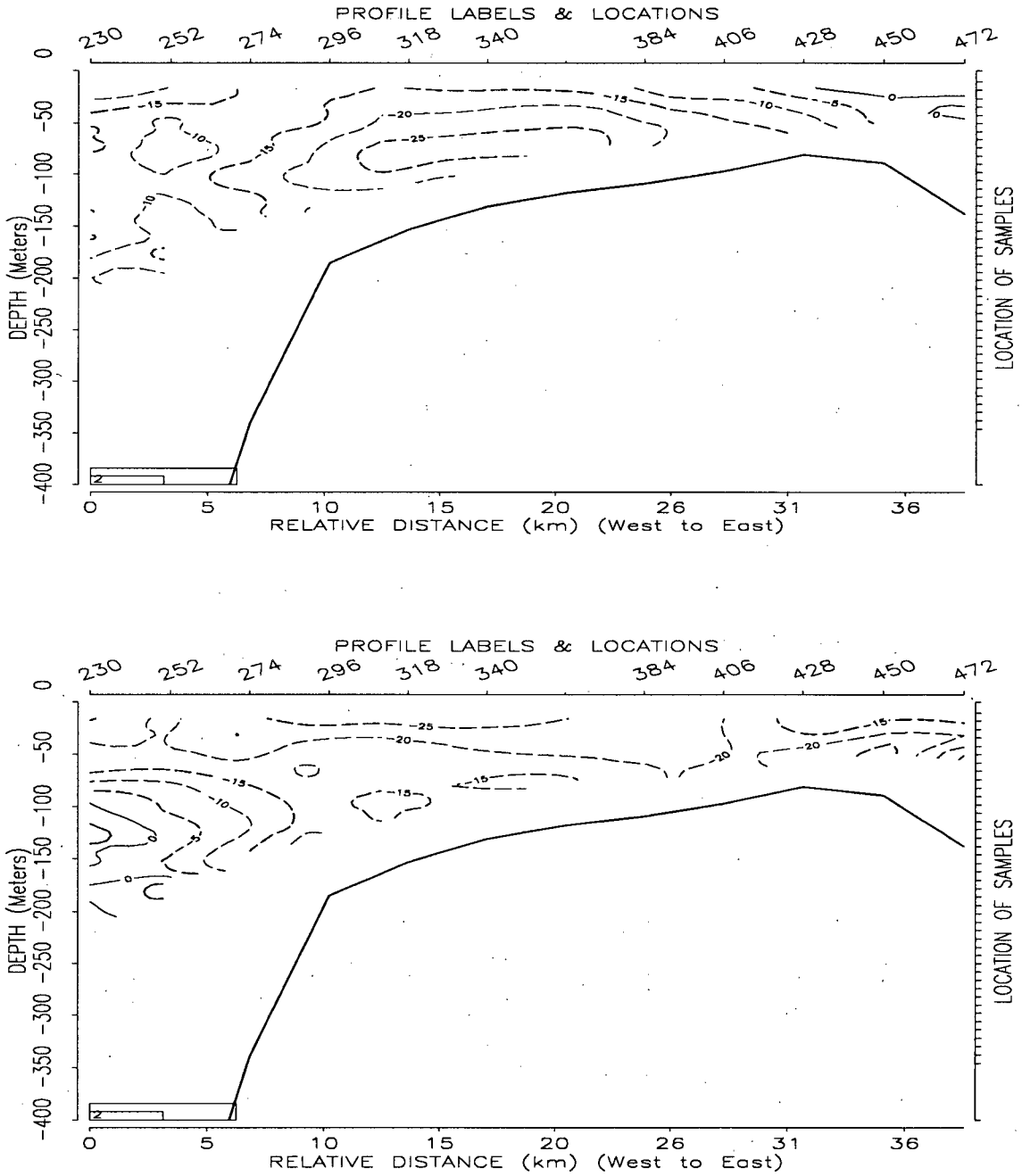

Figure 5.25: Contoured normal (top) and tangential (bottom) currents (cm/s) for section 3. Normal currents are positive to the northwest, tangential currents are positive to the northeast. Data was collected from 22:28 PDT on 19/06/93 to 05:28 PDT on 20/06/93, with the ship steaming onshore.

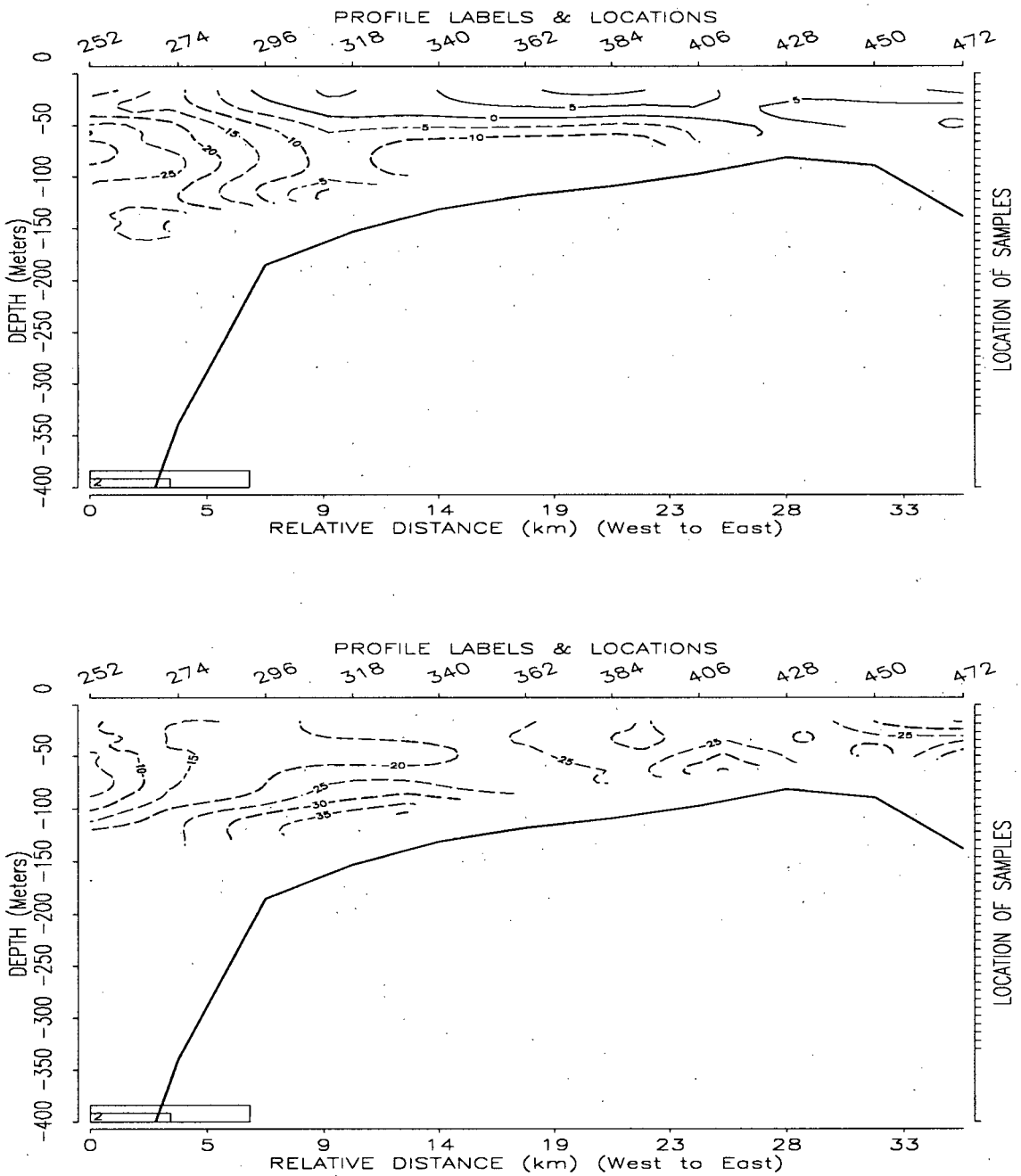

Figure 5.26: Contoured normal (top) and tangential (bottom) currents (cm/s) for section 4. Normal currents are positive to the northwest, tangential currents are positive to the northeast. Data was collected from 05:28 to 11:28 PDT on 20/06/93, with the ship steaming offshore.

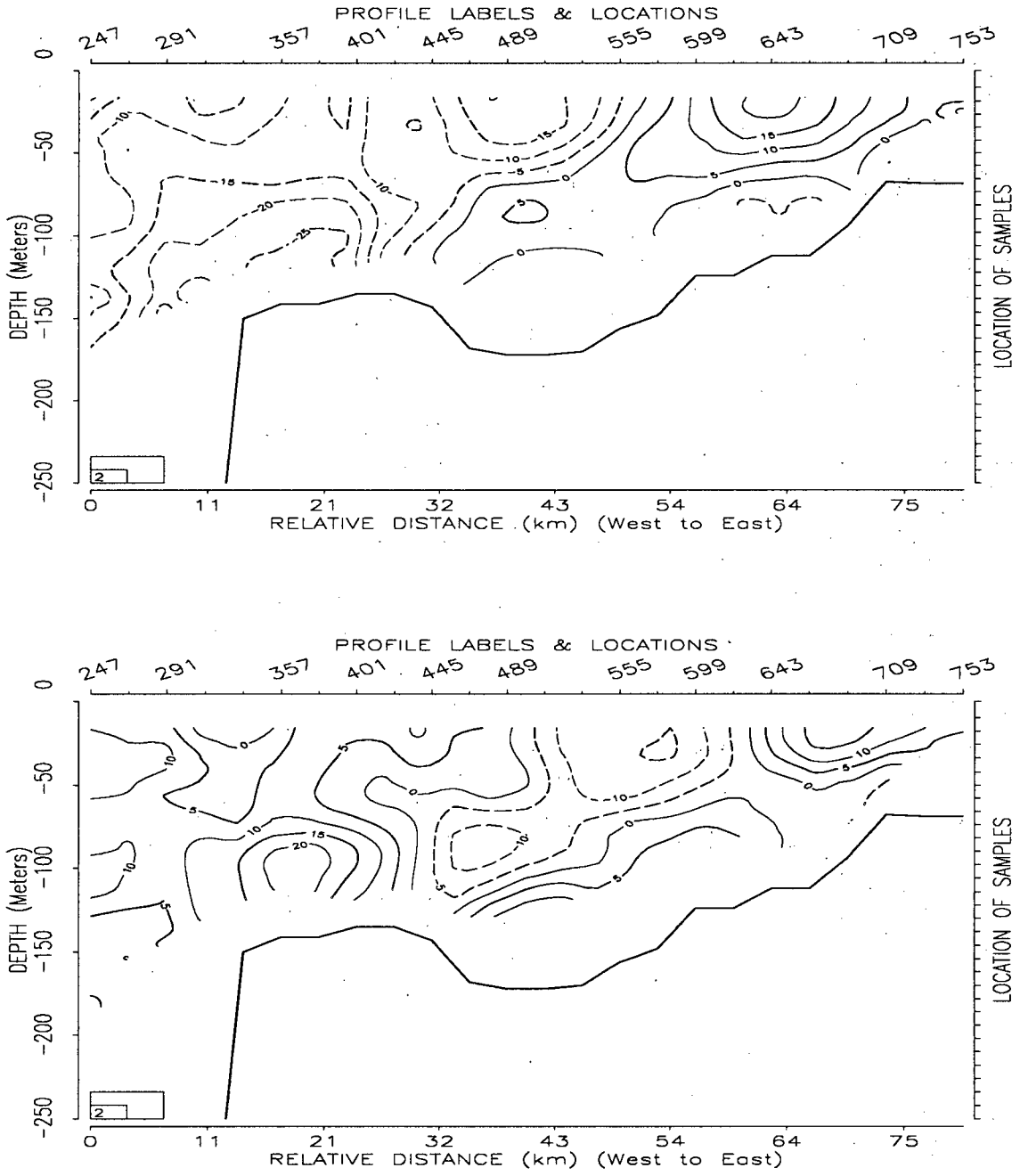

Figure 5.27: Contoured normal (top) and tangential (bottom) currents (cm/s) for section 5. Normal currents are positive to the northwest, tangential currents are positive to the northeast. Data was collected from 05:28 to 11:28 PDT on 20/06/93, with the ship steaming offshore.

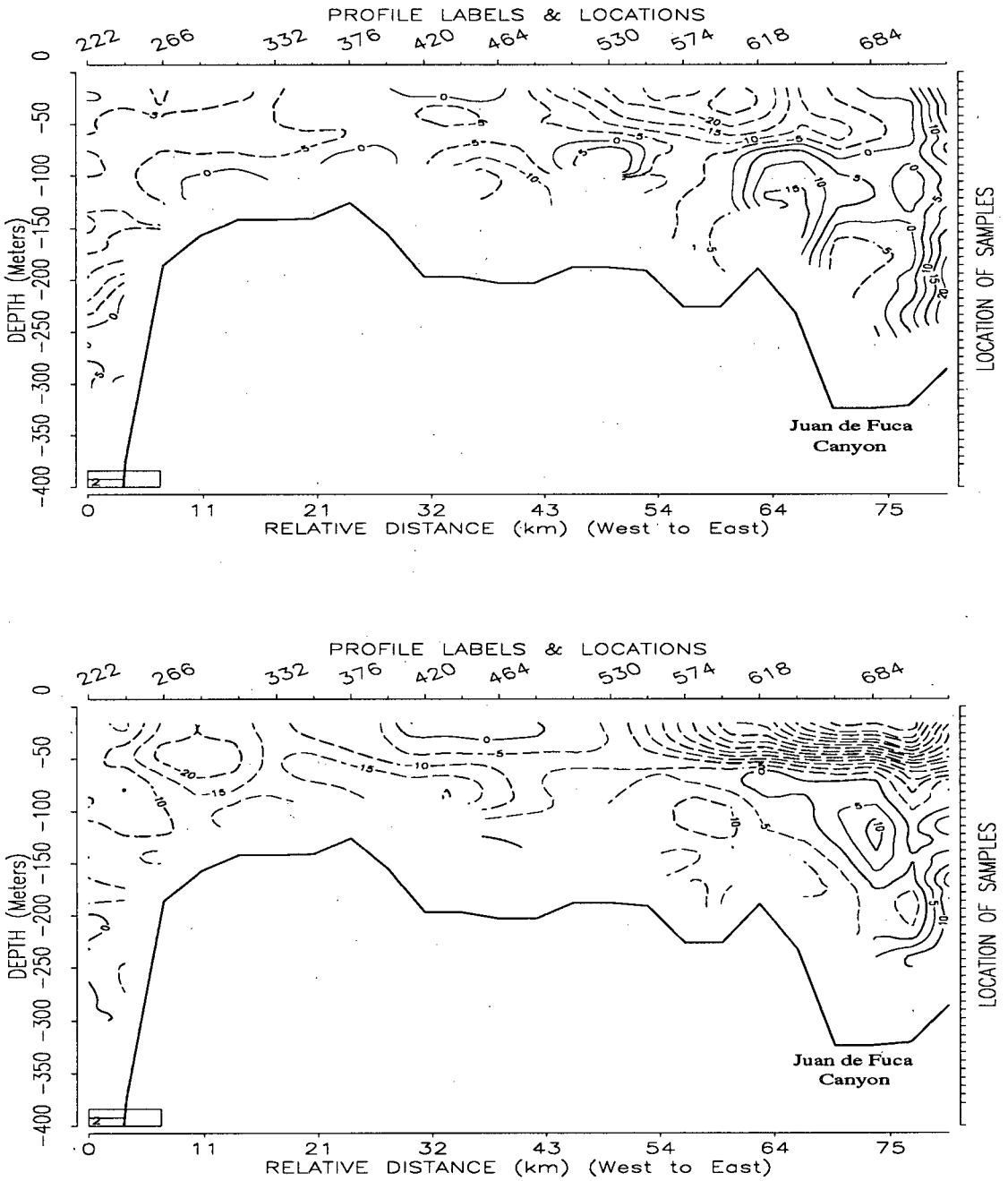

Figure 5.28: Contoured normal (top) and tangential (bottom) currents (cm/s) for section 6. Normal currents are positive to the northwest, tangential currents are positive to the northeast. Data was collected from 05:28 to 11:28 PDT on 20/06/93, with the ship steaming offshore.

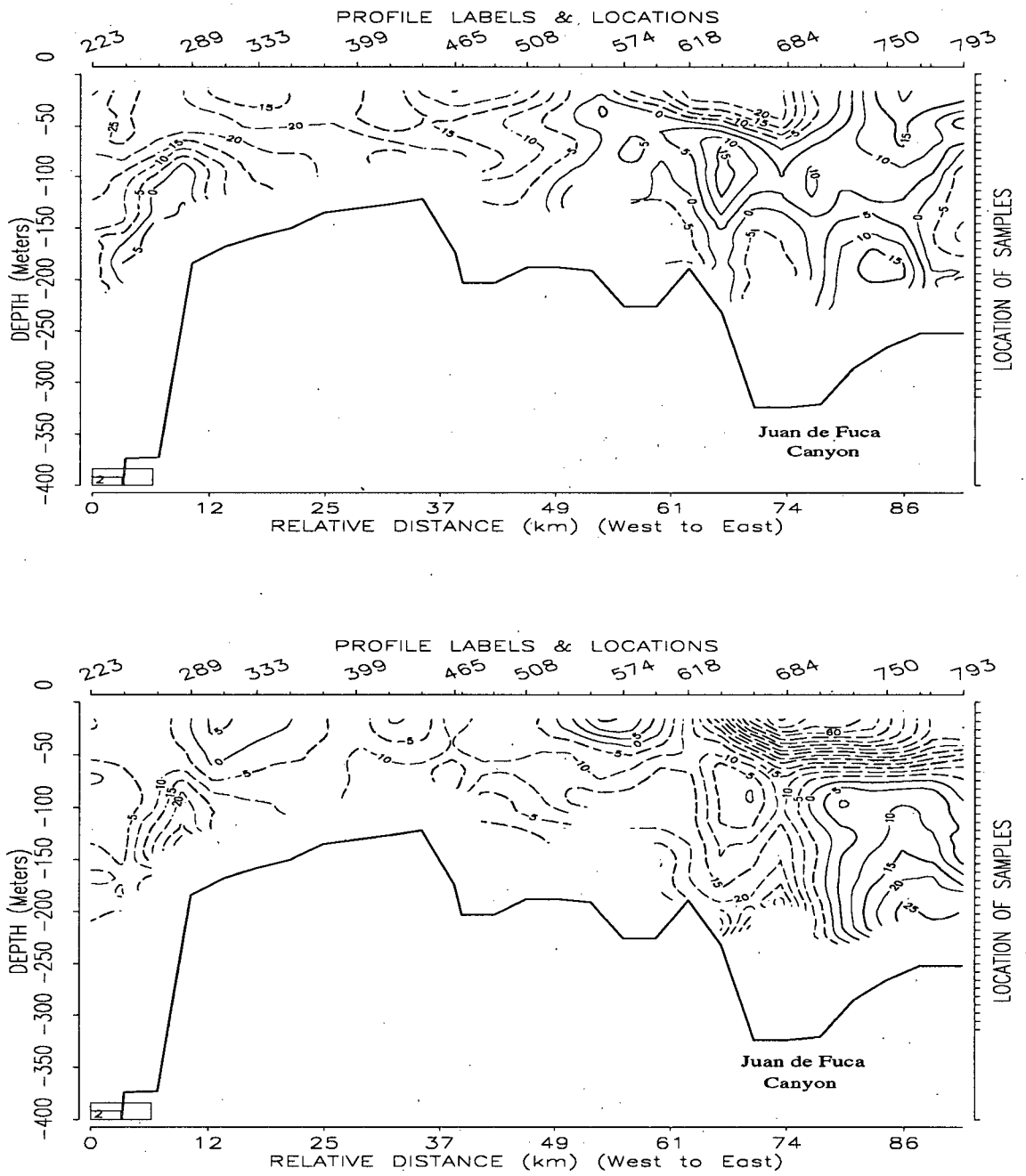

Figure 5.29: Contoured normal (top) and tangential (bottom) currents (cm/s) for section 7. Normal currents are positive to the northwest, tangential currents are positive to the northeast. Data was collected from 05:28 to 11:28 PDT on 20/06/93, with the ship steaming offshore.

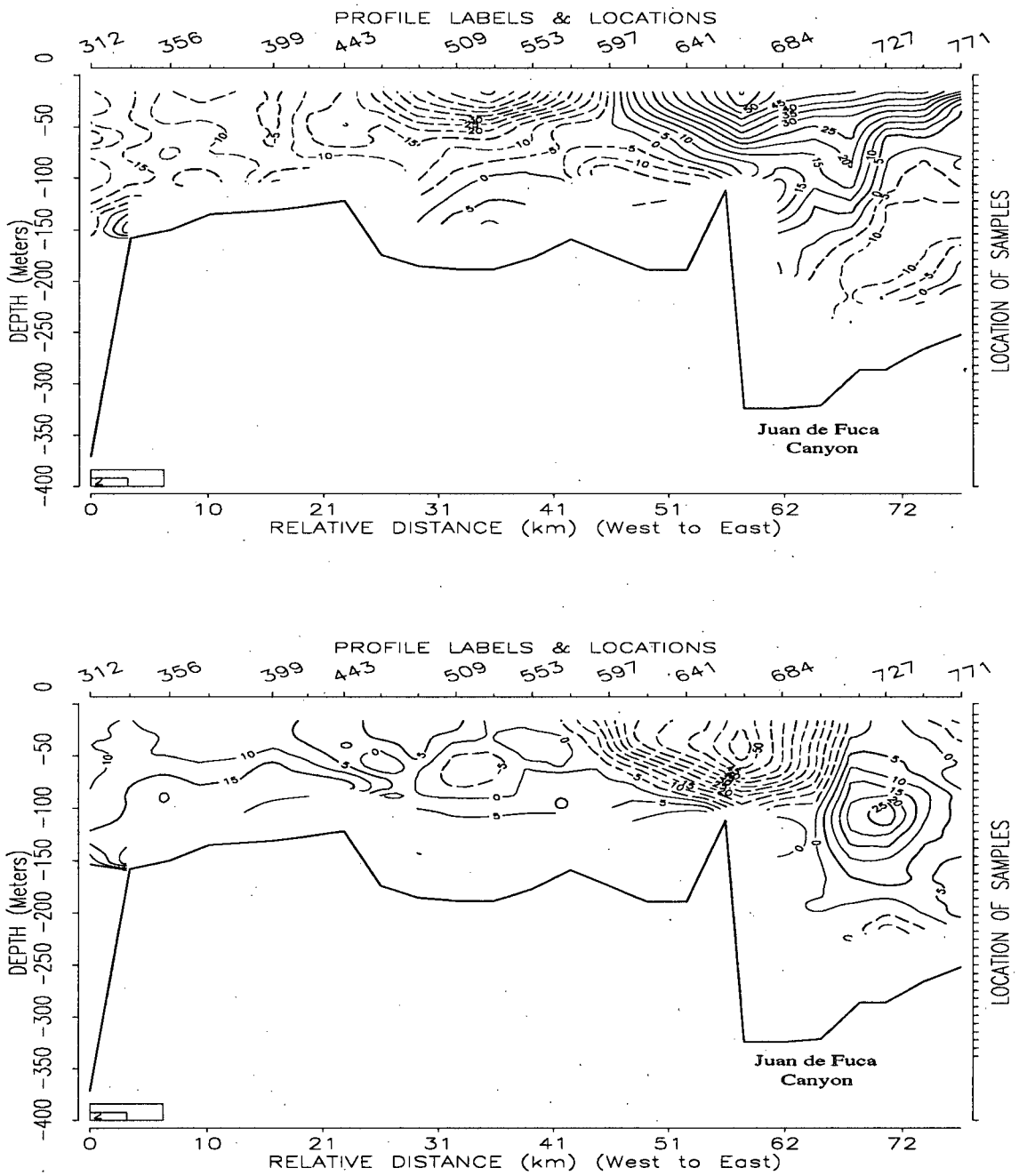

Figure 5.30: Contoured normal (top) and tangential (bottom) currents (cm/s) for section 8. Normal currents are positive to the northwest, tangential currents are positive to the northeast. Data was collected from 05:28 to 11:28 PDT on 20/06/93, with the ship steaming offshore.

Section 8 revealed a shear in the normal component over Juan de Fuca Canyon at relative distances of 65–75 km of about 50 cm/s over 200 m, with normal flows reversing from northwestwards in the upper 50 m to southeastward in the deeper waters.

5.2.4 Spatially Averaged Zooplankton Distributions

The zooplankton distributions over the entire southwest Vancouver Island continental margin can be examined by averaging the June 1993 cruise onto the 22 × 38 grid shown in Figure 4.16, and then into 24 m depth bins. The data initialized 326 of 836 grid-points (39%), with vertical coverage extending from 6 metres depth to about 80% of the bottom depth. Such an average combines data from different times of the month of June, 1993, and therefore must be approached with caution. Large variations in zooplankton distributions on diurnal time scales were observed in Chapter 5.1, especially at times near sunrise and sunset and at locations near the shelf break. Such variability makes an estimate of the seasonal mean zooplankton distribution very difficult, since each grid-point's averaged scattering levels will include only one or two different sampling periods. Typically, at least 3–5 sampling periods are needed to resolve diurnal variations. Thus, in the following analysis, only those large scale patterns observed to be persistent in Chapter 5.2.2 are examined. Any smaller scale variability is not reliable with so little data in the average.

Figures 5.31, 5.33 and 5.35 are horizontal maps of the daytime backscatter residuals averaged over the depth ranges [6,30] m, [78,102] m and [174,198] m, respectively. Figures 5.32, 5.34 and 5.36 are maps of the averaged nighttime backscatter residuals for the same depth ranges. Note that "absolute" backscatter residual levels cannot be compared between daytime and nighttime as different average fit parameters are used for day and night residual calculations.

The upper 30 m revealed a horizontal structure which was roughly uniform (to within

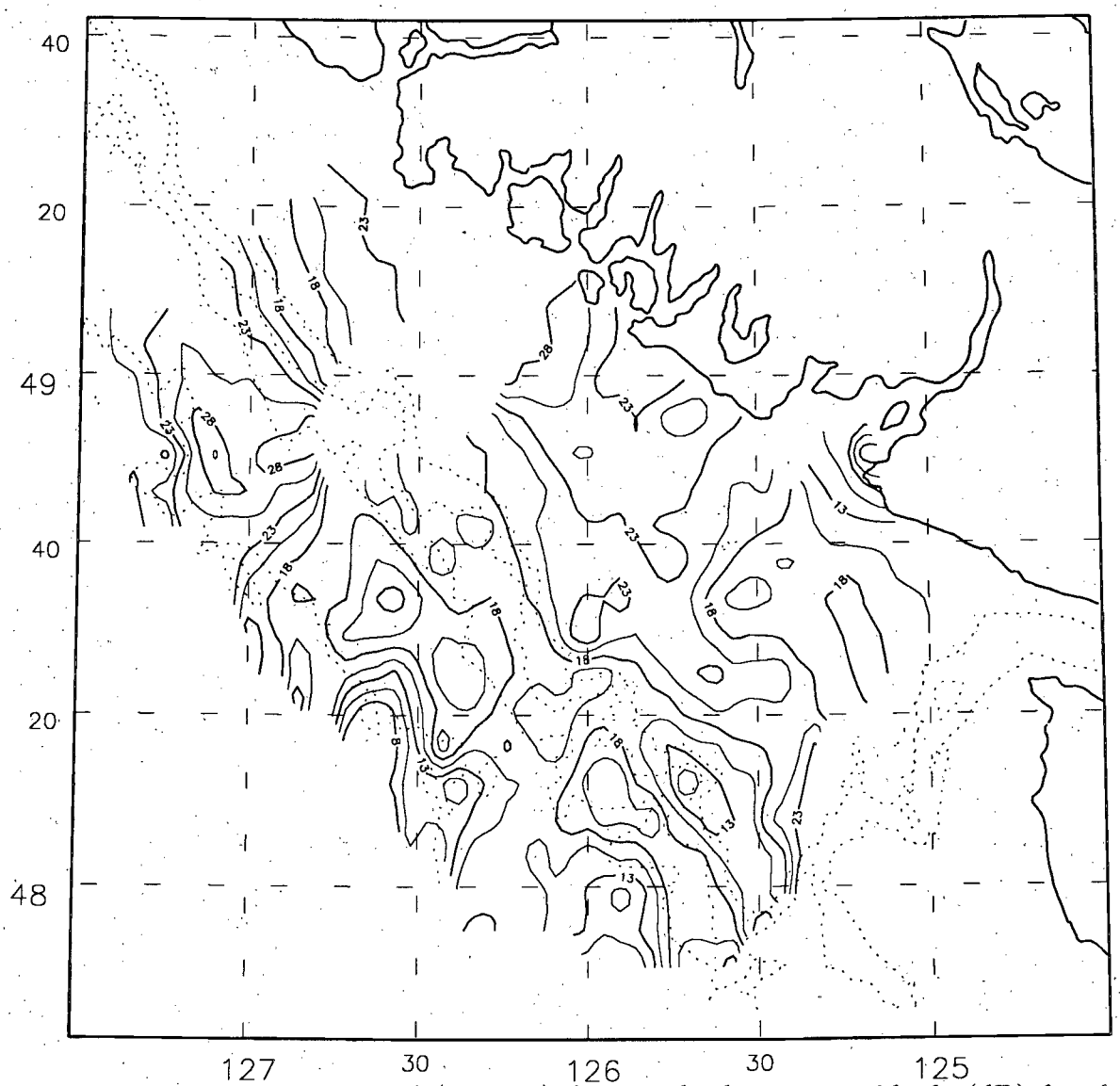

Figure 5.31: Vertically-averaged (6–30 m) daytime backscatter residuals (dB) for the period June 19 - July 7, 1993.

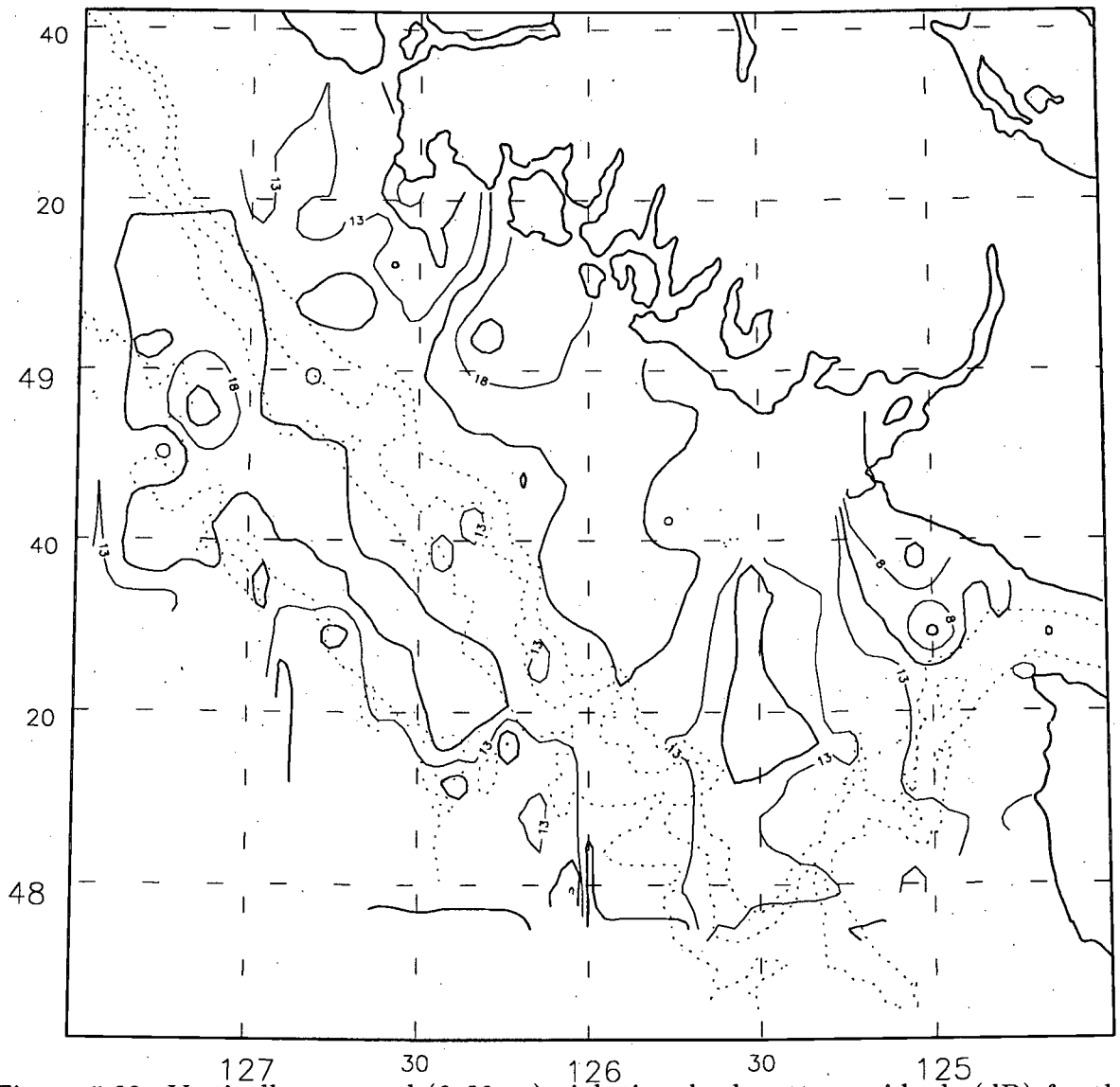

Figure 5.32: Vertically-averaged (6–30 m) nighttime backscatter residuals (dB) for the period June 19 - July 7, 1993.

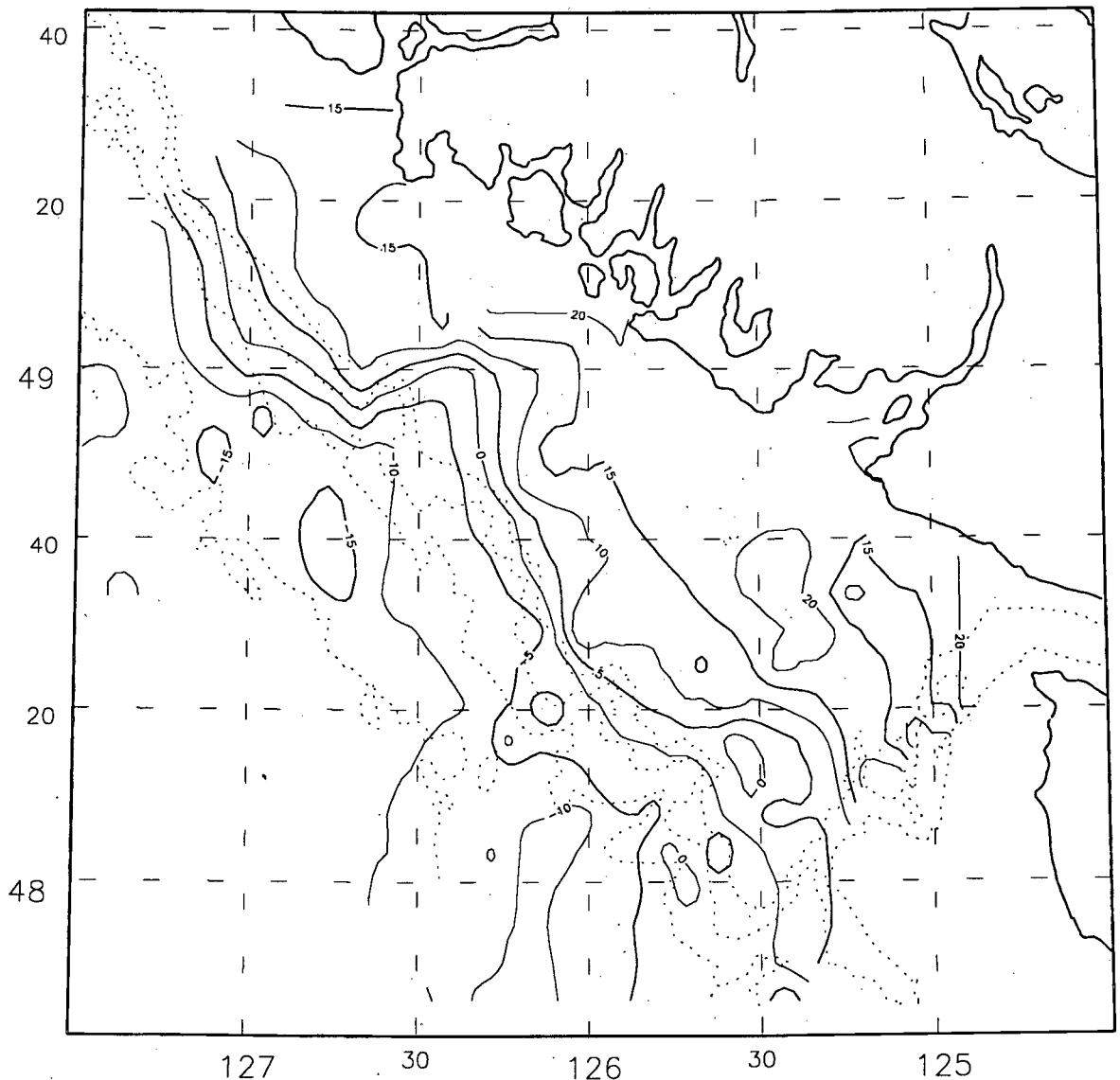

Figure 5.33: Vertically-averaged (78–102 m) daytime backscatter residuals (dB) for the period June 19 - July 7, 1993.

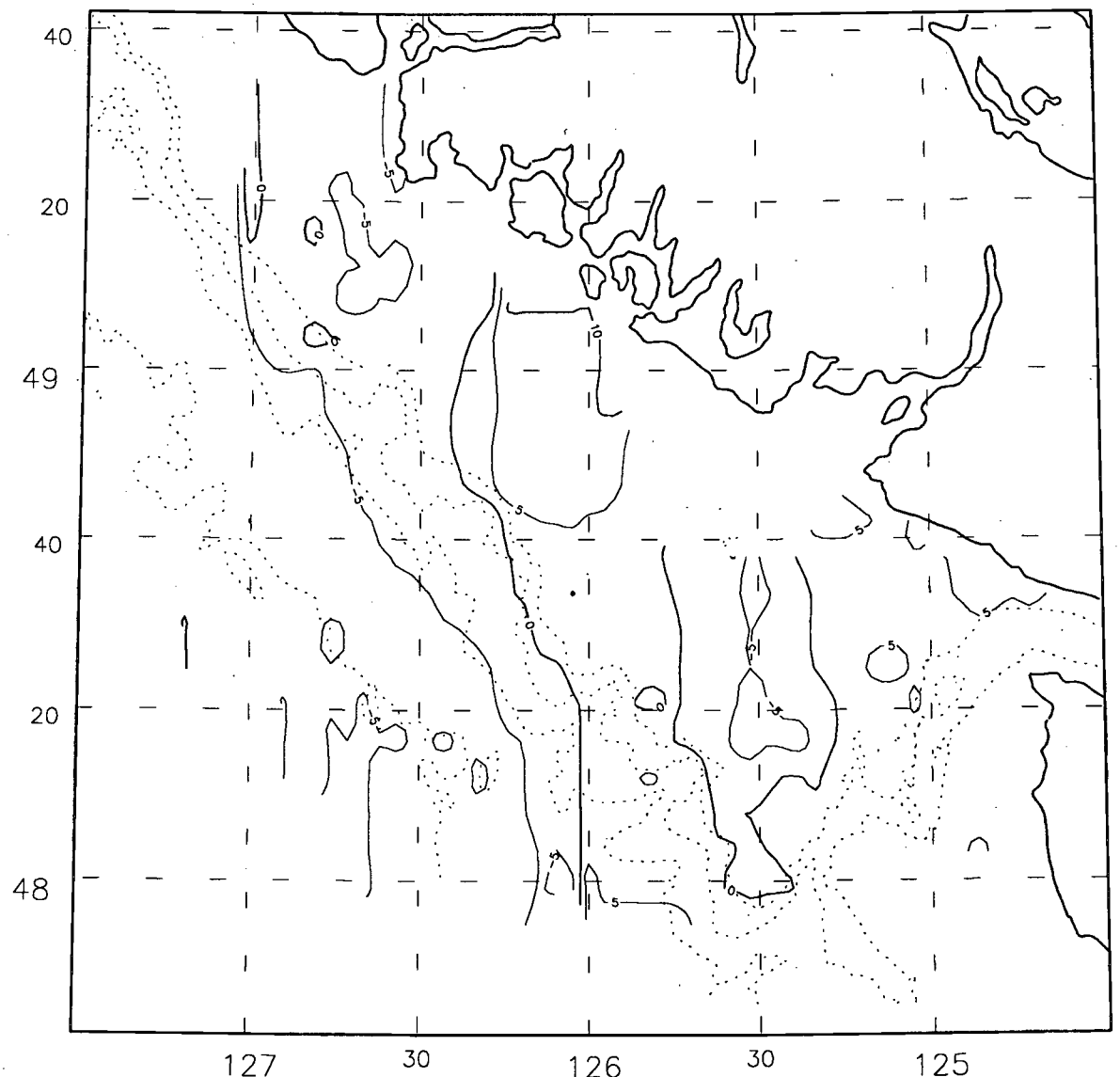

Figure 5.34: Vertically-averaged (78–102 m) nighttime backscatter residuals (dB) for the period June 19 - July 7, 1993.

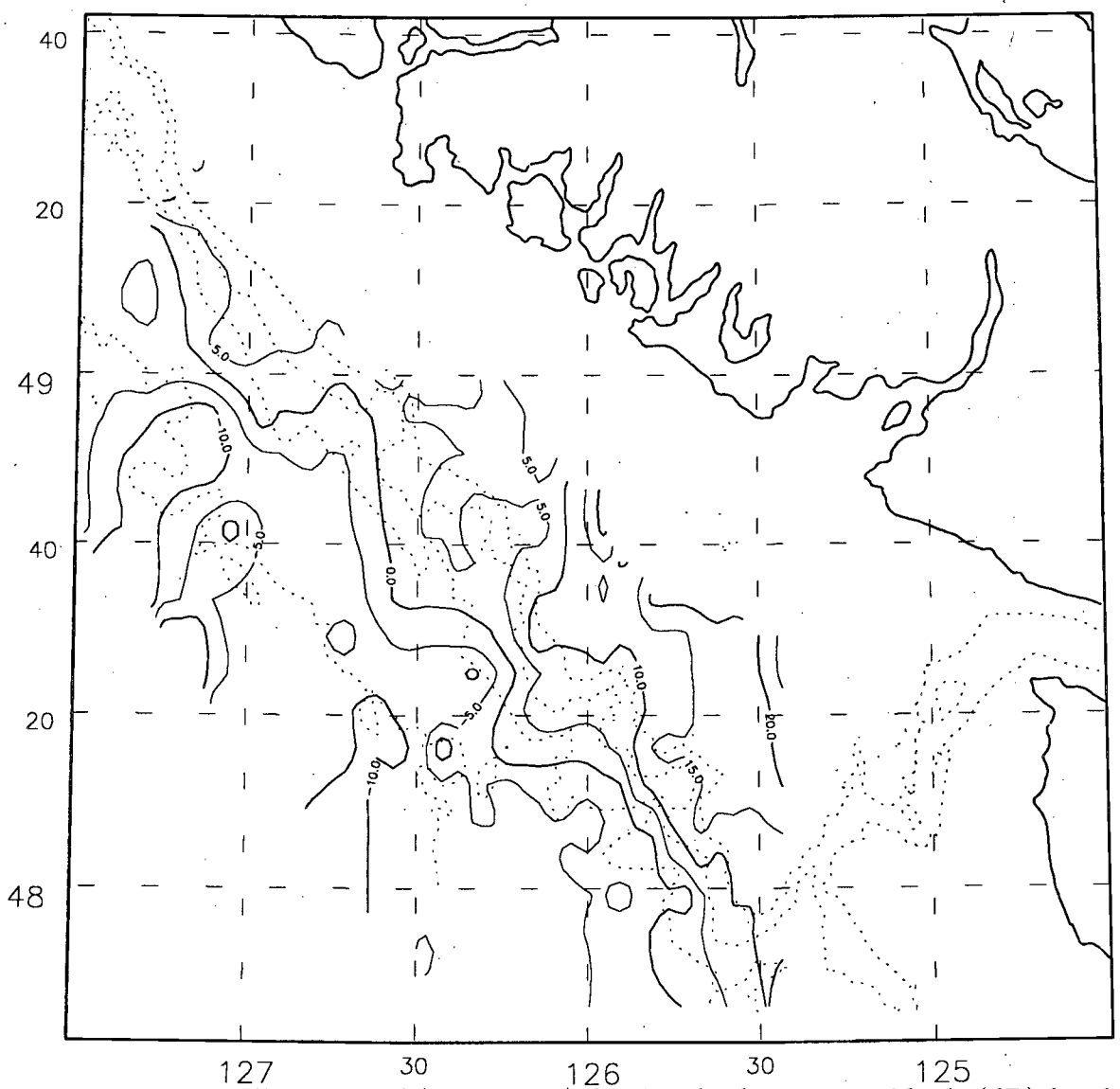

Figure 5.35: Vertically-averaged (174–198 m) daytime backscatter residuals (dB) for the period June 19 - July 7, 1993.

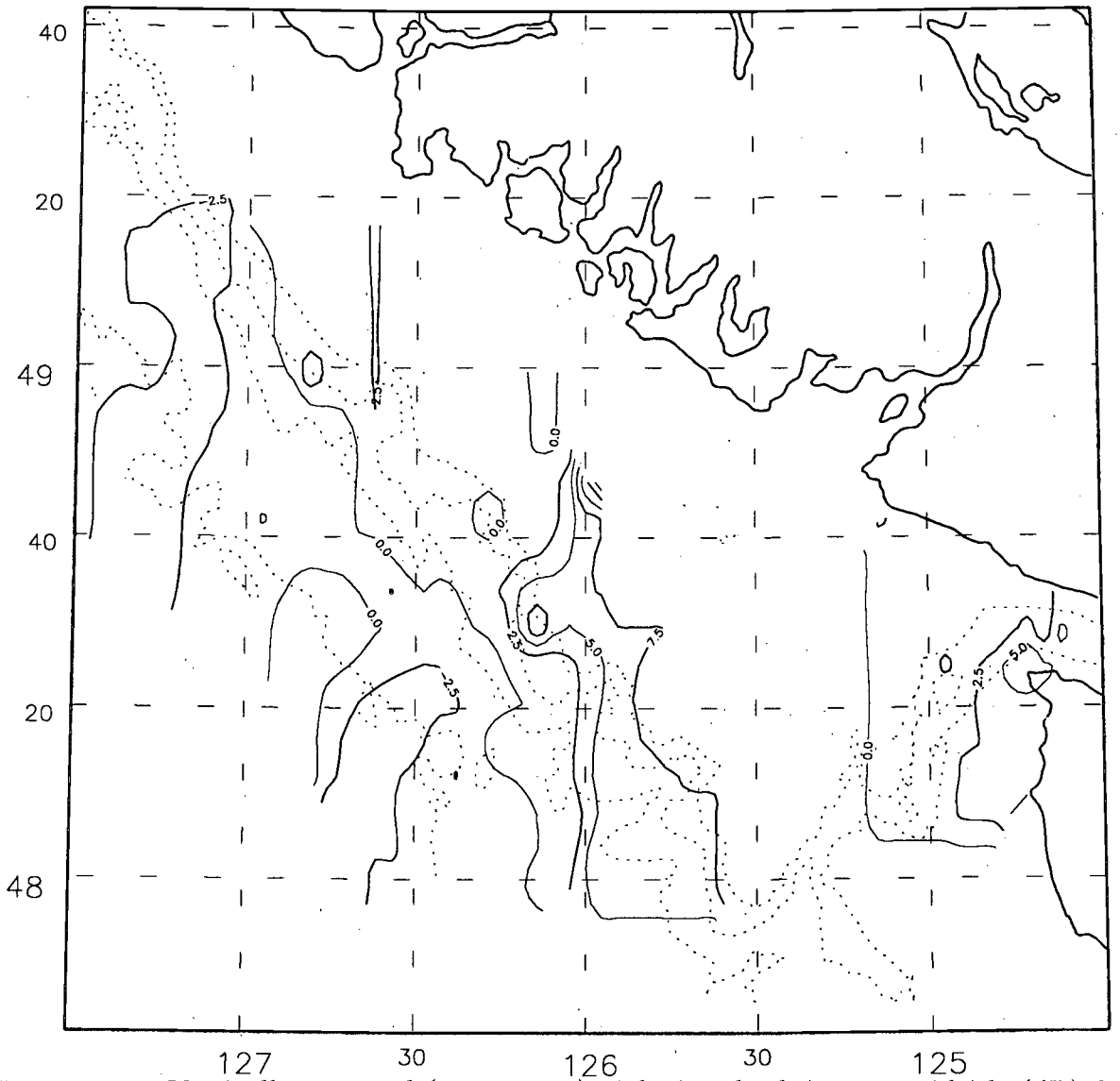

Figure 5.36: Vertically-averaged (174–198 m) nighttime backscatter residuals (dB) for the period June 19 - July 7, 1993.

$\pm 10\,dB$) both night and day, with backscatter residuals of about 20 dB during the day, and about 10–15 dB during the night. A slight depletion region along the shelf break was apparent both day and night in the surface waters, with levels $\approx 5\,dB$ lower than the levels over the shelf and over the slope. The mid-depth water (78–102 m) revealed a more banded structure along the shelf-break both day and night, with higher scattering levels over the shelf (15–20 dB during the day and 5–10 dB at night) than over the shelf-break and slope (−10–0 dB during the day and −5–0 dB at night). Lower scattering levels in the water from 78–102 m correspond to the depletion layer at the same depths seen in most vertical sections examined in the previous sections (e.g. Figures 5.4a–e and 5.15–5.22). The deep water (174–198 m) also revealed a banded structure along the shelf break. Scattering levels over the shelf break at night were 5–10 dB lower than the surface water levels. In contrast, the scattering levels over the shelf break during the day were about 15 dB lower than the surface water levels, due to plankton rising to their daytime depths.

Figure 5.37 shows two schematics of the cross-shelf zooplankton structure present along most of the shelf break in June, 1993 (a) at night and (b) during the day. These schematics show the general features observed in zooplankton distributions in Chapter 5.1 and in Chapter 5.2. High concentrations of zooplankton resided in the surface waters and a depletion region filled the depths from 100–200 m both day and night. Strong concentrations of scatterers resided just over the shelf break at depths of 150–200 m during the day. This shelf-break bottom scattering layer underwent migration into the surface waters at sunset, descending back to its daytime depth at sunrise. The surface scatterers are thought to be comprised of mainly copepods during the day, and of copepods and euphausiids at night. The daytime bottom shelf-break scattering layer is thought to be comprised of mainly euphausiids.

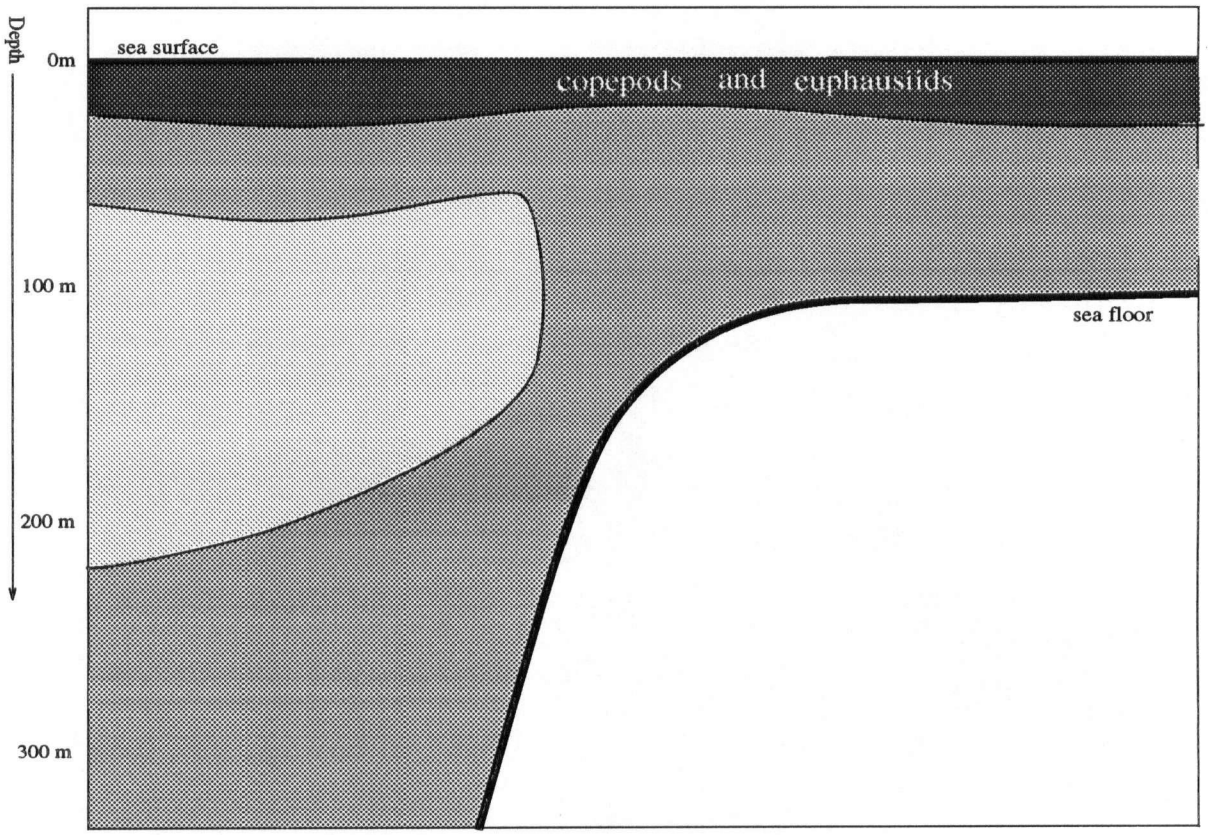

(a)

Figure 5.37: Schematic representations of the zooplankton structures found along the shelf-break in June, 1993 (a) at night. Dark areas indicate high backscatter residuals.

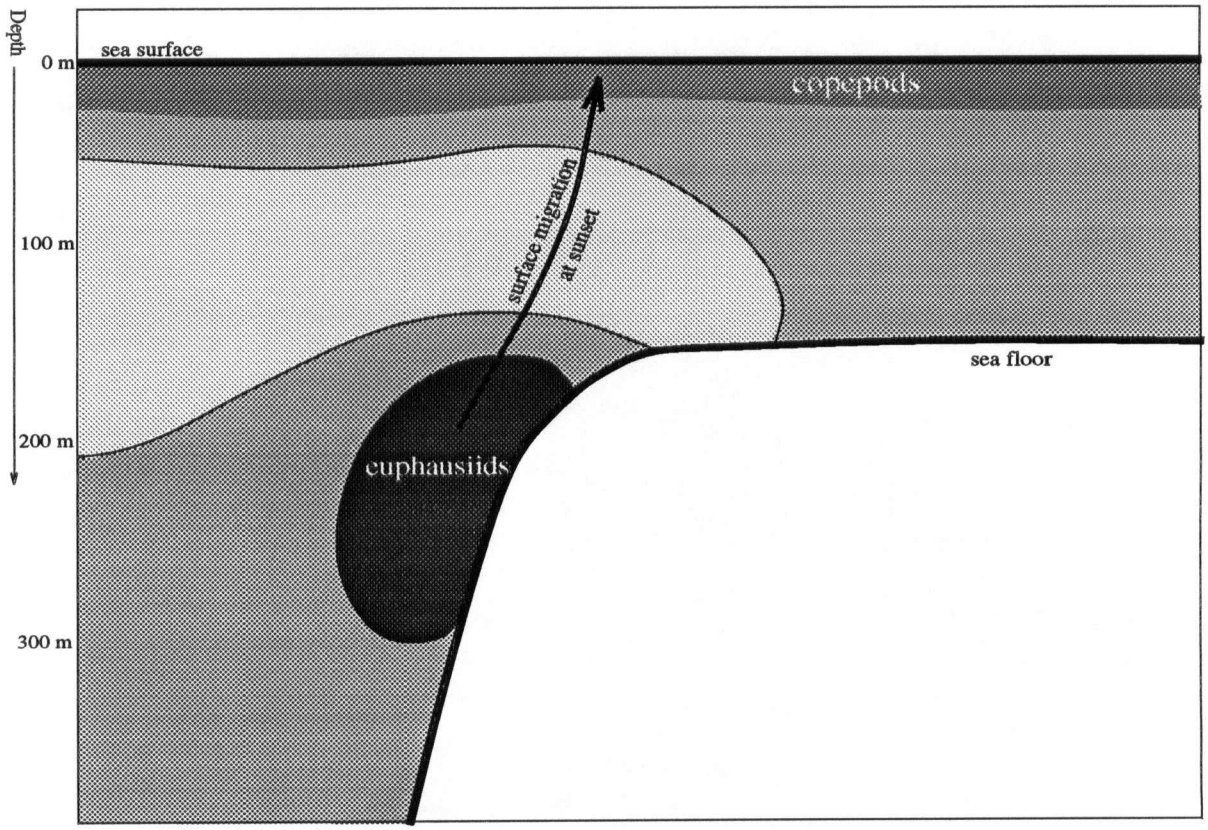

Figure 5.37: (b) during the day. Dark areas indicate high backscatter residuals.

5.2.5 Spatially Averaged Current Patterns

The current patterns over the entire southwest Vancouver Island continental margin are also examined by averaging the June 1993 cruise onto the 22 × 36 grid shown in Figure 4.16, and then into 24 m depth bins. Such an average combines data from different times of the month of June, 1993, and therefore must be approached with caution. Large variations in water flows on diurnal and semi-diurnal time scales due to strong tidal currents were observed in Chapter 5.1. Such variability makes an estimate of the seasonal mean flows very difficult, since each grid-point's averaged water velocities will include only one or two different sampling periods. Typically, about 6–10 different sampling periods would be needed in each average to resolve semi-diurnal variations (M.Foreman, *pers. comm.*). Thus, in the following analysis, only those large scale patterns observed to be persistent in Chapter 5.2.3 are examined. Any smaller scale variability is not reliable with so little data in the average.

Figures 5.38 and 5.39 are horizontal maps of the absolute current vectors averaged over the depth ranges [6,30] m and [78,102] m, respectively. Absolute currents from GPS estimates of ship velocity are included in these maps.

Two predominant features were observed. First, a strong flow ($\approx 20\,cm/s$) to the south-southwest over the shelf break (200 m isobath), as was observed in the vertical sections examined above. This is consistent with observations of a southwestward summer shelf break current by Freeland et al. (1984). Second, a strong outflow ($> 30\,cm/s$) to the northwest from Juan de Fuca Strait, which appeared to be turning to the south and southeast over Juan de Fuca Canyon. This outflow is apparent in the upper 30 m, but is much reduced at 80 m. This is consistent with the two-layer estuarine flow in the strait described by Labrecque et al. (1994), who found a seaward surface flow of relatively fresh water in the upper 80 m, and a landward flow of more saline oceanic

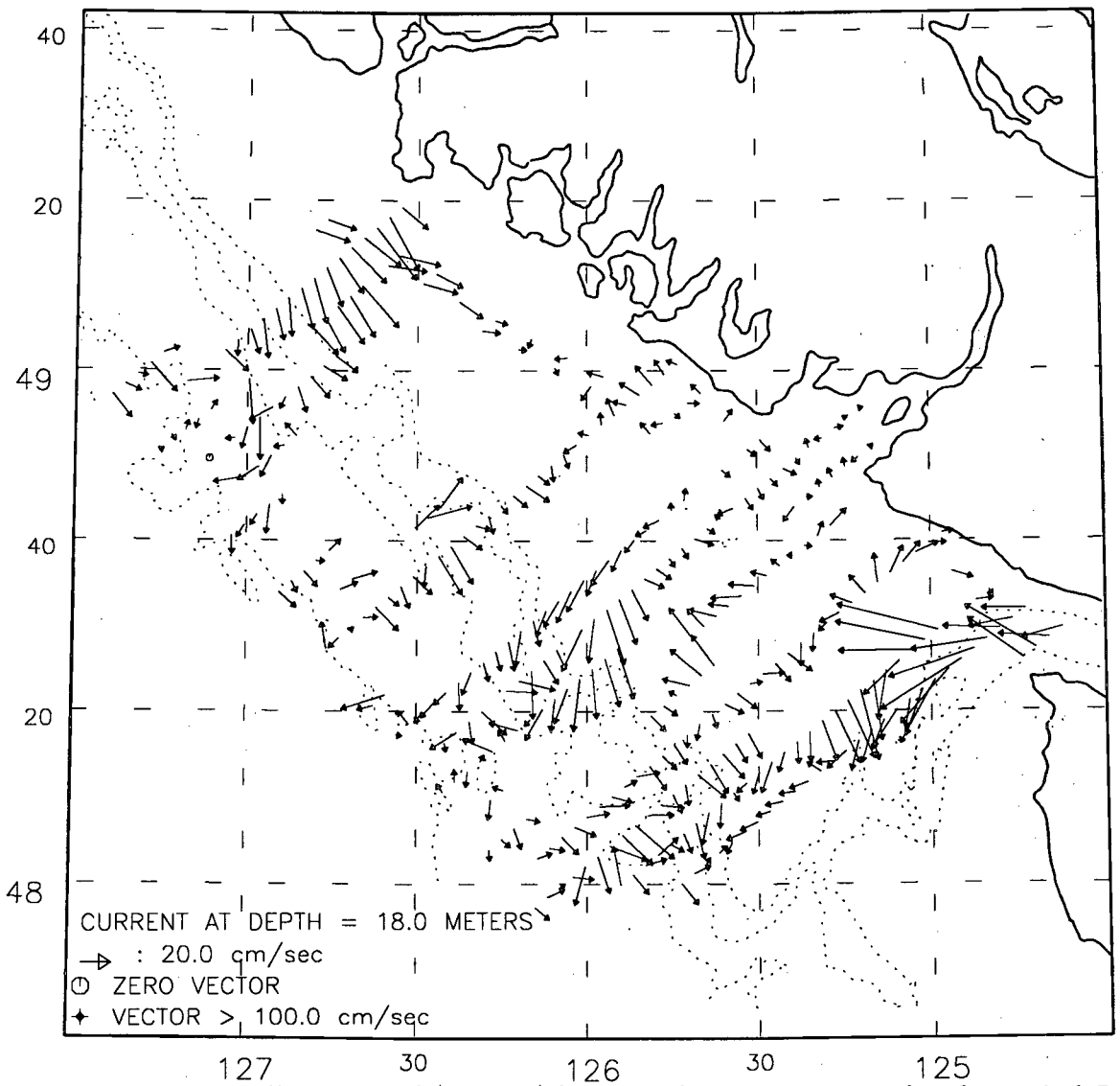

Figure 5.38: Vertically-averaged (6–30 m) horizontal current vectors for the period June 19 - July 7, 1993.

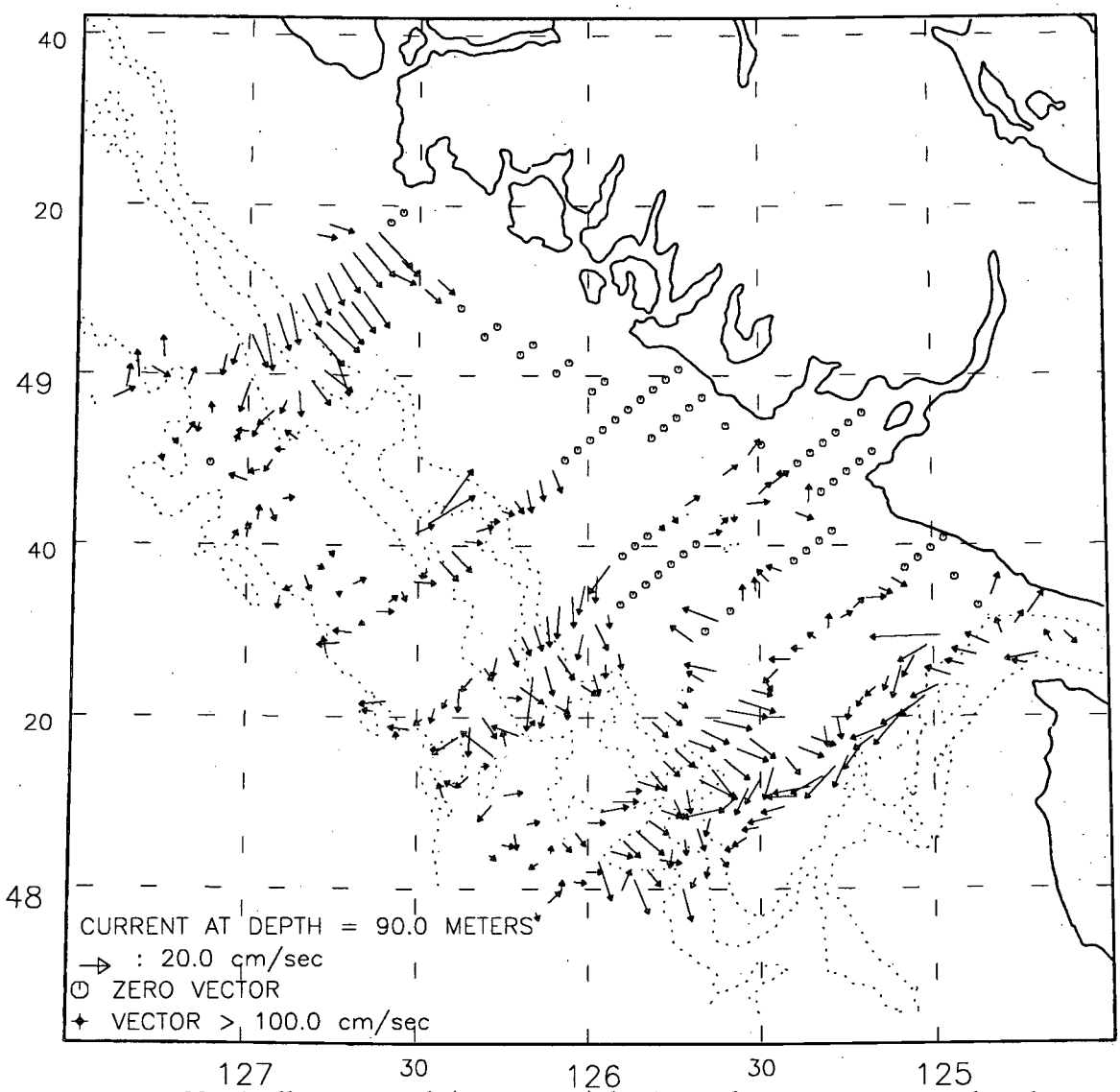

Figure 5.39: Vertically-averaged (78–102 m) horizontal current vectors for the period June 19 - July 7, 1993.

water at depth. A small clockwise eddy also appeared just north of the outflow from Juan de Fuca Strait. The flows over the slope are weak and confused, as expected from the errors in the GPS estimates of ship velocity. The flows over the shelf are also weak and confused, due primarily to a lack of temporal coverage and tidal velocities which are of the same magnitude as the mean velocities. Some evidence of a northwestward flowing coastal current is apparent near the coast off Cox Point (Tofino) at ($49°N$,$125.7°W$). A schematic of the major surface water flow patterns observed in Figure 5.38 is presented in Figure 5.40.

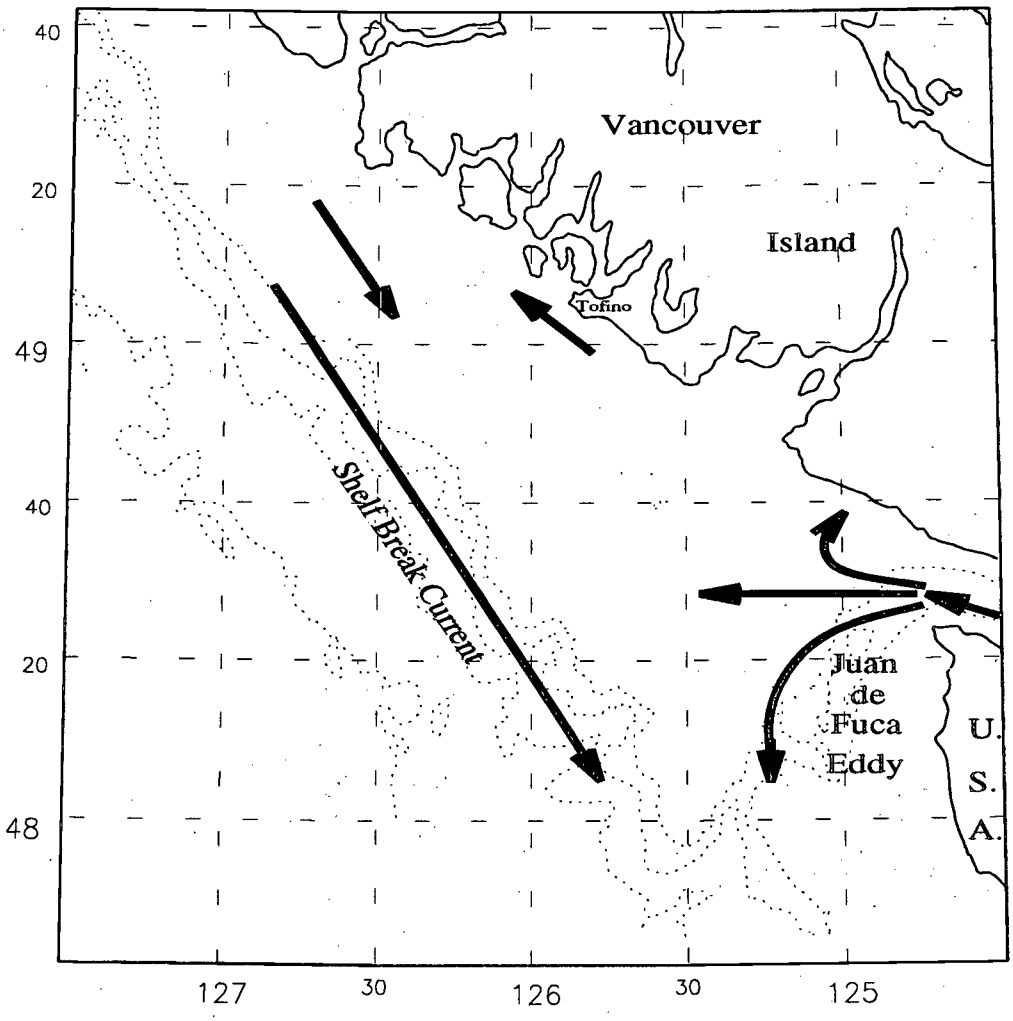

Figure 5.40: Schematic of the major surface water flow patterns in June, 1993.

Chapter 6

Summary and Recommendations

Goals

The goals of this work were first, to develop a consistent protocol for estimating backscatter strengths and current velocity from vessel-mounted ADCP data; and second, to use this protocol to examine spatial and temporal variability of zooplankton distributions off the southwest coast of Vancouver Island. Each of these goals will be addressed in the following summary, including what limitations the ADCP data have in making estimates of the backscatter strengths and currents, and what changes could be made to the present system to improve the data quality and resolution.

Estimating absolute backscatter values

Absolute measures of backscatter were difficult to obtain due to variability in the system parameters used to convert the raw AGC to backscatter strength, S_v. The parameters with the largest effects were the electronics noise, E_r, the power input to the transducer, V_s, and the temperature of the electronics, T_e. These parameters introduced errors in the estimates of S_v of about 5 dB. A measurement of E_r and of V_s, and continuous monitoring of T_e should reduce the error on S_v to below 1 dB. Using such an estimate of S_v, it would be possible to calculate zooplankton biomass using a model of how each species scatters 150 kHz sound and measurements of the relative abundances and weights of zooplankton from net samples taken coincidentally with the ADCP measurements.

Residuals

Most of the system-dependent effects in the backscatter profiles can be removed if the data are only used as a relative measure of zooplankton biomass. This is achieved with the residuals obtained after linear regression analysis on the data. Average regression parameters from 10000 profiles remove all system dependent effects from the backscatter residuals to within about 2 dB. This estimate of the errors in backscatter residuals depends on maximal variations in the system parameters affecting the backscatter strength (Table 4.2), and is probably smaller than 2 dB. A continuous record of the system parameters in Table 4.2 would yield a more precise estimate of the errors in backscatter residuals.

Bottom-scattering effects

Because averaging intervals often covered substantial variations in bottom depths, sidelobe bottom scattering effects in the vessel-mounted ADCP used in this study often contaminated a greater fraction of the water column than the specified 15% (RDI, 1989). Bottom-scattering effects by sidelobes were removed by using the minimum of five estimates of local water depth: Three recorded by the ADCP bottom-tracking pings; and two independent estimates from the Digital Terrain File. Such a method sometimes removes more of the profile than is necessary. However, this is a sacrifice which must be made in order to avoid ambiguities in the resulting backscatter profiles near the bottom. More accurate removal of bottom scattering effects could have been achieved using one of the following methods:

1. Record the minimum of all the depths measured by the ADCP bottom tracking pings in each ensemble averaging interval. In the present configuration, only the average bottom depth of the 20–30 depths was recorded. A simple algorithm could be implemented to record the absolute minimum depth encountered during each

averaging interval.

2. Implement a sonar beam that points vertically downwards in the ADCP (a 5-beam instrument). The bottom profile measured with a vertical beam is not affected by side-lobe bottom scattering. The vertical beam could therefore measure accurate backscatter strengths to within one bin length of the bottom. It could also be used in concert with the other four beams to measure backscatter strengths in the upper 80% of the water column. Gargett (1988) used a single narrow-beam 215 kHz transducer mounted on the vessel pointing straight down. Such a device could be implemented on the C.S.S. *J.P.Tully* and used with the vessel-mounted ADCP already in place to measure scattering strengths close to the bottom.

Separating profiles into day/night

It is important to distinguish between profiles taken during the day and during the night, as the zooplankton distributions change drastically at sunset and at sunrise. Upper limb sunset and sunrise times obtained from astronomical data were chosen as delimiters between day and night. Upper limb sunset and sunrise times are given in UTC, and so it is important to know what time zone the times recorded by the ADCP refer to. Unfortunately, the time zone is not recorded by the data acquisition system (DAS), and so must be found by examining the scientist's log-book in concert with the ADCP data. A record of the time zone referred to by the ADCP would be helpful.

Errors in water velocities

The errors in the absolute water velocities were estimated using the RDI (1989) method to be about 5 cm/s when using bottom-tracking estimates of ship velocity. The errors in absolute water velocities from GPS estimates of ship velocity were estimated to be about 40 cm/s. The bottom-tracking errors were small enough to yield accurate

measurements of local currents, especially when spatially averaged over distances of 4–8 km (which reduces the errors to about 2 cm/s). The GPS errors, on the other hand, were about twice the typical mean currents for the southwest coast of Vancouver Island, and as such were not very useful. Spatial averaging over distances of 4–8 km reduced the errors to about 15–20 cm/s, which is of the same order of magnitude as the local currents. Broad spatial averages over distances of about 30 km would be necessary to reduce the errors in absolute currents from GPS estimates of ship velocity to acceptable levels (5 cm/s). The use of differential GPS or removal of the selectivity mode by the U.S. Navy would improve positional accuracy and hence velocity by about an order of magnitude.

The error estimates in absolute water velocities given in the preceding paragraph must be regarded with some skepticism as they do not include the systematic errors due to the the offset angle and scaling bias of the ADCP mounted on the *J.P.Tully*. These effects have never been measured and were not corrected for in this study. Measurement of these effects would be necessary to make any claims about the accuracy of the water velocity estimates.

ADCP survey line results

The data collected by the vessel-mounted ADCP on the *J.P.Tully* were first examined on small spatial (14 km × 1.5 km) and small temporal (19 h) scales. The backscatter residuals were examined both as *in-situ* vertical sections, as time series for various locations across the shelf break and slope and as time series for various depth bins along the entire line. The current patterns were examined as *in-situ* vertical sections, and as time series for various depth bins along the entire line.

The zooplankton distributions represented by the backscatter residuals exhibited a definite structure which persisted during the first seven daylight hours of the time series.

This structure consisted of a strong surface scattering layer all across the shelf and slope, a depletion region between depths of 80–150 m over the slope, and a strong bottom scattering layer over the shelf break and slope. Horizontal offshore motion of aggregations of scatterers over the shelf was observed and the coincident water flows confirmed that the motion was due to advection by offshore flow. The persistent structure observed during the daytime changed drastically at sunset. The nighttime structure consisted of near-uniform scattering levels throughout the water column over the shelf and shelf break and a strong surface scattering layer across the shelf and slope. The changes observed at sunset were attributed to vertical migrations of euphausiids from depths of 150–200 m over the shelf break to the surface, with mean swimming speeds of 1–1.5 cm/s. A strong scattering layer was present over the shelf in the last few hours of the time series, and is believed to have been comprised of a high concentration of euphausiids which were advected into the area by a reversal in water flow from southeastward to northwestward. Such an advection was confirmed by the coincident ADCP measurements of the alongshore water flow. This scattering layer underwent an abrupt downwards migration from the surface waters to the near-bottom waters (100–120 m) just prior to sunrise, with mean swimming speeds of 3–4 cm/s.

The current patterns were consistent both with the summer mean southeastward-flowing shelf-break current (Freeland et al., 1984; Thomson et al., 1989b) and the tidal flows as calculated by Foreman's barotropic model (Foreman and Walters, 1990). Significant baroclinic tidal effects were observed as periodically occurring vertical shears with 12 hour periods. Absolute water velocities were calculated from bottom-tracking for most of the survey period. The errors in the absolute water velocities from bottom-tracking ship velocities were calculated by assuming uniform flows over horizontal spatial scales of 500 m. The errors were about 5–6 cm/s, which confirmed the estimates of 5 cm/s made previously. The assumption of horizontal uniformity in currents was justified using

estimates of the maximum horizontal shear present over the shelf break. The absolute water velocities from GPS ship velocities were not accurate enough to yield any consistent values, and so were discarded.

Coastwide survey results

The data collected in June 1993 with the ADCP on the *J.P. Tully* were also examined over spatial scales of about 100 km and temporal scales of 1–3 weeks. The zooplankton scattering levels had similar day and night cross-shelf structures to those observed in the ADCP line survey. Current patterns were consistent with a summer mean southeastward flowing shelf-break current (Freeland et al., 1984), an estuarine type flow at the mouth of Juan de Fuca Strait (Labrecque et al., 1994), and a counter-clockwise rotating eddy over Juan de Fuca Canyon (Ware and Thomson, 1992).

The errors in water velocity components were calculated by assuming horizontal uniformity in currents over spatial scales of 500 m, as was done previously for the ADCP survey line data. The errors were found to be 7–8 cm/s when using bottom-tracking to estimate ship velocities, which were consistent (to within 2-3 cm/s) both with the estimates made for the ADCP survey line data (5–6 cm/s) and with the estimates made using the RDI (1989) method (5 cm/s). The errors in water velocity components were about 30 cm/s when using GPS to estimate ship velocities. This estimate was lower than the 40 cm/s estimate based on differences between GPS and bottom-tracking ship velocities. However, the estimate of 30 cm/s is considered more accurate as it does not involve the bottom-tracking errors. The variability in absolute water velocities resulting from GPS estimates of ship velocities was found to be large enough to mask any water flow patterns and therefore, only the estimates of absolute velocities using bottom-tracking were used. Spatial averaging of the absolute velocities using bottom-tracking resulted in water velocity errors of about 2–3 cm/s.

Summer mean patterns

Averaging the data over the month of June revealed only the gross features of both backscatter residuals and water velocities. The zooplankton distributions observed in the *in-situ* vertical sections were found to persist all along the coast from the mouth of Juan de Fuca Strait to Estevan Point. The surface layer (6–30 m depth) revealed uniform backscatter levels both day and night across the shelf and slope. The mid-depth (80–100 m) depletion layer over the slope persisted all along the coast. The mid-depths revealed a banded zooplankton structure along the shelf break which reflected the boundary between the depletion layer over the slope and the higher zooplankton concentrations over the shelf. The deep water (175–200 m depth) also revealed a banded structure along the shelf-break, due to the boundary between the slope water zooplankton concentrations and the high concentrations near the bottom at the shelf-break. The banded structures in the waters below 80 m along the shelf-break were more pronounced (higher cross-shelf gradients in scattering levels) during the day.

The currents observed in the *in situ* vertical sections also were found to persist all along the coast from the mouth of Juan de Fuca Strat to Estevan Point. A southeastward flowing surface shelf-break current with speeds of about 20 cm/s was observed along the shelf break from Estevan Point to the waters over the mouth of Juan de Fuca Canyon. Outflow from Juan de Fuca Strait was observed to be strong (30–40 cm/s) in the surface waters (6–30 m) and weak (5–10 cm/s) in the deeper waters (78–102 m). A counter-clockwise rotating eddy was observed over Juan de Fuca Canyon. These currents were consistent with previous observations (Freeland et al., 1984; Ware and Thomson, 1992; Labrecque et al., 1994).

Viability of spatial averaging

Accurate summer mean zooplankton distributions and currents are difficult to obtain

from vessel-mounted ADCP data due to variability in backscatter residuals and in water velocities at semidiurnal and diurnal frequencies. Zooplankton distributions showed high variability at sunset and sunrise due to migration. Even after separation of the profiles into day and night, the migrations disrupted the mean patterns for a few hours prior to sunset and sunrise. The zooplankton distributions also showed high variability throughout the day due to advection of large patches of zooplankton. Water flow showed high variability at diurnal and semidiurnal frequencies throughout the survey area due to tidal flows.

It was found that there was not enough data sampling to well resolve the mean summer zooplankton distributions and currents. To estimate how many sampling periods [1] (for a given location) would be needed to resolve the mean currents and backscatter residuals to within 5 dB and 5 cm/s, respectively, the variances in the mean spatially averaged water velocity components and backscatter residuals were examined for the data taken off Barkley Sound (vertical sections 1–4; see Chapter 5.2.1). The data in sections 1–4 were averaged onto the 22×38 grid (Figure 4.16), initializing two grid rows. Each cross-shore location (same grid column) in the two initialized grid rows were then averaged together. The standard deviations on these averages are presented in histogram form (Figure 6.1).

The backscatter residuals have significant quantities of data with standard deviations as high as 12 dB. Therefore, the standard errors for one typical cruise with 2–3 sampling periods averaged onto each gridpoint will be 7–9 dB. To reduce this to below 5 dB would require 5–6 sampling periods, which would normally be collected over 2–3 cruises. The currents have significant amounts of data with standard deviations as high as 25 cm/s. Therefore, the standard errors for one typical cruise with 2–3 sampling periods averaged onto a grid point would be about 15 cm/s. To reduce this to about 5 cm/s would require

[1] A 'sampling period' denotes a period of time during which all ADCP profiles were sequential and averaged onto the same grid point

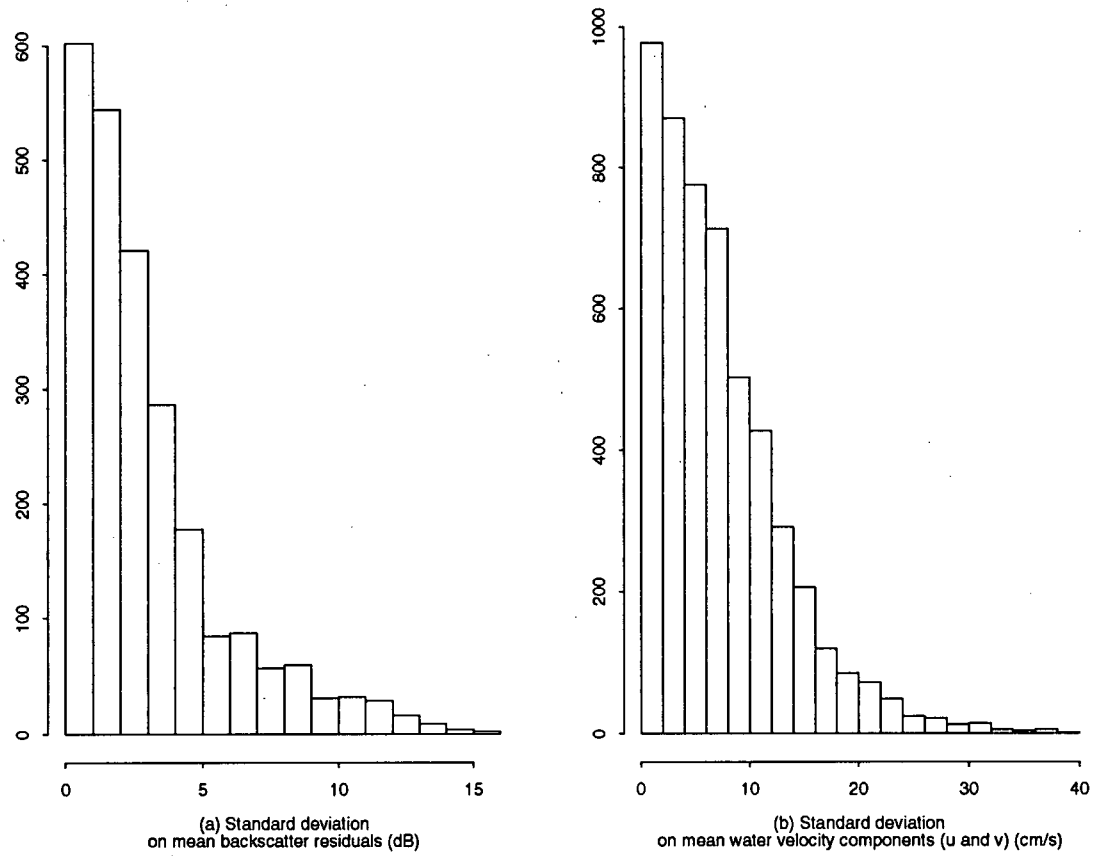

Figure 6.1: Histograms of standard deviations on mean (a) backscatter residuals and (b) water velocity components (u and v) for the June 1993 cruise.

10–15 sampling periods or 5–8 cruises.

The above analysis of sampling needed to resolve mean patterns in ADCP data could be furthered by comparing variances at different locations and at different times of the day to find where and when increased sampling would be needed.

A coverage of 10–15 sampling periods per grid-point is not available for any single month for a given year, since there was typically only one cruise per month to the southwest coast of Vancouver Island with the vessel-mounted ADCP. However, such data sampling is available if the data from all cruises during the last seven years are included in the averages. For example, along with the June, 1993 cruise discussed above, there was one cruise in June for each year from 1989-1991 and two cruises in June, 1988, for a total of six June cruises to the southwest coast of Vancouver Island. The mean structures revealed by such an average would be inter-annually persistent. The variability in the zooplankton distributions and current patterns may be higher than that discussed above due to the longer time scales involved. However, such an average would probably reveal the inter-annual mean structures in backscatter residuals and water velocities to within about 2–3 dB and 5 cm/s, respectively.

Future work

The ADCP survey line conducted in June 1993 yielded some interesting results concerning the mean distribution, the diurnal migratory patterns and the advection of zooplankton on the Vancouver Island continental margin. The ADCP water velocity data was used primarily to examine the effects of the water flow on the zooplankton distributions, but also yielded results concerning the effects of barotropic and baroclinic tidal components on the mean currents. We suggest that a more thorough survey could be completed over the Vancouver Island shelf break as follows:

Measure the offset angle and scaling bias of the ADCP on the *J.P. Tully* using one of the methods suggested by Pollard and Read (1989). Set the ADCP bin length to 4 m, the *blank-beyond-transmit* to 4 m, and the averaging interval to 120 sec.

Steam back and forth along a 3–5 km long survey line over the shelf break. The survey line should span the outer edge (1–2 km) of the shelf and extend a few kilometres seaward of the shelf break. The orientation of the survey line should be perpendicular to the mean orientation of the shelf break (200 m isobath). The ship speed should be roughly constant at about 10 knots, so as to cover the survey line in about two hours.

Steam the survey line for at least a 48 hour period. This would ensure two diurnal and four semidiurnal tidal periods as well as two diurnal plankton migration periods. The ship should be able to steam the survey line about 20 times in 48 hours, yielding enough coverage to give accurate estimates of the mean structures present in the area.

Take water property data at about five selected sites along the survey line. This should include CTD casts to enable calculations of the internal tidal modes and correlations between the ADCP currents, zooplankton distributions and water mass displacements.

Perform net tows at about three locations: Over the shelf; over the shelf break; and over the slope. Net tows at these locations should be done at least once during each day and once during each night. Multiple nets should be used to determine the abundances of zooplankton species at representative depths of 25, 50, 75, 100, 150, 200 and 300 m. This would enable calibration of the backscatter data to yield absolute estimates of biomass throughout the survey line. It would also enable

identification of the species composition of the aggregations of scatterers observed. Preferably, the survey should be completed in the summer when the plankton concentrations are highest. Similar surveys could be completed in the winter and spring to observe the seasonal variations in zooplankton distributions.

Bibliography

Appell, G. F., Bass, P. D., and Metcalf, M. A. (1991). Acoustic Doppler current profiler performance in near surface and bottom boundaries. *Journal of Oceanic Engineering*, 16(4):390–396.

Becker, R. A., Chambers, J. M., and Wilks, A. R. (1988). *The New S Language.* Wadsworth and Brooks/Cole Advanced Books and Software, Pacific Grove, CA.

Bevington, P. R. (1969). *Data Reduction and Error Analysis for the Physical Sciences.* McGraw-Hill Book Company, New York.

Bollens, S. M., Frost, B. W., and Lin, T. S. (1992). Recruitment, growth and diel vertical migration of *euphausia pacifica* in a temperate fjord. *Marine Biology*, 114:219–228.

Burd, B. J. and Thomson, R. E. (1993). Flow volume calculations based on three-dimensional current and net orientation data. *Deep-Sea Research*, 40(6):1141–1153.

Burd, B. J. and Thomson, R. E. (1994). Hydrothermal venting at Endeavour Ridge: effect on zooplankton biomass throughout the water column. *Deep-Sea Research*, 41(9):1407–1423.

Burd, B. J., Thomson, R. E., and Jamieson, G. S. (1992). Composition of a deep scattering layer overlying a mid-ocean ridge hydrothermal plume. *Marine Biology*, 113:517–526.

Crawford, W. R. and Thomson, R. E. (1982). Continental shelf waves of diurnal period along Vancouver Island. *Journal of Geophysical Research*, 87:9516–9522.

Crawford, W. R. and Thomson, R. E. (1984). Diurnal period continental shelf waves along Vancouver Island: A comparison of observations with theoretical models. *Journal of Physical Oceanography*, 14(10):1629–1646.

Cuypers, L. (1993). *Oceanplot 1.01 Manual.* Hermes Computing Services, Victoria, B.C.

Flagg, C. N. and Smith, S. L. (1989). On the use of the acoustic Doppler current profiler to measure zooplankton abundance. *Deep-Sea Research*, 36(3):455–474.

Flather, R. A. (1987). A tidal model of the northeast Pacific. *Atmosphere-Ocean*, 25(1):22–45.

Flather, R. A. (1988). A numerical model investigation of tides and diurnal period continental shelf waves along Vancouver Island. *Journal of Physical Oceanography*, 18:115–139.

Foreman, M. G. and Freeland, H. J. (1991). A comparison of techniques for tide removal from ship-mounted acoustic Doppler measurements along the southwest coast of Vancouver Island. *Journal of Geophysical Research*, 96(C9):17007–17021.

Foreman, M. G. and Walters, R. A. (1990). A finite-element tidal model for the southwest coast of Vancouver Island. *Atmosphere-Ocean*, 28(3):281–287.

Freeland, H. J., Crawford, W. R., and Thomson, R. E. (1984). Currents along the Pacific coast of Canada. *Atmosphere-Ocean*, 22(2):151–172.

Freeland, H. J. and Denman, K. L. (1982). A topograhically controlled upwelling center off southern Vancouver Island. *Journal of Marine Research*, 40:1069–1093.

Gargett, A. E. (1988). A 'large eddy' approach to acoustic remote sensing of turbulent kinetic energy dissipation rate ϵ. *Atmosphere-Ocean*, 26(4):483–508.

Genin, A., Haury, L., and Greenblatt, P. (1988). Interactions of migrating zooplankton with shallow topography: predation by rockfishes and intensification of patchiness. *Deep-Sea Research*, 35(2A):151–175.

Geyer, W. R. and Signell, R. (1990). Measurements of tidal flow around a headland with a shipboard acoustic Doppler current profiler. *Journal of Geophysical Research*, 95(C3):3189–3197.

Greenlaw, C. F. (1977). Backscattering spectra of preserved zooplankton. *Journal of the Acoustical Society of America*, 62(1):44–52.

Guerin-Ancey, O. and David, P. M. (1993). Use of a multibeam-multifrequency sounder to study the distribution of small zooplankton. *Deep-Sea Research*, 40(1):119–128.

Heywood, K. J., Scrope-Howe, S., and Barton, E. D. (1991). Estimation of zooplankton abundance from shipborne ADCP backscatter. *Deep-Sea Research*, 38(6):677–691.

Holliday, D. V. and Pieper, R. E. (1980). Volume scattering strengths and zooplankton distributions at acoustic frequencies between 0.5 and 3 MHz. *Journal of the Acoustical Society of America*, 67(1):135–146.

Huyer, A., Kosro, P. M., Fleishbein, J., Ramp, S. R., Stanton, T., Washburn, L., Chavez, F. P., Cowles, T. J., Pierce, S. D., and Smith, R. L. (1991). Currents and water masses of the coastal transition zone off northern California, June to August 1988. *Journal of Geophysical Research*, 96(C8):14809–14831.

Joyce, T. M., Bitterman, Jr., D. S., and Prada, K. E. (1982). Shipboard acoustic profiling of upper ocean currents. *Deep-Sea Research*, 29(7A):903–913.

Kampa, E. M. (1975). Observations of a sonic-scattering layer during the total solar eclipse, 30 June, 1973. *Deep-Sea Research*, 22(6):417–423.

Kaneko, A., Koterayama, W., Honji, H., Mizuno, S., Kawatate, K., and Gordon, R. L. (1990). Cross-stream survey of the upper 400m of the Kuroshio by an ADCP on a towed fish. *Deep-Sea Research*, 37(5):875–889.

Kosro, P., Huyer, A., Ramp, S. R., Smith, R. L., Chavez, F. P., Cowles, T. J., Abbott, M. R., Strub, P. T., Barber, R. T., Jessen, P., and Small, L. F. (1991). The structure of the transition zone between coastal waters and the open ocean off northern California, winter and spring 1987. *Journal Geophysical Research*, 96(C8):14707–14730.

Kosro, P. M. (1985). *Shipboard Acoustic Current Profiling During the Coastal Ocean Dynamics Experiment.* PhD thesis, University of California, San Diego.

Labrecque, A. M., Thomson, R. E., Stacey, M. W., and Buckley, J. R. (1994). Residual currents in Juan de Fuca Strait. *Atmosphere-Ocean*, 32(2):375–394.

Mackas, D. L. (1992). Seasonal cycle of zooplankton off southwestern British Columbia. *Canadian Journal of Fisheries and Aquatic Sciences*, 49:903–921.

Mackas, D. L., Louttit, G. C., and Austin, M. J. (1980). Spatial distribution of zooplankton and phytoplankton in British Columbia coastal waters. *Canadian Journal of Fisheries and Aquatic Sciences*, 37(10):1476–1487.

Parsons, T. R., Takahashi, M., and Hargrave, B. (1984). *Biological Oceanographic Processes.* Pergamon Press, 3^{rd} edition.

Pieper, R. E. (1971). *A Study of the Relationship Between Zooplankton and High-Frequency Scattering of Underwater Sound.* PhD thesis, University of British Columbia.

Pollard, R. and Read, J. (1989). A method for calibrating shipmounted acoustic Doppler profilers and the limitations of gyro compasses. *Journal of Atmospheric and Oceanic Technology*, 6(6):859–865.

Ramp, S. R., Jessen, P. F., Brink, K. H., Niler, P. P., Daggett, F. L., and Best, J. S. (1991). The physical structure of cold filaments near Point Arena, California, during june 1987. *Journal of Geophysical Research*, 96(C8):14859–14883.

RDI (1989). *Acoustic Doppler Current Profilers Principles of Operation: A Practical Primer.* RD Instruments, San Diego, CA.

RDI (1990). Calculating absolute backscatter. Technical Report ADCP-90-04, RD Instruments, San Diego, CA.

Richter, K. E. (1985). Acoustic determination of small-scale distributions of individual zooplankters and zooplankton aggregations. *Deep-Sea Research*, 32(2):163–182.

Simard, Y., de Ladurantaye, R., and Therriault, J.-C. (1986). Aggregation of euphausiids along a coastal shelf in an upwelling environment. *Marine Ecology*, 32:203–215.

Simard, Y. and Mackas, D. L. (1989). Mesoscale aggregations of euphausiid sound scattering layers on the continental shelf of Vancouver Island. *Canandian Journal of Fisheries and Aquatic Sciences*, 46:1238–1249.

Stat. Sci. (1991). *S-PLUS 3.0 Reference Manual.* Statistical Sciences, Inc., Seattle, Washington.

Thomson, R. E., Burd, B. J., Dolling, A. G., Gordon, R., and Jamieson, G. S. (1992a). The deep scattering layer associated with the Endeavour Ridge hydrothermal plume. *Deep-Sea Research*, 39(1):55–73.

Thomson, R. E., Gordon, R. L., and Dolling, A. G. (1991). An intense acoustic scattering layer at the top of a mid-ocean ridge hydrothermal plume. *Journal of Geophysical Research*, 96(C3):4839–4844.

Thomson, R. E., Gordon, R. L., and Dymond, J. (1989a). Acoustic Doppler current profiler observations of a mid-ocean ridge hydrothermal plume. *Journal of Geophysical Research*, 94(C4):4709–4720.

Thomson, R. E. and Gower, J. F. (1985). A wind-induced mesoscale eddy over the Vancouver Island continental slope. *Journal of Geophysical Research*, 90(C5):8981–8993.

Thomson, R. E., Healey, M. C., Morris, J. F., and Borstand, G. A. (1992b). Commercial troll fishing vessel distribution off Vancouver Island during July 1988: relation to observed physical oceanography. *Canadian Journal of Fisheries and Aquatic Sciences*, 49(4):820–832.

Thomson, R. E., Hickey, B. M., and LeBlond, P. H. (1989b). The Vancouver Island Coastal Current: fisheries barrier and conduit. In Beamish, R. and McFarlane, G., editors, *Effects of Ocean Variability on Recruitment and an Evaluation of Parameters Used in Stock Assessment Models*, volume 108, pages 265–296. Canadian Special Publication of Fisheries and Aquatic Sciences.

Trump, C. L. (1986). Estimating absolute current velocities by merging shipboard Doppler current profiler data with Loran-C data. In *Proceedings of the IEEE third working Conference on Current Measurements*, pages 177–183.

Urick, R. J. (1983). *Principles of Underwater Sound.* McGraw-Hill.

Ware, D. M. and Thomson, R. E. (1988). Oceanic factors affecting the distribution and recruitment of west coast fisheries. In Sinclair, editor, *Report from the National Workshop on Recruitment.*, volume 1636, pages 31–64. Canadian Technical Report of Fisheries Aquatic Sciences.

Ware, D. M. and Thomson, R. E. (1992). La Perouse Project: *Seventh annual progress report 1991.* DFO Reports.

Wilson, C. and Firing, E. (1992). Sunrise swimmers bias acoustic Doppler current profiles. *Deep-Sea Research*, 39(5):885–892.

Appendix A

Derivation of the Biomass Formula

This appendix describes how to calculate the biomass per unit volume, W, from the acoustic backscatter per unit volume, S_v. To begin, recall (3.3), which related the total acoustic cross section per unit volume, σ_v, to S_v:

$$S_v = 10 \log(\frac{\sigma_v}{4\pi}). \tag{A.1}$$

For n scatterers per unit volume, each with an acoustic cross section, σ, the total acoustic cross section per unit volume is:

$$\sigma_v = n\,\sigma. \tag{A.2}$$

If each scatterer has a weight, w, then the total biomass per unit volume is:

$$W = n\,w, \tag{A.3}$$

Combining (A.1), (A.2) and (A.3), the total biomass per unit volume is:

$$W = 4\pi 10^{S_v/10} \left(\frac{w}{\sigma}\right). \tag{A.4}$$

If there are m different types of scatterers present, each with an acoustic cross section, σ_i, a weight, w_i, and an abundance per unit volume, n_i, (i = 1 to m) then (A.2) and (A.3) become:

$$\sigma_v = \sum_{i=1}^{m} n_i\,\sigma_i, \tag{A.5}$$

and:

$$W = \sum_{i=1}^{m} n_i\,w_i. \tag{A.6}$$

Thus, (A.4) becomes:

$$W = 4\pi 10^{S_v/10} \left(\frac{\sum_{i=1}^{m} n_i \, w_i}{\sum_{i=1}^{m} n_i \, \sigma_i} \right). \tag{A.7}$$

The abundances n_i in (A.7) can be re-written in terms of relative abundances, ξ_i, by dividing the top and bottom of (A.7) by the total number of scatterers per unit volume, n, as follows:

$$W = 4\pi 10^{S_v/10} \left(\frac{\sum_{i=1}^{m} \frac{n_i}{n} \, w_i}{\sum_{i=1}^{m} \frac{n_i}{n} \, \sigma_i} \right), \tag{A.8}$$

but, since

$$n = \sum_{i=1}^{m} n_i, \tag{A.9}$$

and

$$\xi_i = \frac{n_i}{n} = \frac{n_i}{\sum_{i=1}^{m} n_i}, \tag{A.10}$$

The total biomass per unit volume is given by:

$$W = 4\pi 10^{S_v/10} \left(\frac{\sum_{i=1}^{m} \xi_i \, w_i}{\sum_{i=1}^{m} \xi_i \, \sigma_i} \right). \tag{A.11}$$

Appendix B

Errors on Absolute Velocity from Bottom Tracking

The absolute, earth-referenced water velocities, (u, v), were given by (4.17):

$$\begin{pmatrix} u \\ v \end{pmatrix} = \begin{pmatrix} \sin\theta & -\cos\theta \\ \cos\theta & \sin\theta \end{pmatrix} \begin{pmatrix} (V_w)_{\|} - V_b \\ (V_w)_{\perp} \end{pmatrix} \tag{B.1}$$

where $(V_w)_{\|}$= along-ship component of relative water velocity,

$(V_w)_{\perp}$= cross-ship component of relative water velocity,

θ = ship heading from compass (degrees),

V_b = bottom speed (cm/s).

Equation (B.1) can be re-written in terms of absolute water velocities as:

$$\begin{pmatrix} u \\ v \end{pmatrix} = \begin{pmatrix} \sin\theta & -\cos\theta \\ \cos\theta & \sin\theta \end{pmatrix} \begin{pmatrix} V_{\|} \\ V_{\perp} \end{pmatrix} \tag{B.2}$$

where $V_{\|} = (V_w)_{\|} - V_b$,

$V_{\perp} = (V_w)_{\perp}$.

The variances in (u, v) due to variances in θ, $V_{\|}$ and $V_{\perp}$ (σ_θ, $\sigma_{V_{\|}}$, and $\sigma_{V_{\perp}}$) are found using ((Bevington, 1969), (4-9)):

$$\begin{pmatrix} \sigma_u \\ \sigma_v \end{pmatrix}^2 = \left[\frac{\partial}{\partial\theta}\begin{pmatrix} u \\ v \end{pmatrix}\right]^2 \sigma_\theta^2 + \left[\frac{\partial}{\partial V_{\|}}\begin{pmatrix} u \\ v \end{pmatrix}\right]^2 \sigma_{V_{\|}}^2 + \left[\frac{\partial}{\partial V_{\perp}}\begin{pmatrix} u \\ v \end{pmatrix}\right]^2 \sigma_{V_{\perp}}^2 \tag{B.3}$$

where the square of a matrix is defined here as a matrix of the squares of each row.

Expanding the first term in (B.3):

$$\left[\frac{\partial}{\partial\theta}\begin{pmatrix} u \\ v \end{pmatrix}\right]^2 \sigma_\theta^2 = \left[\begin{pmatrix} \cos\theta & \sin\theta \\ -\sin\theta & \cos\theta \end{pmatrix}\begin{pmatrix} V_{\|} \\ V_\perp \end{pmatrix}\right]^2 \sigma_\theta^2$$

$$= \begin{pmatrix} V_{\|}\cos\theta + V_\perp \sin\theta \\ V_\perp \cos\theta - V_{\|}\sin\theta \end{pmatrix}^2 \sigma_\theta^2$$

$$= \begin{pmatrix} (V_{\|} + V_\perp \tan\theta)^2 \\ (V_\perp - V_{\|}\tan\theta)^2 \end{pmatrix} \cos^2\theta\, \sigma_\theta^2 \qquad \text{(B.4)}$$

Expanding the second term in (B.3):

$$\left[\frac{\partial}{\partial V_{\|}}\begin{pmatrix} u \\ v \end{pmatrix}\right]^2 \sigma_{V_{\|}}^2 = \left[\begin{pmatrix} \sin\theta & -\cos\theta \\ \cos\theta & \sin\theta \end{pmatrix}\begin{pmatrix} 1 \\ 0 \end{pmatrix}\right]^2 \sigma_{V_{\|}}^2$$

$$= \begin{pmatrix} \sin^2\theta \\ \cos^2\theta \end{pmatrix}\sigma_{V_{\|}}^2 \qquad \text{(B.5)}$$

Expanding the third term in (B.3):

$$\left[\frac{\partial}{\partial V_\perp}\begin{pmatrix} u \\ v \end{pmatrix}\right]^2 \sigma_{V_\perp}^2 = \left[\begin{pmatrix} \sin\theta & -\cos\theta \\ \cos\theta & \sin\theta \end{pmatrix}\begin{pmatrix} 0 \\ 1 \end{pmatrix}\right]^2 \sigma_{V_\perp}^2$$

$$= \begin{pmatrix} \cos^2\theta \\ \sin^2\theta \end{pmatrix}\sigma_{V_\perp}^2 \qquad \text{(B.6)}$$

However,

$$V_{\|} = (V_w)_{\|} - V_b \qquad \text{(B.7)}$$

$$V_\perp = (V_w)_\perp, \qquad \text{(B.8)}$$

and so, since the fluctuations in water velocities are uncorrelated to the fluctuations in bottom velocities, the errors in absolute water velocities in the ship's reference frame,

$$\sigma_{V_{\|}}^2 = \sigma_w^2 + \sigma_b^2 \qquad \text{(B.9)}$$

$$\sigma_{V_\perp}^2 = \sigma_w^2 \qquad \text{(B.10)}$$

where σ_w = random error in water velocity (cm/s),

σ_b = random error in bottom tracking velocity (cm/s).

Thus, combining (B.4), (B.5), (B.6), (B.9) and (B.10):

$$\begin{pmatrix} \sigma_u^2 \\ \sigma_v^2 \end{pmatrix} = \begin{pmatrix} ((V_w)_{\|} - V_b + (V_w)_{\perp} \tan\theta)^2 \\ ((V_w)_{\perp} - ((V_w)_{\|} - V_b) \tan\theta)^2 \end{pmatrix} \cos^2\theta \, \sigma_\theta^2 + \begin{pmatrix} \sin^2\theta \\ \cos^2\theta \end{pmatrix} \sigma_b^2 + \sigma_w^2 \quad \text{(B.11)}$$

If $(V_w)_{\|} \approx (V_w)_{\perp} \equiv V$, then (B.11) is:

$$\begin{pmatrix} \sigma_u^2 \\ \sigma_v^2 \end{pmatrix} = \begin{pmatrix} 1 + \tan^2\theta + 2\tan\theta \\ 1 + \tan^2\theta - 2\tan\theta \end{pmatrix} V^2 \cos^2\theta \, \sigma_\theta^2 + \begin{pmatrix} \sin^2\theta \\ \cos^2\theta \end{pmatrix} \sigma_b^2 + \sigma_w^2 \quad \text{(B.12)}$$

Assuming a maximum heading error of $\sigma_\theta = 4°$, a maximum water speed of $V = 30\,cm/s$, and a water velocity error of $\sigma_w = 5\,cm/s$, the first term on the right hand side of (B.12) will change the values of σ_u and σ_v by at most 7.5% of σ_w, or $0.4\,cm/s$. Thus, to a good approximation (to within about $0.4\,cm/s$), the errors on water velocities derived from bottom-tracking estimates of ship speed are:

$$\sigma_u = \sqrt{\sigma_w^2 + \sin^2\theta \, \sigma_b^2}, \quad \text{(B.13)}$$

$$\sigma_v = \sqrt{\sigma_w^2 + \cos^2\theta \, \sigma_b^2}. \quad \text{(B.14)}$$